

Theoretical Design and Synthesis of Low Band Gap Conjugated Copolymers for Photovoltaic and Nonlinear Optical Applications

Thesis submitted to
Cochin University of Science and Technology
in partial fulfilment of the requirements
for the award of the degree of
Doctor of Philosophy
in
Chemistry
Under the Faculty of Science

by

Anjali C. P.



Department of Applied Chemistry
Cochin University of Science and Technology
Kochi - 22

July 2017

Theoretical Design and Synthesis of Low Band Gap Conjugated Copolymers for Photovoltaic and Nonlinear Optical Applications

Ph.D. Thesis under the Faculty of Science

By

Anjali C. P.

Research Fellow

Department of Applied Chemistry

Cochin University of Science and Technology

Kochi, India 682022

Email: anjali.acp4@gmail.com

Supervising Guide

Dr. K. Sreekumar

Professor

Department of Applied Chemistry

Cochin University of Science and Technology

Kochi, India 682022

Email: drksreekumar@gmail.com, ksk@cusat.ac.in

Department of Applied Chemistry
Cochin University of Science and Technology
Kochi, India 682022

July 2017

**DEPARTMENT OF APPLIED CHEMISTRY
COCHIN UNIVERSITY OF SCIENCE AND TECHNOLOGY
KOCHI - 682022, INDIA**



Dr. K. Sreekumar
Professor

Ph: 9447121530
E-mail: ksk@cusat.ac.in

Date: 19th July 2017

Certificate

This is to certify that the thesis entitled “**Theoretical Design and Synthesis of Low Band Gap Conjugated Copolymers for Photovoltaic and Nonlinear Optical Applications**” is an authentic record of research work carried out by **Ms. Anjali C. P.**, under my supervision in partial fulfilment of the requirements for the award of the degree of Doctor of Philosophy in Chemistry under the Faculty of Science of Cochin University of Science and Technology, and further that no part thereof has been presented before for the award of any other degree. All the relevant corrections and modifications suggested by the audience and recommended by the doctoral committee of the candidate during the presynopsis seminar have been incorporated in the thesis.

Dr. K. Sreekumar
(Supervising Guide)

Declaration

I hereby declare that the thesis entitled “**Theoretical Design and Synthesis of Low Band Gap Conjugated Copolymers for Photovoltaic and Nonlinear Optical Applications**” submitted for the award of the Ph. D Degree, is based on the original research work done by me under the guidance of Dr. K. Sreekumar, Professor, Department of Applied Chemistry, Cochin University of Science and Technology and further that it has not previously formed the basis for the award of any other degree.

Kochi-22
19/07/2017

Anjali C. P.

*Success is not final, failure is not fatal:
it is the courage to continue that counts.*

Winston S. Churchill

Acknowledgement

First and foremost, I would like to express my sincere gratitude to my supervising guide and mentor, Dr. K. Sreekumar, Professor, Department of Applied Chemistry, Cochin University of Science and Technology for the continuous support, invaluable guidance and motivation during my research work. Without his unimaginable patience and compassion, this thesis would not have materialized. I thank him for giving me intellectual freedom in my work and I could not have imagined having a better advisor and mentor for my research.

I extend my gratitude to Dr. K. Girish Kumar, Head as well as my Doctoral Committee Member, Department of Applied Chemistry, Cochin University of Science and Technology and all other former Heads of the Department for providing me the best platform and necessary facilities to accomplish the research work. I greatly acknowledge the help and guidance of all the faculty members of the Department of Applied Chemistry, throughout my research work. I record my sincere thanks to Dr. M. R. Prathapachandra Kurup and Dr. M. R. Anantharaman, former directors of Inter University Centre for Nanomaterials and Devices (IUCND). I thank all non-teaching staff of the department for the timely help and co-operation extended to me during my research work.

It is my privilege to acknowledge Dr. K. P. Vijayakumar, Professor, Department of Physics, CUSAT and Dr. P. Predeep, Professor, NIT, Calicut for allowing me to do photovoltaic studies in their labs. I extend my gratitude to the Director, International School of Photonics, CUSAT for the Nonlinear Optical studies.

My heartfelt thanks to Dr. Mahesh Kumar for helping me in Quantum Chemical calculations and solving the theoretical chemistry problems. I whole heartedly thank Mr. S. Mathew, ISP, CUSAT for helping me to carryout NLO measurements. My sincere gratitude to Ms. R. Geethu, Department of Physics, and Ms. Rose Mary, NITC for the Photovoltaic studies of the polymers and timely help

during the last stages of my research work. My heartfelt thanks to Unni Sivasankaran, Analytical lab, for the Cyclic Voltammetric studies.

I always cherish the sincere friendship of my former colleagues, Dr. Anoop, Dr. Kannan, Dr. Mangala, Dr. Elizabeth, Ms. Jabia, Mr. Jithin, Ms. Smrithy Vasudevan, Ms. Anu, Mr. Rajkumar, Ms. Saritha for their love and support in the initial stages of my work.

I extend my sincere thanks to my loving lab mates Dr. Sherly, Dr. Smitha, Dr. Jiby, Dr. Sinija, Dr. Jisha, Ms. Anjaly Jacob, Dr. Jaimy, Ms. Letcy, Ms. Shaibuna, Ms. Shebitha for rendering their helping hand during difficult times and for all the fun we have had in the lab. I extend my gratefulness to new juniors Avudaiappan, Hiba and Priya.

I am really thankful to Sowmya Xavier for her immense support and motivation during my hard times. She stood by my side like a sister with extreme care and love when I felt depressed and struggled. Without her constant motivation, this thesis would not have become a reality. My special thanks to Sona for her love and support during the difficult times of my research. She was always there for helping me personally at any time. I specially acknowledge Sona for helping me to carryout NLO measurements. I express my sincere thanks to Jisha Pillai for her timely help especially for the thermal analysis. I remember with deepest gratitude for all the personal support and care she had given to me. I also remember my special friends Bhavya and Suma for the wonderful and joyous days in hostel and all the fun we had together. No words of gratitude are enough to acknowledge the help, support and care given by them.

I remember Reshma, Sandhya chechi, Pravitha, Sajitha chechi, Cisy, Remya, Jomon chettan, Rakesh, Eason for their valuable friendship, love and support. I specially thank Aswathy, Vineetha, Nithya, Kala for their love and friendship. I would like to thank all my friends in the Department of Applied Chemistry, Department of Physics and Department of Polymer Science and Rubber Technology for their help and care. I would like to acknowledge IUCND and CUSAT for

providing the financial support to carry out my research work, I am also thankful to Dr. Shibu, and Mr. Saji, SAIIF-STIC, CUSAT, for all Spectral analysis.

My deepest gratitude goes to my family for their unflagging love and support throughout my work, I thank my father and my mother for their prayer and blessings. I also remember my sisters with affection. They form the backbone; their unconditional love and support helped to achieve my goal. I can't find enough words to thank them.

Last but not the least, words fall short in expressing my thanks to Jayesh, my beloved husband for his love, care and support. He is the constant and the best source of inspiration and motivation to take this research work to its logical end. Without his unflinching support and cooperation, I would not have been able to complete this work, I hope he will forgive me for social distancing from him which was resorted to whenever was needed for quite longer duration due to the research work. At this moment, I remember with gratitude his entire family members for their whole hearted support to achieve this goal in my life.

Above all, I thank god for giving me this wonderful opportunity to do research.

Anjali C. P.

||| Preface |||

Conjugated polymers have received considerable technological interest due to the combination of physical properties of polymers (low density, processibility, solubility, *etc.*) with the optoelectronic properties of semiconductors and have been extensively studied due to their potential applications in organic optoelectronic devices, such as photovoltaic cells, thin film transistors, organic light emitting diodes, electrochromic devices *etc.* In addition to this, conjugated organic polymers have received considerable attention, because of their advantages, such as being light weight, flexible and having a facile large-scale fabrication. These are considered to be one of the most promising materials to lower the cost of the energy generated when compared to inorganic material based solar cells. Such conjugated polymeric materials are used as active layers in optoelectronic devices. For instance, conjugated polymers and their doped forms were considered as potential alternatives for metals in the field of device fabrication. The major intention of the present study was to synthesize low band gap conjugated polymers which have the ability to absorb from the visible region and possessing both photovoltaic and nonlinear optical property.

Major objectives of the present study are:

- Theoretical designing of low band gap conjugated polymers using Density Functional Theory (DFT) in the periodic boundary condition (PBC).
- Synthesis of Monomers and designed low band gap polymers using different synthetic strategies including Direct Arylation Polymerization, Suzuki Coupling Polymerization, Gilch Polymerization and Knoevenagel Polycondensation.
- Explore the third-order nonlinear optical properties of synthesized polymers.

- Explore the application of the conjugated polymers as active layer in photovoltaic devices and fabrication of solar cells using different configurations.

The thesis is divided into six chapters

The first chapter gives a concise introduction to conjugated polymers and their applications in different optoelectronic devices. The first section of the introduction chapter describes the fundamental concepts and structural aspects of conjugated polymers. Second section deals with the concepts of theoretical investigation and designing of conjugated polymers. Various routes for the synthesis of conjugated polymers are discussed in the third section of this chapter. Fourth section illustrates the various technological aspects of device fabrication in organic photovoltaics and donor-acceptor concept in band gap modelling. The last section describes the fundamentals of nonlinear optical properties of conjugated polymers and their application in optical limiting devices.

The second chapter includes the methods for the synthesis of monomers. Seven dibromo derivatives of different monomers were synthesized which were suitable for the synthesis of conjugated copolymers via Direct Arylation and Suzuki Polymerization routes. Two bromomethylated derivatives of monomers were synthesized for Gilch Polymerization reaction and one cyanomethyl derivative of monomer was synthesized for the synthesis of cyanovinylene polymer. All the monomers synthesized were characterized by different spectroscopic and analytical techniques.

Third chapter deals with the theoretical studies of monomers, D-A binary units and polymers using Gaussian 09 software. Monomers and D-A units were optimized using density functional theory (DFT) and total optimization process included DFT/B3LYP/6-31G formalism. Band gap, oscillator strength and excitation energies were calculated using time dependent density functional theory (TD-DFT) calculations. Conjugated polymers were optimized by applying periodic boundary condition (PBC).

In the fourth chapter, the synthesis of twelve conjugated copolymers by different synthetic strategies like Direct Arylation Polymerization, Suzuki Coupling Polymerization, Gilch Polymerization and Knoevenagel Polycondensation were demonstrated. The synthesized polymers were characterized by different spectroscopic techniques including ^1H NMR and IR spectroscopy. GPC (Gel Permeation Chromatography) technique was used for finding the molecular weights of polymers. Absorption spectra were recorded for all the samples and from the onset value of absorption peak, optical band gaps were calculated. Emission spectra of copolymers were measured in different solvents and found to be in the visible range. Thermal stability of polymers was investigated by TG-DTA. The redox behavior of all the copolymers was investigated using cyclic voltammetry. HOMO and LUMO energy values and electrochemical band gaps of copolymers were calculated. Band gaps obtained from optical and electrochemical methods are in good agreement with the band gaps obtained from theoretical calculations.

Fifth chapter is about the Photovoltaic and Nonlinear Optical applications of the synthesized polymers. Summary and conclusion of the work done is presented in the sixth chapter. References are given at the end of each chapter.

Contents

Chapter 1

AN INTRODUCTION TO CONJUGATED POLYMERS

AND THEIR APPLICATIONS.....01 - 44

1.1	Introduction.....	01
1.1.1	Strategies for Band Gap Reduction	04
1.1.2	The Donor-Acceptor Approach in Band Gap Control.....	06
1.2	Computational Methods	07
1.3	General Routes for the Synthesis of Conjugated Polymers.....	09
1.3.1	Suzuki Coupling Polymerization Reaction	10
1.3.2	Heck Polymerization	11
1.3.3	Sonogashira Coupling Reaction	12
1.3.4	Stille Coupling Reaction.....	13
1.3.5	Yamamoto Coupling Reaction	13
1.3.6	Gilch Polymerization Reaction	14
1.3.7	Direct Arylation Polymerization	16
1.4	Organic Photovoltaics	17
1.4.1	Bilayer Heterojunction Devices	19
1.4.2	Bulk Heterojunction Devices	20
1.4.3	Design and Structural Organization of Polymeric Materials for Photovoltaic Device Architecture	23
1.4.3.1	D-A Copolymer as p-type Material.....	23
1.5	Nonlinear Optics	25
1.5.1	Nonlinear Absorption (NLA)	27
1.5.1.1	Two Photon Absorption (TPA)	28
1.5.1.2	Multiphoton Absorption	29
1.5.1.3	Saturable Absorption (SA)	29
1.5.1.4	Reverse Saturable Absorption (RSA).....	30
1.5.1.5	Free Carrier Absorption (FCA)	30
1.5.2	Optical Power Limiting	30
1.5.3	Nonlinear Refraction (NLR)	31
1.5.4	Z-scan Technique for NLO Characterization.....	32
1.5.4.1	Open Aperture (OA) Z-scan.....	33
1.5.4.2	Closed Aperture (CA) Z-scan.....	34
1.6	Scope of the thesis.....	35
	References.....	36

Chapter 2

SYNTHESIS AND CHARACTERIZATION OF MONOMERS45 - 77

2.1	Introduction.....	45
2.2	Results and Discussion.....	52

2.2.1	Synthesis of Monomers	52
2.2.1.1	Synthesis of Fluorene Based Monomers	53
2.2.1.2	Synthesis of 3,4-dimethoxythiophene	54
2.2.1.3	Synthesis of 3,7-dibromo-10-octylphenothiazine	55
2.2.1.4	Synthesis of 4, 4'-dibromotriphenylamine	55
2.2.1.5	Synthesis of 3,6-bis(4-bromophenyl) 2,5-dihydropyrrolo[3,4-c] pyrrole-1,4-dione	56
2.2.1.6	Synthesis of 1,4-dibromo-2,5-bis (octyloxy) benzene	57
2.2.1.7	Synthesis of 1,4-bis (bromomethyl)-2,5-bis (octyloxy) benzene	58
2.2.1.8	Synthesis of 1,4-bis (bromomethyl)-2-((2-ethylhexyl)oxy)-5-methoxybenzene	59
2.2.1.9	Synthesis of 2,2'-((2,3-dihydrothieno[3,4-b][1,4]dioxine-5,7-diyl) bis(4,1- phenylene)) diacetonitrile ⁵³	60
2.3	Experimental Procedure	60
2.3.1	Synthesis of Fluorene Based Monomers.....	60
2.3.1.1	2,7-Dibromofluorene	60
2.3.1.2	2, 7-Dibromo-9,9-dioctylfluorene	61
2.3.1.3	Synthesis of 2,7-bis (4,4,5,5-tetramethyl-1,3,2-dioxaborolan-2-yl)-9,9-dioctylfluorene	61
2.3.1.4	Synthesis of 2,7-dibromofluorenone	63
2.3.1.5	Synthesis of 9,9-Bis(4-diphenylaminophenyl)-2,7-dibromofluorene	64
2.3.2	Synthesis of 3,7-Dibromo-10-(octyl)phenothiazine	65
2.3.3	Synthesis of 4, 4'-dibromotriphenylamine.....	66
2.3.4	Synthesis of 3,6-bis (4-bromophenyl) 2,5-dihydropyrrolo [3,4-c] pyrrole-1,4-dione.....	67
2.3.5	Synthesis of 1,4-dibromo-2,5-bis (octyloxy) benzene 1,4-bis (octyloxy) benzene.	68
2.3.6	Synthesis of 1,4-bis (bromomethyl)-2,5-bis (octyloxy) benzene	69
2.3.7	Synthesis of 1,4-bis (bromomethyl)-2-((2-ethylhexyl)oxy)-5-methoxybenzene	70
2.3.8	Synthesis of Thiophene Based Monomers	71
2.3.8.1	Diethyl thiodiglycolate	71
2.3.8.2	3,4-Dimethoxy-2,5-dicarbethoxythiophene.....	71
2.3.8.3	3,4-Dimethoxythiophene-2,5-dicarboxylic acid.....	72
2.3.8.4	Synthesis of 3,4-dimethoxythiophene.....	72
2.3.9	Synthesis of 2,2'-((2,3-dihydrothieno [3,4-b][1,4]dioxine-5,7-diyl)bis(4,1phenylene)) diacetonitrile.....	79
2.4	Conclusion	74
	References.....	74

Chapter 3

THEORETICAL STUDIES OF MONOMERS, D-A UNITS

AND POLYMERS.....	79 - 116
3.1 Introduction.....	79
3.2 Theoretical Calculation	82
3.3 Results and Discussion	84
3.3.1 Thiophene Based Polymers.....	89
3.3.1.1 Band Structure of P(EDT-TPAFL) and P(DMT-TPAFL).....	89
3.3.1.2 Band Structure of P(EDT-TPA) and P(DMT-TPA).....	93
3.3.1.3 Band Structure of P(EDT-DOB)	96
3.3.2 Fluorene Based Polymers	99
3.3.2.1 Band Structure of P(FL-TPAFL) and P(FL-DPPPh).....	99
3.3.2.2 Band Structure of P(FL-TPA) and P(FL-BP).....	103
3.3.3 Anthracene-phenothiazine Polymer	106
3.3.4 Phenylenevinylene polymers	109
3.4 Conclusion.....	113
References.....	114

Chapter 4

SYNTHESIS AND CHARACTERIZATION OF

DESIGNED CONJUGATED POLYMERS 117 - 167

4.1 Introduction.....	117
4.1.1 Palladium Catalyzed Polymerization Reactions.....	118
4.1.2 Synthesis of PPV Polymers.....	121
4.2 Results and Discussion	121
4.2.1 Synthesis of Thiophene Based Polymers	121
4.2.1.1 P(EDT-TPAFL) and P(DMT-TPAFL).....	121
4.2.1.1.1 Optical Properties	124
4.2.1.1.2 Thermal Properties	126
4.2.1.1.3 Electrochemical Studies	127
4.2.1.2 P(EDT-TPA), P(DMT-TPA) and P(EDT-DOB).....	128
4.2.1.2.1 Optical Properties	131
4.2.1.2.2 Thermal Properties	133
4.2.1.2.3 Electrochemical Studies	135
4.2.2 Synthesis of fluorene based polymers	136
4.2.2.1 P(FL-TPAFL) and P(FL-DPPPh).....	136
4.2.2.1.1 Optical Properties	139
4.2.2.1.2 Thermal Properties	140
4.2.2.1.3 Electrochemical Studies	141
4.2.2.2 P(FL-TPA) and P(FL-BP)	142
4.2.2.2.1 Optical Properties	145
4.2.2.2.2 Thermal Properties	146

4.2.2.2.3	Electrochemical Studies	147
4.2.3	Synthesis of Anthracene-phenothiazine Copolymer P(ANT-PHENO)	148
4.2.3.1	Optical Properties	150
4.2.3.2	Thermal and Electrochemical Properties	151
4.2.4	Synthesis of phenylenevinylene Polymers (PPV)	153
4.2.4.1	DOC-MEH PPV and EDTh CN PPV	153
4.2.4.1.1	Optical Properties	155
4.2.4.1.2	Thermal Properties	157
4.2.4.1.3	Electrochemical Studies	157
4.3	Experimental	158
4.3.1	Synthesis of Thiophene Based Polymers	158
4.3.1.1	General Procedure for the Polymerization	158
4.3.1.1.1	Synthesis of P(EDT-TPAFL)	159
4.3.1.1.2	Synthesis of P(DMT-TPAFL)	159
4.3.1.1.3	Synthesis of P(EDT-TPA)	160
4.3.1.1.4	Synthesis of P(DMT-TPA)	160
4.3.1.1.5	Synthesis of P(EDT-DOB)	161
4.3.2	Synthesis of fluorene based polymers	161
4.3.2.1	General Procedure for Polymerization through Suzuki Coupling	161
4.3.2.1.1	Synthesis of P(FL-TPAFL)	162
4.3.2.1.2	Synthesis of P(FL-DPPPh)	162
4.3.2.1.3	Synthesis of P(FL-TPA).....	163
4.3.2.1.4	Synthesis of P(FL-BP)	163
4.3.3	Synthesis of Anthracene-phenothiazine copolymer P(ANT-PHENO).....	164
4.3.4	Synthesis of Phenylenevinylene Polymers	164
4.3.4.1	Synthesis of DOC-MEH PPV.....	164
4.3.4.2	Synthesis of EDTh CN PPV	165
4.4	Conclusion	165
	References.....	166

Chapter 5

NONLINEAR OPTICAL AND PHOTOVOLTAIC

APPLICATIONS OF CONJUGATED POLYMERS169 - 201

5.1	Introduction.....	169
5.1.1	Nonlinear Optics	170
5.1.1.1	Z-Scan Technique.....	171
5.1.1.2	Optical Power Limiting	173
5.1.2	Photovoltaics	174
5.1.2.1	Bulk Heterojunction Devices.....	174
5.1.2.1.1	Conventional Photovoltaic Devices	174

5.1.2.1.2	Inverted Photovoltaic Devices	175
5.1.2.2	I-V Characteristics of a Photovoltaic Device	175
5.1.2.3	Open Circuit Voltage.....	177
5.1.2.4	Short Circuit Current	177
5.1.2.5	Fill Factor	177
5.2	Results and Discussion	178
5.2.1	Open Aperture (OA) Z-Scan Measurements of the Polymers	178
5.2.1.1	Thiophene Based Polymers	179
5.2.1.2	Fluorene Based Polymers	184
5.2.1.3	Anthracene-Phenothiazine Copolymer P(ANT-PHENO) ...	187
5.2.1.4	Phenylenevinylene Polymers (PPVs)	189
5.2.2	Photovoltaic Device Fabrication	191
5.2.2.1	Photovoltaic Performance of Conventional Solar Cells Constructed Using Synthesized Polymers	192
5.2.2.2	Photovoltaic Performance Of Inverted Solar Cells Constructed Using Synthesized Polymers	194
5.3	Conclusion	197
	References.....	198

Chapter 6

SUMMARY AND OUTLOOK.....	203 - 208
6.1 Summary of the Work.....	203
6.2 Major Achievements	207
6.3 Future Outlook.....	208

List of Publication.....	209 - 210
---------------------------------	------------------

List of Abbreviation	211 - 213
-----------------------------------	------------------

**AN INTRODUCTION TO CONJUGATED
POLYMERS AND THEIR APPLICATIONS**

Contents	<i>1.1 Introduction</i>
	<i>1.2 Computational Methods</i>
	<i>1.3 General Routes for the Synthesis of Conjugated Polymers</i>
	<i>1.4 Organic Photovoltaics</i>
	<i>1.5 Nonlinear Optics</i>
	<i>1.6 Scope of the Thesis</i>

1.1 Introduction

Conjugated polymers have received considerable technological interest due to the combination of physical properties of polymers like low density, processibility, solubility, etc. and the optoelectronic properties of semiconductors. The semiconducting behavior of conjugated polymers make them applicable in organic optoelectronic devices¹⁻⁴ such as photovoltaic cells,^{5,6} thin film transistors,⁷ organic light emitting diodes,^{8,9} electrochromic devices etc.¹⁰ As being light weight, flexible and having facile processes for large-scale fabrication, conjugated polymers are considered to be one of the most promising materials to lower the cost of the energy generated when compared to inorganic material based solar cells.¹¹⁻¹⁶ Conjugated polymeric materials and their doped forms are used as active layers in optoelectronic devices and were considered as potential alternatives for metals in the field of device fabrication.¹⁷⁻¹⁹

The first section of the introductory chapter describes the fundamental concepts and structural aspects of conjugated polymers. Second section deals with the concepts of theoretical investigation and designing of conjugated polymers. Various routes for the synthesis of conjugated polymers are discussed in the third section of this chapter. Fourth section illustrates the various technological aspects of device fabrication in organic photovoltaics and donor-acceptor concept in band gap modelling. The last section describes the fundamentals of nonlinear optical properties of conjugated polymers and their application in optical limiting devices.

The band gap of a polymer is directly related to its conjugation along the backbone. Another factor which affects the band gap of the organic material is the bond length alteration (BLA). Band gap can be controlled through reduction of bond length alteration. Increasing the aromaticity of the polymer backbone does not ensure a low band gap, but it is more stable and thus represents the ground-state structure. Instead, more effective way of lowering the band gap in conjugated systems is increasing the quinoid character thereby decreasing the bond length alteration of the polymeric backbone (Figure 1.1).²⁰⁻²²

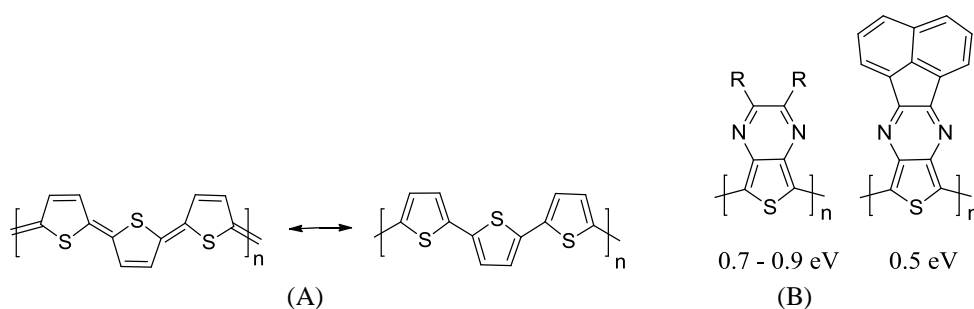


Figure 1.1: (A) Aromatic and quinoid resonance structures of polythiophene; (B) band gap reduction of polymer due to enhanced quinoidal character²⁰

Another important factor which affects the band gap is the planarity of the polymer backbone. Monomer aromaticity and heteroatom in heterocyclic systems are responsible for the planarity (Figure 1.2). The strong electron affinity of heteroatom leads to lower band gap values.²³ It has also been proposed that monomer aromaticity determines the confinement potential and delocalization of the π -electrons. As the confinement within the ring becomes stronger, the delocalization length along the backbone decreases, resulting in larger E_g values.²⁴ The last factor to consider is interchain coupling that can occur via stacking in the solid state, resulting in increased electron delocalization and a reduction in band gap. Reduced molecular ordering can increase the spatial distance between polymer chains, reducing interchain coupling and increasing band gap. Such molecular ordering can also directly affect the charge mobility of materials.

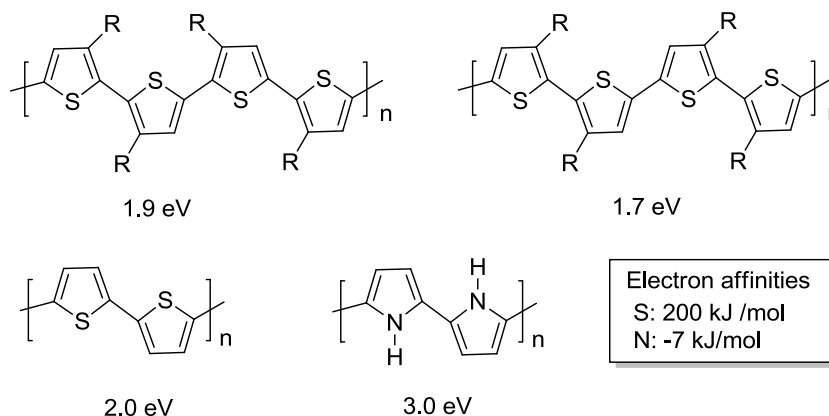


Figure 1.2: Illustrative examples of molecular effects on band gap²⁴

Band gap control has always been an essential synthetic strategy in the field of conjugated polymers. In 1992, Wynberg and co-workers introduced the concept of the donor-acceptor (D-A) approach to conjugated polymer

design.²⁵ Various strategies like ladder polymerization, donor-acceptor polymerization etc. are used for band gap control. The donor-acceptor (D-A) approach as a powerful synthetic tool in controlling the band gaps of conjugated polymers, was first introduced by Havinga et al.^{25,26} which was utilized to achieve narrow and low band gap polymers. The donor-acceptor concept is important not only for the band gap control, but also for providing the possibility of combining properties of two different moieties. In the donor-acceptor copolymers, the low band gap is ascribed to an intramolecular charge transfer (ICT) between the electron-rich and electron poor units. The actual band gap correlates with the energy difference between the highest occupied molecular orbital (HOMO) of the electron-rich donor unit and the lowest unoccupied molecular orbital (LUMO) of the electron-poor acceptor moiety. The band gap can be narrowed or widened on the basis of the strength of donor and acceptor units. Therefore, the strength of the donor and acceptor materials that are combined has a significant effect on the resulting band gap. One advantage of utilizing conjugated polymers for technological applications is the ability to tune the material properties at the molecular level. This is typically accomplished through synthetic modification of the monomeric units.²⁷⁻²⁹

1.1.1 Strategies for Band Gap Reduction

This section discusses the general design strategies used to control the band gaps of conjugated polymers. Considering the skeleton of a polyaromatic conjugated polymer such as polyphenylene, poly(phenylene vinylene), and polythiophene, there are two possible resonance structures for the ground state with nondegenerate energy. The first is called the aromatic form. In the case of thiophene polymers (Figure 1.1A), each thiophene unit maintains its

aromaticity with confined π -electrons. Delocalization of the π -electrons along the conjugated backbone converts double bonds into single bonds and synchronously transforms single bonds into double bonds, leading to a resonance structure referred to as the quinoid form.²⁰ The quinoid form is energetically less stable when compared to the aromatic form. Quinoid structure has a small band gap because it requires destruction of the aromaticity and a loss in the stabilization energy.²² As the quinoid contribution increases, the carbon-carbon single bonds between two adjacent rings adopt more double bond character and the bond length alteration starts to decrease. Overall, the HOMO-LUMO band gap decreases linearly as a function of the increasing quinoid character. For example, polyisothianaphthene (PITN)³⁰ tend to favor the quinoid form to selectively maintain the benzene aromaticity which make PITN a low band gap conjugated polymer.

In a similar manner, quinoidization by aromatic exchange, poly(thieno [3,4-*b*]pyrazine)³¹ or poly(thieno [3,4-*b*] thiophene)³² with primary thiophene rings fused with another aromatic pyrazine or thiophene ring at the β -position have also been synthesized to promote quinoid population and achieve low band gap conjugated polymers (Figure 1.3).



Poly (thieno [3,4-*b*] pyrazine)

Poly (thieno [3,4-*b*] thiophene)

Figure 1.3: Chemical Structures of Poly (thieno [3,4-*b*] pyrazine) and Poly (thieno [3,4-*b*] thiophene)

There are other various useful strategies for reducing the band gap of conjugated polymers including molecular modification used to impose steric or electronic effects on conjugated main chains and planarization between adjacent aromatic units which allows parallel p-orbital interactions to extend conjugation and facilitate delocalization. This in turn results in band gap reduction by reducing the BLA.³³

1.1.2 The Donor-Acceptor Approach in Band Gap Control

A more powerful strategy in designing low band gap conjugated polymers is the synthesis of alternating donor-acceptor (D-A) copolymers.³⁴ Through the introduction of push-pull driving forces, electron delocalization and the formation of quinoid mesomeric structures over the conjugated backbone can be facilitated, resulting in the reduction of BLA. By introducing electron rich donor unit and electron deficient acceptor unit in the same polymer backbone, the valence and conduction bands get broadened and a small HOMO-LUMO separation in between. This can be elucidated in a more simple way by introducing the concept of hybridization of the molecular orbital between the donor and acceptor in the D-A polymer (Figure 1.4).

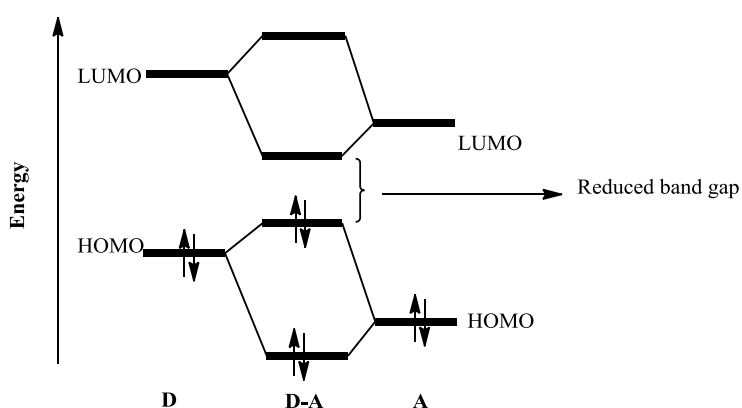


Figure 1.4: Illustration of hybridization of the molecular orbital

According to the rules of perturbation theory, the HOMO of the donor segment will interact with the HOMO of the acceptor segment to yield two new HOMOs for the D-A polymer. Similarly, the LUMO of the donor will interact with that of the acceptor to produce two new LUMOs of the D-A polymer. After the electrons redistribute themselves from their original non interacting orbitals to the new hybridized orbitals of the polymer, a higher lying HOMO and a lower lying LUMO are formed. This leads to a narrowing of the optical band gap.³⁵ Figure.1.4 shows the hybridization process of the HOMOs and LUMOs of a D-A system. This concept has served as a basis for structural modification of many conjugated systems. By carefully selecting the structures of the donors and acceptors and their respective electron donating and withdrawing strengths, conjugated polymers with controlled energy levels and band gaps can be synthesized.

1.2 Computational Methods

The major aspect of the conjugated polymer research is the synthesis of organic polymeric materials with suitable electronic and structural characteristics for the various applications. Theoretical modelling of monomeric units and conjugated polymers will help to avoid the expense and wastage of chemicals and thereby helps to design conjugated polymers with low band gaps. A theoretical model or method is a way to model a system using a specific set of approximations. These approximations are combined with a calculation algorithm and are applied to atomic orbitals, defined by the basis set in order to compute molecular orbitals and energy.³⁶

In general, the methods can be separated into 4 main types: semi empirical, ab initio, density functional and molecular mechanics. The

selection of theoretical model depends on the size of the system and on the level of approximation. Density functional theory (DFT) methods are becoming more and more popular because the results obtained are comparable to the ones obtained using ab initio methods. DFT methods account for electron correlation by estimating the interaction of an electron with the total electron density.^{37,38} Most popular DFT method is B3LYP (Becke, three-parameter, Lee-Yang-Parr). (Becke 3-Parameter³⁹ method for calculating that part of the molecular energy due to overlapping orbitals, plus the Lee-Yang-Parr (LYP)⁴⁰ method of accounting for correlation).

Two different types of theoretical methods are available for the band gap calculation of conjugated polymers. The first method is the oligomer method. Using this method, band gap of polymers can be calculated by plotting the reciprocal of oligomer length ($1/n$) as a function of HOMO-LUMO gap (in eV) of oligomer which requires repeated calculations until convergence is reached.⁴¹⁻⁴⁴ Second method is the periodic boundary condition (PBC) method along with the density functional calculations. PBCs are a set of boundary conditions which are used for approximating large polymeric systems by using a small part of the chain (unit cell). The PBC-DFT method was implemented in the Gaussian 03⁴⁵ and Gaussian 09⁴⁶ quantum chemical codes. Gaussian type orbitals (GTOs) are implemented in the Gaussian software packages.⁴⁷ For calculating the periodic boundary condition of polymers, Bloch Functions were employed to transform Gaussian type orbitals to crystal orbitals.⁴⁸ Band gaps obtained by DFT method by applying periodic boundary conditions are usually in good agreement with that obtained by experimental data. T. M. Pappenfus et al.,

have performed DFT calculations on a series of D-A copolymers using the oligomer method and periodic boundary conditions.⁴⁹ They have demonstrated that the two methods agree well with one another and correlated with experimental data obtained.

On the basis of band structure and electronic property studies of a series of vinylene-linked polymers by performing hybrid functional with periodic boundary conditions in conjunction with nucleus-independent chemical shift (NICS) and bond length alteration (BLA), B. M. Wong et al. came to a conclusion that the aromatic \leftrightarrow quinoidal level-crossing is a more effective way of lowering the band gap in conjugated systems.⁵⁰ Heyd-Scuseria-Ernzerhof (HSE06) functional⁵¹ incorporating a screened Hartree-Fock interaction has been introduced which was more computationally effective than traditional hybrid functional, B3LYP. In the present work, HSE06 in combination with 6-31G basis set was used for calculating the electronic properties of the D-A conjugated polymers.

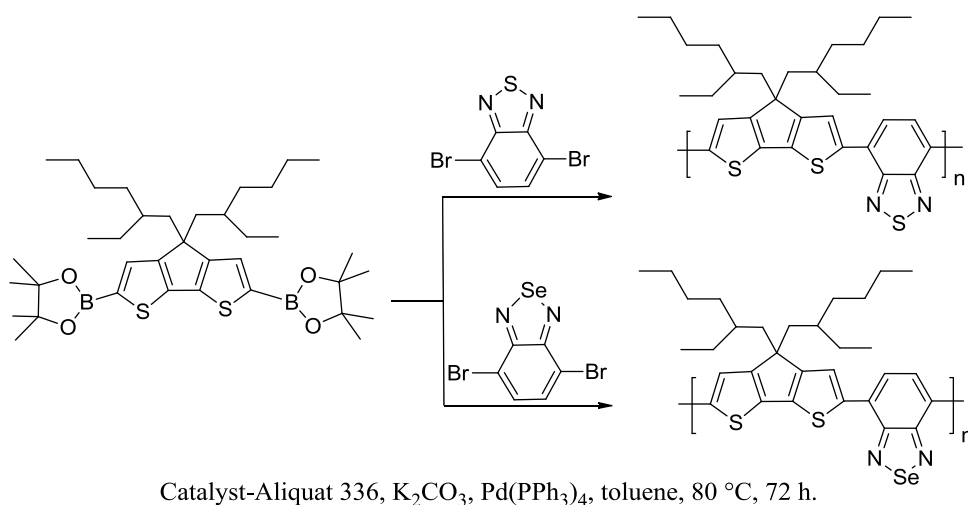
1.3 General Routes for the Synthesis of Conjugated Polymers

During the past decades, considerable knowledge (theoretical and experimental) has been gained and many synthetic strategies are available for the synthesis of conjugated polymers. In addition to chemical oxidative⁵² or electrochemical⁵³⁻⁵⁵ polymerizations, transition metal catalyzed cross-coupling reactions provide a particularly powerful synthetic strategy for Csp^2-Csp^2 and $Csp-Csp^2$ bond formation.⁵⁶ This section discusses the general introduction to metal mediated polymerization and Knoevenagel polycondensation, with a particular focus on Pd and Ni catalyzed polymerization reactions. Pd catalyzed (Suzuki,⁵⁷ Negishi,⁵⁸ Heck,⁵⁹ Sonogashira⁶⁰ and Stille⁶¹ coupling

polymerizations) and Nickel catalyzed (Kumada Corriu⁶²) reactions are often used for the synthesis of conjugated polymers.

1.3.1 Suzuki Coupling Polymerization Reaction

The Suzuki cross-coupling of aryl halides with organoboronic acids or esters has become one of the most widely investigated and used synthetic methods for C-C bond formation. It is widely used to synthesize polyolefins, styrenes, and substituted biphenyls. The general scheme for the Suzuki coupling reaction includes a carbon-carbon single bond formation by coupling an organoboron species with a halide using a palladium catalyst and a base. The advantage of Suzuki coupling polymerization is the less toxic nature, mild reaction conditions, economical and ecofriendly (even water can be used as solvent) nature of the reaction.



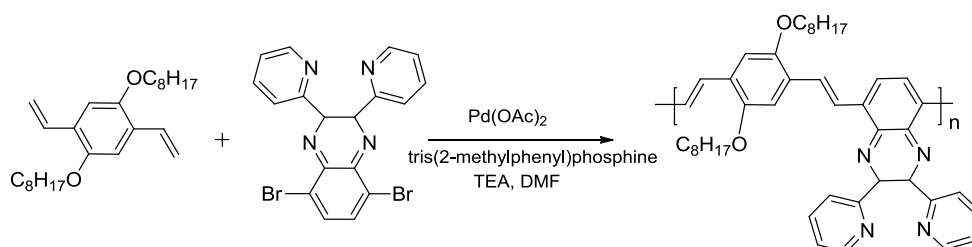
Scheme 1.1: Synthesis of Benzochalcogenadiazole Based Polymers⁶³

L. Gregory et al. synthesized two cyclopentadithiophene benzochalcogenadiazole donor-acceptor (D-A) copolymers via Suzuki

polymerization reaction (Scheme 1.1). The band gaps of S- and Se- containing polymers were calculated to be 1.59 eV and 1.46 eV respectively. The results imply that the substitution of heavy atoms into the acceptor can narrow the band gap of a D-A polymer.⁶³

1.3.2 Heck Polymerization

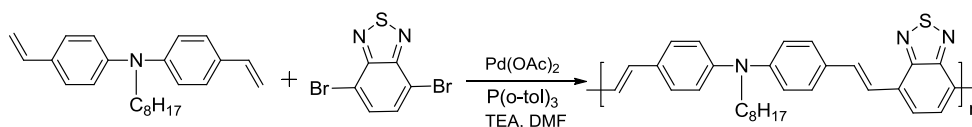
A new conjugated copolymer, poly[1,4-dioctyloxyphenylene-2,5-diethenylene-(2,3-dipyridine-2-ylquinoxaline-5,8-diyl)ethylene] (PPV-BD) was synthesized successfully by Chen et al., in which the electron-donating unit was alkoxy substituted phenyl ring, and the electron-accepting unit was a quinoxaline (Scheme 1.2). The resulting polymer had a low band-gap of 1.98 eV. The results showed that introduction of quinoxaline units has led to a reduction of the band gap of poly(p-phenylenevinylene) (PPV) copolymers and can be used for detection of TNT in solution.⁶⁴



Scheme 1.2: Synthesis of PPV-BD Polymer

Huo et al. synthesized alternating copolymers of electron-rich arylamine/dialkoxyphenylene and electron-deficient 2,1,3-benzothiadiazole. They studied the photovoltaic properties of the copolymers by fabricating the bulk heterojunction device.⁶⁵ The bulk heterojunction-type polymer solar cell was fabricated with the blend of the copolymer, DP-BT and

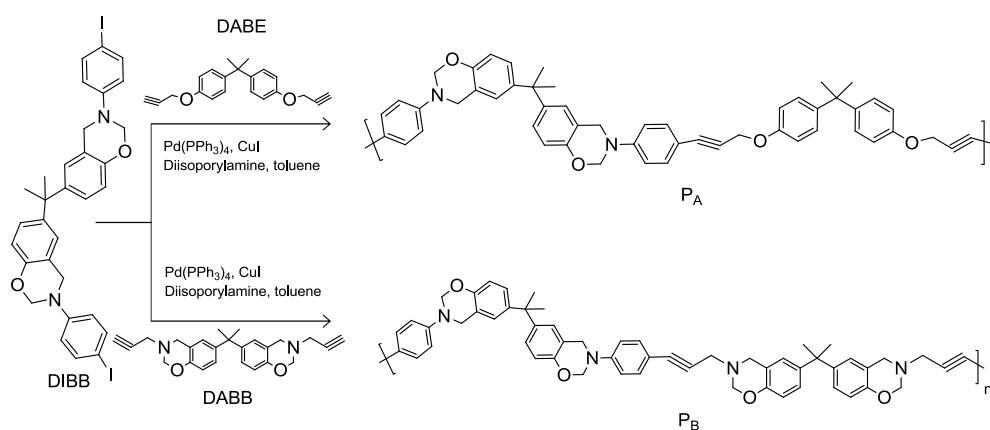
PCBM as the photosensitive layer which gave a power conversion efficiency of 0.39 % (Scheme 1.3).



Scheme 1.3: Synthesis of DP-BT Polymer

1.3.3 Sonogashira Coupling Reaction

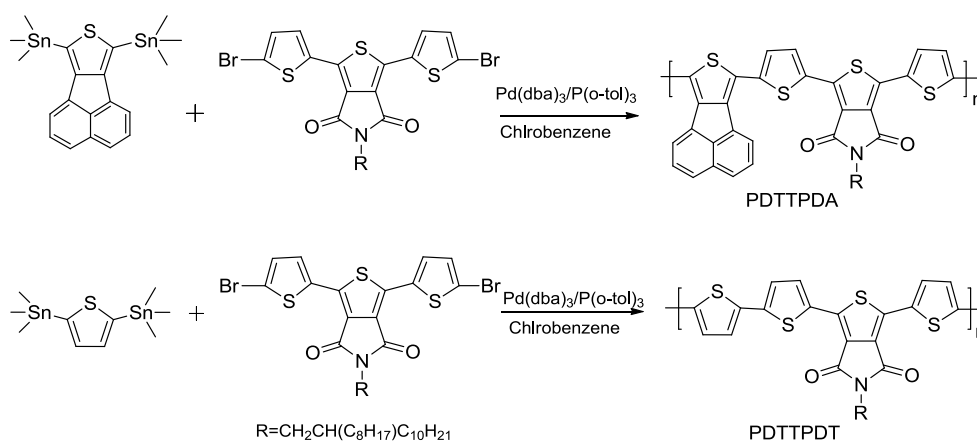
The traditional reactants in the Sonogashira coupling reaction are vinyl or aryl halides and terminal alkynes. The reaction has been generally performed in a system involving a Palladium catalyst, Copper Iodide co-catalyst, and supplemental amines.⁶⁶ Demir et al. synthesized thermally curable polybenzoxazines from Diiodobisbenzoxazine (DIBB), Diacetylene bisbenzoxazine (DABB), and Diacetylene bisether (DABE) by Sonogashira coupling reaction⁶⁷ (Scheme 1.4).



Scheme 1.4: Synthesis of Benzoxazine Polymers by Sonogashira Coupling

1.3.4 Stille Coupling Reaction

The Stille cross-coupling reaction is a versatile C-C bond forming reaction between organic stannane and organic halides. This reaction is more suitable for thiophene-containing polymers using monomers with stannyl groups on the thiophene ring. W. H. Lee et al. synthesized two donor-acceptor conjugated polymers composed of new acenaphtho[1,2-c] thiophene or thiophene as electron donors and 1,3-dithien-2-yl-thieno[3,4-c]pyrrole-4,6-dione (DTTPD) as the electron acceptor by Stille cross-coupling reaction (Scheme 1.5). They observed that polymer: PCBM bulk heterojunction device fabricated showed power conversion efficiency (PCE) of up to 3.28 %.⁶⁸

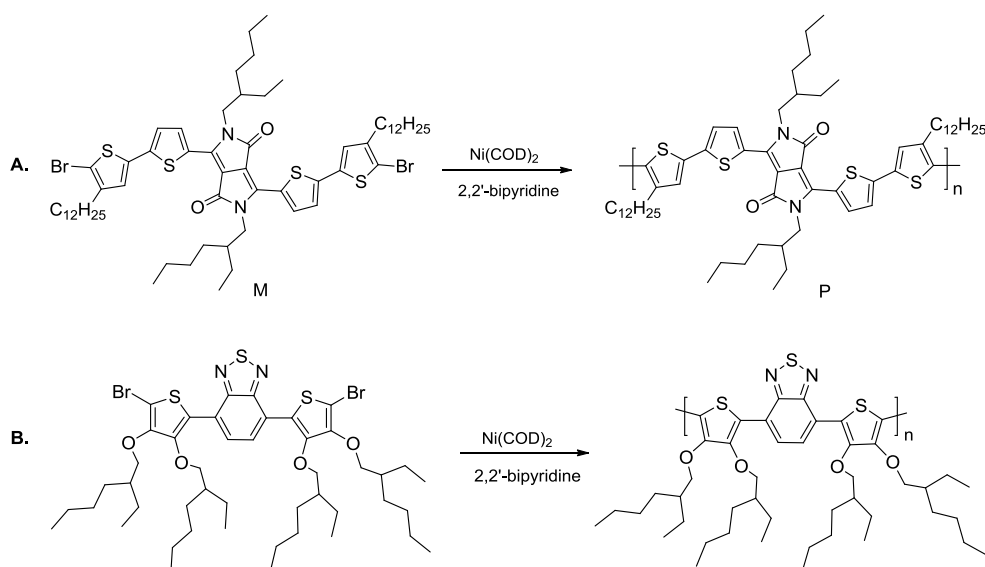


Scheme 1.5: Synthesis of Polymers by Stille Coupling Reaction

1.3.5 Yamamoto Coupling Reaction

Yamamoto dehalogenation coupling reactions provide Nickel-mediated self-polymerization of single monomers. The advantage of Yamamoto coupling is that only a single component of monomer can self-polymerize to afford the alternating D-A polymer with moderate to high molecular weight. Janssen and

co-workers reported a new conjugated polymer based on alternating electron-rich quaterthiophene and electron-deficient diketopyrrolopyrrole units⁶⁹ by the Yamamoto coupling which exhibited an ideal band gap of 1.4 eV (Scheme 1.6.A). The device using P/PCBM gave power conversion efficiency (PCE) of 3.2 %. They also reported side chain substituted conjugated polymer (Scheme.1.6.B) that consisted of alternating electron-rich bithiophene and electron deficient benzothiadiazole unit.⁷⁰

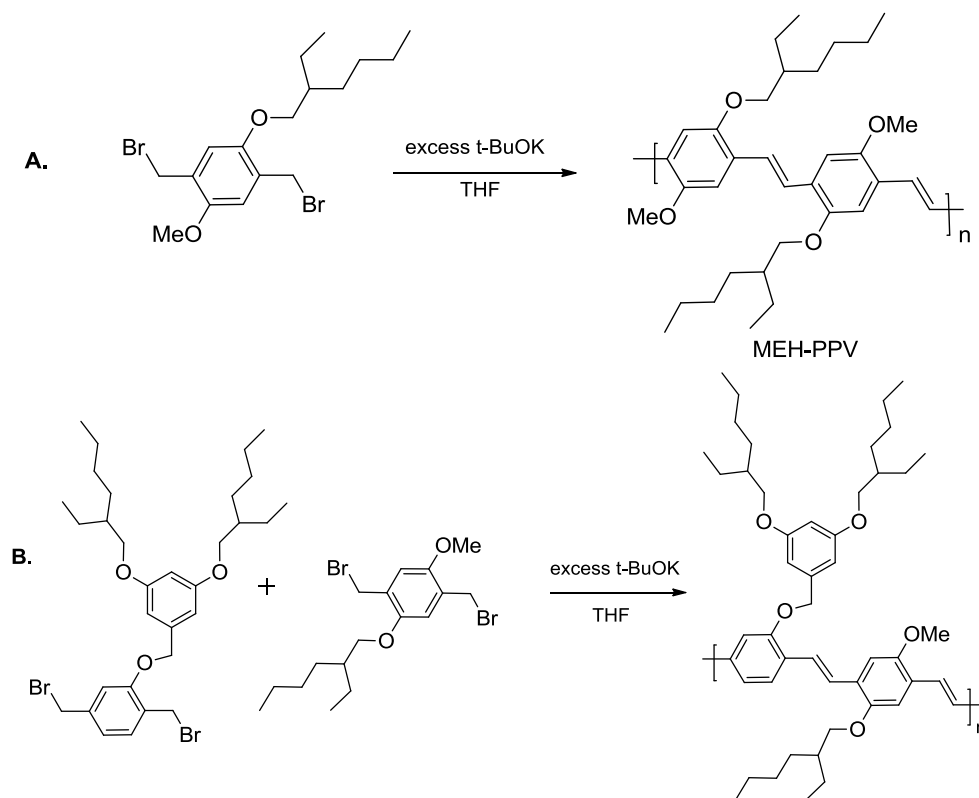


Scheme 1.6: Synthesis of Polymers by Yamamoto Coupling Reaction

1.3.6 Gilch Polymerization Reaction

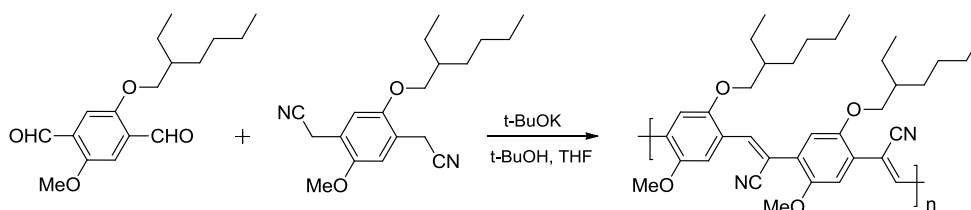
This reaction is useful in the synthesis of phenylene vinylene polymers. Usually Gilch polymerization route is used for the self-polymerization of monomers in the presence of potassium tert-butoxide to yield homopolymer. Neef et al. published a typical Gilch route to the synthesis of solution-processable poly(2-methoxy-5-((2'-ethylhexyloxy)-1,4-phenylene vinylene)

(MEH-PPV) which is depicted in Scheme 1.7A.⁷¹ In addition to PPV homopolymer derivatives, monomers with different side chains can also be randomly copolymerized by the Gilch route to afford a variety of interesting PPV derivatives. Tan et al. synthesized 3,5-dialkoxybenzyl pendant containing MEH-PPV derivatives. The feeding ratio of two monomers can be varied to fine-tune the steric and electronic properties of the resultant polymer (Scheme.1.7B); a photovoltaic device was fabricated using a Polymer: PCBM blend which showed PCE value of 1.41 %.⁷²



Scheme 1.7: Synthesis of PPV Polymers via Gilch Route

The molecular orbital energy levels of phenylene vinylene polymers can also be tuned by incorporating electronic substituents into the conjugated vinylene backbone. M. Ganstrom et al. synthesized cyano group incorporated phenylene vinylene polymer (CN-PPV) by means of a facile Knoevenagel polycondensation between terephthalaldehyde and 1,4-bis (cyanomethyl) benzene in the presence of the base, *t*-BuOK (Scheme 1.8). Compared to MEH-PPV, the new CN-PPV lowered both the LUMO and HOMO levels by ~ 0.5 eV. Electron-withdrawing effect of the cyano side group creates a low-lying LUMO level so that it can function as a suitable electron acceptor in photovoltaic devices, in either a bilayer or a bulk heterojunction configuration. For example, a bilayer device fabricated by CN-PPV as the n-type layer showed PCE of 1.9 %.⁷³

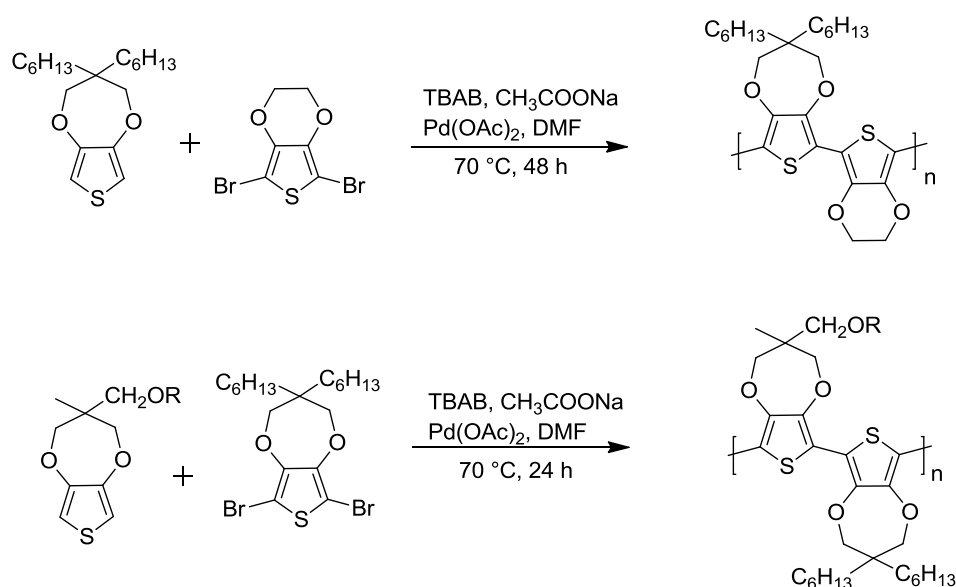


Scheme 1.8: Synthesis of CN-PPV by Knoevenagel Polycondensation Reaction

1.3.7 Direct Arylation Polymerization

Direct Arylation polymerization is an important methodology that emerged only recently. This reaction is the coupling of aryl halides with catalytically activated C-H bonds which provides a desirable and economical alternative to standard cross-coupling reactions for the construction of new C-C bonds. Direct arylation is used to synthesize polymers that were previously difficult to prepare due to the instability of organometallic monomers. The

major drawback of direct (hetero) arylation, however, is the lack of C-H bond selectivity which results in cross-linked material during polymerization reactions. The cross-linking can be avoided by blocking the 3- and 4- positions of thiophene based monomers. A. Kumar et al. reported a single step reductive polymerization of ProDOT derivatives in the presence of Pd catalyst which gave the corresponding direct arylated polymers⁷⁴ (Scheme.1.9).



Scheme 1.9: Synthesis of Thiophene Based Polymers by Direct Arylation Polymerization Route

1.4 Organic Photovoltaics

Conjugated polymers fulfill the two most important requirements needed for photovoltaic device materials: they absorb light effectively and are able to carry charge. Therefore, they are used as active material in organic photovoltaic (OPV) devices. Two general classes of OPVs are organic small molecule based

devices and organic polymer semiconductor based devices. Small molecule semiconductor based devices are generally processed by vapor deposition under high vacuum, while the polymer semiconductor based devices are processed from solution. Here, active layer is sandwiched between two electrodes and it consists of organic polymeric materials instead of inorganic silicon. Organic layer has two phases: donor, an electron donator, and electron withdrawing acceptor. Conjugated materials are commonly used in both roles.⁷⁵

The general working principle in such solar cells involves the photoexcitation of the donor material by absorbing light energy to generate excitons. This electron-hole pair diffuses to the donor-acceptor (D-A) interface and dissociates into holes and electrons. The fully separated free charge carriers transport to the respective electrodes in the opposite direction with the aid of the internal electric field, which generates the photocurrent and photovoltage. The process of conversion of light into electricity can be schematically described by the following Figure 1.5.

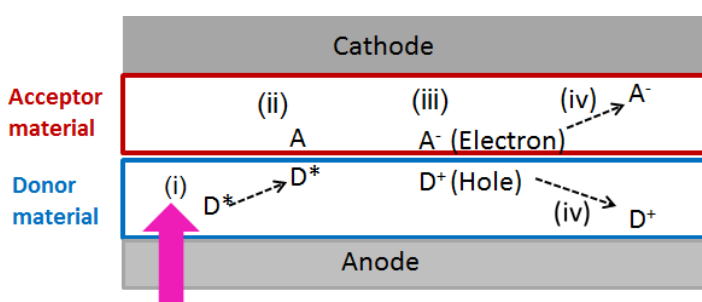


Figure1.5: Energy conversion process in photovoltaic devices

1.4.1 Bilayer Heterojunction Devices

Tang implemented a bilayer heterojunction architecture containing a p-type layer for hole transport and an n-type layer for electron transport to improve the photocurrent of the solar cell device.⁷⁶ The bilayer device structure is shown in Figure 1.6. The donor layer and acceptor layer are deposited on the transparent conducting oxide coated glass plate layer by layer. The metal electrode was coated on the top of the active layer by vacuum evaporation technique. By absorbing photons from sun light, donor and acceptor creates excitons. These excited species move towards the interface and dissociated into free charges. In bilayer heterojunction devices, the separated layer of donor and acceptor has small interfacial area which limits the amount of free charge carriers from reaching the interface. The limited lifetime of excitons only allow the electron-hole pair to diffuse a short distance, probably between 5 nm and 14 nm.⁷⁷⁻⁸¹ If the donor creates excitons far away from the heterojunction interface, which will result in the decay of excitons to the ground state without the chance to reach the acceptor. This leads to the loss of absorbed photons and quantum efficiency. Consequently, the performance of bilayer heterojunction devices is greatly limited by the small area of charge-generating interface between the donor and acceptor.

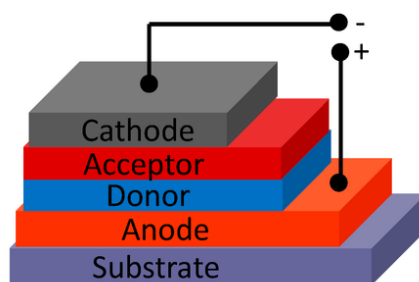


Figure 1.6: Schematic representation of bilayer heterojunction

1.4.2 Bulk Heterojunction Devices

Yu et al. introduced the concept of a bulk heterojunction (BHJ) to overcome the difficulty of reduced quantum efficiency in the case of bilayer heterojunction devices.⁸² By blending donor and acceptor materials together, an interpenetrating network with a large D-A separation between the two components in bulk was obtained. In this way, much enhanced quantum efficiency of charge separation can be achieved by any absorbing site in the composite which is within a few nanometers of the donor-acceptor interface. The formation of a continuous network creates two channels to transport holes in the donor domain and electrons in the acceptor domain, resulting in efficient charge collection. The fabrication of the device can be simplified by employing solution processing techniques as the bulk heterojunction configuration requires only single active layer to create an internal D-A heterojunction, without having any interfacial erosion problems which bilayer configuration faced. Figure 1.7 illustrates the standard bulk heterojunction architecture where an active layer of the D-A polymer is sandwiched between two electrodes. Sariciftci and co-workers discovered efficient photo induced electron transfer in conjugated polymer-fullerene composites.⁸³ Buckminsterfullerene (C_{60}) has proven to be an ideal n-type material due to its various intrinsic advantages.

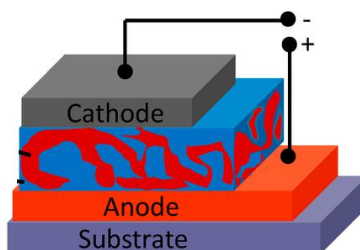


Figure 1.7: Schematic representation of bulk heterojunction

In the case of polymer/fullerene organic photovoltaic devices, active layers are composed of hole-transporting polymeric materials as donors and electron transporting fullerene derivatives as acceptors.⁸⁴ Well defined nanostructured active layer is essential for the effective photoelectric conversion processes. First, it possesses a relatively low-lying lowest unoccupied molecular orbital(LUMO) energy level which is thermodynamically favorable to accepting electrons from an excited p-type material. The triply degenerate C₆₀ LUMO enables it to be reduced by up to six electrons, which reflects its unique stabilization of negative charges.⁸⁴

Yokozawa et al.⁸⁵ and McCullough et al.⁸⁶⁻⁸⁸ developed the controlled polymerization of regioregular poly(3-hexylthiophene). A number of regioregular polythiophene-based donor-type block copolymers have been developed⁸⁹⁻⁹² and investigations have been carried out on their application as donor materials in OPVs. For example, poly(3-hexylthiophene)-*block*-poly(3-(2-ethylhexyl)thiophene),⁹³ poly(butylthiophene)-*block*-poly (octylthiophene)^{94,95} and poly(4-vinyl triphenylamine)-*block*-poly(3-hexylthiophene)-*block* poly(4-vinyl triphenylamine)⁹⁶ were found to exhibit clear lamellar phase separation and have been studied widely because of their potential applications as acceptor materials instead of fullerene derivatives in OPVs.⁹⁷⁻¹⁰¹ In contrast to donor materials, the fullerene derivative, PCBM, is the only conventional acceptor material for OPVs. One of the major reasons for using PCBM is its high electron mobility (*ca.* 0.002 cm²/V s). However, there are also considerable drawbacks for use in OPVs:

- (i) Negligible light absorption in the visible-near-IR regions.
- (ii) Less compatibility with donor polymeric materials.
- (iii) High cost for synthesis and purification.

S. H. Park et al.¹⁰² fabricated bulk heterojunction solar cell using copolymer, poly[N-9'-heptadecanyl-2,7-carbazole-alt-5,5-(4,7-di-2-thienyl-2,1,3-benzothiadiazole) (PCDTBT) by blending with PC₇₀BM acceptor, gave a power conversion efficiency of 6.1 %. Y. Liang et al.¹⁰³ developed bulk heterojunction solar cells by blending thieno[3,4-b]thiophene and benzodithiophene polymers with PC₇₁BM as active layer and achieved a power conversion efficiency of 7.4 %.

The investigation of non-fullerene acceptor materials that can potentially replace PCBM in OPVs is, thus, increasingly necessary, which gives rise to the possibility of fabricating all-polymer (polymer/polymer) photovoltaic device. (Figure 1.8 B). All-polymer photovoltaic architecture offers potential advantages over conventional fullerene-based OPVs, such as more efficient light absorption due to the acceptor polymer and relatively high open-circuit voltages.¹⁰⁴ Although D-A block copolymer have electron-transporting properties, broad light absorption and nano morphology derived from the D-A block structure, the number of D-A block copolymers as acceptor material is still limited. Even though these polymers have synthetic difficulties, the recent advancements in the synthesis and applications of D-A block copolymer for all-polymer photovoltaics are highlighted.¹⁰⁵

Y. Zhou et al.¹⁰⁶ fabricated all polymer solar cell by selecting isoindigo polymers as the donor material because of their low band gaps, strong absorption, good hole charge transport etc. and substituted N,N'-Dioctyl-3,4,9,10-perylenedicarboximide (PTCDI) polymer as the acceptor polymer due to its good electron transporting property and good solubility. This all-PSC achieved a power conversion efficiency of 4.2 %. Z. Li et al.¹⁰⁷

constructed all polymer solar cells (all-PSCs) with naphthalenediimide-bithiophene-thiophene random polymers. The acceptor polymer, PNDI-T10 is miscible with the low band gap donor polymer PTB7-Th, and the blend promotes efficient exciton dissociation and charge transport. The balanced hole and electron mobility gave the best solar cell performance with a power conversion efficiency of 7.6 %.

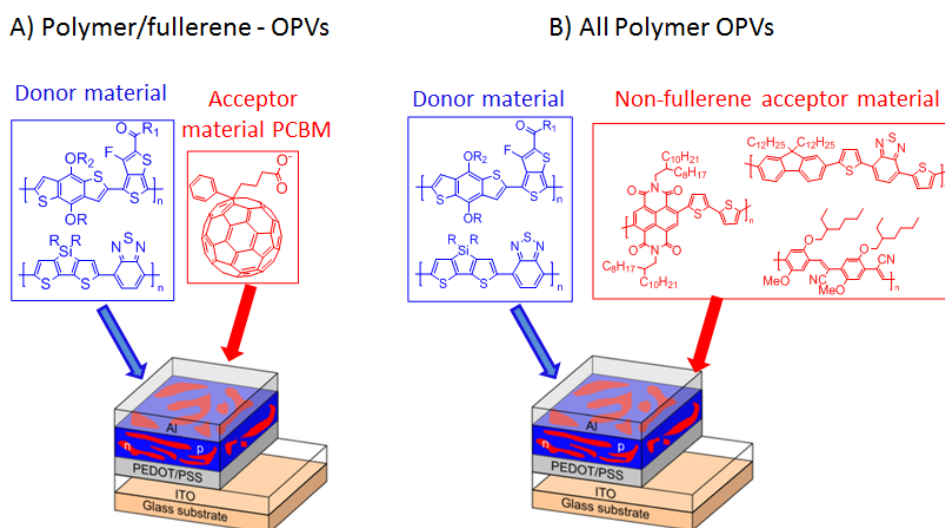


Figure 1.8: Device architecture of (A) polymer/fullerene organic photovoltaics (OPVs) and (B) all-polymer OPVs.

1.4.3 Design and Structural Organization of Polymeric Materials for Photovoltaic Device Architecture

1.4.3.1 D-A Copolymer as p-type Material

The most important characteristics for determining the optical and electrical properties of a conjugated polymer are the band gap and the HOMO-LUMO energy levels which in turn greatly influence the ultimate photovoltaic performance. The photovoltaic mechanism involves the

conversion of light energy to electrical energy in a device by absorbing sunlight by the photoactive materials. The wavelength of the maximum photon flux density of the solar spectrum is located at approximately 700 nm, which corresponds to a low energy of 1.77 eV.¹⁰⁸ The absorption spectrum of a conjugated polymer needs to cover both the red and near infrared ranges to exploit the endless source of solar energy and match the greater part of the solar spectrum. Hence it can harvest the maximum photon flux. It is highly desirable to develop conjugated polymers with broader absorption through narrowing their optical band gap. The low band gap conjugated polymers have been intensely studied by realizing the ultimate goal of developing organic conducting metals without the need of doping. The band gap can be reduced by either raising the HOMO or lowering the LUMO level of the polymer or by compressing the two levels closer together simultaneously. It has been demonstrated that the open-circuit voltage in BHJ photovoltaics with ohmic contacts is linearly dependent on the magnitude of the built-in potential, defined as the difference between the HOMO level of a p-type polymer and the LUMO level of an n-type material. The donor with the lower HOMO level will better reach the theoretically attainable open circuit voltage (V_{oc}), whereas reduction in a polymer's band gap to broaden the absorption coverage by lifting up the HOMO level will inevitably result in a loss of open circuit voltage. On the other hand, the LUMO level of p-type materials has to be at least 0.3 eV higher than that level of the n-type material to guarantee the formation of a downhill driving force for the energetically favorable electron transfer and overcome the binding energy of the intrachain exciton.¹⁰⁹⁻¹¹¹ Achieving a narrow band gap for conjugated polymer may result in the lowering of

LUMO level eventually being lower than that of the fullerene, thus hampering the efficient electron transfer. The effort to find new p-type polymers for polymer solar cells is not solely directed to pursuing low band gaps, but also to controlling the band gap by modulating the HOMO-LUMO levels to their optimal values.

Z. Zhang et al.¹¹² synthesized copolymers from benzodithiophene and benzotriazole units, namely, poly{4,8-bis(2-ethylhexyloxy)benzo[1,2-b;3,4-b]dithiophene-2,6-diyl-alt-2-octyl-4,7-di(thiophen-2-yl)-2*H*-benzo[d][1,2,3]triazole-5',5''-diyl} (PBDTDTBTz) and poly{4,8-bis(2-ethylhexyloxy)benzo[1,2-b;3,4-b]dithiophene-2,6-diyl-alt-2-dodecylbenzotriazole-4,7-diyl} (PBDTBTz), via Stille coupling polymerization method. Photovoltaic performance of the synthesized copolymers blended with PCBM as acceptor, were investigated. The photovoltaic device with the PBDTDTBTz/PC₇₁BM showed a power conversion efficiency of 1.7 %, while PBDTBTz gave a power conversion efficiency of 1.4 %, under illumination.

1.5 Nonlinear Optics

Nonlinear optics (NLO) is the branch of optics that describes the behavior of light in nonlinear media. More specifically, NLO includes the studies of the interaction of light with matter in which the response of the material system to the applied electromagnetic field is nonlinear in the amplitude of this field. At low intensity of light, typical of non-laser sources, the properties of materials remain independent of the intensity of illumination.¹¹³ The superposition principle holds true in this regime, and light waves can pass through materials or be reflected from boundaries and interfaces without interacting with each other. Laser sources, on the other

hand, can provide sufficiently high light intensities to modify the optical properties of materials. Light waves can then interact with each other, exchanging momentum and energy, and the superposition principle is no longer valid. This interaction of light waves can result in the generation of optical fields at new frequencies, including optical harmonics of incident radiation or sum- or difference-frequency signals.¹¹⁴

The physical origin of nonlinearities involving transition between discrete molecular states is the electric dipole interaction between the electrons in atoms and molecules and an electromagnetic field. The dielectric polarization P responds nonlinearly to the applied optical field. In an optical system, a nonlinear response can occur when there is sufficiently intense illumination. The nonlinearity is exhibited in the polarization ($\vec{\rho}$) of the material, which is often represented by a power series expansion of the total applied optical field (\vec{E}):

$$(\vec{\rho}) = \epsilon_0 (\chi^{(1)} \vec{E}_1 + \chi^{(2)} \vec{E}_2 + \chi^{(3)} \vec{E}_3 + \dots) \dots\dots\dots(1.1)$$

Here $\chi^{(1)}$ is the linear susceptibility representing the linear response (i.e. linear absorption and the refractive index) of the material. The two lowest order nonlinear responses are accounted for by the second and third order nonlinear susceptibilities $\chi^{(2)}$ and $\chi^{(3)}$.¹¹⁵

The nonlinearity may be of microscopic or macroscopic origin. The polarization density $P = N \rho$ is a product of the individual dipole moment ρ induced by the applied electric field and the number density of dipole moments N . The nonlinear behavior may reside either in ρ or in N (Figure 1.9).

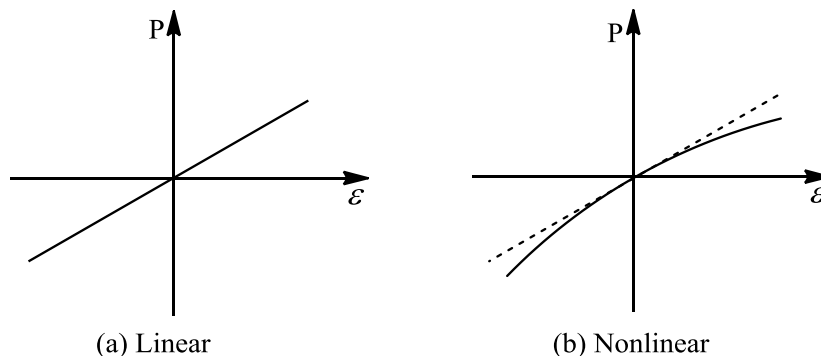


Figure 1.9: The P- ϵ relation for (a) a linear dielectric medium and (b) a nonlinear medium

The relation between P and ϵ is linear when ϵ is small, but becomes nonlinear when ϵ acquires values comparable to inter atomic electric fields, which are typically $\sim 10^5$ - 10^8 V/m. Figure 1.9 shows the linear and nonlinear behavior of light in a medium. The origin of a nonlinear response of an optical material to light is the dependence of the number density N on the optical field. If the external applied optical electric fields are typically small in comparison with characteristic interatomic or crystalline fields, even when focused laser light is used, the nonlinearity is usually weak.¹¹⁶

1.5.1 Nonlinear Absorption (NLA)

At high input optical intensities, there is an intensity-dependent change in a material's refractive index, which results in an intensity-dependent absorption change. Nonlinear refractive index and absorption changes play the key role in many important nonlinear phenomena such as optical switching or soliton generation.¹¹⁷ There is a possibility for a material to absorb more than one photon before relaxing to the ground state in the case of higher intensity of radiation. The nonlinear absorption is

arising from either direct multiphoton absorption, saturation of the single photon absorption, or free-carrier absorption in the case of solids.

1.5.1.1 Two Photon Absorption (TPA)

Two-photon absorption is the simultaneous absorption of two photons of identical or different frequencies in order to excite a molecule from the ground state to a higher energy state. The sum of the energies of the two photons is equal to the energy difference between the involved lower and upper states of the molecule. Two-photon absorption is a third-order process which is several orders of magnitude weaker than linear absorption at low light intensities. Figure 1.10 shows the schematic representation of two photon absorption process. The atomic transition rate due to TPA depends on the square of the light intensity, thus it is a nonlinear optical process, and can dominate over linear absorption at high intensities.¹¹⁸

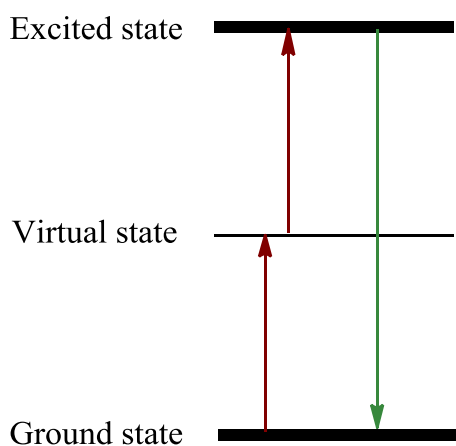


Figure 1.10: Energy scheme of a two photon excitation process

The nonlinear absorption is proportional to the intensity of incident light (I) and is given by equation (1.2)¹¹⁹

$$\frac{dI}{dZ} = -\alpha I - \beta I^2 \dots \dots \dots (1.2)$$

where α is the linear absorption coefficient and β is the two photon absorption coefficient.

1.5.1.2 Multiphoton Absorption

Multiphoton absorption means simultaneous absorption of a number (>2) of photons, accompanied by the transition of an absorbing molecule from a lower energy level to a higher level.¹²⁰ The absorption of (n+1) photons from a single beam is given by equation (1.3)

$$\frac{dI}{dZ} = -(\alpha + \gamma^{(n+1)} I^n) I \dots \dots \dots (1.3)$$

where $\gamma^{(n+1)}$ is the (n+1) photon absorption coefficient.

1.5.1.3 Saturable Absorption (SA)

Saturable absorption is a property of materials where the absorption of light decreases with increasing light intensity. Most materials show some saturable absorption only at very high optical intensities. When the absorption cross-section from excited state is smaller than that from ground state, molecules in the ground state of a material become excited into an upper energy state at such a rate that there is insufficient time for them to decay back to the ground state before the ground state becomes depleted, and the absorption subsequently saturates.¹²¹

1.5.1.4 Reverse Saturable Absorption (RSA)

Reverse saturable absorption is a class of nonlinear absorption in which the excited state absorption is large compared to the ground state absorption. It is known as reverse saturable absorption. At high incident laser energies, the nonlinear absorber gives large absorption and low incident laser energies results in lower absorption. The performance of such nonlinear optical materials can be limited by the accompanying linear absorption at low input energy. However, transparency is at low input energy, but higher absorption at high input energy can be achieved with multi-photon absorbers (MPA) in which two or more photons are absorbed simultaneously.¹²¹

1.5.1.5 Free Carrier Absorption (FCA)

In semiconductors, if the absorbed photon has energy greater than the band gap, the electron will be promoted to the conduction band and it acts as a free carrier. The free carrier generated will contribute to current flow when a field is applied. The excited electron will rapidly relax to the bottom of the conduction band, where it will recombine with an excited hole in the valence band after a characteristic recombination time. However, while retaining in the conduction band, it can absorb another photon if the intensity is sufficiently high. This process is called free carrier absorption.¹²¹

1.5.2 Optical Power Limiting

With the extensive use of high power laser in various applications, much interest is currently being directed towards the search for new nonlinear optical materials for passive optical limiters which are used to protect human eyes and solid state optical sensors from intense laser

beams.¹²² Optical limiter exhibits linear transmittance at low powers, but it becomes slightly opaque at high incident intensities. Optical limiting effect results from intensity dependent optical nonlinear processes like (a) nonlinear absorption (NLA), (b) nonlinear scattering (NLS), (c) nonlinear refraction (NLR) (d) optically induced phase transitions and (e) photo refraction (PR).¹²³ An optical limiter is a device designed to keep the power, irradiance, energy or fluence transmitted by an optical system below some specified maximum value regardless of the magnitude of the input which maintains a high transmittance at low input powers.

The minimum criteria identified for a material to act as an effective optical limiter are,¹²⁴

- Having a high linear transmittance
- A fast response time (e.g. picoseconds or faster)
- A low limiting threshold (the input corresponding to the break point in the curve).
- Low optical scattering
- A broad band response (e.g. the entire visible spectrum)

1.5.3 Nonlinear Refraction (NLR)

Nonlinear refraction is the change in spatial distribution of the refractive index of a medium when a material is exposed to electromagnetic radiation of suitable frequency. The nonlinear refraction property of a material could be due to Raman induced Kerr effect, electronic polarization, molecular orientation effects, thermal contributions, and photorefractive

effects. The nonlinear refraction property of a material can be utilized for various applications like optical switching, optical data processing, optical logic gates and passive laser mode-locking. The relation between nonlinear refraction and intensity of illumination is given by equation (1.4),¹²⁵

$$n = n_0 + n_2 I \dots\dots\dots(1.4)$$

where ‘ n_0 ’ is the linear refractive index and ‘ n_2 ’ is nonlinear refraction coefficient. Several physical mechanisms like molecular orientational effect, Raman induced Kerr effect, electronic polarization etc. contribute to the nonlinear refraction property of a material.¹¹⁹

1.5.4 Z-scan Technique for NLO Characterization

In 1989, Sheik Bahae developed Z-scan single beam technique for measuring the magnitude of nonlinear absorption as well as sign and magnitude of nonlinear refraction.^{126,127} This technique offers simplicity and high sensitivity when compared to other methods. Z-scan is based on the principle of spatial beam distortion. When a laser beam of high intensity propagates through a nonlinear material, the variation in photo-induced refractive index may lead to self-focusing of the beam. The propagation and self-refraction can be studied using this technique. The third order nonlinear optical properties of solids, liquids and liquid crystals can be studied by this method.

The experimental setup for single beam z-scan is given in Figure 1.11. In this set up, if the transmitted light is measured through a finite aperture placed in the far field as the sample is moved in z-direction, then it is referred to as closed aperture (CA) Z-scan technique. However, if the

transmitted light is measured without an aperture, then it is referred to as open aperture (OA) Z-scan technique. Here the output is sensitive only to non-linear absorption of a material. Closed aperture and open aperture z-scan methods yield the real and imaginary parts of nonlinear susceptibility, respectively.^{125,126}

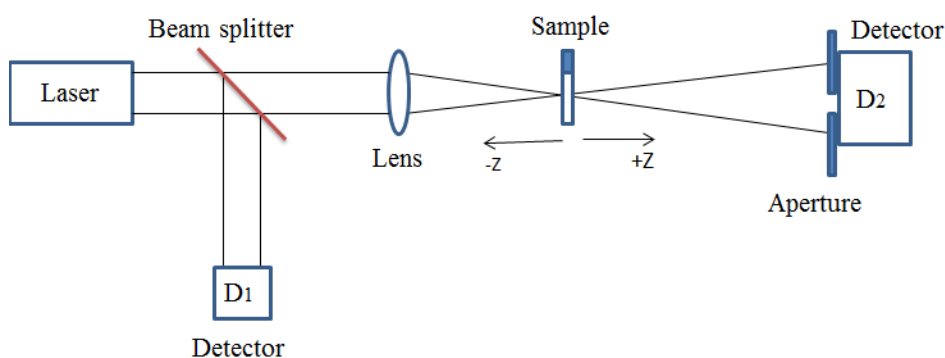


Figure 1.11: Schematic representation of the experimental setup for Z-scan technique.

1.5.4.1 Open Aperture (OA) Z-scan

In open aperture Z-scan, the detector is sensitive only to intensity variations of the transmitted light and not the phase variations of the light. Open aperture Z-scan is used to measure the nonlinear absorption of the medium. If the sample has two photon absorption (TPA), the measure of transmitted light will be minimum at the focal point.¹²⁶ On the other hand, transmission maximum will be obtained at focal point if the sample is a saturable absorber. S. Narayanan et al.¹²⁷ investigated the third order nonlinear optical properties of copolymer, poly(2,5-(3,4-ethylenedioxythiophene)-alt-2,7-(9,9-dioctylfluorene)) by Z-scan technique. The open aperture Z-scan traces of the polymers gave a reverse saturable absorption graph with a positive

nonlinear absorption coefficient. The study showed that the nonlinear absorption fitted well with the theoretical fit derived from two photon absorption (TPA). The third-order nonlinear optical properties of 3,4-ethylenedioxythiophene-quinoxaline copolymers were also reported by S. Narayanan et al.¹²⁸ The open aperture Z-scan traces showed that the copolymers exhibited reverse saturable absorption with positive nonlinear absorption. The theoretical fitting confirmed that two photon absorption (TPA) could be the process involved in the optical absorption.

1.5.4.2 Closed Aperture (CA) Z-scan

Apart from the open aperture technique, closed aperture Z-scan is based on the self-refraction and self-phase modulation effects. The high intense light is allowed to pass through an aperture and the transmitted light is measured as a function of the sample position Z with respect to the focal plane using a single Gaussian beam. In closed aperture z-scan technique, the medium behaves like thin lens of variable focal length due to change in refractive index at each position ($n = n_0 + n_2I$).¹¹⁹ The beam irradiance enhances when the material with negative non-linear refractive index is brought closer to focus. This enhancement leads to self-lensing in the sample. A negative self-lensing prior to focus will tend to collimate the beam, which will result in beam narrowing at the aperture which causes an increase in transmission (peak). As the sample passes the focal plane to the right in z direction, the same self-defocusing enhances the beam divergence causing a beam broadening at the aperture, leads to a decreased transmission (valley). A peak in the transmittance curve followed by valley in the transmittance curve reveals the negative non-linearity of a material.

Whereas, valley-peak configuration represents positive nonlinear refraction of the medium.¹²⁶ In order to determine the sign and magnitude of nonlinear refraction property of copolymer, poly(2,5-(3,4-ethylenedioxythiophene)-alt-2,7-(9,9-dioctylfluorene)), closed aperture Z-scan technique was performed.¹²⁷ The closed aperture trace of the polymer showed peak-valley characteristics which indicated the negative nonlinear refractive index due to self-defocusing. S. Narayanan et al.¹²⁸ reported the nonlinear refractive indices of 3,4-ethylenedioxythiophene-quinoxaline copolymers by closed aperture Z-scan studies. The copolymers showed negative nonlinear refraction coefficient and peak-valley traces because of the self-defocusing behavior.

1.6 Scope of the Thesis

- Designing of novel conjugated polymers whose band gap lies in the semiconducting range using Density Functional Theory in the Periodic Boundary Condition (PBC) formalism.
- Synthesis of Conjugated polymers by adopting appropriate synthetic Procedures.
- Explore the application of the synthesized conjugated polymers as active layer in the heterojunction photovoltaic devices using ZnO and LiF as the electron transport materials and MoO₃ and PEDOT: PSS as hole transport layers.
- Explore the application of conjugated polymers in nonlinear optical devices.

References

- [1] J. Roncali, *Chem. Rev.* 1997, **97**, 173.
- [2] H. A. M. van Mullekom, J. A. J. M. Vekemans, E. E. Havinga, E. W. Meijer, *Mater. Sci. Eng.*, 2001, **32**, 1.
- [3] N. Matsumi, Y. Chujo, *Polym. J.*, 2008, **40**, 77.
- [4] E. Bundgaard, F. C. Krebs, *Sol. Energy Mater. Sol. Cells.*, 2007, **91**, 954.
- [5] F. Zhang, W. Mammo, L. M. Andersson, S. Admassie, M. R. Andersson, O. Inganäs, *Adv. Mater.*, 2006, **18**, 2169.
- [6] C. Soci, I.-W. Hwang, D. Moses, Z. Zhu, D. Waller, R. Gaudiana, C. J. Brabec, A. J. Heeger, *Adv. Funct. Mater.*, 2007, **17**, 632.
- [7] W. Y. Lee, C. W. Chen, C. C. Chueh, C. C. Yang, W. C. Chen, *Polym. J.*, 2008, **40**, 249.
- [8] W. C. Wu, W. Y. Lee, W. C. Chen, *Macromol. Chem. Phys.*, 2006, **207**, 1131.
- [9] A. P. Kulkarni, Y. Zhu, S. A. Jenekhe, *Macromolecules.*, 2005, **38**, 1553.
- [10] F. Fusalba, H. A. Ho, L. Breau, D. Belanger, *Chem. Mater.*, 2000, **12**, 2581.
- [11] S. Gunes, H. Neugebauer, N.S. Sariciftci, *Chem. Rev.*, 2007, **107**, 1324.
- [12] G. Dennler, M. C. Scharber, C. J. Brabec. *Adv. Mater.*, 2009, **21**, 1323.
- [13] B. C. Thompson, , J. M. J. Fréchet, *Angew. Chem. Int. Ed.*, 2008, **47**, 58.
- [14] H. Zhou, L. Yang, W. You, *Macromolecules*, 2012, **45**, 607.
- [15] L. M. Chen, Z. Hong, G. Li, Y. Yang., *Adv. Mater.* 2009, **21**, 1434.
- [16] A. Facchetti, *Chem. Mater.*, 2011, **23**, 733.
- [17] D. M. de Leeuw, E. Cantatore, *Mat. Sci. Semicond. Process*, 2008, **11**, 199.
- [18] S. C. Rasmussen, K. Ogawa, S. D Rothstein: *Handbook of Organic Electronics and Photonics*, American Scientific Publishers: Stevenson Ranch, CA, 2008.
- [19] K. J. Allen, *Proc. IEEE.*, 2005, **93**, 1394.

- [20] S. C. Rasmussen, M. Pomerantz, "Low Band gap Conducting Polymers," in *Conjugated Polymers: Theory, Synthesis, Properties, and Characterization*, T. A. Skotheim and J. R. Reynolds, Eds.; Handbook of Conducting Polymers, 3rd Ed., CRC Press: Boca Raton, FL, 2007.
- [21] J. L. Brédas, *J. Chem. Phys.*, 1985, **82**, 3808.
- [22] J. L. Brédas: *Aromatic Polymers: Electronic Properties of Polymers and Related Compounds*, Springer Series in Solid-State Sciences, Springer-Verlag: Berlin, 1985.
- [23] G. R. Hutchison, Y. J. Zhao, B. Delley, A. J. Freeman, M. A. Ratner, T. J. Marks, *Phys. Rev. B.*, 2003, **68**, 35204.
- [24] V. Hernandez, C. Castiglioni, M. Del Zoppo, G. Zerbi, *Phys. Rev. B.*, 1994., **50**, 9815.
- [25] E. E. Havinga, W. ten Hoeve, H. Wynberg, *Synth. Met.* 1993, **55**, 299.
- [26] E. E. Havinga, W. Hoeve, H. Wynberg, *Polym. Bull.* 1992, **29**, 119.
- [27] G. Öktem, A. Balan, D. Baran, L. Toppare, *Chem. Commun.*, 2011, **47**, 3933.
- [28] A. W. Hains, Z. Liang, M. A. Woodhouse, B. A. Gregg, *Chem. Rev.*, 2010, **110**, 6689.
- [29] C. Shen, Y. Rubin, F. Wudl, *Angew. Chem. Int. Ed.*, 2004, **116**, 1524.
- [30] F. Wudl, M. Kobayashi, A. J. Heeger, *J. Org. Chem.*, 1984, **49**, 3382.
- [31] a) M. Pomerantz, B. Chaloner-Gill, L. O. Harding, J. J. Tseng, W. J. Pomerantz, *J. Chem. Soc. Chem. Commun.*, 1992, 1672.
b) M. Pomerantz, X. Gu, *Synth. Met.*, 1997, **84**, 243.
- [32] L. Cuff, M. Kertesz, *Synth. Met.*, 1993, **55**, 960.
- [33] H. Brisset, G. C. Thobie, A. Gorgues, M. Jubault, J. Roncali, *J. Chem. Soc., Chem. Commun.* 1994, **11**, 1305.
- [34] C. Kitamura, S. Tanaka, Y. Yamashita, *Chem. Mater.*, 1996, **8**, 570.
- [35] G. Brocks, A. Tol, *J. Phys. Chem.*, 1996, **100**, 1838.

- [36] D. Young: Computational Chemistry: A Practical Guide for Applying Techniques to Real World Problems, John Wiley & Sons, USA, 2001.
- [37] F. Jensen, Introduction to Computational Chemistry, 2nd ed.; John Wiley & Sons, inc: England, 2007.
- [38] J. B. Foresman, A. Frisch, Exploring Chemistry with Electronic Structure Methods, 2nd ed., Gaussian, Pittsburgh, PA, 1996.
- [39] C. Lee, W. Yang, R. G. Parr, *Phys. Rev. B.*, 1988, **37**, 785.
- [40] K. Burke, J. P. Perdew, Y. Wang, J. F. Dobson, G. Vignale, M. P. Das, (Eds.), Electronic Density Functional Theory: Recent Progress and New Directions, Plenum Press, New York, 1998.
- [41] S. S. Zade, N. Zamoshchik, M. Bendikov, *Acc. Chem. Res.*, 2011, **37**, 785
- [42] L. Zhang, Q. Zhang, H. Ren, H. Yan, J. Zhang, H. Zhang, J. Gu, *Sol. Energ. Mat. Sol. Cells.*, 2008, **92**, 581.
- [43] C. S. Ra, S. Yim, G. Park, *Bull. Korean Chem. Soc.*, 2008, **29**, 891.
- [44] U. Salzner, J. B. Lagowski, P. G. Pickup, R. A. Poirier, *Synth. Met.*, 1998, **96**, 177.
- [45] M. J. Frisch, G. W. Trucks, H. B. Schlegel, G. E. Scuseria, M. A. Robb, J. R. Cheeseman, J. A.; Montgomery, T. Vreven, K. N. Kudin, J. C. Burant, Millam, J. S. Iyengar, J. Tomasi, V. Barone, B. Mennucci, M. Cossi, G. Scalmani, N. Rega, G. A. Petersson, H. Nakatsuji, M. Hada, M. Ehara, K. Toyota, R. Fukuda, J. Hasegawa, M. Ishida, T. Nakajima, Y. Honda, O. Kitao, H. Nakai, M. Klene, X. Li, J. E. Knox, H. P. Hratchian, J. B. Cross, V. Bakken, C. Adamo, J. Jaramillo, R. Gomperts, R. E. Stratmann, O. Yazyev, A. J. Austin, R. Cammi, C. Pomelli, J. W. Ochterski, P. Y. Ayala, K. Morokuma, G. A. Voth, Salvador, J. J. Dannenberg, V. G. Zakrzewski, S. Dapprich, A. D. Daniels, M. C. Strain, O. Farkas, D. K. Malick, A. D. Rabuck, K. Raghavachari, J. B. Foresman, J. V. Ortiz, Cui, A. G. Baboul, S. Clifford, J. Cioslowski, B. B. Stefanov, G. Liu, A. Liashenko, P. Piskorz, I. Komaromi, R. L. Martin, D. J. Fox, T. Keith, M. A. Al-Laham, C. Y. Peng, A. Nanayakkara, M. Challacombe, P. M. W. Gill, B. Johnson, W. Chen, M. W. Wong, C. Gonzalez, J. A. Pople, Gaussian, Inc., 2004.

- [46] M. J. Frisch, G. W. Trucks, H. B. Schlegel, G. E. Scuseria, M. A. Robb, J. R. Cheeseman, G. Scalmani, V. Barone, B. Mennucci, G. A. Petersson, H. Nakatsuji, M. Caricato, X. Li, H. P. Hratchian, A. F. Izmaylov, J. Bloino, G. Zheng, J. L. Sonnenberg, M. Hada, M. Ehara, K. Toyota, R. Fukuda, J. Hasegawa, M. Ishida, T. Nakajima, Y. Honda, O. Kitao, H. Nakai, T. Vreven, J. A. Montgomery, J. E. Peralta, F. Ogliaro, M. Bearpark, J. J. Heyd, E. Brothers, K. N. Kudin, V. N. Staroverov, R. Kobayashi, J. Normand, K. Raghavachari, A. Rendell, J. C. Burant, S. S. Iyengar, J. Tomasi, M. Cossi, N. Rega, N. J. Millam, M. Klene, J. E. Knox, J. B. Cross, V. Bakken, C. Adamo, J. Jaramillo, R. Gomperts, R. E. Stratmann, O. Yazyev, A. J. Austin, R. Cammi, C. Pomelli, J. W. Ochterski, R. L. Martin, K. Morokuma, V. G. Zakrzewski, G. A. Voth, P. Salvador, J. J. Dannenberg, S. Dapprich, A. D. Daniels, Ö. Farkas, J. B. Foresman, J. V. Ortiz, J. Cioslowski, Fox, D. J. Gaussian, Inc., Wallingford CT, 2009.
- [47] K. N. Kudin, G. E. Scuseria, *Phys. Rev. B.*, 2000, **61**, 16440.
- [48] Pisani, C. Ed. *Lecture Notes in Chemistry*, Springer-Verlag, Heidelberg, 1996,
- [49] S. S. Zade, M. Bendikov, *Org. Lett.*, 2006, **8**, 5243.
- [50] B. M. Wong, J. G. Cordaro, *J. Phys. Chem. C*, 2011, **115**, 18333.
- [51] J. Heyd, G. E. Scuseria, M. J. Ernzerhof, *J. Chem. Phys.*, 2003, **118**, 8207.
- [52] N. Toshima, S. Hara, *Prog. Polym. Sci.*, 1995, **20**, 155.
- [53] S. Sadki, P. Schottland, N. Brodie, G. Sabouraud, *Chem. Soc. Rev.*, 2000, **29**, 283.
- [54] G. A. Sotzing, J. R. Reynolds, P. J. Steel, *Adv Mater.*, 2004, **9**, 795.
- [55] R. J. Waltman, J. Bargon, *Can. J. Chem.*, 1986, **64**, 76.
- [56] Y. J. Cheng, T. Y. Luh, *J. Organomet. Chem.*, 2004, **689**, 4137.
- [57] (a) N. Miyaura, K. Yamada, A. Suzuki, *Tetrahedron Lett.*, 1979, **20**, 3437.
(b) N. Miyaura, A. Suzuki, *J. Chem. Soc., Chem. Commun.*, 1979, 866.
(c) A. Suzuki, *J. Organomet. Chem.*, 1999, **576**, 147. (d) N. Miyaura, T. Yanagi, A. Suzuki, *Synth. Commun.*, 1981, **11**, 513.

- [58] (a) E. Negishi, A. O. King, N. Okukado, *J. Org. Chem.*, 1977, **42**, 1821.
(b) A. O. King, N. Okukado, E. I. Negishi, *J. Chem. Soc.-Chem. Commun.*, 1977, 683. (c) E. I. Negishi, *Acc. Chem. Res.*, 1982, **15**, 340.
- [59] (a) T. Mizoroki, K. Mori, A. Ozaki, *Bull. Chem. Soc. Jpn.*, 1971, **44**, 58.
(b) R. F. Heck, J. P. Nolley, *J. Org. Chem.*, 1972, **37**, 2320.
- [60] K. Sonogashira, *J. Organomet. Chem.*, 2002, **653**, 46.
- [61] D. Milstein, J. K. Stille, *J. Am. Chem. Soc.*, 1978, **100**, 3636.
- [62] K. Tamao, K. Sumitani, M. Kumada, *J. Am. Chem. Soc.*, 1972, **94**, 4374.
- [63] L. Gregory, L. Gibson, T. M. McCormick, D. S. Seferos, *J. Am. Chem. Soc.*, 2012, **134**, 539
- [64] S. J. Chen, Q. Y. Zhang, J. W. Gu, M. L. Ma, L. Zhang, J. Zhou, Y. Y. Zhou, *Polymer Letters*, 2012, **6**, 454.
- [65] L. Huo, C. He, M. Han, E. Zhou, Y. Li, *J. Polym. Sci. Part A: Poly. Chem.*, 2007, **45**, 3861.
- [66] Y. Liang, J. Xie Li, *J. Org. Chem.*, 2006, **71**, 379.
- [67] K. D. Demir, B. Kiskan, Y. Yagci., *Macromolecules*. 2011, **44**, 1801.
- [68] W. H. Lee, S. K. Lee, W. S. Shin, S. J. Moon, M. J. Park, S. H. Lee, *Sol. Energ. Mat. Sol. Cells.*, 2014, **122**, 190.
- [69] M. M. Wienk, M. Turbiez, J. Gilot, R. A. Janssen, *J. Adv. Mater.*, 2008, **20**, 2556.
- [70] M. M. Wienk, M. G. R. Turbiez, M. P. Struijk, M. Fonrodona, R. A. J. Janssen, *Appl. Phys. Lett.*, 2006, **88**, 153511.
- [71] C. F. Neef, J. P. Ferraris, *Macromolecules*, 2000, **33**, 2311.
- [72] Z. Tan, R. Tang, E. Zhou, Y. He, C. Yang, F. Xi, Y. Li, *J. Appl. Polym. Sci.*, 2008, **107**, 514.
- [73] M. Granstrom, K. Petritsch, A. C. Arias, A. Lux, M. R. Andersson, R. H. Friend, *Nature*, 1998, **395**, 257.
- [74] A. Kumar, A. Kumar, *Polym. Chem.*, 2010, **1**, 286.

- [75] B. W. Boudouris, C. D. Frisbie, M. C. Hillmyer, *Macromolecules*, 2008, **41**, 67.
- [76] C. W. Tang, *Appl. Phys. Lett.*, 1986, **48**, 183.
- [77] J. J. M. Halls, K. Pichler, R. H. Friend, S. C. Moratti, A. B. Holmes, *Appl. Phys. Lett.* 1996, **68**, 3120.
- [78] M. Theander, A. Yartsev, D. Zigmantas, M. V. Sundstro, W. Mammo, M. R. Andersson, S. O. Ingana, *Phys. Rev. B.*, 2000, **61**, 12957.
- [79] A. Haugeneder, M. Neges, C. Kallinger, W. Spirkl, U. Lemmer, J. Feldmann, U. Scherf, E. Harth, A. Gu gel, K. Mullen, *Phys. Rev. B.*, 1999, **59**, 15346.
- [80] T. Stubinger, W. Brutting, *J. Appl. Phys.*, 2001, **90**, 3632.
- [81] D. E. Markov, E. Amsterdam, P. W. M. Blom, A. B. Sieval, J. C. Hummelen, *J. Phys. Chem. A.*, 2005, **109**, 5266.
- [82] G. Yu, J. Gao, J. C. Hummelen, F. Wudl, A. J. Heeger, *Science*, 1995, **270**, 1789.
- [83] N. S. Sariciftci, L. Smilowitz, A. J. Heeger, F. Wudl, *Science*, 1992, **258**, 1474.
- [84] J. You, L. Dou, K. Yoshimura, T. Kato, K. Ohya, T. Moriarty, K. Emery, C. C. Chen, J. Gao, G. Li, *Nat. Commun.*, 2013, **4**, 1446.
- [85] R. Miyakoshi, A. Yokoyama, T. Yokozawa, *J. Am. Chem. Soc.*, 2005, **127**, 17542.
- [86] M. C. Iovu, E. E. Sheina, R. R. Gil, R. D. McCullough, *Macromolecules*, 2005, **38**, 8649.
- [87] R. S. Loewe, S. M. Khersonsky, R. D. McCullough, *Adv. Mater.*, 1999, **11**, 250.
- [88] R. S. Loewe, P. C. Ewbank, J. Liu, L. Zhai, R. D. McCullough, *Macromolecules*, 2001, **34**, 4324.
- [89] I. Osaka, R. D. McCullough, *Acc. Chem. Res.*, 2008, **41**, 1202.
- [90] B. W. Boudouris, C. D. Frisbie, M. C. Hillmyer, *Macromolecules*, 2008, **41**, 67.
- [91] B. W. Boudouris, F. Molins, D. A. Blank, C. D. Frisbie, M. A. Hillmyer, *Macromolecules*, 2009, **42**, 4118.

- [92] K. Ohshimizu, M. Ueda, *Macromolecules*, 2008, **41**, 5289.
- [93] P. T. Wu, G. Ren, F. S. Kim, C. Li, R. Mezzenga, S. A. Jenekhe, *J. Polym. Sci., Part. A: Polym. Chem.*, 2010, **48**, 614.
- [94] P. T. Wu, G. Ren, C. Li, R. Mezzenga, S. A. Jenekhe, *Macromolecules*, 2009, **42**, 2317.
- [95] P. T. Wu, G. Ren, S. A. Jenekhe, *Macromolecules*, 2010, **43**, 3306.
- [96] J. H. Tsai, Y. C. Lai, T. Higashihara, C. J. Lin, M. Ueda, W. C. Chen, *Macromolecules*, 2010, **43**, 6085.
- [97] M. J. Robb, S. Y. Ku, G. J. Hawker, *Adv. Mater.*, 2013, **25**, 5686.
- [98] J. Wang, T. Higashihara, *Polym. Chem.*, 2013, **4**, 5518.
- [99] U. Scherf, A. Gutacker, N. Koenen, *Acc. Chem. Res.*, 2008, **41**, 1086.
- [100] A. Yassar, L. Miozzo, R. Girona, G. Horowitz, *Prog. Polym. Sci.*, 2013, **38**, 791.
- [101] X. Guo, M. Baumgarten, K. Müllen, *Prog. Polym. Sci.*, 2013, **38**, 1832.
- [102] S. H. Park, A. Roy, S. Beaupre, S. Cho, N. Coates, J. S. Moon, D. Moses, M. Leclerc, K. Lee, A. Heeger, *Nature Photonics*, 2009, **3**, 297.
- [103] Y. Liang, Z. Xu, J. Xia, S. T. Tsai, Y. Wu, G. Li, C. Ray, L. Yu, *Adv. Mater.*, 2010, **22**, 35.
- [104] A. Facchetti, *Mater. Today*, 2013, **16**, 123.
- [105] K. Nakabayashi, H. Mori, *Materials*, 2014, **7**, 3274.
- [106] Y. Zhou, T. Kurosawa, W. Ma, Y. Guo, L. Fang, K. Vandewal, Y. Diao, C. Wang, Q. Yan, J. Reinspach, J. Mei, A. L. Appleton, G. I. Koleilat, Y. Cao, S. C. B. Mannsfeld, A. Salleo, H. Ade, D. Zhao, Z. Bao, *Adv. Mater.*, 2014, **26**, 3767.
- [107] Z. Li, X. Xu, W. Zhang, X. Meng, W. Ma, A. Yartsev, O. Inganas, M. R. Andersson, R. A. J. Janssen, E. Wang, *J. Am. Chem. Soc.*, 2016, **138**, 10935.
- [108] C. Gueymard, *Solar Energy*, 2004, **76**, 423.

- [109] C. J. Brabec, C. Winder, N. S. Sariciftic, J. C. Hummelen, A. Dhanabalan, P. A. van Hal, R. A. J. Janssen, *Adv. Funct. Mater.*, 2002, **12**, 709.
- [110] J. J. M. Halls, J. Cornil, D. A. dos Santos, R. Silbey, D. H. Hwang, A. B. Holmes, J. L. Bredas, R. H. Friend, *Phys. Rev. B.*, 1999, **60**, 5721.
- [111] L. J. A. Koster, V. D. Mihailetschi, P. W. M. Blom, *Appl. Phys. Lett.*, 2006, **88**, 093511.
- [112] Z. Zhang, B. Peng, B. Liu, C. Pan, Y. Li, Y. He, K. Zhou, Y. Zou, *Polym. Chem.*, 2010, **1**, 1441.
- [113] Y. R. Shen: *The Principles of Nonlinear Optics*, Wiley, New York, 1984.
- [114] K. Rottwitt, P. T. Lichtenb, *Nonlinear Optics: Principles and Applications*, CRC Press, New York, 2014.
- [115] M. Bass, E. W. van Stryland, J. M. Enoch, W. L. Wolfe, *Handbook of Optics*, Vol. IV, Chapter. 17, McGraw Hill Professional, 2000.
- [116] E. A. S. Bahaa, M. C. Teich, *Nonlinear Optics*, Wiley, New York, 2001.
- [117] N. Demetrios, Christodoulides, I. C. Khoo, J. Gregory, Salamo, I. George, Stegeman, W. Eric, V. Stryland, *Adv. Opt. Photonics.*, 2010, **2**, 60.
- [118] Nikolai V. Tkachenko, *Optical Spectroscopy: Methods and Instrumentations*. Elsevier, 2006.
- [119] Richard. L. Sutherland, *Handbook of Nonlinear Optics*, CRC press, 2003.
- [120] S. H. Guang, L. S. Tan, Q. Zheng, P. N. Prasad, *Chem. Rev.*, 2008, **108**, 1245.
- [121] Litty Irimpan, *Spectral and nonlinear optical characterization of ZnO Nanocomposites*, Ph.D Thesis, Cochin University of Science and Technology, 2008
- [122] C. Zhang, Y. L. Song, Y. Xu, H. K. Fun, G. Y. Fang, Y. X. Wang, X. Q. Xin, *J. Chem. Soc., Dalton Trans.*, 2823, 2000.
- [123] J. A. Herman, J. Staromlynska, *Int. J. Nonlinear Opt. Phy.* 2, **271**, 1993.
- [124] R. Tong, H. Wuc, B. Lia, R. Zhua, G. Youa, S. H. Qian, *Physica B Condens. Matter*, 2005, **366**, 192.

- [125] M. S. Bahae, A. A. Said, E. W. Van Stryland, *Opt. Lett.*, 1989, **14**, 955.
- [126] M. S. Bahae, A. A. Said, T. H. Wei, D. J. Hagan, E. W. Van Stryland, *IEEE J. Quant. Electron.*, 1990, **26**, 760.
- [127] S. Narayanan, A. Abbas, S. P. Raghunathan, K. Sreekumar, C. S. Kartha, R. Joseph, *RSC Adv.*, 2015, **5**, 8657.
- [128] S. Narayanan, S. P. Raghunathan, S. Mathew, M. V. Mahesh Kumar, A. Abbas, K. Sreekumar, C. S. Kartha, R. Joseph, *Eur. Polym J.*, 2015, **64**, 157.

.....❧.....

**SYNTHESIS AND CHARACTERIZATION OF
MONOMERS**

- 2.1 *Introduction*
- 2.2 *Results and Discussion*
- 2.3 *Experimental Procedure*
- 2.4 *Conclusion*

The optoelectronic properties of conjugated polymeric materials can be utilized for the fabrication of organic electronic and photonic devices. When key structural requirements are met, these materials exhibit unique properties such as solution processability, large charge transporting capabilities, broad optical absorption etc. Herein, the synthesis and characterization of monomers which are used for preparing the desired conjugated polymers are reported. Detailed description of experimental procedures are presented.

2.1 Introduction

The development of bulk heterojunction polymer solar cells (PSCs) has become an interesting area of research because of the high manufacturing cost of inorganic material based solar cells.^{1,2} Researchers have focused on the synthesis of new photovoltaic conjugated polymers and the development of device fabrication technologies based on low cost, light weight, easily processable organic semiconductors.³ Conjugated polymers with low band gaps, suitable energy levels and high charge carrier mobility are responsible

for the performance of PSCs.⁴⁻⁶ For device applications, it is important to control the electronic band structure of the polymer to achieve a band gap of the desired magnitude and frontier orbitals, HOMO (highest occupied molecular orbital) and LUMO (lowest unoccupied molecular orbital), of proper energies.⁷ The band gap can be tuned by introducing suitable donor and acceptor moieties or introducing linker units. The combination of high-lying HOMO levels (residing on the donor units) and low-lying LUMO levels (residing on the acceptor units) result in an overall low band gap for the polymer. The band gap can be narrowed or widened on the basis of the choice of donor and acceptor units, or more specifically, the difference in electron density between the donor and acceptor units along the polymer backbone.⁸ Another strategy is the introduction of electron-withdrawing groups in particular positions in the conjugated polymer chain.^{9,10} Organic materials with a large absorption range (low band gap) can be synthesized which can harvest photons at longer wavelength and improve the efficiency of organic photovoltaic devices, due to a better overlap of the absorption spectrum and the solar spectrum.

One advantage of utilizing conjugated polymers for technological applications is the ability to tune the material properties at the molecular level. This is typically accomplished through synthetic modification of the monomeric units or the combination of dissimilar units to make copolymeric systems.¹¹ Donor-acceptor (D-A) conjugated polymers are promising candidates for high mobility polymeric semiconductors.¹²⁻¹⁸ M. He et al. have developed polycyclic aromatic unit comprising six rings, (5,11-bis(2-octyldodecyl) dithieno[3,2-b:3',2'-b']naphtho-[1,2-b:5,6-b']dithiophene) (DTNDT). Four donor-acceptor (D-A) conjugated polymers, which are named P-BT, P-2FBT,

P-IID, and P-DPP, were synthesized with DTNDDT as the donor unit and 2,1,3-benzothiadiazole (BT), 5,6-difluorobenzo[*c*][1,2,5]thiadiazole (2FBT), isoindigo (IID), and diketopyrrolopyrrole (DPP) as the acceptor unit, respectively.

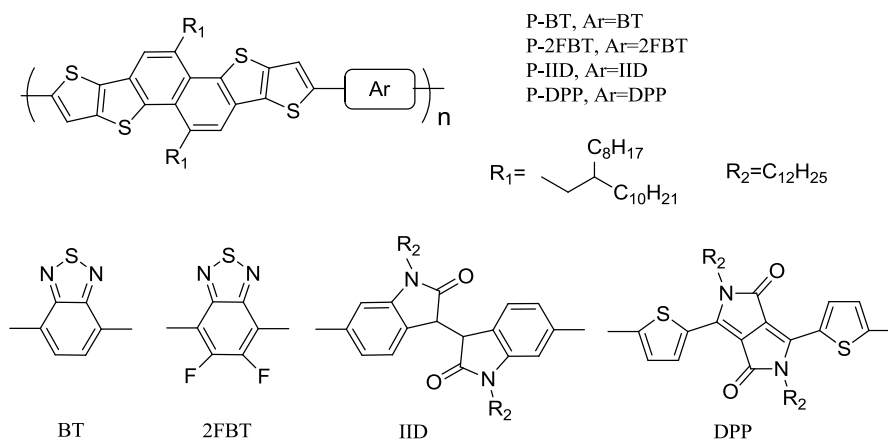


Figure 2.1: Chemical Structures of D–A Conjugated Polymers, P-BT, P-2FBT, P-IID, and P-DPP

The semiconducting properties of the polymers were characterized with bottom gate and top contact (BGTC) organic thin film transistors (OTFTs). All four polymers showed p-type transport behavior, and the hole mobilities were 0.023, 0.078, 0.50, and 1.80 $\text{cm}^2/(\text{V s})$ for P-BT, P-2FBT, P-IID, and P-DPP, respectively.¹⁹ The study indicated that DTNDDT is a promising building block for high performance polymeric semiconductors.

A. Zhang et al.²⁰ investigated the influence of chemical structures on the microstructure of the conjugated polymers and hence affecting their performance in organic field effect transistors (OFETs). It has been widely reported that, by using the coplanar conjugated backbone^{21,22} and the flexible side chains by introducing van der Waals interactions,²³ conjugated polymers can exhibit good crystal properties. Many reports show that

conjugated polymers containing fluorine atoms show enhanced crystallinity with “edge-on” orientation, resulting in high mobilities in OFETs compared to the nonfluorinated polymers (Figure 2.2). In this study, fluorinated DPP polymers provided hole mobilities below $1.80 \text{ cm}^2 \text{ V}^{-1} \text{ s}^{-1}$ (Figure 2.2 B), while nonfluorinated DPP polymers exhibited high hole mobilities up to $11.16 \text{ cm}^2 \text{ V}^{-1} \text{ s}^{-1}$ (Figure 2.2 A), which is also among the highest reported hole mobilities. Less crystallinity and enhanced “face-on” orientation of the polymers are responsible for the poor hole mobilities in FET devices. These results help to understand the relation between chemical structure and charge transport properties, which can be used to design new conjugated polymers towards high performance OFETs.²⁰ Functionalization of conjugated polymers with conjugated side chains includes introducing spacer group between the polymer backbone and side chain. This may influence the electronic properties of the polymer and in turn efficiency. It is very important to design suitable monomers for the synthesis of polymers as it may affect the method of polymerization and yields.

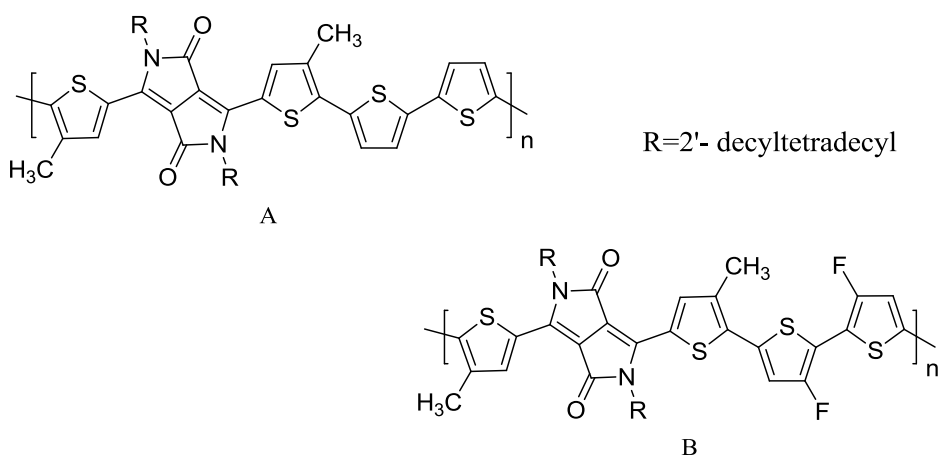


Figure 2.2: Nonfluorinated and fluorinated DPP Polymers

Poly(phenylenevinylene) (PPV)-based polymers are commonly used as donor materials in organic solar cells. Poly[2-methoxy-5-(2-ethylhexyloxy)-1,4-phenylenevinylene] (MEH-PPV) and poly[2-methoxy-5-(3',7'-dimethyloctyloxy)-1,4-phenylene vinylene] (MDMO-PPV) are two representatives of PPV-based polymers that have exhibited efficiencies of ~2 % in organic solar cells, when used in combination with PCBM as electron acceptor.²⁴⁻²⁷ The band gap of PPV-based organic materials is in the range of 2.3 eV. Therefore, it does not capture the near-infrared region of the electromagnetic spectrum.^{28,29} This limits the short-circuit current of PPV-based organic solar cells and ultimately the power conversion efficiency. Figure 2.3 shows the two widely used examples of PPV-based organic materials.

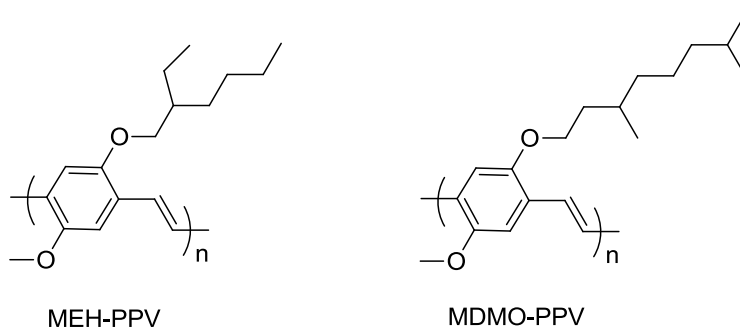


Figure 2.3: Structure of the most common poly(phenylvinylene) materials, MEH-PPV and MDMO-PPV

Common problems with the materials already discussed above are the large band gap and high-lying HOMO level. In order to harvest a greater fraction of energy from the sun and also improve the Voc, it is essential that the band gap of the polymer materials is reduced and the HOMO level is lowered. One strategy that has been used successfully to

achieve this is to construct organic materials with backbone having alternating electron-donor and electron-acceptor units forming D-A co-polymers.³⁰⁻³² Thiophene is the most commonly used building block for the synthesis of conjugated copolymers for photovoltaic and optoelectronic applications because of its excellent electrical and optical properties.³³ One polymer that was designed based on the repeating alternating electron-donor and electron-acceptor units is poly[N-9'-heptadecanyl-2,7-carbazole-alt-5,5-(4',7'-di-2-thienyl-2',1',3'-benzothiadiazole)] (PCDTBT)³⁴ which contains repeating units of electron-donating carbazole and electron-withdrawing benzothiadiazole. PCDTBT has a band gap of 1.88 eV and HOMO level of 5.50 eV. The device made from PCDTBT showed a PCE of 3.6 %. By modifying PCDTBT-based device through addition of optical spacer, solution processing and device engineering, the efficiency has been raised to ~7 %.^{35,36} Polymers based on repeating units of cyclopenta [2,1-b:3,4-b'] dithiophene (CPDT) and dithieno [3,2-b:2',3'-d] silole (DTS) showed lower band gaps of approximately 1.5 eV.^{37,38} The polymers, poly [(4,4-bis(2-ethylhexyl)-cyclopenta-[2,1-b:3,4-b'] dithiophene)-2,6-diyl-alt-(2,1,3-benzothiadiazole-4,7-diyl)] (PCPDTBT) and poly[(4,4'-bis(2-ethylhexyl) dithieno[3,2-b:2',3'-d]silole)-2,6-diyl-alt-(2,1,3-benzothiadiazole-4,7-diyl)] (PSBTBT) synthesized from these units showed absorption up to 850 nm and showed PCE of ~ 5 %. The performance of the polymers can be related to the strong intramolecular interactions between the donor and acceptor units. The structures of PCPDTBT and PSBTBT are shown in Figure 2.4.

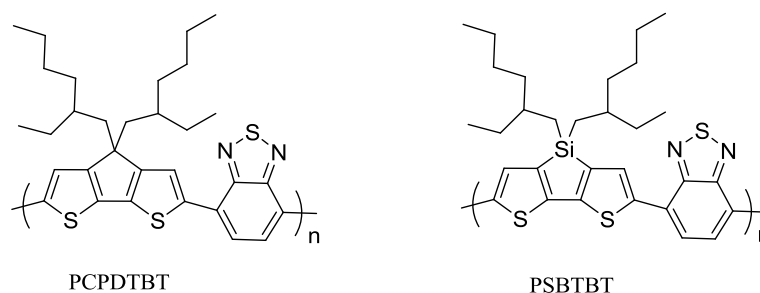


Figure 2.4: Structures of PCPDTBT and PSBTBT which gave PCE of 5% in organic photovoltaic cell

Fluorene based conjugated polymers have been widely used in organic light emitting diodes, and photovoltaics due to their high photoluminescence quantum yield, chemical and high thermal stability and good charge transport properties. Polyfluorene has a band gap of ~ 3.0 eV, which limits its ability to harvest light from the solar spectrum and application in photovoltaic cells. Therefore, in order to achieve low band gap value, it is necessary to introduce electron withdrawing units to fluorene backbone by copolymerization procedure. Electron-deficient 2,1,3-benzothiadiazole units have been widely incorporated into PF-based copolymers to alter the energy levels and fine-tune the emitting color over the entire visible region.³⁹ In spite of the high hole mobility and weak electron transport nature of polyfluorene, alternating poly(9,9-dioctylfluorene- *co*-benzothiadiazole) (PF1) exhibited a reduced LUMO level and thereby enhanced electron mobility (10^{-3} cm²/(V s)). Thus the electron deficient benzothiadiazole units can be considered as an electron-transport material.⁴⁰

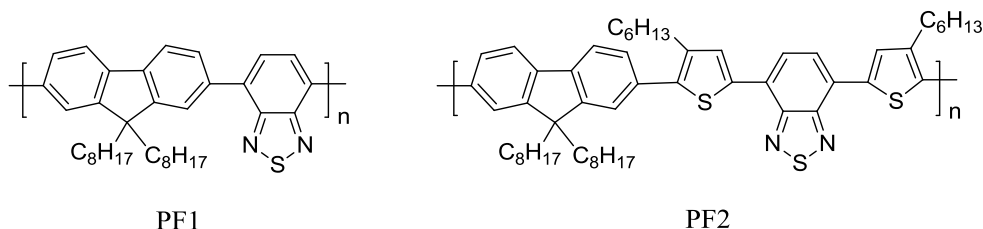


Figure 2.5: Chemical structures of PF1 and PF2

The photovoltaic performance of the ternary blend solar cell based on P3HT:PCBM:PF1 (1.0:0.6:1.4, wt %) showed a higher PCE value of 1.94 % than that of the binary blend P3HT:PCBM (1:2, wt %). The charge-carrier properties of PF1 can be further modulated by copolymerizing fluorene with the 4,7-bis(3-hexylthiophen-5-yl)-2,1,3-benzothiadiazole unit to yield the polymer PF2.⁴¹ With two additional electron-rich thiophene rings attached to both sides of the benzothiadiazole unit, the hole mobility of PF2 was expected to be improved compared to that of PF1.³¹

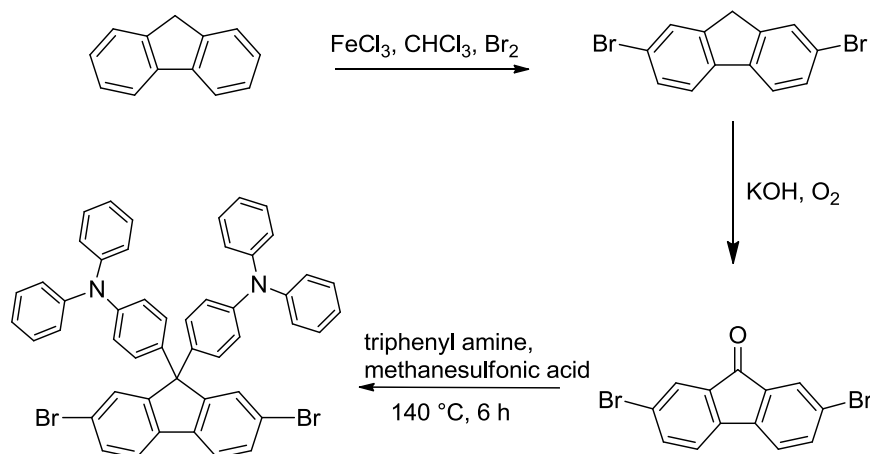
2.2 Results and Discussion

2.2.1 Synthesis of Monomers

3,4-ethylenedioxythiophene, 9,10-anthracenediboronic acid bis(pinacol) ester, 4,4'-dibromobiphenyl and 2,5-thiophene dicarboxaldehyde were purchased from Sigma Aldrich and used directly without further purification. All other monomers were synthesized according to reported procedures and characterized by spectroscopic techniques. HPLC grade solvents were used directly and other solvents were dried and distilled when necessary according to the standard procedures.

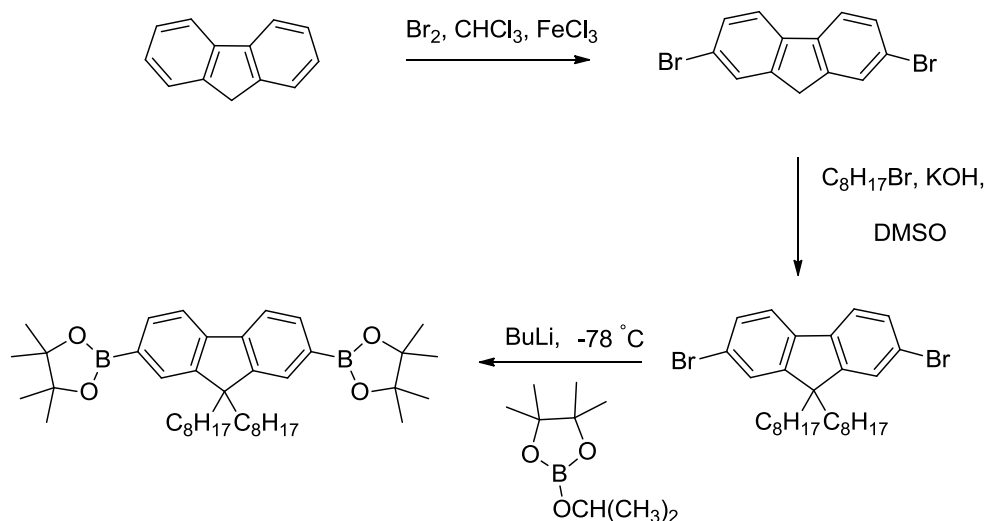
2.2.1.1 Synthesis of Fluorene Based Monomers

2,7-Dibromofluorene⁴² was prepared by the bromination of 9H-Fluorene which on air oxidation in the presence of KOH in THF gave 2,7-dibromofluorenone.⁴³ 9,9-bis(4-diphenylaminophenyl)-2,7-dibromofluorene⁴⁴ was synthesized by treating 2,7-dibromofluorenone with triphenylamine in the presence of methanesulfonic acid at 140 °C. The synthetic route for the preparation of the compounds is shown in Scheme 2.1.



Scheme 2.1: Synthesis of 9,9-bis(4-diphenylaminophenyl)-2,7-dibromofluorene

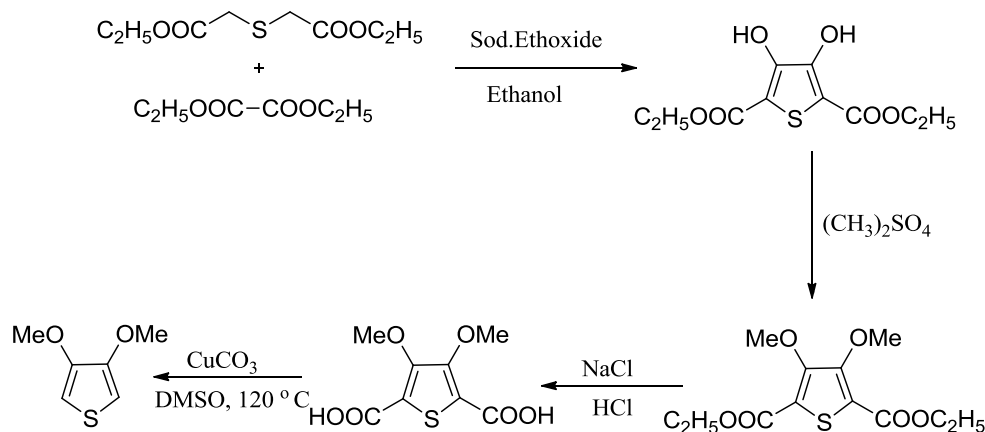
The dibromofluorene was treated with 1-bromooctane in the presence of KOH in DMSO to give 2,7- dibromo-9,9-dioctylfluorene). The above product was treated with n-butyl lithium and 2-isopropoxy-4,4,5,5-tetramethyl-1,3,2-dioxaborolane in dry THF at -78 °C to form 2,7-bis (4,4,5,5-tetramethyl-1,3,2-dioxaborolan-2-yl)-9,9-dioctylfluorene⁴⁵ (Scheme 2.2).



Scheme 2.2: Synthesis of 2,7-bis(4,4,5,5-tetramethyl-1,3,2-dioxaborolan-2-yl)-9,9-dioctylfluorene

2.2.1.2 Synthesis of 3,4-dimethoxythiophene

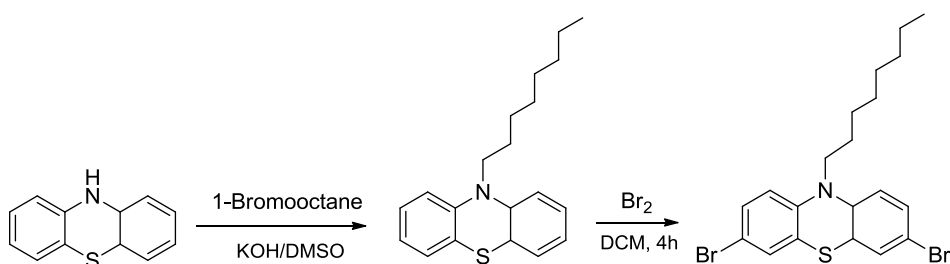
In the synthesis of 3,4-dimethoxythiophene,⁴⁶ first step involved the condensation of diethyl thiodiglycolate and diethyloxalate to give the 3,4-dihydroxythiophene dicarboxylic ester followed by methylation using freshly prepared dimethyl sulphate. This was followed by the hydrolysis of the ethyl ester with conc. HCl to form 3,4-dimethoxythiophene 2,5-dicarboxylic acid. Finally, the above product was decarboxylated at 120 °C to obtain the 3,4-dimethoxy thiophene as dark coloured liquid which was purified with column chromatography to yield a colourless liquid as the final product (Scheme 2.3).



Scheme 2.3: Synthesis of 3,4-dimethoxythiophene

2.2.1.3 Synthesis of 3,7-dibromo-10-octylphenothiazine

3,7-dibromo-10-octylphenothiazine⁴⁷ was synthesized in two steps starting from phenothiazine. First step involved the alkylation of phenothiazine and bromination of alkylated phenothiazine gave the product as pale yellow coloured liquid (Scheme 2.4).

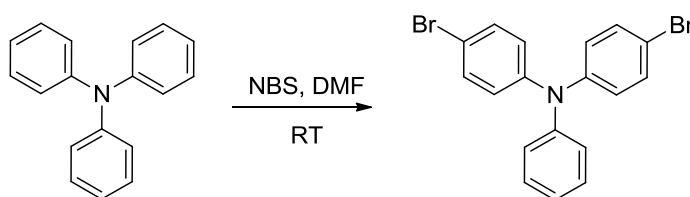


Scheme 2.4: Synthesis of 3,7-dibromo-10-octylphenothiazine

2.2.1.4 Synthesis of 4, 4'-dibromotriphenylamine

Dibromo derivative of triphenylamine was synthesized by treating triphenylamine with N-bromosuccinimide (NBS) at room temperature and

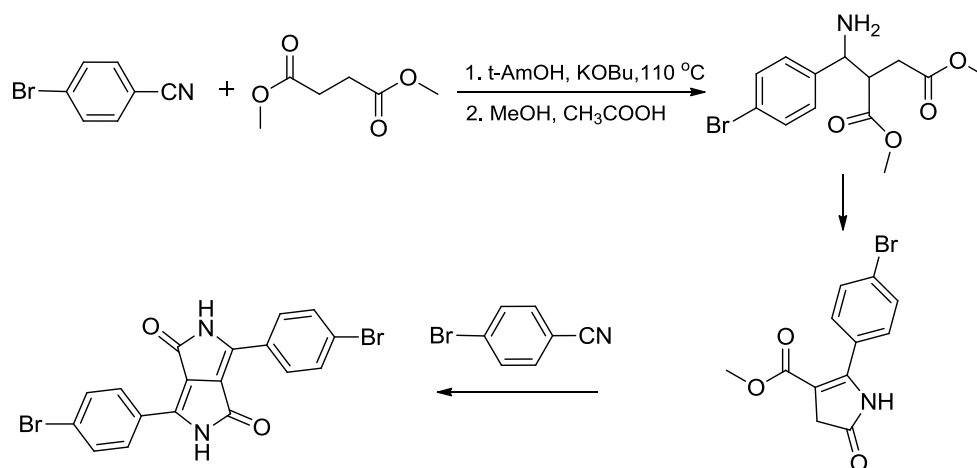
stirred for 24 h. Dichloromethane was added to the solution and washed with water and organic layer was dried using MgSO_4 followed by solvent evaporation which gave the crude product. Column chromatography of the residue over silica gel (Hexane: DCM, 5:1) gave the product as curdy white powder⁴⁸ (Scheme 2.5).



Scheme 2.5: Synthesis of 4, 4'-dibromotriphenylamine

2.2.1.5 Synthesis of 3,6-bis(4-bromophenyl)-2,5-dihydropyrrolo[3,4-c]pyrrole-1,4-dione

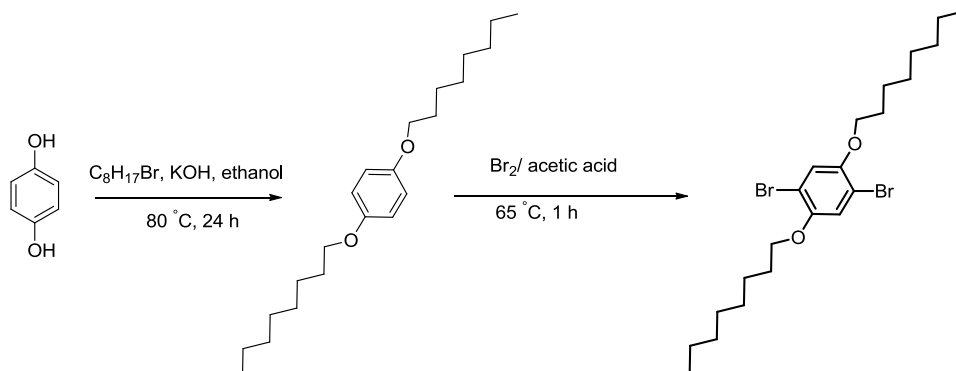
The succinic ester route is widely used for preparing DPP compounds. Dimethyl succinate was stirred with 2 equivalents of aromatic nitrile and a strong base. The carbonitrile was selected according to the type of the target DPP monomer. For example, phenyl carbonitrile gave diphenyl-DPP product. Dimethyl succinate first reacts with one nitrile molecule to form a pyrrolinone ester, a single ring system, which further reacted with another aromatic nitrile to close the second ring. The reaction sequence for the monomer prepared is shown in Scheme 2.6. 4-Bromobenzonitrile reacted with dimethyl succinic ester to give enaminoester and after ring closure, pyrroline ester. Repeating the stages with another nitrile gave 3,6-bis(4-bromophenyl) 2,5-dihydropyrrolo [3,4-c] pyrrole-1,4-dione.⁴⁹



Scheme 2.6: Synthesis of 3,6-bis(4-bromophenyl)-2,5-dihydropyrrolo [3,4-c] pyrrole-1,4-dione

2.2.1.6 Synthesis of 1,4-dibromo-2,5-bis (octyloxy) benzene

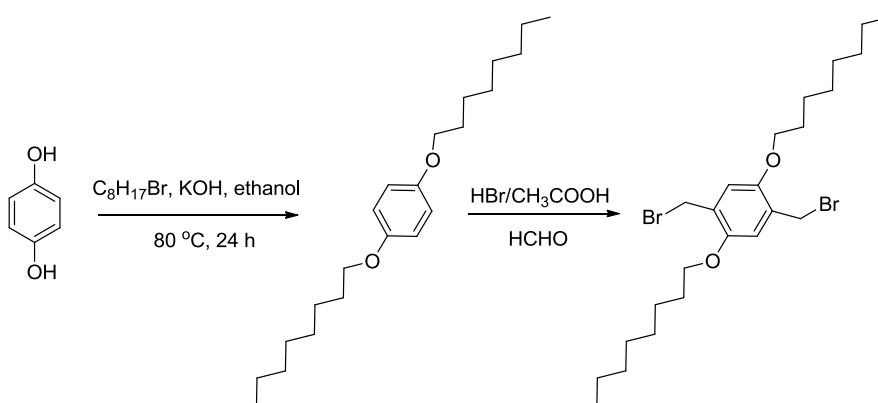
A mixture of quinol and potassium hydroxide in ethanol was refluxed for 1 h at 80 °C. After cooling to room temperature, 1-bromooctane was added dropwise and again stirred at 80 °C for 24 h. The mixture was poured into water and precipitated product was washed with methanol to afford 1,4-bis (octyloxy) benzene as white powder. A solution of Br₂ in glacial acetic acid was added to the solution of 1,4-bis(octyloxy) benzene in glacial acetic acid at 65 °C. The reaction mixture was cooled to room temperature and poured into water and made alkaline with NaOH solution. The precipitated product was filtered and washed with bicarbonate solution which gave the product as white powder⁵⁰ (Scheme 2.7).



Scheme 2.7: Synthesis of 1,4-dibromo-2,5-bis (octyloxy) benzene

2.2.1.7 Synthesis of 1,4-bis (bromomethyl)-2,5-bis (octyloxy) benzene

1,4 –bis (octyloxy) benzene, paraformaldehyde and glacial acetic acid were placed in an ice bath. HBr in glacial acetic acid was carefully added drop wise into this flask, and the mixture was stirred for 24 h at $60\text{--}70\text{ }^\circ\text{C}$. The mixture was poured into saturated $NaHCO_3$ solution. It was cooled to room temperature and extracted with dichloromethane. The solvent was removed on a rotary vacuum flash evaporator. The residue was purified by column chromatography with the mixture of hexane and CH_2Cl_2 (8:1) to offer 1,4-bis (bromomethyl)-2,5-bis (octyloxy) benzene^{51,52} (Scheme 2.8).



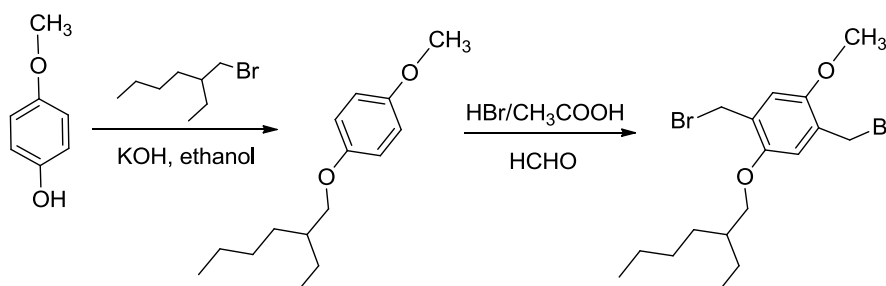
Scheme 2.8: Synthesis of 1,4-bis (bromomethyl)-2,5-bis (octyloxy) benzene

2.2.1.8 Synthesis of 1,4-bis (bromomethyl)-2-((2-ethylhexyl)oxy)-5-methoxybenzene

1-Methoxy-4-(2-ethylhexyloxy) benzene

A mixture of 4-methoxyphenol and KOH in ethanol was refluxed for 1 h at 80 °C under nitrogen atmosphere. After cooling to room temperature, 2-ethylhexyl bromide was added drop wise and further refluxed for 24 h. When the brownish solution was turned to yellow, the reaction mixture was poured into distilled water and the brown liquid was extracted with diethyl ether. Vacuum distillation gave the product as colourless liquid.

1,4-Bis-(bromomethyl) methoxy-4-(2-ethylhexyloxy) benzene

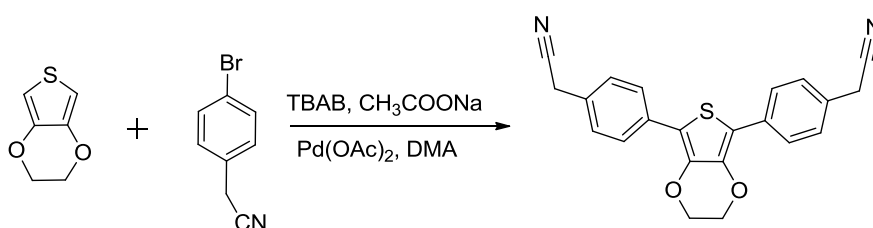


Scheme 2.9: Synthesis of 1,4-bis (bromomethyl)-2-((2-ethylhexyl)oxy)-5-methoxybenzene

1-methoxy-4-(2-ethylhexyloxy)benzene, paraformaldehyde and glacial acetic acid were placed in an ice bath. HBr in glacial acetic acid was carefully added drop wise into this flask, and the mixture was stirred for 24 h at 60-70 °C. The mixture was poured into saturated NaHCO₃ solution and extracted with dichloromethane. The crude product was washed several times with Brine solution and water and recrystallized from hexane twice to obtain the product as a white powder⁵² (Scheme 2.9).

2.2.1.9 Synthesis of 2,2'-((2,3-dihydrothieno[3,4-b][1,4]dioxine-5,7-diyl)bis(4,1-phenylene)) diacetonitrile⁵³

To a stirred solution of ethylenedioxythiophene in dimethyl acetamide (DMAc) was added tetrabutylammonium bromide and sodium acetate. The reaction mixture was stirred at room temperature for 15 min followed by addition of 4-bromophenyl acetonitrile and 10 mol % palladium acetate. The reaction mixture was stirred at room temperature for 24 h. The reaction mixture was cooled to room temperature and poured in to cold methanol. The precipitate was filtered and washed with methanol. The product was dissolved in minimum amount of Chloroform and precipitated from methanol and dried in vacuum (Scheme 2.10).



Scheme 2.10: Synthesis of 2,2'-((2,3-dihydrothieno[3,4-b][1,4]dioxine-5,7-diyl)bis(4,1-phenylene)) diacetonitrile

2.3 Experimental Procedure

2.3.1 Synthesis of Fluorene Based Monomers

2.3.1.1 2,7-Dibromofluorene

Bromine (4 mL) was added drop wise to a solution of 9H-fluorene (6 g, 36 mmol) and ferric chloride (92 mg, 1.6 mmol) in CHCl₃ (100 mL) at 0 °C. The mixture was stirred for 12 h and it was poured into 50 mL water. The precipitate was washed with NaHCO₃ and NaHSO₃ solution. The organic layer was extracted with CHCl₃ and dried over anhydrous magnesium

sulphate. After filtration, the solvent was removed using rotary vacuum evaporation and the residue was recrystallized from ethanol resulting in white crystalline product (Yield: 76 %). m.p. 160-164 °C. ¹H NMR (400 MHz, CDCl₃), δ: 7.66 (s, 2H), 7.60-7.59 (d, 2H), 7.51-7.49 (d, 2H), 3.87 (s, 2H).

2.3.1.2 2, 7-Dibromo-9,9-dioctylfluorene

KOH solution (10 mL, 50 %) and 1-Bromooctane (5.60 g, 29 mmol) was added drop wise to a mixture of 2,7-dibromofluorene (3.88 g, 12 mmol), tetrabutylammonium bromide (0.0225 g, 0.0975 mmol) in DMSO (50 mL) under N₂ atmosphere. The reaction mixture was stirred at 80 °C for 2 days. The mixture was poured into 500 mL of water. The organic layer was extracted with dichloromethane. The combined organic layer was dried over anhydrous MgSO₄. The solvent was removed under reduced pressure. The crude product was purified by recrystallization from hexane to yield colourless crystals (Yield: 89 %). m.p. 59-63 °C. ¹H NMR (400 MHz, CDCl₃), δ: 7.51 (s, 2H), 7.45 (m, 4H), 1.90 (m, 4H), 1.25-0.86 (m, 24H), 0.83 (t, 6H). ¹³C NMR (CDCl₃, 100 MHz), ppm: 153.2, 139.8, 131.2, 126.2, 122.3, 121.1, 46.4, 41.8, 31.7, 29.6, 29.0, 23.9, 22.8, 14.1. m/z: 548.4

2.3.1.3 Synthesis of 2,7-bis (4,4,5,5-tetramethyl-1,3,2-dioxaborolan-2-yl)-9,9-dioctylfluorene

To a stirred solution of 2,7-dibromo-9,9-dioctylfluorene (5.0 g, 9.1 mmol) in THF (70 mL) at -78 °C was added drop wise n-butyl lithium in hexane (7.6 mL, 2.5 M, 19 mmol) and kept the mixture at -78 °C for 10 minutes. The mixture was warmed to 0 °C for 15 min and cooled back to -78 °C. 2-isopropoxy-4,4,5,5-tetramethyl-1,3,2-dioxaborolane (4 g, 21.5 mmol) was

added rapidly to the solution. The resulting mixture was warmed to room temperature and stirred for 24 h. The mixture was poured into water and extracted with diethyl ether. The organic extract was washed with brine and dried over magnesium sulphate. The solvent was removed under reduced pressure, and the crude product was purified by column chromatography, eluting with 2 % ethyl acetate and hexane to give 2,7-bis (4,4,5,5-tetramethyl-1,3,2-dioxaborolan-2-yl)-9,9-dioctylfluorene as a pale yellow solid (Yield: 65 %). ^1H NMR (400 MHz, CDCl_3), δ : 7.83 (d, 2H), 7.76 (s, 2H), 7.73 (d, 2H), 2.05 (m, 4H), 1.44 (s, 24H), 1.25-1.09 (m, 24H), 0.82 (t, 6H).

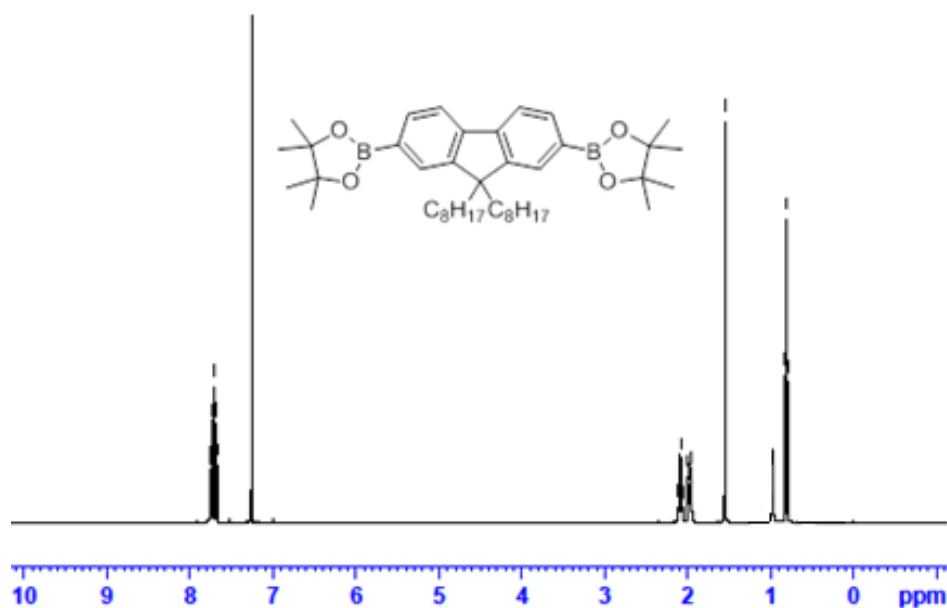


Figure 2.6: ^1H NMR spectrum of 2,7-bis (4,4,5,5-tetramethyl-1,3,2-dioxaborolan-2-yl)-9,9-dioctylfluorene

2.3.1.4 Synthesis of 2,7-dibromofluorenone

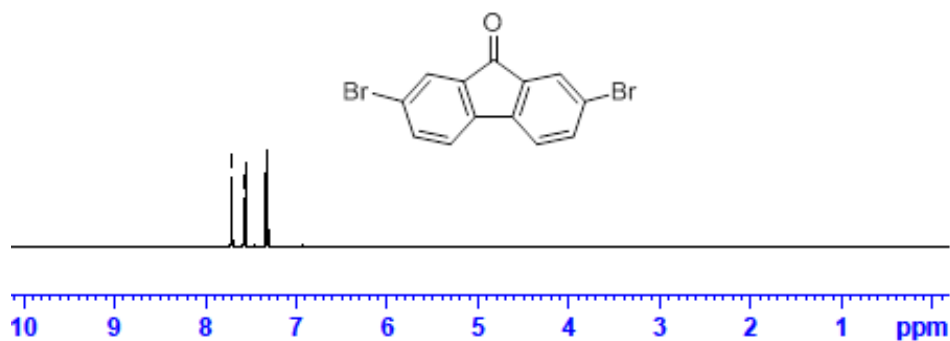


Figure 2.7: ¹H NMR spectrum of 2,7-dibromofluorenone

Into a 100 mL, two-necked round bottom flask equipped with a magnetic stirrer and an air condenser were charged 2,7-dibromofluorenone (3.24 g, 5 mmol), KOH (0.56 g, 10 mmol) and THF (30 mL). The reaction mixture was stirred at room temperature and air was introduced for 5 minutes in every 30 minutes to ensure that there was sufficient oxygen with minimal loss of solvent. The reaction mixture was filtered to remove KOH and the filtrate was concentrated to obtain the crude product. The crude product was washed with water (3×100 mL) and dried column chromatography of the crude product (Hexane/ DCM, 4:2) gave 2,7-dibromofluorenone as yellow solid (Yield: 98 %). m.p. 202-205 °C. ¹H NMR (400 MHz, CDCl₃), δ: 7.85 (d, 2H), 7.56 (d, 2H), 7.37 (d, 2H). m/z: 337

2.3.1.5 Synthesis of 9,9-Bis(4-diphenylaminophenyl)-2,7-dibromofluorene

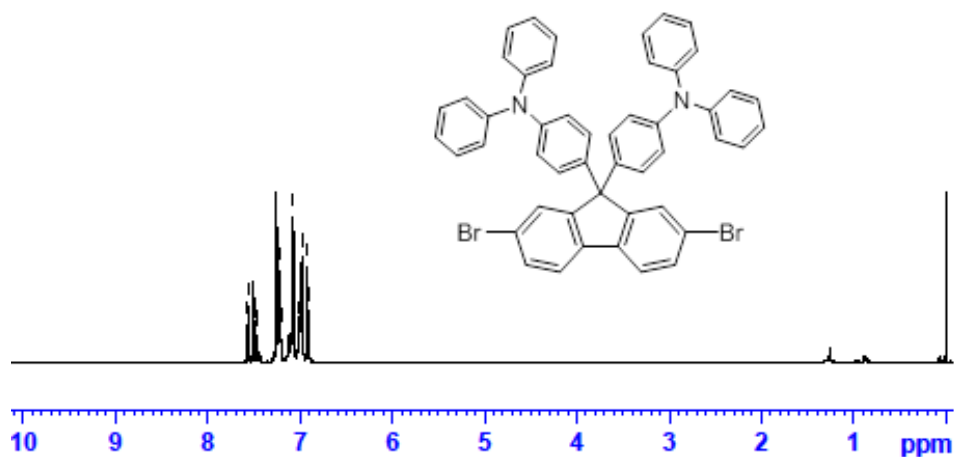


Figure 2.8: ¹H NMR spectrum of 9,9-Bis (4-diphenylaminophenyl)-2,7-dibromofluorene

A mixture of dibromofluorenone (2.46 g, 7.28 mmol) and triphenylamine (25 g, 0.102 mol) with methane sulfonic acid (0.7 g, 7.28 mmol) was heated at 140 °C with constant stirring under an inert atmosphere for 6 h. The cooled mixture was extracted with DCM, and the extract was washed with sodium carbonate solution, dried and concentrated. Chromatography of the residue on silica, eluting with hexane/DCM, followed by recrystallization from acetone gave 9,9-bis(4-diphenylaminophenyl)-2,7-dibromofluorene as pale yellow powder (Yield-70 %). m.p. 310-312 °C. ¹H NMR (400 MHz, CDCl₃), δ: 7.57 (d, 4H), 7.48 (d, 2H), 7.20 (d, 8H), 7.00-7.08 (m, 8H), 6.92-7.98 (m, 8H), 6.88 (d, 4H). m/z: 810

2.3.2 Synthesis of 3,7-Dibromo-10-(octyl)phenothiazine

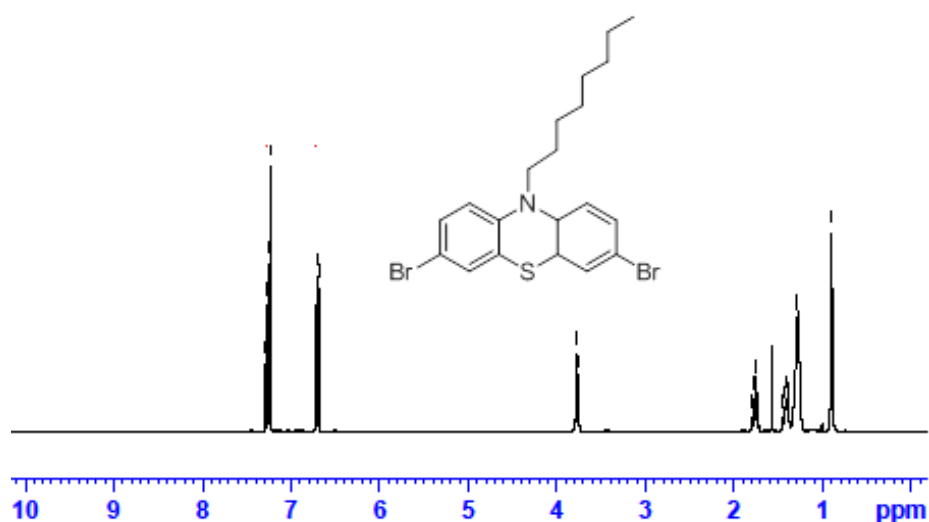


Figure 2.9: ¹H NMR spectrum of 3,7-Dibromo-10-(octyl)phenothiazine

10-n-Octylphenothiazine (7.5 g, 0.024 mol) was dissolved in 50 mL of dichloromethane, and bromine (8.0 g, 0.05 mol) was injected into the solution using a syringe and stirred for 4 h at room temperature. Dilute aqueous sodium hydroxide (20 mL) was added to the reaction mixture and kept for 30 min. The reaction mixture was extracted three times using dichloromethane and brine, and the organic layer was separated and concentrated. The crude product was purified by column chromatography using hexane as the eluent which gave yellow oil. ¹H NMR (400 MHz, CDCl₃), δ : 6.68-7.28 (m, 6H), 3.78 (t, 2H), 1.38-1.79 (m, 12H), 0.88 (d, 3H).

2.3.3 Synthesis of 4, 4'-dibromotriphenylamine

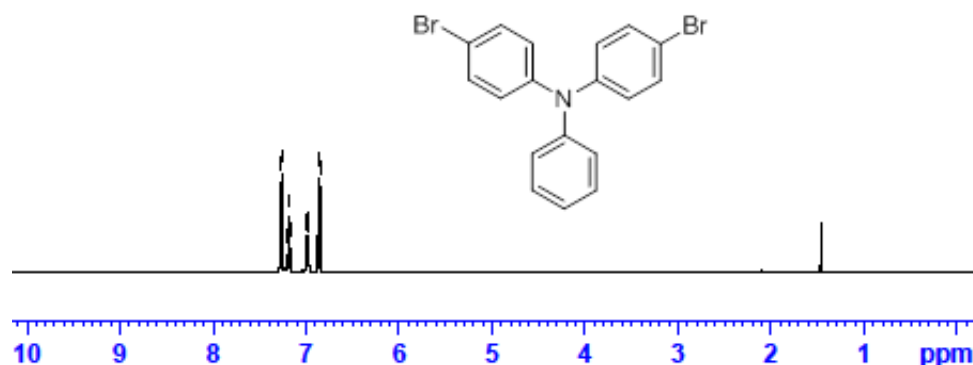


Figure 2.10: ¹H NMR spectrum of 4, 4'-dibromotriphenylamine

To a mixture of triphenylamine (2.43 g, 10 mmol) in DMF (50 mL) was added NBS (3.56 g, 10 mmol) in small portions. The colour of the solution changed from colorless to clear green and then to light yellow. The solution was stirred at room temperature for 24 h and 100 mL of DCM was added to the solution. The reaction mixture was washed with water (1 × 60 mL, 4 × 30 mL). Organic layer was dried over MgSO₄ and the solvent was evaporated using rotary vacuum evaporator. Column chromatography of the residue over silica gel (Hexane: DCM at 5:1) gave the product as curdy white powder. ¹H NMR (400 MHz, CDCl₃), δ: 6.92 (d, 4H), 7.01 (d, 2H), 7.15 (m, 1H), 7.20 (m, 2H), 7.35 (d, 4H).

2.3.4 Synthesis of 3,6-bis (4-bromophenyl) 2,5-dihydropyrrolo [3,4-c] pyrrole-1,4-dione

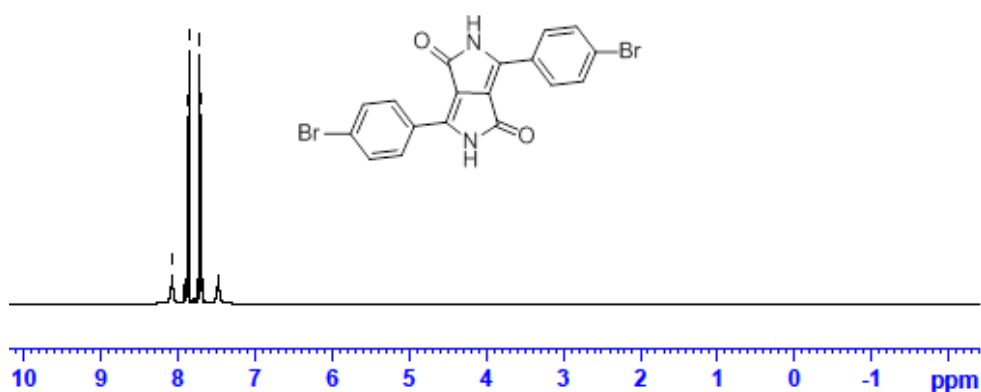


Figure 2.11: ^1H NMR spectrum of 3,6-bis (4-bromophenyl) 2,5-dihydropyrrolo [3,4-c] pyrrole-1,4-dione

Potassium tert-butoxide (4 g, 35.7 mmol) was added to a round bottom flask with argon protection. A solution of t-amyl alcohol (25 mL) and 4-bromobenzonitrile (5.46 g, 30 mmol) was injected by a syringe in one portion. The mixture was warmed up to 100-110 °C and a solution of dimethyl succinate (1.46 g, 10 mmol) in tert-amyl alcohol (8 mL) was dropped slowly in 1 h. When the addition was completed, the reaction was kept at the same temperature for 1 h and the reaction mixture was kept for 2 h. The mixture was cooled to 65 °C and diluted with 50 mL of methanol. The mixture was neutralized with acetic acid and refluxed for another 10 minutes. The suspension was filtered and the red filter cakes was washed with hot methanol and water twice each and dried in vacuum. The product could be used directly to the next step without further purification. ^1H NMR (400 MHz, CDCl_3), δ : 8.07 (s, 2H), 7.88 (d, 4H), 7.68 (d, 4H).

2.3.5 Synthesis of 1,4-dibromo-2,5-bis (octyloxy) benzene 1,4-bis (octyloxy) benzene

A solution of quinol (0.25 mol) in 100 mL of ethanol was slowly added to a stirred solution of KOH (0.63 mol) in 350 mL of ethanol at room temperature. The reaction mixture was stirred for 1 h. A solution of 1-octylbromide (0.75 mol) in 50 mL of ethanol was added drop wise. The reaction mixture was refluxed overnight. Ethanol was removed by rotary vacuum evaporation and the reaction mixture was partitioned between ethyl acetate and sodium carbonate solution. After drying over sodium sulfate, the product was obtained by reduced pressure distillation to get the product (Yield: 72 %). ^1H NMR (400 MHz, CDCl_3), δ : 6.89 (s, 4H), 4.05 (t, 4H), 1.76(m, 4H), 1.42-1.28 (m, 20H), 0.90 (t, 6H).

1,4-dibromo-2,5-bis (octyloxy) benzene

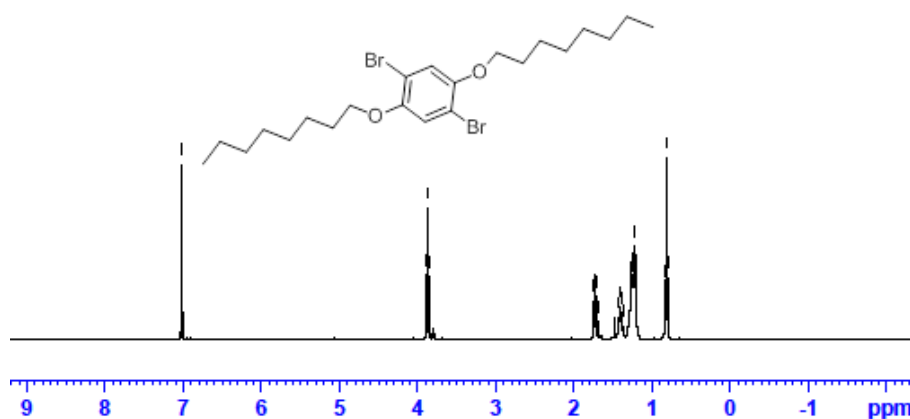


Figure 2.12: ^1H NMR spectrum of 1,4-dibromo-2,5-bis (octyloxy) benzene

A solution of Br_2 (9.6 g, 60 mmol) in glacial acetic acid (30 mL) was added dropwise to a solution of 1,4-dioctyloxybenzene (10 g, 30 mmol) in glacial acetic acid (45 mL) at 65 °C. The reaction mixture was stirred for

45 minutes at the same temperature. The temperature was raised to reflux and kept for one hour. The solution was cooled to room temperature and subsequently poured into water (500 mL) and made alkaline with 2N NaOH (600 mL). The precipitate was filtered and washed thoroughly with sodium bicarbonate solution to give 1,4-dibromo-2,5-bis (octyloxy) benzene as white solid (76 %). ^1H NMR (400 MHz, CDCl_3), δ : 7.01(s, 2H), 3.88 (t, 4H), 1.76(m, 4H), 1.42-1.28 (m, 20H), 0.83 (t, 6H).

2.3.6 Synthesis of 1,4-bis (bromomethyl)-2,5-bis (octyloxy) benzene

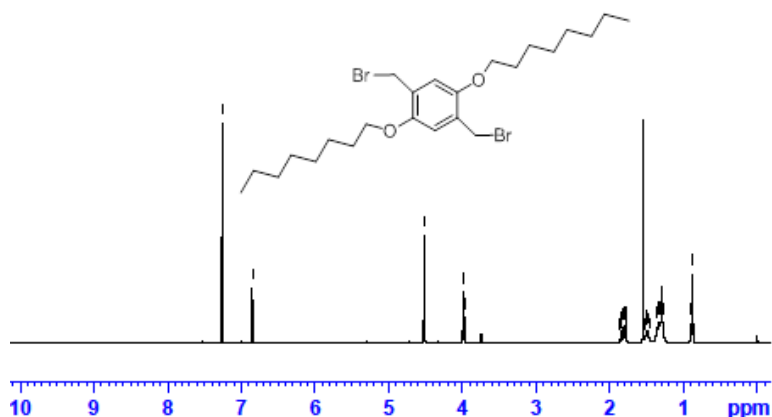


Figure 2.13: ^1H NMR spectrum of 1,4-bis (bromomethyl)-2,5-bis (octyloxy) benzene

A three necked flask containing 1,4-bis (octyloxy) benzene (0.01 mol), paraformaldehyde (0.035 mol), and glacial acetic acid (40 mL) was placed in an ice bath. 33 % HBr in glacial acetic acid was carefully added drop wise into this flask, and the mixture was stirred for 24 h at 60-70 °C. The mixture was poured into 200 mL of saturated NaHCO_3 solution after being cooled to room temperature and extracted with DCM. The solvent was removed on a rotary vacuum evaporator, the residue was purified by column chromatography with the mixture of hexane and CH_2Cl_2 (8:1) to offer 1,4-bis (bromomethyl)-2,5-bis

(octyloxy) benzene. ^1H NMR (400 MHz, CDCl_3), δ : 7.26 (s, 2H), 4.52 (s, 4H), 3.99 (t, 4H), 1.86 (t, 4H), 1.53-1.45 (m, 20H), 0.98 (s, 6H).

2.3.7 Synthesis of 1,4-bis (bromomethyl)-2-((2-ethylhexyl)oxy)-5-methoxybenzene

1-Methoxy-4-(2-ethylhexyloxy) benzene

A mixture of 4-methoxyphenol (0.08 mol, 10 g) and KOH (0.16 mol, 9 g) in ethanol (40 mL) was refluxed for 1 h at 80 °C under nitrogen atmosphere. After cooling to room temperature, 2-ethylhexyl bromide (0.08 mol) was added drop wise and further refluxed for 24 h. When the brownish solution turned to yellow, the reaction mixture was poured into 200 mL of distilled water and the brown liquid was extracted with diethyl ether. The crude product was washed several times with aqueous sodium carbonate solution and water and was recrystallized. ^1H NMR (400 MHz, CDCl_3), δ : 6.71 (d, 4H), 3.80 (d, 2H), 3.62 (s, 3H), 1.76 (s, 1H), 1.54-1.24 (m, 8H), 0.90 (t, 6H).

1,4-bis(bromomethyl)-2-((2-ethylhexyl)oxy)-5-methoxybenzene

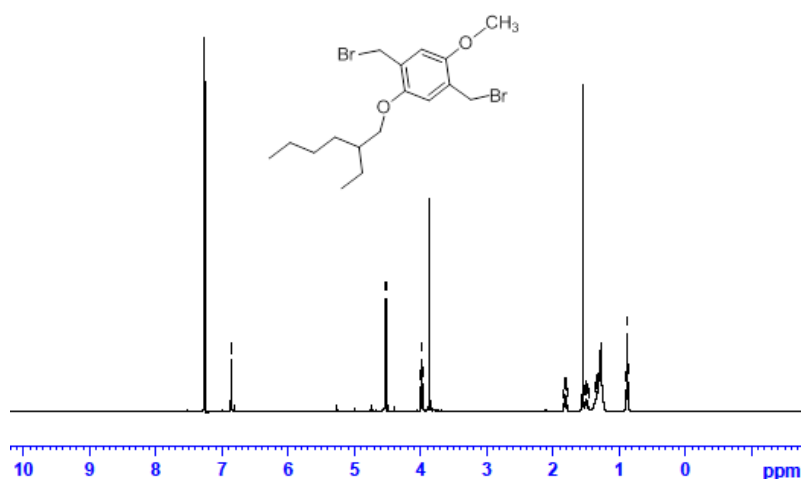


Figure 2.14: ^1H NMR spectrum of 1,4-bis (bromomethyl)-2-((2-ethylhexyl)oxy)-5-methoxybenzene

A three necked flask containing 1-methoxy-4-(2-ethylhexyloxy) benzene (0.01 mol), paraformaldehyde (0.035 mol), and glacial acetic acid (40 mL) was placed in an ice bath. 33 % HBr in glacial acetic acid was carefully added drop wise into this flask, and the mixture was stirred for 24 h at 60-70 °C. The mixture was poured into 200 mL of saturated NaHCO₃ after being cooled to room temperature and extracted with DCM. The crude product was washed several times with Brine solution and water and recrystallized from hexane twice to obtain compound as a white crystal Yield: 82 %. ¹H NMR (400 MHz, CDCl₃), δ: 6.85 (s, 2H), 4.53 (s, 4H), 4.03 (d, 2H), 3.86 (s, 3H), 1.84 (t, 1H), 1.70-1.32 (m, 8H), 0.90 (t, 6H).

2.3.8 Synthesis of Thiophene Based Monomers

2.3.8.1 Diethyl thiodiglycolate

In a 500 mL round bottom flask, thiodiglycolic acid (10 g, 0.06 mol) was dissolved in dry ethanol (25 mL) and conc. sulphuric acid (1 mL) was added drop wise to it. The resulting mixture was refluxed for 24 h. The excess methanol was evaporated and the residue was dissolved in ethyl acetate, washed with saturated sodium bicarbonate solution until the aqueous layer was neutral. The organic layer was dried over sodium sulfate and the solvent was removed on a rotary evaporator to afford a light yellow liquid. Yield: 89 %. ¹H NMR (400 MHz, CDCl₃), δ: 4.2 (q, 4H), 3.4 (s, 4H), 1.4 (t, 6H).

2.3.8.2 3,4-Dimethoxy-2,5-dicarbethoxythiophene

A solution of 1 g of sodium metal in 10 mL of dry ethanol was cooled at 0-5 °C. To this, a solution of 2.06 g of diethyl thiodiglycolate and 1.18 g of diethyl oxalate was added and stirred. The temperature was maintained at 0 °C. The sodium salt was precipitated as a yellow solid. The reaction was

completed by heating the reaction mixture to reflux for 2 h. After cooling, the solid was filtered and dried. The sodium salt of diester (1.5 g, 5.43 mmol) was taken in 7 mL of freshly distilled dimethyl sulfate and the mixture was heated at 100 °C for 1 h. The excess dimethyl sulfate was distilled at low pressure and the crude product was dissolved in ethyl acetate (10 mL) and washed with cold 5 % NaOH solution (5 mL). The organic layer was extracted and dried over sodium sulfate and solvent was evaporated to afford the compound as a pure light yellow solid. Yield: 64 %. ^1H NMR (400 MHz, CDCl_3), δ : 4.1 (q, 4H), 3.9 (s, 6H), 4.1 (q, 4H), 1.2(t, 6H).

2.3.8.3 3,4-Dimethoxythiophene-2,5-dicarboxylic acid

In a 100 mL round bottom flask 3,4-dimethoxy-2,5-dicarbethoxy thiophene (0.9 g, 3.5 mmol) was taken and 10 % NaOH (5 mL) was added to it. The mixture was refluxed for 1 h. The reaction mixture was cooled to room temperature and conc. HCl was added to it with stirring. The precipitate thus formed was collected in a Buchner funnel and dried in an oven to give the above product as a white solid. Yield: 84 %. ^1H NMR (400 MHz, CDCl_3), δ : 10.2 (s, 2H), 4 (s, 6H)

2.3.8.4 Synthesis of 3,4-dimethoxythiophene

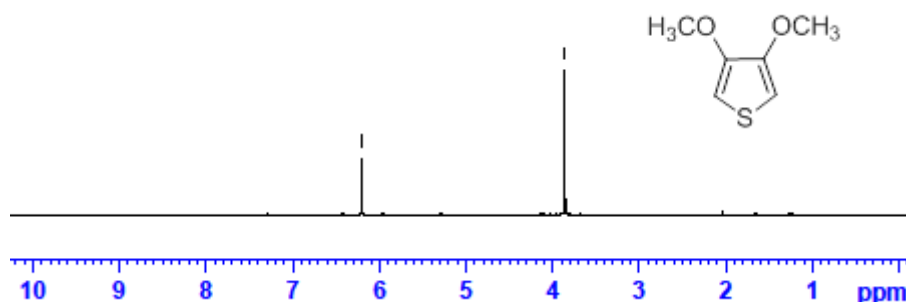


Figure 2.15: ^1H NMR spectrum of 3,4-dimethoxythiophene

A 100 mL dry three necked round bottom flask was charged with 3,4-dimethoxythiophene-2,5-dicarboxylic acid (9 g, 43.3 mmol), copper chromite (0.56 g, 4 mol %) and dry quinoline (30 mL). The mixture was heated at 160 °C for 4 h under argon atmosphere. The reaction mixture was vacuum distilled and the pink liquid obtained was dissolved in 50 mL of ethyl acetate and washed repeatedly with 5 % HCl and water. The organic layer was dried over anhydrous Na₂SO₄, filtered and the solvent was evaporated to give a crude brown coloured liquid. The crude compound was purified by column chromatography using silica gel as adsorbent and eluting using ethyl acetate/ petroleum ether mixture to afford the product as colourless liquid (Yield: 56 %). ¹H NMR (400 MHz, CDCl₃), δ: 6.2 (s, 2H), 3.8 (s, 6H). ¹³C NMR (CDCl₃, 100 MHz), ppm : 57, 36, 96, 35, 147, 90. m/z = 144

2.3.9 Synthesis of 2,2'-((2,3-dihydrothieno [3,4-b][1,4] dioxine-5,7-diyl)bis(4,1phenylene)) diacetonitrile

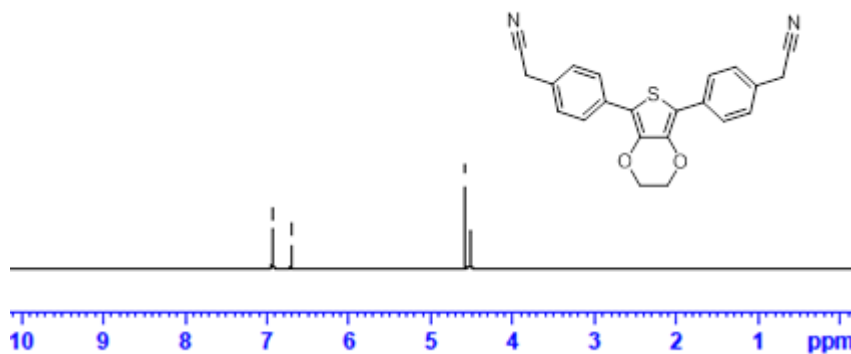


Figure 2.16: ¹H NMR spectrum of 2,2'-((2,3-dihydrothieno [3,4-b][1,4] dioxine-5,7-diyl)bis(4,1phenylene)) diacetonitrile

To a stirred solution of ethylenedioxythiophene (0.15 g, 1.06 mmol) in 60 mL DMAc was added tetrabutylammonium bromide (0.349 g, 1.06 mmol)

and sodium acetate (0.586 g, 4.2 mmol). The reaction mixture was stirred at room temperature for 15 minutes followed by addition of 4-bromophenyl acetonitrile (0.4156 g, 2.12 mmol) and 10 mol % palladium acetate. The reaction mixture was stirred at room temperature for 24 h. The reaction mixture was cooled to room temperature and poured in to cold methanol. The precipitate was filtered and washed with methanol. The product was dissolved in minimum amount of chloroform and precipitated from methanol and dried in vacuum. ^1H NMR (400 MHz, CDCl_3), δ : 6.98 (s, 4H), 6.75 (s, 4H), 4.6 (s, 4H), 4.5 (s, 4H).

2.4 Conclusion

A series of monomers were successfully synthesized. The strategies used for synthesizing the monomers were discussed in this chapter. All the compounds synthesized were spectroscopically characterized.

References

- [1] V. Balzani, A. Credi, M. Venturi, *ChemSusChem.*, 2008, **1**, 26.
- [2] D. Wöhrle, D. Meissner, *Adv. Mater.*, 1991, **3**, 129.
- [3] N. S. Sariciftci, *Mater. Today.*, 2004, **7**, 40.
- [4] J. Y. Kim, K. Lee, N. E. Coates, D. Moses, T. Q. Nguyen, M. Dante, A. J. Heeger, *Science*, 2007, **317**, 222.
- [5] M. C. Scharber, D. Mühlbacher, M. Koppe, P. Denk, C. Waldauf, A. J. Heeger, C. J. Brabec, *Adv. Mater.*, 2006, **18**, 789.
- [6] H. H. Fong, V. A. Pozdin, A. Amassian, G. G. Malliaras, D. M. Smilgies, M. He, S. Gasper, F. Zhang, M. Sorensen, *J. Am. Chem. Soc.*, 2008, **130**, 13202.
- [7] (a) A Moliton, R. C. Hiorns, *Polym. Int.*, 2004, **53**, 1397.
(b) J. Roncali, *Chem. Rev.*, 1997, **97**, 173.

- [8] L. G. Gregory, M. M. Theresa, S. S. Dwight, *J. Am. Chem.Soc.*, 2012, **134**, 539.
- [9] H. A. Ho, H. Brisset, P. Fre` re, J. Roncali, *J. Chem. Soc., Chem. Commun.* 1995, **71**, 2309.
- [10] H. A. Ho, H. Brisset, E. Elandaloussi, P. Fre` re, J. Roncali, *Adv. Mater.*, 1996, **8**, 990.
- [11] S. C. Rasmussen, K. Ogawa, S. D. Rothstein, *The Handbook of Organic Electronics and Photonics*, H. S. Nalwa, Ed.; American Scientific Publishers: Stevenson Ranch, CA, 2008.
- [12] H. Sirringhaus, *Adv. Mater.*, 2014, **26**, 1319.
- [13] Z. Yi, S. Wang, Y. Liu, *Adv. Mater.*, 2015, **27**, 3589.
- [14] S. Holliday, J. E. Donaghey. I. McCulloch, *Chem. Mater.*, 2014, **26**, 647.
- [15] T. Lei, J. Wang, J. Pei, *Acc. Chem. Res.*, 2014, **47**, 1117.
- [16] E. Wang, W. Mammo, M. R. Andersson, *Adv. Mater.*, 2014, **26**, 1801.
- [17] H. Yan, Z. Chen, Y. Zheng, C. J. R Newman, Quinn, F. Dötz, M. Kastler, A. Facchetti, *Nature.*, 2009, **457**, 679.
- [18] S. G. Bucella, A. Luzio, L. Gann, L. Thomsen, C. R. McNeill, G. Pace, A. Perinot, Z. Chen, A. Facchetti, M. Caironi, *Nat. Commun.*, 2015, **6**, 8394.
- [19] M. He, W. Li, Y. Gao, H. Tian, J. Zhang, H. Tong, D. Yan, Y. Geng, F. Wang, *Macromolecules*, 2016, **49**, 825.
- [20] A. Zhang, C. Xiao, Y. Wu, C. Li, Y. Ji, L. Li, W. Hu, Z. Wang, W. Ma, W. Li, *Macromolecules*, 2016, **49**, 6431.
- [21] W. Zhang, Y. Han, X. Zhu, Z. Fei, Y. Feng, N. D Treat, H. Faber, N. Stingelin, I. McCulloch, T. D Anthopoulos, Heeney, *Adv. Mater.*, 2016, **28**, 3922.
- [22] H. Chen, Y. Guo, G. Yu, Y. Zhao, J. Zhang, D. Gao, H. Liu, Y. Liu, *Adv. Mater.*, 2012, **24**, 4618.
- [23] A. R. Han, G. K. Dutta, J. Lee, H. R. Lee, S. M. Lee, H. Ahn, T. J. Shin, J. H. Oh, C. Yang, *Adv. Funct. Mater.*, 2015, **25**, 247.

- [24] H. Hoppe, T. Glatzel, M. Niggemann, W. Schwinger, F. Schaeffler, A. Hinsch, M.C LuxSteiner, N. S Sariciftci, *Thin Solid Films*, 2006, **511**, 587.
- [25] M. T. Rispens, A. Meetsma, R. Rittberger, C. J. Brabec, S. N. Sariciftci, J. C. Hummelen. *Chem. Commun.*, 2003, **17**, 2116.
- [26] J. M. Kroon, M. M. Wienk, W. J. H. Verhees, J. C. Hummelen, *Thin Solid Films*, 2002, **7**, 223.
- [27] S. Shao, F. Liu, Z. Xie, L. Wang. *J. Phys. Chem. C.*, 2010, **114**, 9161.
- [28] L. Qian, Y. Zheng, K. R. Choudhury, D. Bera, F. So, J. Xue, P.H. Holloway, *Nano Today*, 2010, **5**, 384.
- [29] D. K. Chambers, S. Selmic, *Mater. Res. Soc. Symp. Proc.*, 2005, **871**.
- [30] P. L. T. Boudreault, A. Najari, M. Leclerc, *Chem. Mater.*, 2011, **23**, 456.
- [31] Y. J. Cheng, S. H. Yang, C. S. Hsu, *Chem. Rev.*, 2009, **109**, 5868.
- [32] Y. Liang, Y. Luping. *Acc. Chem. Res.*, 2010, **43**, 1227.
- [33] W. Ma, C. Yang, X. Gong, K. Lee, A. J. Heeger, *Adv. Funct. Mater.*, 2005, **15**, 1617.
- [34] N. Blouin, A. Michaud, M. Leclerc, *Adv. Mater.*, 2007, **19**, 2295.
- [35] Z. M. Beiley, E. T. Hoke, R. Noriega, J. Dacuña, G. F. Burkhard, J. A. Bartelt, A. Salleo, M. F. Toney, M. D. McGehee, *Adv. Energy Mater.*, 2011, **47**, 954.
- [36] S. H. Park, A. Roy, S. Beaupré, S. Cho, N. Coates, J. S. Moon, D. Moses, M. Leclerc, K. Lee, A.J. Heeger, *Nat. Photon.*, 2009, **3**, 297.
- [37] Z. Zhu, D. Waller, R. Gaudiana, M. Morana, D. Muhlbacher, M. Scharber, C. Brabec, *Macromolecules*, 2007, **40**, 1981.
- [38] J. Hou, H. Y. Chen, S. Zhang, G. Li, Y. Yang, *J. Am. Chem. Soc.*, 2008, **130**, 16144.
- [39] P. Herguth, X. Jiang, M. S. Liu, A. K. Y. Jen, *Macromolecules*, 2002, **35**, 6094.
- [40] A. J. Campbell, D. D. C. Bradley, H. Antoniadis, *Appl. Phys. Lett.*, 2001, **79**, 2133.

- [41] C. R. McNeill, J. J. M. Halls, R. Wilson, G. L. Whiting, S. Berkebile, M. G. Ramsey, R. H. Friend, N. C. Greenham, *Adv. Funct. Mater.*, 2008, **18**, 2309.
- [42] R. Zhao, X. Zhan, J. Yao, G. Sun, Q. Chen, Z. Xie, Y. M., *Polym. Chem.*, 2013, **4**, 5382.
- [43] X. Zhang, X. Ji, S. Jiang, L. Liu, B. L. Weeks, Z. Zhang, *Green Chem.*, 2011, **13**, 1891.
- [44] E. Christophe, C. Andrew, F. U. Grimsdale, Y. Gang, S. Gordana and A. Mullen, *Adv. Mater.*, 2002, **14**, 11.
- [45] P. Sonar, J. Zhang, A. C. Grimsdale, K. Mullen, M. Surin, R. Lazzaroni, P. Leclerc, S. Tierney, M. Heeney, I. McCulloch, *Macromolecules*, 2004, **37**, 709.
- [46] E. W. Fager, *J. Am. Chem. Soc.*, 1945, **67**, 2217.
- [47] S. Guangyi, Z. Yingping, L. Yongfang, *J. Phys. Chem. C.*, 2008, **112**, 12058.
- [48] Y. Zhu, A. R. Rabindranath, T. Beyerlein, B. Tieke, *Macromolecules*, 2007, **40**, 6981.
- [49] D. Cao, Q. Liu, W. Zeng, S. Han, J. Peng, S. Liu, *J. Polym. Sci. Part A.*, 2006, **44**, 2395.
- [50] M. Ramos, M. T. Rispens, J. K. J. van Duren, J. C. Hummelen, R. A. J. Janssen, *J. Am. Chem. Soc.*, 2001, **123**, 6714.
- [51] H. G. Gilch, W. L. Wheelwright, *J. Polym. Sci. Part A: Polym Chem.*, 1966, **4**, 1337.
- [52] R. Li, Y. Mo, R. Shi, P. Li, C. Li, Z. Wang, S. Li, *Monatsh Chem.*, 2014, **145**, 85.
- [53] M. Granstrom, K. Petritsch, A. C. Arias, A. Lux, M. R. Andersson and R. H. Friend, *Nature.*, 1998, **395**, 257.

.....✂.....

**THEORETICAL STUDIES OF MONOMERS,
D-A UNITS AND POLYMERS**

- 3.1 Introduction
- 3.2 Theoretical Calculations
- 3.3 Results and Discussion
- 3.4 Conclusion

Design of conjugated polymeric materials with low band gap and suitable molecular orbital energy levels has been playing a key role in optoelectronic device fabrication. Theoretical designing is an appropriate method to accelerate the search of conjugated polymeric materials with desirable properties. A detailed description of Quantum Chemical calculations for the theoretical designing of conjugated polymers with suitable electronic and structural properties is presented. The properties of the designed polymers were investigated using Gaussian calculation setup. Optimization procedure involved quantum chemical calculations, based on density functional theory (DFT) methods. The conjugated polymers were optimized by applying periodic boundary condition (PBC). The methods provided valuable guidance for designing conjugated polymers with desirable device characteristics.

3.1 Introduction

Donor-acceptor (D-A) conjugated polymers are promising candidates for high mobility polymeric semiconductors.¹⁻³ By using different donor and acceptor units, absorption spectra and energy levels of conjugated polymers

can be easily tuned.^{4,5} For device applications, it is especially important to control the electronic band structure of the polymer to achieve a band gap of the desired magnitude and frontier orbitals of the proper energies. To attain such precise control over the polymer electronic structure is a key aspect for the advancement of the field, some methodologies should be developed.^{6a,b} The equally important thing is the control of physical properties of the materials. The development of novel polymers that are soluble in common organic solvents and processable by industrially relevant techniques, such as spin coating, spray-coating or roller coating, is necessary for the practical application of conjugated polymers. Such processable polymers with tailored electronic structures also possess the possibility to be multifunctional materials that can find application in numerous device architectures.

Special interesting classes of conjugated polymers are the soluble, low band gap polymers. Such polymers offer a broad range of attractive features for use in a variety of device architectures, such as a strong overlap with the solar spectrum (photovoltaics), ease of oxidation and reduction as well as the potential for high electron and hole mobility and a potentially transparent oxidized state. Although several approaches have been taken towards the development of low band gap polymers,^{6b,7} soluble and processable systems are rare. The major advantage of the donor-acceptor approach is that proper choice of the donor and acceptor groups allows one to select the approximate HOMO and LUMO energies of the resulting polymer. This is especially attractive for the development of polymers for electronic device applications. To increase the number of photons absorbed at peak solar wavelengths, it is necessary to shift the absorption spectrum of the donor polymer towards the

red end of the visible spectrum, and thus, the synthesis of new, low band gap polymers is required.⁸

To overcome the time consuming conventional chemical approach in synthesizing conducting polymers, the application of predictive computational design combined with chemical intuition leads to a more efficient approach. Theoretical calculations offer significant advantages like time and cost effectiveness and reduction in the number of synthetic targets for experimental design.⁹ The density functional theory (DFT) is presently the most successful quantum chemical approach to compute the electronic structures of polymers using the functional of the electron density.¹⁰ Pure local and gradient-corrected functionals (i.e., LDA and PBE) severely underestimate semiconductor band gaps and do not account for excitonic effects,¹¹⁻¹³ while hybrid functionals partially overcome this problem by mixing in a fraction of nonlocal Hartree-Fock exchange. Recently, methodological progress has been made in using range-separated DFT techniques for both molecular applications¹⁴⁻¹⁹ and periodic organic systems.²⁰ In particular, the recent Heyd Scuseria-Ernzerhof (HSE) functional²¹ incorporates a screened Hartree-Fock interaction for small distances and is, therefore, more computationally efficient than traditional hybrid functionals.

B. M. Wong et al. investigated the band structure and electronic properties in vinylene-linked heterocyclic polymers using density functional theory (DFT) calculations.⁹ They focussed on vinylene-linked polymers because, the vinylene group significantly enhances π -conjugation by delocalizing electrons along the backbone, leading to heterocyclic polymers with very low band gap values. DFT calculations utilize hybrid functionals

with fully periodic boundary conditions (PBC) to obtain accurate band gaps in these conjugated polymers.²²⁻²⁵ However, most of these studies are primarily focused on isolated oligomers and did not address band-structure properties in a fully-periodic geometry. The oligomer calculations are only approximate for molecular systems and unable to capture the full electronic band structure as a function of electron momentum. Molecular calculations on extended oligomers are incapable of determining whether a polymer has a direct (or indirect) band gap. Since the modelling of systems using oligomers can introduce spurious border effects related to the finite size of the oligomer, the use of fully-periodic approaches for an accurate description of band structure and band gap is mandatory.^{26,27}

3.2 Theoretical Calculations

The electronic and structural properties of the designed polymers were investigated using Gaussian calculation setup. Optimization procedure involved quantum chemical calculations, based on density functional theory (DFT) methods.¹⁰ Structure of Monomers and D-A units of the designed polymers were optimized by means of DFT at B3LYP (Becke's three parameter²⁸ hybrid functional using the Lee-Yang-Parr (LYP)²⁹ level of theory using 6-31G basis set.³⁰ In the case of polymers, as more and more donor-acceptor units are joined together, the overlapping of the π -orbitals spans a much wider range of energy level, and the energy gap (band gap, Eg.) between the highest occupied molecular orbital (often referred to as HOMO level) and the lowest unoccupied molecular orbital (referred to as the LUMO level) become smaller. HOMO and LUMO energy levels were obtained from the occupied and virtual energy values and this energy levels describe optoelectronic and electron transport

efficiencies of the donor-acceptor systems.³¹ The frontier molecular orbital distribution and band gap of monomers and D-A units of the polymers were obtained from energy calculations obtained by DFT using B3LYP/6-31G basis set. For the simplification in computational calculations, the long alkyl side chains on the donor and acceptor units were replaced with methyl groups and other types of substituents were retained as such. The backbone of the polymers were simplified to two repeating units.

Oscillator strength and activation energy of monomers and D-A units were obtained from Time-dependent density functional theory (TD-DFT) calculations using DFT/B3LYP and 6-31G formalism. The periodic boundary condition approach (PBC) was used to determine the electronic properties of copolymers. The PBC-DFT method was implemented in the Gaussian 09 package.³² To get a better fit with experiments, hybrid exchange correlation functionals were used in the PBC/DFT formalism. Widely used hybrid DFT methods include correlation functional B3LYP and HSE06 (full Heyd-Scuseria-Ernzerh functional).²⁰ The starting unit cell geometries for the PBC calculation were taken from the central portion of the optimized D-A unit and optimized inside a given lattice length on the constraints of periodic boundary condition by assuming that the unit cell was repeated identically an infinite number of times along the translation vector. Band structure in which lowest 4 unoccupied and highest 4 occupied bands in the positive region of the first Brillouin zone (between $k = 0$ and $k = \pi/a$) were plotted.³³

Oscillator strengths (f_{osc}) of all the monomers and donor-acceptor units of polymers were calculated using TD-DFT (B3LYP/6-31G) basis set. The present approach is able to provide a systematic evaluation of the electronic

properties of the polymers, and theoretical studies show that the computational methods used in the present studies can be applied for this purpose. Electronic structure, band gap, absorption and emission properties of polymers obtained from the studies suggest whether the designed polymers are good candidates for the intended applications or not.

3.3 Results and Discussion

Fluorene and 3,4-ethylenedioxythiophene based monomers, oligomers, and polymers have much synthetic flexibility and solution processability. The thiophene based polymers provide highly conducting and especially stable doped states. They also provide a range of optical properties with electronic band gaps varying across the entire visible spectrum, leading to enhanced redox properties and making them useful for numerous electrochemical and photovoltaic devices.³⁴ Academic and industrial researchers are interested in fluorene based polymers because of their optical and electrical properties. They have high photoluminescence quantum yields, which can be tuned to emit light throughout the entire visible region. They are currently being investigated for use in light-emitting diodes, field-effect transistors, and plastic solar cells.³⁵

Here, the theoretical investigation of thiophene and fluorene based monomers, donor-acceptor binary units and polymers have been performed to evaluate their electronic and optical properties by employing Gaussian 09. To investigate the effect of donor and acceptor strength of the polymeric backbone on the electronic properties and band gaps, different donor-acceptor combinations were taken into account. The present study focused on the effect of donor or acceptor strength of thiophene based and fluorene based

polymers and checked the electronic properties and band gap in such a way that the donor unit is fixed by keeping the acceptor unit constant and vice versa.

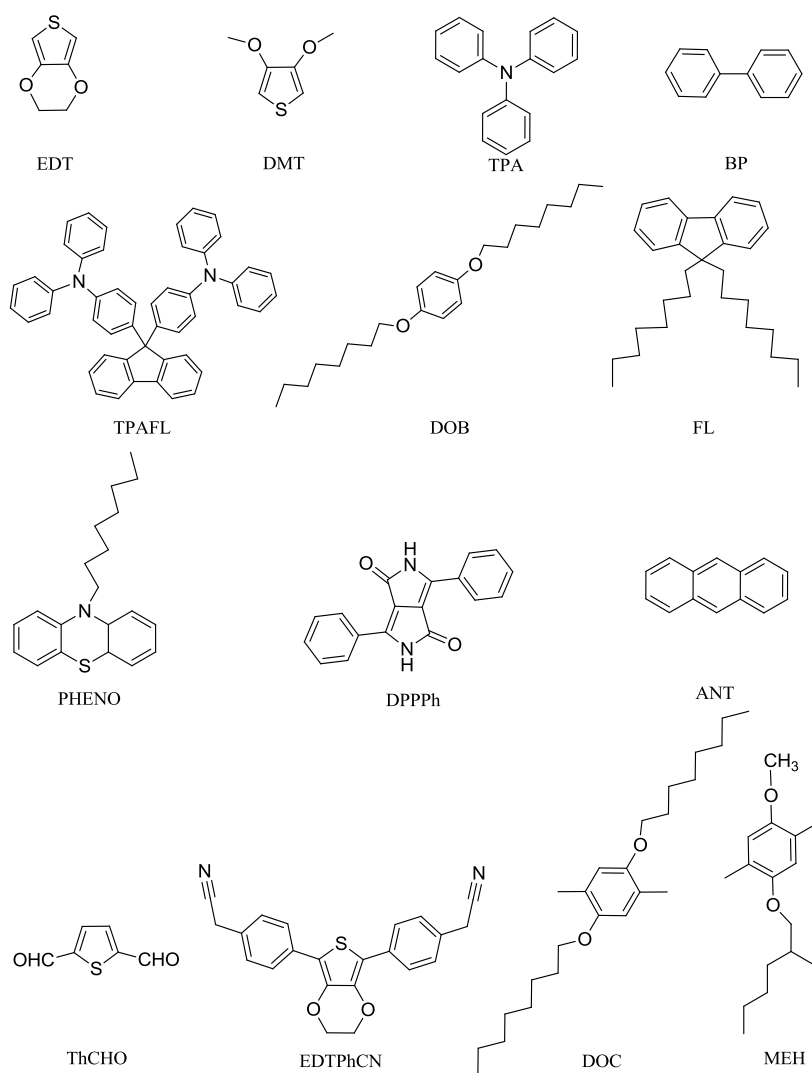


Figure 3.1: Building units as donor/acceptor moieties

Figure 3.1 gives the structure of monomer units taken for the theoretical investigation and thereby synthesis of polymers. All the monomers are abbreviated using appropriate symbols.

The above mentioned monomeric units were optimized by means of DFT/B3LYP/6-31G formalism. Figure 3.2 shows the optimized structure of the monomers.

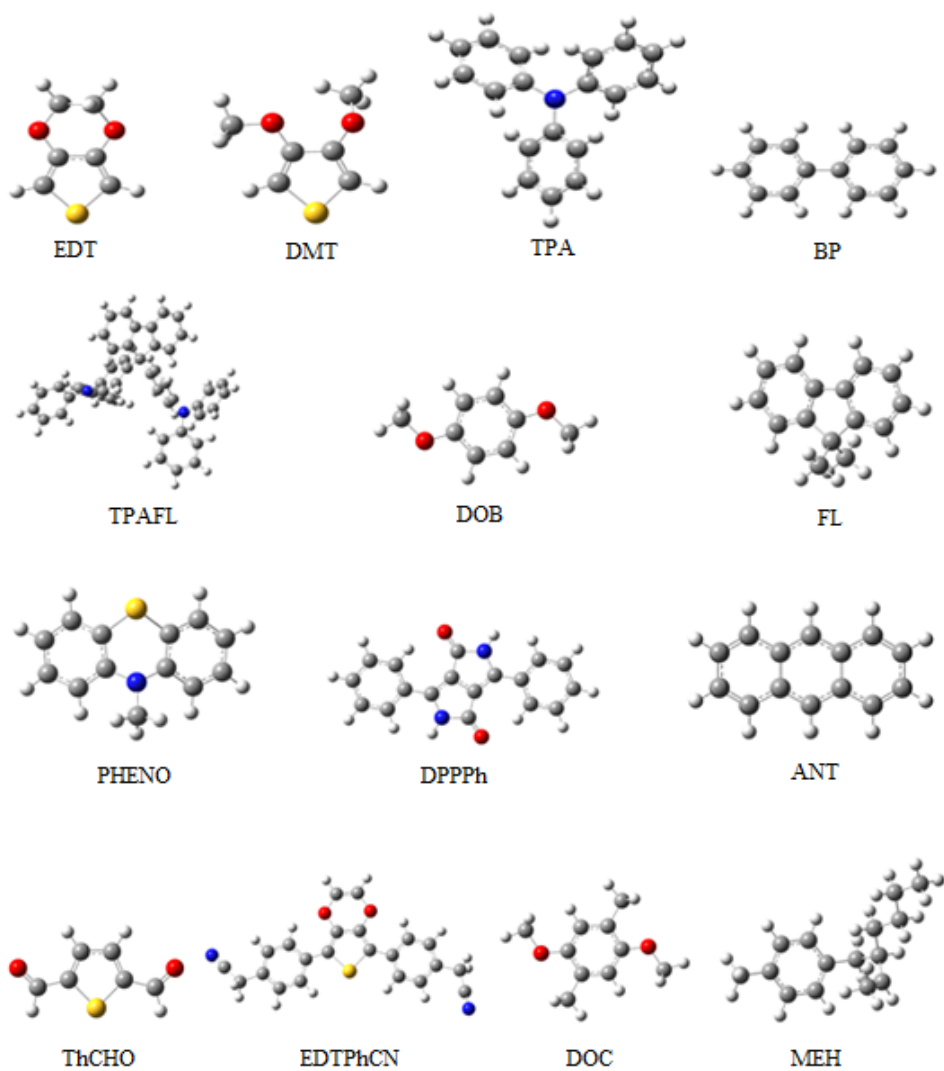


Figure 3.2: Optimized geometries of monomers obtained by DFT/B3LYP/6-31G

The HOMO and LUMO energy levels of all the monomers and donor-acceptor binary units of each polymer were optimized by DFT calculations. Vertical excitation energies, oscillator strength (f_{osc}) and excitation wave length of each monomer unit (Table 3.1) and donor-acceptor binary units (Table 3.2) were computed by applying Time Dependent – Density Functional Theory (TD-DFT) calculations on the optimized geometries and the values are tabulated. Absorption intensity of the polymer can be predicted by this method, which is an important factor governing the performance of the polymer.

Table 3.1: Energy values of $E_{excitation}$ (eV), f_{osc} and λ_{max} (nm) of the monomer units obtained by TD-DFT/B3LYP/6-31G

Monomer	f_{osc}	$E_{excitation}$ (eV)	λ_{max} (nm)
TPA	0.02	3.96	312
EDT	0.15	5.53	234
DOB	0.05	4.78	258
BP	0.54	4.82	257
PHENO	0.01	3.91	317
TPAFL	0.01	3.62	342
DPPPh	0.47	2.68	461
FL	0.26	4.69	263
DMT	0.14	5.34	232
ANT	0.06	3.35	370
DOC	0.07	4.85	255
MEH	0.06	4.84	256
EDTPhCN	0.08	3.56	348
ThCHO	0.42	4.26	290

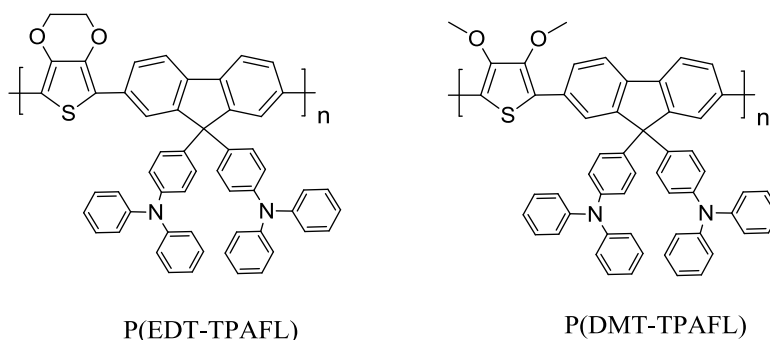
Table 3.2: Energy values of $E_{\text{excitation}}$ (eV), f_{osc} and λ_{max} (nm) of the donor-acceptor binary units obtained by TD-DFT/B3LYP/6-31G

D-A Unit	f_{osc}	$E_{\text{excitation}}$ (eV)	λ_{max} (nm)
EDT-TPAFL	0.003	3.14	395
DMT-TPAFL	0.004	3.12	397
EDT-TPA	0.67	3.34	370
DMT-TPA	0.65	3.39	365
EDT-DOB	0.26	3.91	316
FL-TPAFL	0.008	3.29	376
FL-DPPPh	0.96	2.51	493
FL-TPA	0.82	3.43	361
FL-BP	1.28	3.94	315
ANT-PHENO	0.03	3.02	410
DOC-MEH	0.85	3.59	345
EDPhCNThA	0.97	2.47	502

The absorption wavelengths arising from $S_0 \rightarrow S_1$ electronic transition increase progressively with the increase of conjugation length. It is reasonable to argue that HOMO \rightarrow LUMO transition is predominant in $S_0 \rightarrow S_1$ electronic transition. The results show that there is a decrease of the LUMO and an increase of the HOMO level resulting in a reduced band gap. From the investigations on the energy level and band gap values of the various monomers and donor-acceptor binary units, few polymers were designed and evaluated.

3.3.1 Thiophene Based Polymers

3.3.1.1 Band Structure of P(EDT-TPAFL) and P(DMT-TPAFL)



Here, a few thiophene based copolymers were designed and studied the electronic properties of monomers and donor-acceptor binary units. HOMO and LUMO energy levels of each monomeric and donor-acceptor binary unit were computed using DFT/B3LYP/6-31G level. The frontier molecular orbitals of each unit were obtained from the optimized structures. The energy level diagram of the monomers and D-A units of two thiophene based polymers, poly (3,4-ethylenedioxythiophene--9,9-bis(4-diphenylaminophenyl fluorene)), P(EDT-TPAFL) and poly (3,4-dimethoxythiophene--9,9-bis(4-diphenylaminophenyl fluorene)), P(DMT-TPAFL) were plotted together as one of the monomers is common for these two copolymers. It is observed that the HOMO level of 9,9-bis(4-diphenylaminophenyl fluorene) monomer, TPAFL unit is higher than that of EDT and DMT units showing higher donor strength. The HOMO level of TPAFL monomer is -5.42 eV where as in EDT monomers, it is -6.05 eV and for DMT monomer, it is -6.17 eV. The band gap calculated for three monomer units, EDT, DMT and TPAFL are 5.69 eV, 5.76 eV and 4.75 eV respectively. The band gap calculated for the two donor-

acceptor units EDT-TPAFL and DMT-TPAFL are 4.24 eV and 4.14 eV respectively. A reduction in band gap was observed when monomer units were joined to form single donor-acceptor unit. Here, from the frontier molecular orbitals of D-A units, it is clear that HOMO is localized on the TPAFL unit, which acts as the donor moiety. Computed energy and FMO sketches of HOMO-LUMO levels of monomers (EDT, DMT, and TPAFL) and D-A units (EDT-TPAFL, DMT-TPAFL) of designed polymers are shown in Figure 3.3.

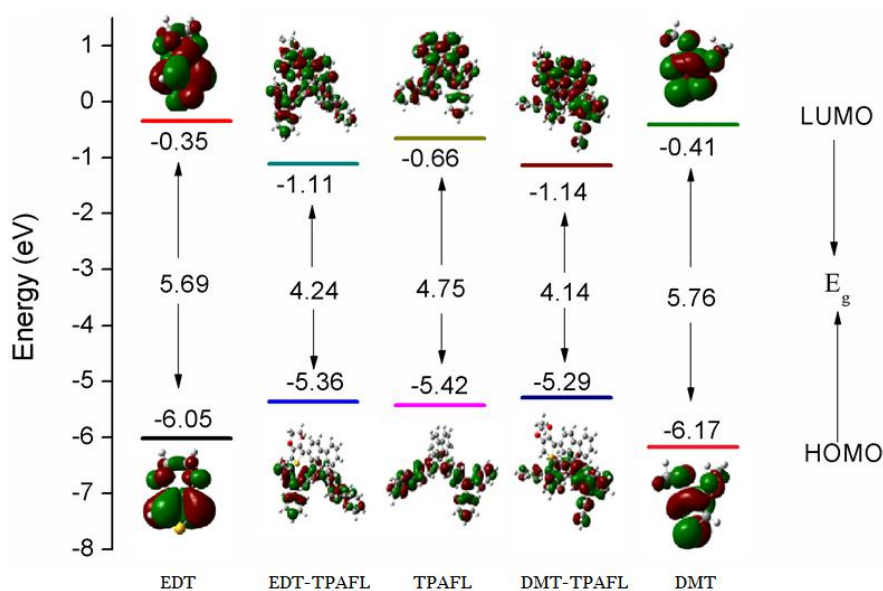


Figure 3.3: Sketch of DFT/B3LYP/6-31G computed energy and HOMO-LUMO levels of monomers (EDT, DMT, TPAFL) and D-A units (EDT-TPAFL, DMT-TPAFL)

The energy levels and band gap of the polymers were calculated by DFT/PBC/HSE06/6-31G method. The energy levels of the HOMO and LUMO were determined from the maximum point of the highest occupied

molecular orbital level and the minimum point of the lowest unoccupied molecular orbital levels respectively. The energy gap (E_g) is evaluated as the difference between the HOMO and LUMO energies. Band gap of the polymers, P(EDT-TPAFL) and P(DMT-TPAFL) are 2.27 eV and 2.36 eV respectively. The reduction in band gaps of two polymers from their corresponding donor-acceptor units are shown in Figure 3.4. Electronic band structures of the polymers are shown in Figure 3.5. All band structures were calculated using a 32 k -point mesh obtained from B3LYP/6-31G periodic DFT calculations. The lower blue lines denote valence bands, and the upper red lines represent conduction bands. The optimized repeating unit for the periodic boundary calculation is given in Figure 3.6. Horizontal line represents the translational vector which is equal to the one dimensional cell size.

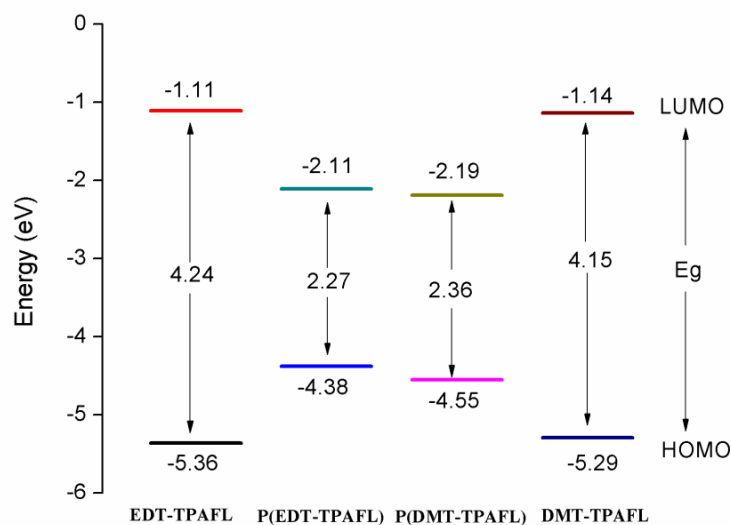


Figure 3.4: Sketch of computed energy levels of HOMO and LUMO for D-A units (EDT-TPAFL and DMT-TPAFL) and designed polymers P(EDT-TPAFL) and P(DMT-TPAFL)

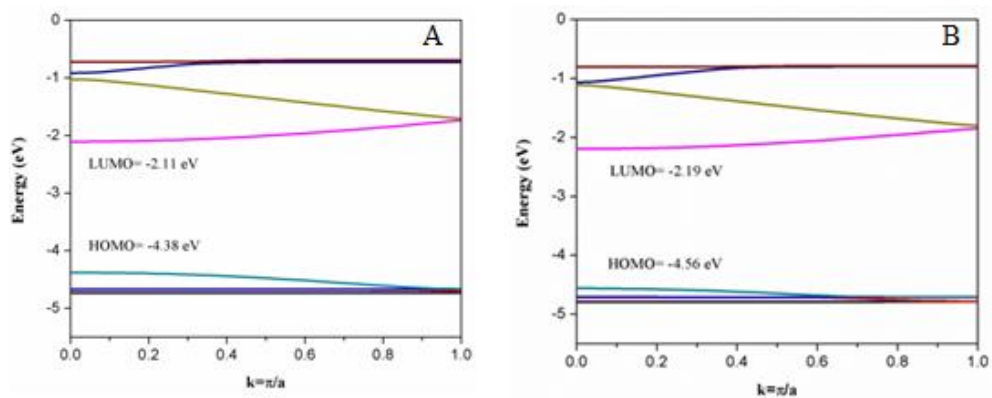


Figure 3.5: Band structure of (A) P(EDT-TPAFL) and (B) P(DMT-TPAFL).

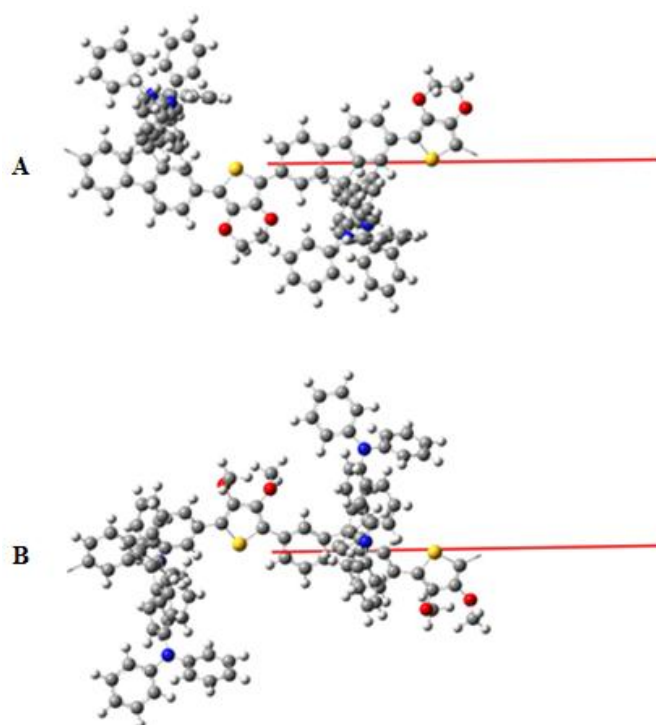
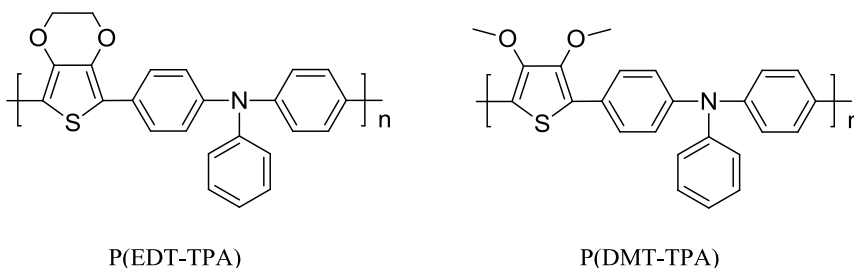


Figure 3.6: Unit cell of the Polymers (A) P(EDT-TPAFL) and (B) P(DMT-TPAFL) for PBC/HSE06/6-31G calculation. Red line represents the translational vector

3.3.1.2 Band Structure of P(EDT-TPA) and P(DMT-TPA)



The energy level diagram of the monomers and D-A units of another set of two thiophene based polymers, P(EDT-TPA) and P(DMT-TPA) were plotted together as one of the monomers is common for these two copolymers. It is observed that the HOMO level of triphenylamine monomer unit is higher than that of EDT and DMT units showing higher donor strength. The HOMO level of TPA monomer is -5.82 eV whereas in EDT monomers, it is -6.05 eV and for DMT monomer, it is -6.17 eV. The band gap calculated for three monomer units, EDT, DMT and TPAFL are 5.69 eV, 5.76 eV and 5.26 eV respectively. The band gap calculated for the two donor-acceptor units EDT-TPA and DMT-TPA are 4.43 eV and 4.49 eV respectively. A reduction in band gap was observed when monomer units were joined to form single donor-acceptor unit. Here, from the frontier molecular orbitals of D-A units, it is clear that HOMO is localized on the TPA unit, which acts as the donor moiety. Computed energy and FMO sketches of HOMO-LUMO levels of monomers (EDT, DMT, and TPA) and D-A units (EDT-TPA, DMT-TPA) of designed polymers are shown in Figure 3.7.

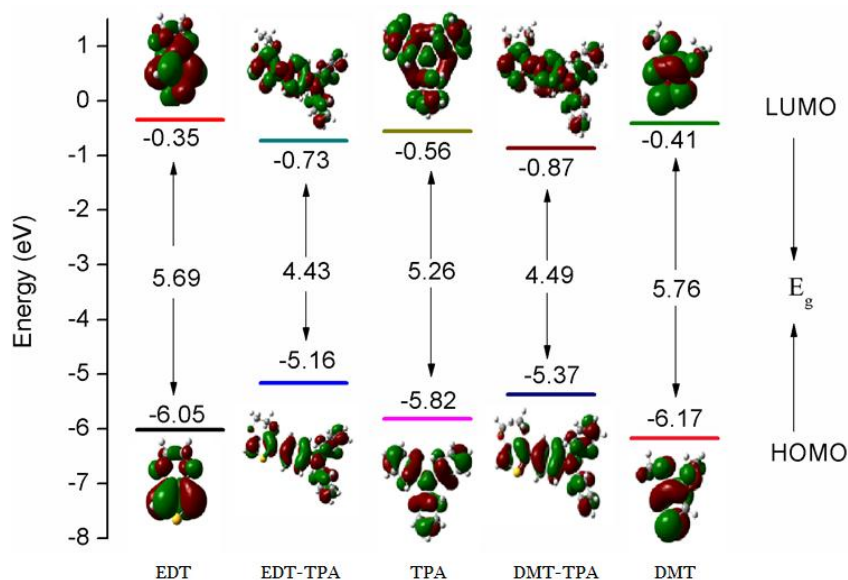


Figure 3.7: Sketch of DFT/B3LYP/6-31G computed energy and HOMO-LUMO levels of monomers (EDT, DMT, TPA) and D-A units (EDT-TPA, DMT-TPA)

The energy levels of the HOMO and LUMO of polymers were determined from the maximum point of the highest occupied molecular orbital level and the minimum point of the lowest unoccupied molecular orbital levels respectively by DFT/PBC/HSE06/6-31G method. The band gap is evaluated as the difference between the HOMO and LUMO energies. Band gap of the polymers, P(EDT-TPA) and P(DMT-TPA) are 2.53 eV and 2.77 eV respectively. The reduction in band gaps of two polymers from their corresponding donor-acceptor units are shown in Figure 3.8. Electronic band structures of the polymers are shown in Figure 3.9. All band structures were calculated using a 32 k -point mesh obtained from B3LYP/6-31G periodic DFT calculations. The lower lines denote valence bands, and the upper lines represent conduction bands. The optimized repeating unit for the

periodic boundary calculation is given in Figure 3.10. Horizontal line represents the translational vector which is equal to the one dimensional cell size.

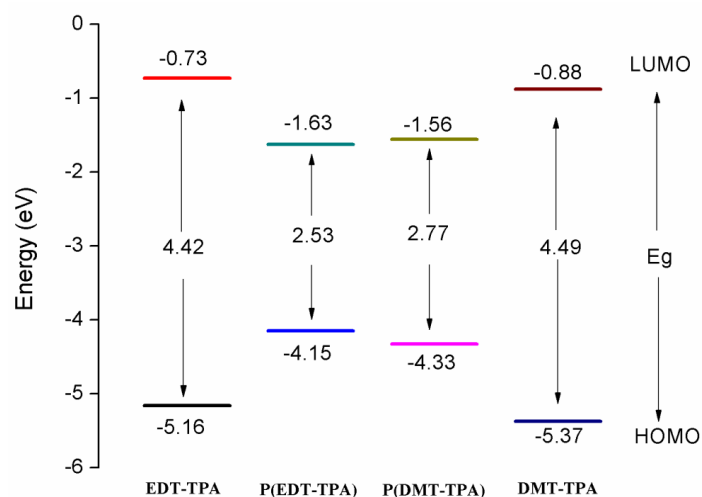


Figure 3.8: Sketch of computed energy levels of HOMO and LUMO for D-A units (EDT-TPA and DMT-TPA) and designed polymers P(EDT-TPA) and P(DMT-TPA)

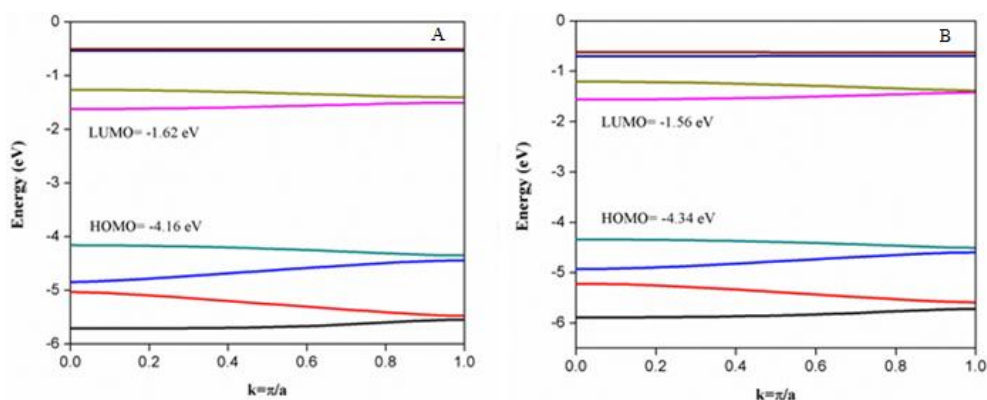


Figure 3.9: Band structure of (A) P(EDT-TPA) and (B) P(DMT-TPA)

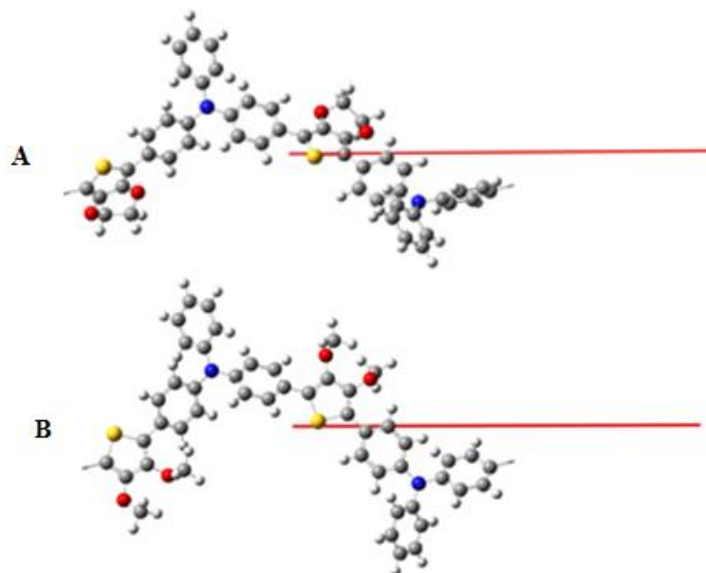
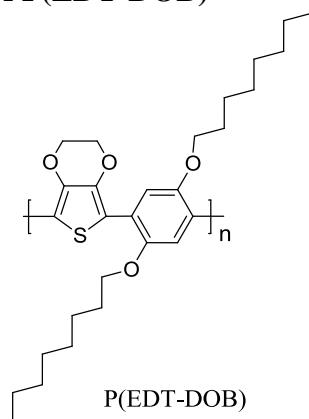


Figure 3.10: Unit cell of the Polymers (A) P(EDT-TPA) and (B) P(DMT-TPA) for PBC/HSE06/6-31G calculation. Red line represents the translational vector

3.3.1.3 Band Structure of P(EDT-DOB)



The energy levels and band gap of the polymer, P(EDT-DOB) was calculated by DFT/PBC/HSE06/6-31G formalism. The energy levels of the HOMO and LUMO of monomers and D-A binary unit were calculated from occupied and virtual eigen values respectively which were obtained from raw data output of DFT/B3LYP/6-31G calculation. The band gap is evaluated as

the difference between the HOMO and LUMO energies. The energy level diagram of the monomers and D-A unit of thiophene based polymer, P(EDT-DOB) was plotted. It is observed that the HOMO level of 1,4-dioctyloxybenzene (DOB) monomer unit is higher than that of EDT unit showing higher donor strength. The HOMO level of DOB monomer is -5.74 eV where as in EDT monomer, it is -6.05 eV. The band gap calculated for two monomer units, EDT and DOB are 5.69 eV and 5.44 eV respectively. The band gap calculated for the donor-acceptor unit EDT-DOB is 4.54 eV. A reduction in band gap was observed when monomer units were joined to form single donor-acceptor unit. Here, from the frontier molecular orbitals of D-A unit, it is clear that HOMO is localized on the DOB unit, which acts as the donor moiety. Computed energy and FMO sketches of HOMO-LUMO levels of monomers (EDT and DOB) and D-A unit (EDT-DOB) of designed polymer are shown in Figure 3.11.

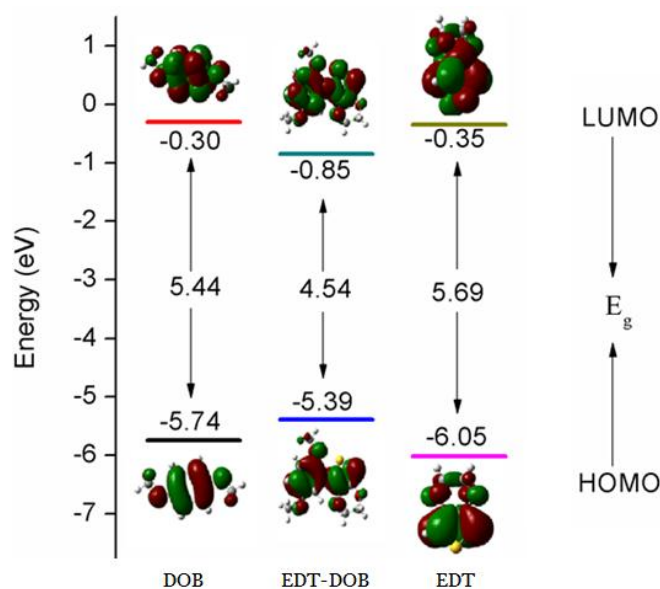


Figure 3.11: Sketch of DFT/B3LYP/6-31G computed energy and HOMO-LUMO levels of monomers (EDT and DOB) and D-A unit (EDT-DOB)

Band gap of the polymer, P(EDT-DOB) was obtained as 2.44 eV. The reduction in band gap of the polymer from its corresponding donor-acceptor unit is shown in Figure 3.12. Electronic band structure of the polymer is shown in Figure 3.13. The band structures were calculated using a 32 k -point mesh obtained from B3LYP/6-31G periodic DFT calculations. The lower blue lines denote valence bands, and the upper red lines represent conduction bands. The optimized repeating unit for the periodic boundary calculation is given in Figure 3.14. Horizontal line represents the translational vector which is equal to the one dimensional cell size.

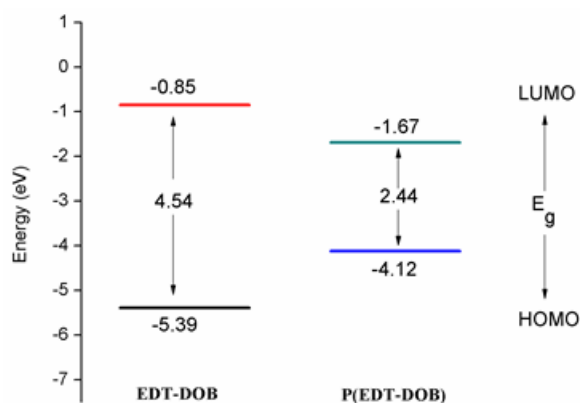


Figure 3.12: Sketch of computed energy levels of HOMO and LUMO for D-A unit (EDT-DOB) and designed polymer P(EDT-DOB)

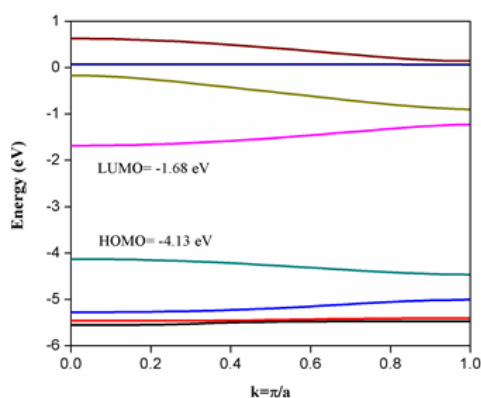


Figure 3.13: Band structure of P(EDT-DOB)

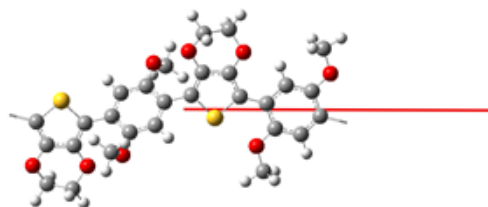
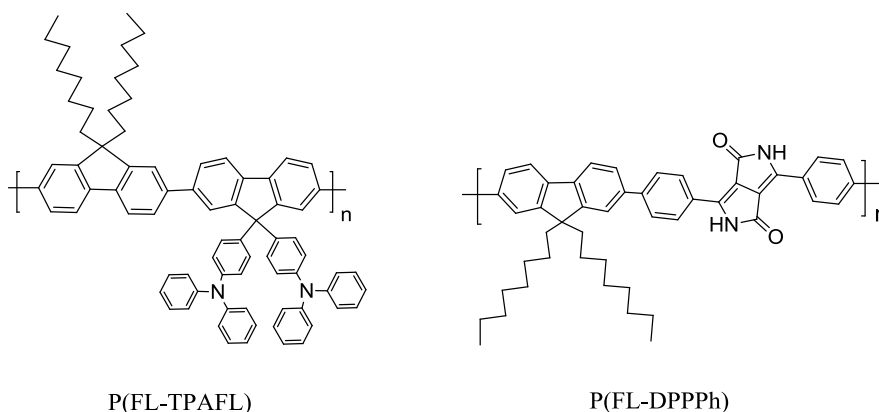


Figure 3.14: Unit cell of the Polymer P(EDT-DOB) for PBC/HSE06/6-31G calculation. Red line represents the translational vector

3.3.2 Fluorene Based Polymers

3.3.2.1 Band Structure of P(FL-TPAFL) and P(FL-DPPPh)



A few fluorene based copolymers were designed and the electronic properties of monomers and donor-acceptor binary units were studied. The energy level diagram of the monomers and D-A units of first set of two fluorene based polymers, P(FL-TPAFL) and P(FL-DPPPh) were plotted together as one of the monomers is common for these two copolymers. It is observed that the HOMO level of 9,9-bis (4-diphenylaminophenyl fluorene) monomer (TPAFL) unit is higher than that of 9,9-dioctylfluorene (FL) monomer showing higher donor strength of TPAFL monomer unit. Whereas, the HOMO level of diketopyrrolopyrrole monomer (DPPPh) unit is lower

than that of 9,9-dioctylfluorene (FL) monomer showing higher acceptor strength of DPPPh unit when compared to the FL unit. The HOMO levels of TPAFL and DPPPh monomers are -5.42 eV and -5.92 eV, whereas in FL monomers, it is -5.73 eV. The band gap calculated for three monomer units, TPAFL, FL and DPPPh are 4.75 eV, 5.09 eV and 3.09 eV respectively. The band gap calculated for the two donor-acceptor units FL-TPAFL and FL-DPPPh are 4.13 eV and 2.77 eV respectively. Here, from the frontier molecular orbitals of D-A unit, FL-TPAFL, it is clear that HOMO is localized on the TPAFL unit, which acts as the donor moiety. But in the case of FL-DPPPh, HOMO is localized on the 9,9-dioctylfluorene (FL) unit. Computed energy and FMO sketches of HOMO-LUMO levels of monomers (TPAFL, FL and DPPPh) and D-A units (FL-TPAFL and FL-DPPPh) of designed polymers are shown in Figure 3.15.

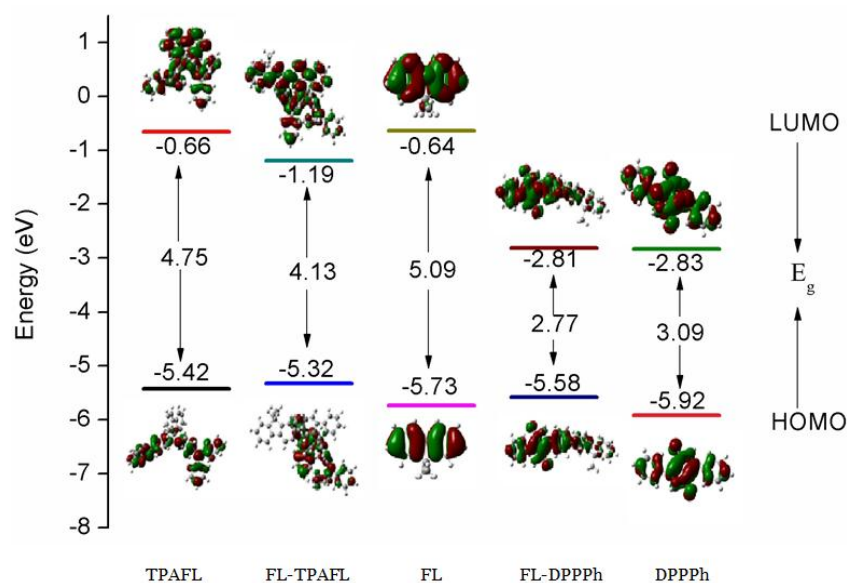


Figure 3.15: Sketch of DFT/B3LYP/6-31G computed energy and HOMO-LUMO levels of monomers (FL, TPAFL, DPPPh) and D-A units (FL-TPAFL, FL-DPPPh)

The band gap is evaluated as the difference between the HOMO and LUMO energies which were obtained directly from the raw data output of DFT/PBC/HSE06/6-31G calculation. Band gap of the polymers, P(FL-TPAFL) and P(FL-DPPPh) are 2.80 eV and 1.96 eV respectively. The reduction in band gap of the two polymers from their corresponding donor-acceptor units is shown in Figure 3.16. Electronic band structures of the polymers are shown in Figure 3.17. All band structures were calculated using a 32 k -point mesh obtained from B3LYP/6-31G periodic DFT calculations. The lower lines denote valence bands, and the upper lines represent conduction bands. The optimized repeating unit for the periodic boundary calculation is given in Figure 3.18. Horizontal line represents the translational vector which is equal to the one dimensional cell size.

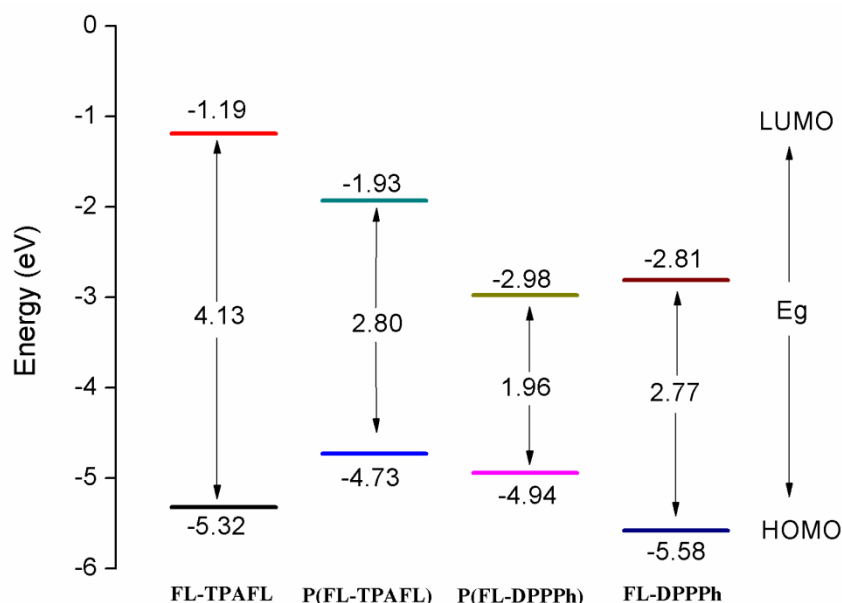


Figure 3.16: Sketch of computed energy levels of HOMO and LUMO for D-A units (FL-TPAFL and FL-DPPPh) and designed polymers P(FL-TPAFL) and P(FL-DPPPh)

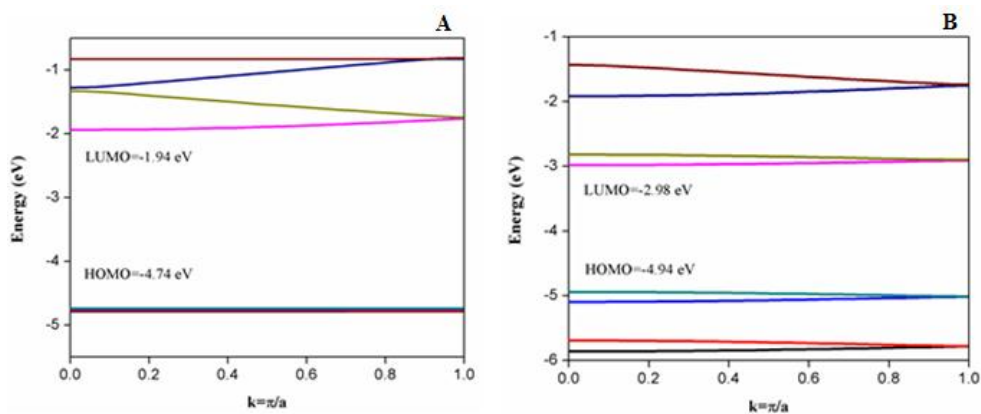


Figure 3.17: Band structure of (A) P(FL-TPAFL) and (B) P(FL-DPPPh)

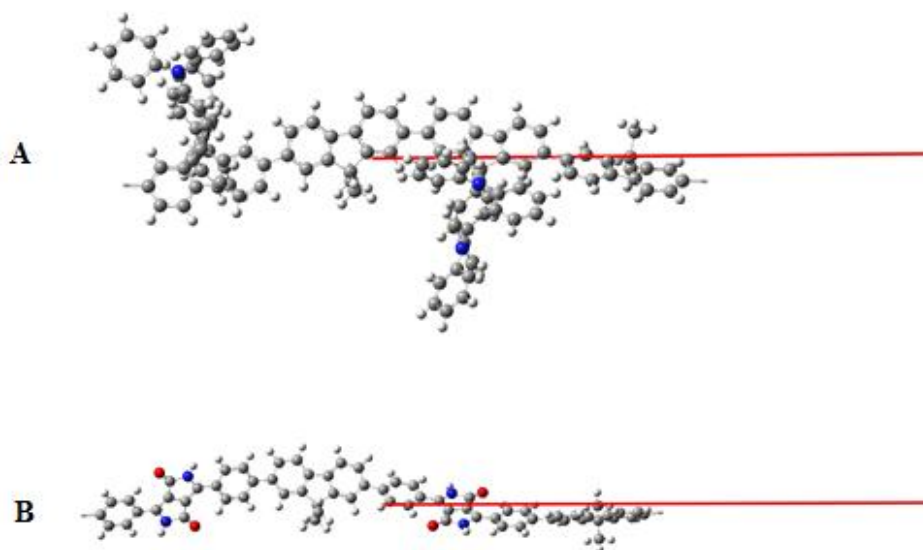
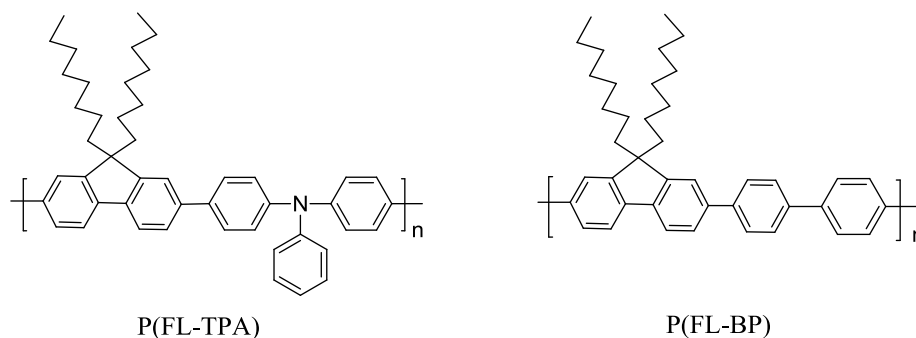


Figure 3.18: Unit cell of the Polymers (A) P(FL-TPAFL) and (B) P(FL-DPPPh) for PBC/HSE06/6-31G calculation. Red line represents the translational vector

3.3.2.2 Band Structure of P(FL-TPA) and P(FL-BP)



The energy level diagram of the monomers and D-A units of second set of two fluorene based polymers, P(FL-TPA) and P(FL-BP) were plotted together as one of the monomers is common for these two copolymers. It is observed that the HOMO level of 9,9-dioctylfluorene (FL) monomer unit is higher than that of both TPA and BP monomer units showing higher donor strength of FL monomer unit. The HOMO levels of TPA and BP monomers are -5.82 eV and -5.96 eV respectively, where as in FL monomer, it is -5.73 eV. The band gap calculated for three monomer units, TPA, FL and BP are 5.26 eV, 5.09 eV and 5.15 eV respectively. The band gap calculated for the two donor-acceptor units FL-TPA and FL-BP are 4.18 eV and 4.27 eV respectively. A reduction in band gap was observed when monomer units were joined to form single donor-acceptor unit because of the extended conjugation. Here, from the frontier molecular orbitals of D-A units, it is clear that HOMO is localized on the FL unit, which acts as the donor moiety. Computed energy and FMO sketches of HOMO-LUMO levels of monomers (TPA, FL, and BP) and D-A units (FL-TPA, FL-BP) of designed polymers are shown in Figure 3.19.

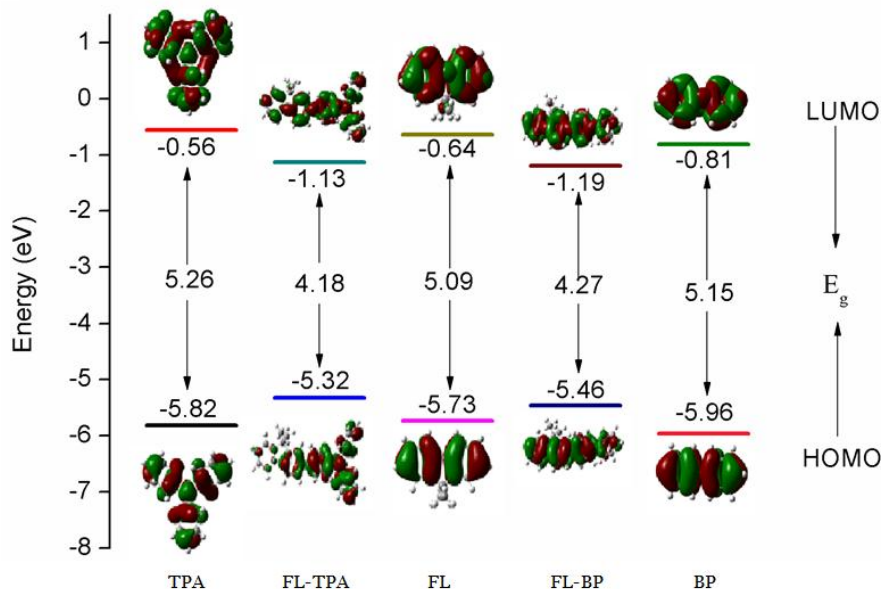


Figure 3.19: Sketch of DFT/B3LYP/6-31G computed energy and HOMO-LUMO levels of monomers (FL, TPA, BP) and D-A units (FL-TPA, FL-BP)

The energy levels and band gap of the polymers were calculated by DFT/PBC/HSE06/6-31G method. The HOMO and LUMO energies were obtained directly from the output. Band gap of the polymers, P(FL-TPA) and P(FL-BP) are 2.94 eV and 3.27 eV respectively. The reduction in band gaps of two polymers from their corresponding donor-acceptor units are shown in Figure 3.20. Electronic band structures of the polymers are shown in Figure 3.21. All band structures were calculated and plotted using a 32 k -point mesh obtained from B3LYP/6-31G periodic DFT calculations. The lower lines denote valence bands, and the upper lines represent conduction bands. The optimized repeating unit for the periodic boundary calculation is given in Figure 3.22. Horizontal line represents the translational vector which is equal to the one dimensional cell size.

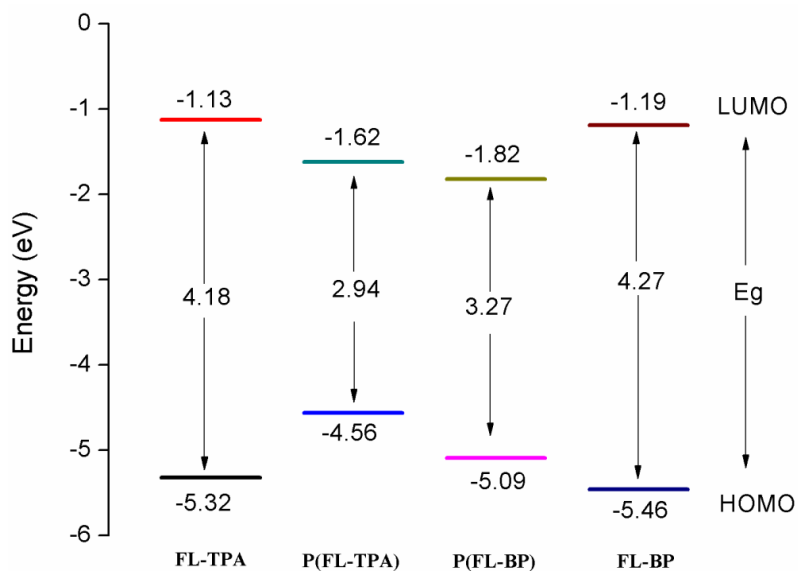


Figure 3.20: Sketch of computed energy levels of HOMO and LUMO for D-A units (FL-TPA and FL-BP) and designed polymers P(FL-TPA) and P(FL-BP)

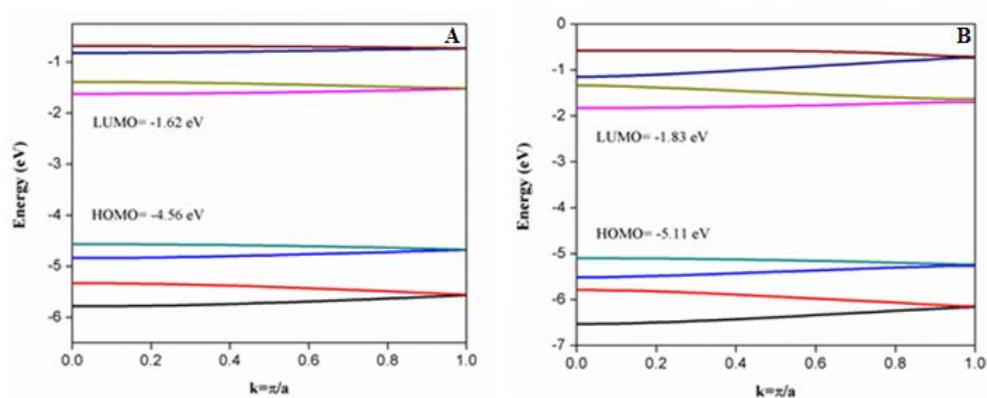


Figure 3.21: Band structure of (A) P(FL-TPA) and (B) P(FL-BP)

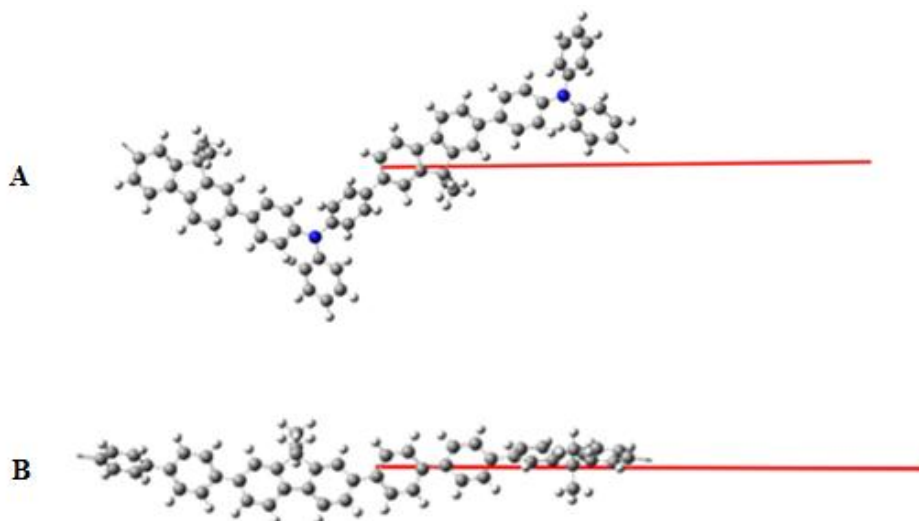
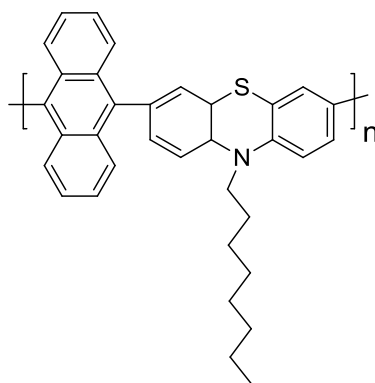


Figure 3.22: Unit cell of the Polymers (A) P(FL-TPA) and (B) P(FL-BP) for PBC/HSE06/6-31G calculation. Red line represents the translational vector

3.3.3 Anthracene-phenothiazine Polymer



P(ANT-PHENO)

The energy level diagram of the monomers and D-A unit of anthracene-phenothiazine polymer, P(ANT-PHENO) was plotted. It is observed that the HOMO level of N-octyl phenothiazine (PHENO) monomer unit is higher than that of anthracene unit (ANT) showing higher donor strength. The

HOMO level of PHENO unit is -4.98 eV whereas in ANT unit, it is -5.28 eV. The band gap calculated for two monomer units, PHENO and ANT are 4.43 eV and 3.34 eV respectively. The band gap calculated for the donor-acceptor unit ANT-PHENO is 2.90 eV. A reduction in band gap was observed when monomer units were joined to form single donor-acceptor unit. Computed energy and FMO sketches of HOMO-LUMO levels of monomeric units (PHENO and ANT) and D-A unit (ANT-PHENO) of designed polymer are shown in Figure 3.23.

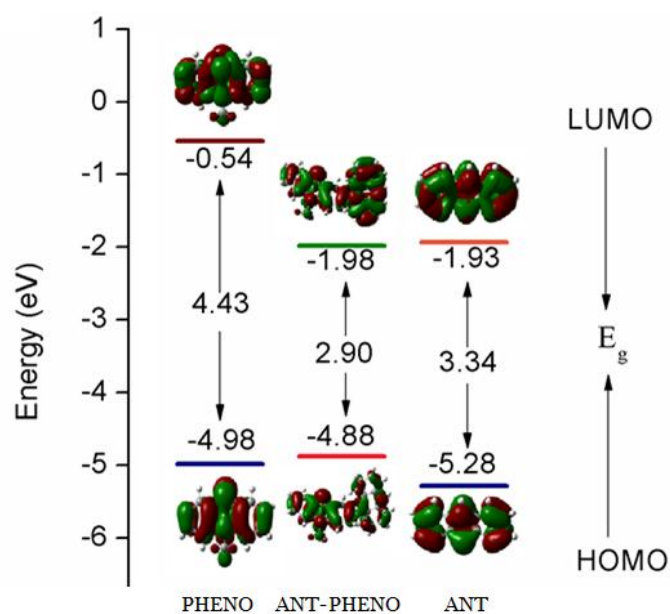


Figure 3.23: Sketch of DFT/B3LYP/6-31G computed energy and HOMO-LUMO levels of monomers (PHENO and ANT) and D-A unit (ANT-PHENO)

The band gap of the polymer, P(ANT-PHENO) is 2.85 eV. The reduction in band gap of the polymer from its corresponding donor-acceptor unit is shown in Figure 3.24. Electronic band structure of the polymer is shown in

Figure 3.25. The band structure was calculated using a 32 k -point mesh obtained from B3LYP/6-31G periodic DFT calculations. The lower lines denote valence bands, and the upper lines represent conduction bands. The optimized repeating unit for the periodic boundary calculation is given in Figure 3.26. Horizontal line represents the translational vector which is equal to the one dimensional cell size.

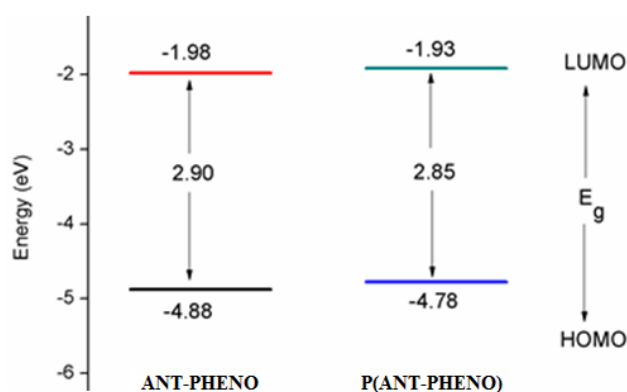


Figure 3.24: Sketch of computed energy levels of HOMO and LUMO for D-A unit (ANT-PHENO) and designed polymer P(ANT-PHENO)

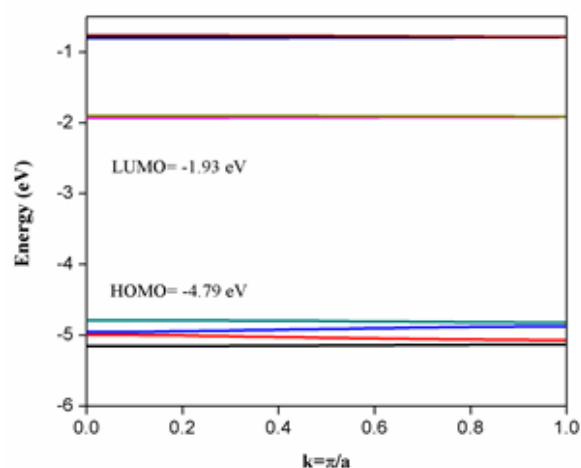


Figure 3.25: Band structure of P(ANT-PHENO)

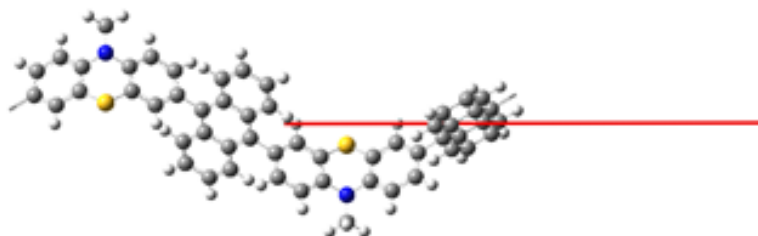
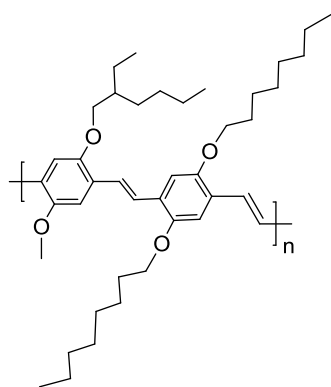


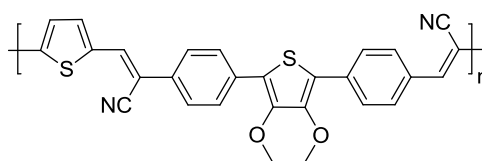
Figure 3.26: Unit cell of the polymer P(ANT-PHENO) for PBC/HSE06/6-31G calculation. Red line represents the translational vector

3.3.4 Phenylenevinylene Polymers

Generally, a conjugated polymer has three major components like conjugated backbone, side chains and substituents. In addition to the main chain, substituents and side chains also determine the electronic properties of the polymers.³⁶ Here, two Phenylenevinylene polymers, one with electron withdrawing cyano group and one without cyano group were considered for evaluating their electronic properties by theoretical methods.



DOC-MEH PPV



EDTh CN PPV

DFT studies of a set of two phenylenevinylene polymers were performed including the electronic properties of monomers and their binary units. The most appropriate theoretical tool for studying their properties is DFT and TD-DFT (Time Dependent Density Functional Theory). HOMO and LUMO energy levels of each monomeric and binary units were computed using DFT/B3LYP/6-31G level. The frontier molecular orbitals of each unit were obtained from the optimized structures. The energy level diagram of the monomers and polymers, DOC-MEH PPV and EDTh CN PPV were plotted together. It is observed that the HOMO level of 1,4-dioctyloxybenzene (DOC) unit is higher than that of 1-((2-ethylhexyl)oxy)-4-methoxybenzene (MEH) unit, showing higher donor strength of DOC monomer unit. Whereas, the HOMO level of EDTPhCN unit is higher than that of thiophene 2,5-dicarboxaldehyde (ThCHO) monomer showing higher donor strength of EDTPhCN unit. The HOMO levels of DOC and MEH monomers are -5.48 eV and -5.84 eV. The HOMO levels of EDTPhCN and ThCHO units are -5.32 eV and -7.13 eV, respectively. The band gap calculated for the monomer units, DOC, MEH, EDThCN and ThCHO are 5.47 eV, 5.77 eV, 3.52 eV and 2.87 eV respectively. The band gap calculated for the donor-acceptor units DOC-MEH and EDPhCNThA are 4.38 eV and 2.97 eV respectively. A reduction in band gap was observed when monomer units were joined to form single donor-acceptor unit. Computed energy and FMO sketches of HOMO-LUMO levels of monomers and binary units of designed polymers are shown in Figure 3.27.

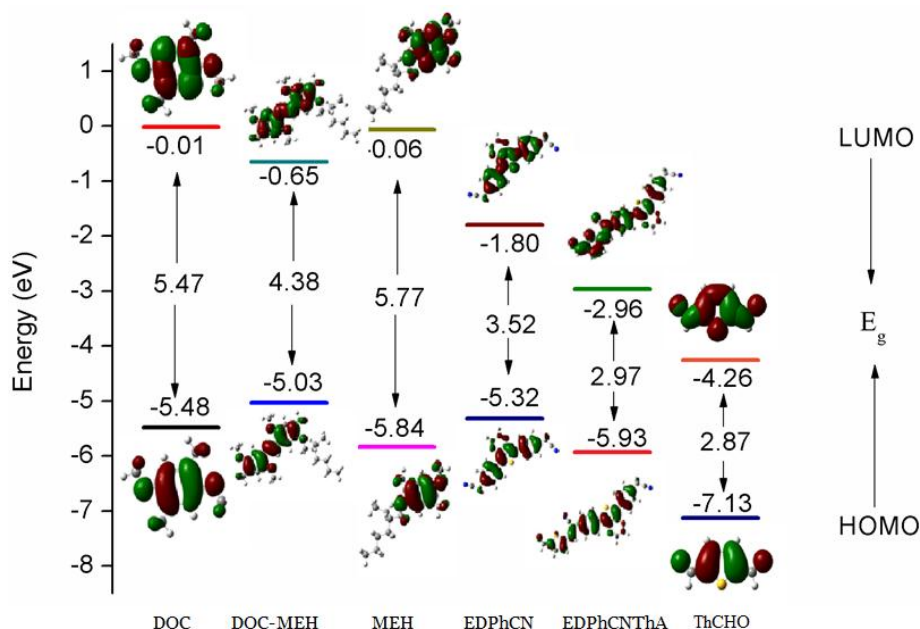


Figure 3.27: Sketch of DFT/B3LYP/6-31G computed energy and HOMO-LUMO levels of monomeric units and D-A units

The band gap of the PPV polymers, DOC-MEH PPV and EDTh CN PPV obtained directly from the raw data output of DFT/PBC/HSE06/6-31G calculation and the values are 1.79 eV and 1.81 eV respectively. The reduction in band gaps of two polymers from their corresponding donor-acceptor units are shown in Figure 3.28. Electronic band structures of the polymers are shown in Figure 3.29. All band structures were calculated using a 32 k -point mesh obtained from B3LYP/6-31G periodic DFT calculations. The lower lines denote valence bands, and the upper lines represent conduction bands. The optimized repeating unit for the periodic boundary calculation is given in Figure 3.30. Horizontal lines represent the translational vector which are equal to the one dimensional cell size.

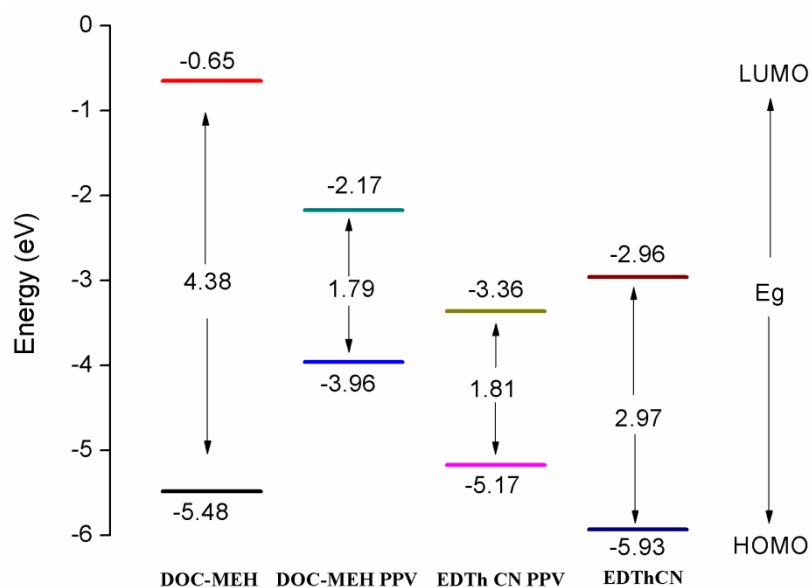


Figure 3.28: Sketch of computed energy levels of HOMO and LUMO for D-A units (FL-TPA and FL-BP) and designed polymers DOC-MEH PPV and EDTh CN PPV

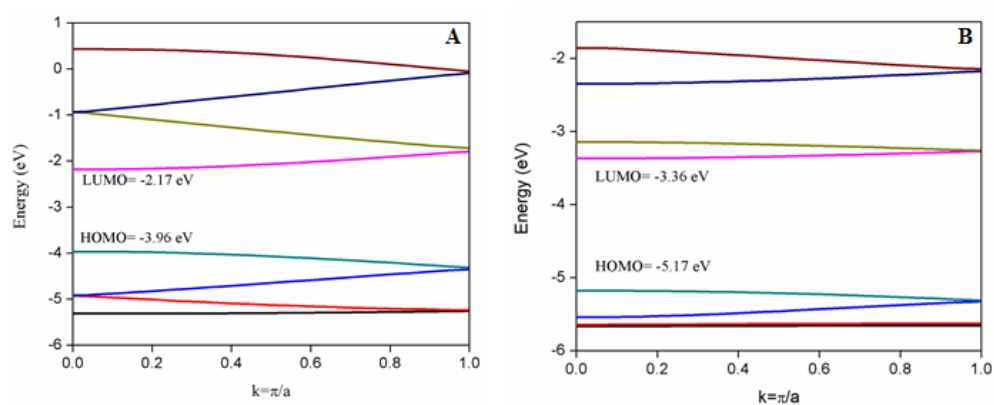


Figure 3.29: Band structure of (A) DOC-MEH PPV and (B) EDTh CN PPV

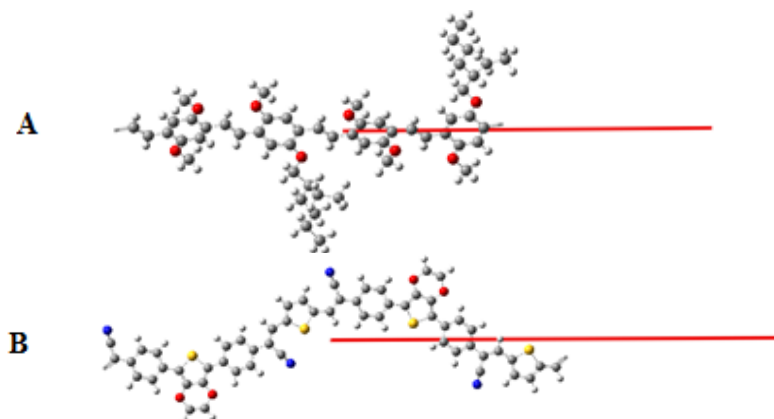


Figure 3.30: Unit cell of the Polymers (A) DOC-MEH PPV and (B) EDTh CN PPV for PBC/HSE06/6-31G calculation. Red line represents the translational vector

3.4 Conclusion

Twelve polymers were designed and their electronic structures were calculated using PBC/HSE06/6-31G method. Out of twelve polymers, five are thiophene based, four are fluorene based, one is phenothiazine based and remaining two are phenylenevinylene polymers. The frontier molecular orbitals of monomers and donor acceptor units of all the polymers were obtained from the energy calculations using DFT/B3LYP/6-31G formalism. It was found that the HOMO and the LUMO energy levels of the monomers are very important factors to determine whether effective charge transfer will take place between donor and acceptor. The reduction of band gap is a function of the acceptor or donor strength. Studies implied that different structural variations, especially the type of monomeric units play key role on the electronic properties (HOMO and LUMO) of the polymers. Time-dependent DFT (TD-DFT) calculations were performed to assess the excited-state vertical transition energies and oscillator strengths based on the optimized molecular geometries.

References

- [1] H. Siringhaus, *Adv. Mater.*, 2014, **26**, 1319.
- [2] Z. Yi, S. Wang, Y. Liu, *Adv. Mater.*, 2015, **27**, 3589.
- [3] S. Holliday, J. E. Donaghey, I. McCulloch, *Chem. Mater.*, 2014, **26**, 647.
- [4] E. Wang, W. Mammo, M. R. Andersson, *Adv. Mater.*, 2014, **26**, 1801.
- [5] H. Usta, C. Newman, Z. Chen, A. Faccetti, *Adv. Mater.*, 2012, **24**, 3678.
- [6] (a) A. Moliton, R. C. Hiorns, *Polym. Int.*, 2004, **53**, 1397.
(b) J. Roncali, *Chem. Rev.*, 1997, **97**, 173.
- [7] H. A. M. Van Mullekom, J. A. J. M. Vekemans, E. E. Havinga, E. W. Meijer, *Mater. Sci. Eng.*, 2001, **32**, 1.
- [8] C. Winder, N. S. Sariciftci, *J. Mater. Chem.*, 2004, **14**, 1077.
- [9] B. M. Wong, D. Lacina, I. M. B. Nielsen, J. Graetz, M. D. Allendorf, *J. Phys. Chem. C.*, 2011, **115**, 7778.
- [10] R. G. Parr and W. Yang, *Density-Functional Theory of Atoms and Molecules*, Oxford University Press, New York, 1989.
- [11] S. Tretiak, K. Igumenshchev, V. Chernyak, *Phys. Rev. B.*, 2005, **71**, 033201.
- [12] B. M. Wong, *J. Phys. Chem. C.*, 2009, **113**, 21921.
- [13] B. M. Wong, T. H. Hsieh, *J. Chem. Theory Comput.*, 2010, **6**, 3704.
- [14] B. M. Wong, J. G. Cordaro, *J. Chem. Phys.*, 2008, **129**, 214703.
- [15] B. M. Wong, M. Piacenza, F. Della Sala, *Phys. Chem. Chem. Phys.*, 2009, **11**, 4498.
- [16] D. Jacquemin, E. A. Perpète, G. Scalmani, M. J. Frisch, R. Kobayashi, C. Adamo, *J. Chem. Phys.*, 2007, **126**, 144105

- [17] D. Jacquemin, E. A. Perpète, O. A. Vydrov, G. E. Scuseria, C. J. Adamo, *Chem. Phys.*, 2007, **127**, 094102.
- [18] D. Jacquemin, E. A. Perpète, G. E. Scuseria, I. Ciofini, C. Adamo, *J. Chem. Theory Comput.*, 2008, **4**, 123.
- [19] K. Kornobis, N. Kumar, B. M. Wong, P. Lodowski, M. Jaworska, T. Andruniów, K. Ruud, P. M. Kozłowski, *J. Phys. Chem. A.*, 2011, **115**, 1280.
- [20] J. Heyd, G. E. Scuseria, M. Ernzerhof, *J. Chem. Phys.*, 2003, **118**, 8207.
- [21] J. Heyd, G. E. Scuseria, M. Ernzerhof, *J. Chem. Phys.*, 2006, **124**, 219906.
- [22] S. Y. Hong, S. J. Kwon, S. C. Kim, *J. Chem. Phys.*, 1995, **103**, 1871.
- [23] U. Salzner, J. B. Lagowski, P. G. Pickup, R. A. Poirier, *Synth. Met.*, 1998, **96**, 177.
- [24] S. Yamaguchi, Y. Itami, K. Tamao, *Organometallics*, 1998, **17**, 4910.
- [25] D. Delaere, M. T. Nguyen, L. G. Vanquickenborne, *Phys. Chem. Chem. Phys.*, 2002, **4**, 1522.
- [26] P. Deák, *Phys. Status Solidi B.*, 2000, **217**, 9.
- [27] A. Zunger, *J. Phys. Chem. C.*, 1974, **7**, 76
- [28] C. Lee, W. Yang and R.G. Parr, *Phys. Rev. B.*, 1988, **37**, 785.
- [29] K. Burke, J. P. Perdew, Y. Wang, J. F. Dobson, G. Vignale and M. P. Das, (Eds.), *Electronic Density Functional Theory: Recent Progress and New Directions*, Plenum Press, New York, 1998.
- [30] (a) A. D. Becke, *J. Chem. Phys.*, 1993, **98**, 5648.
(b) C. Lee, W. Yang and R. G. Parr, *Phys. Rev. B: Condens. Matter Mater. Phys.*, 1994, **37**, 785. (c) P. J. Stephens, F. J. Devlin, C. F. Chabalowski and M. J. Frisch, *J. Phys. Chem.*, 1994, **98**, 11623.
- [31] S. S. Zade, N. Zamoshchik and M. Bendikov, *Acc. Chem. Res.*, 2010, **44**, 14.

- [32] M. J. Frisch, G. W. Trucks, H. B. Schlegel, G. E. Scuseria, M. A. Robb, J. R. Cheeseman, G. Scalmani, V. Barone, B. Mennucci, G. A. Petersson, H. Nakatsuji, M. Caricato, X. Li, H. P. Hratchian, A. F. Izmaylov, J. Bloino, G. Zheng, J. L. Sonnenberg, M. Hada, M. Ehara, K. Toyota, R. Fukuda, J. Hasegawa, M. Ishida, T. Nakajima, Y. Honda, O. Kitao, H. Nakai, T. Vreven, J. A. Montgomery, J. E. Peralta, F. Ogliaro, M. Bearpark, J. J. Heyd, E. Brothers, K. N. Kudin, V. N. Staroverov, R. Kobayashi, J. Normand, K. Raghavachari, A. Rendell, J. C. Burant, S. S. Iyengar, J. Tomasi, M. Cossi, N. Rega, N. J. Millam, M. Klene, J. E. Knox, J. B. Cross, V. Bakken, C. Adamo, J. Jaramillo, R. Gomperts, R. E. Stratmann, O. Yazyev, A. J. Austin, R. Cammi, C. Pomelli, J. W. Ochterski, R. L. Martin, K. Morokuma, V. G. Zakrzewski, G. A. Voth, P. Salvador, J. J. Dannenberg, S. Dapprich, A. D. Daniels, O. Farkas, J. B. Foresman, J. V. Ortiz, J. Cioslowski, Gaussian 09, Revision B02, D. J. Fox, Gaussian, Inc., Wallingford CT, 2009.
- [33] M. J. Frisch, G. W. Trucks, H. B. Schlegel, G. E. Scuseria, M. A. Robb, Cheeseman et al., Gaussian 03, revision E. 01. Pittsburg, PA:Gaussian, Inc, 2003.
- [34] L. Groenendaal, F. Jonas, D. Freitag, H. Pielartzik, J. R. Reynolds, *Adv. Mater.*, 2000, **12**, 481.
- [35] T. A. P. Hai, R. Sugimoto, *Polymer Journal*, 2016, **48**, 1115.
- [36] H. Zhou, L. Yang, W. You, *Macromolecules*, 2012, **45**, 607.

.....✂.....

**SYNTHESIS AND CHARACTERIZATION OF
DESIGNED CONJUGATED POLYMERS**

Contents	4.1 <i>Introduction</i>
	4.2 <i>Results and Discussion</i>
	4.3 <i>Experimental</i>
	4.4 <i>Conclusion</i>

This chapter discusses the synthesis of designed polymers by means of Direct Arylation polymerization, Suzuki Coupling polymerization, Gilch polymerization and Knoevenagel polycondensation reactions. The synthesized polymers were characterized by UV-Vis, ¹H NMR spectroscopic techniques, thermogravimetric and electrochemical techniques etc. Detailed synthetic and characterization data are presented.

4.1 Introduction

Conjugated polymers exhibit variety of technologically relevant applications because of their ability to absorb and emit light¹⁻⁴ and photoconductivity,⁵ which makes them useful materials for the applications in light emitting diodes^{6,7} and photovoltaics.^{8,9} These polymers have the advantage of light weight and can be processed easily from solution by spin coating or inkjet printing.^{10,11} This makes them cheaper for device fabrication.

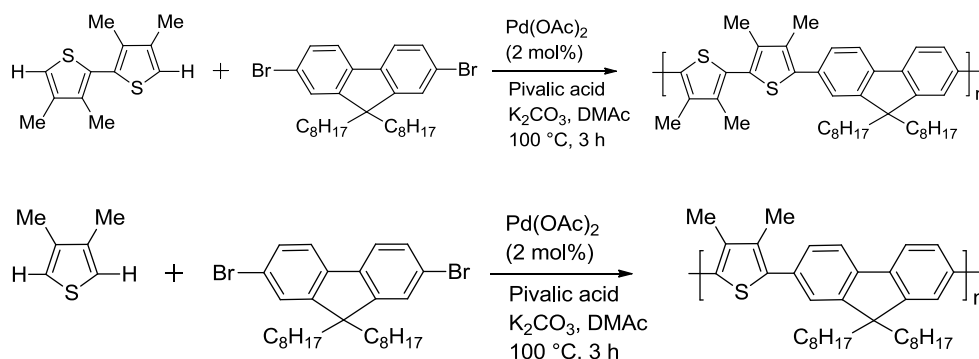
The conjugated polymers have low band gaps and exhibit semiconductor properties. Conductivity and color of a polymer depends on the band gap. Low band gap polymers find wide range of applications in optoelectronic field due to their high conductivity without doping. To increase the conductivity, band gap can be reduced by doping process.¹² Variation in band gap energy allows changing the optical and electronic properties of conjugated polymers by adopting new strategies for the synthesis of conjugated polymers. Band gap modifications are also possible by changing planarity, interchain interaction, bond length variation or presence of donor and acceptor groups on the polymer backbone. Donor-acceptor method has the advantage over other methods.¹³ Palladium catalyzed cross-coupling reactions are widely used for the synthesis of donor-acceptor conjugated copolymers.

4.1.1 Palladium Catalyzed Polymerization Reactions

In the present work, the two palladium catalyzed polymerization reactions adopted for the synthesis of conjugated polymers are Direct Arylation polymerization reaction and Suzuki Coupling polymerization reaction. Direct Arylation is the coupling of aryl halides with catalytically activated aryl C-H bonds which provides a desirable and atom-economical alternative to standard cross-coupling reactions for the construction of new C-C bonds. It is a base-assisted, concerted metalation-deprotonation (CMD) pathway.¹⁴ During this process, carboxylate or carbonate anions coordinate to the metal center, typically palladium, in situ and assist in the deprotonation transition state. Thiophene substrates have demonstrated high reactivity towards C-H bond activation when appropriately substituted with electron-

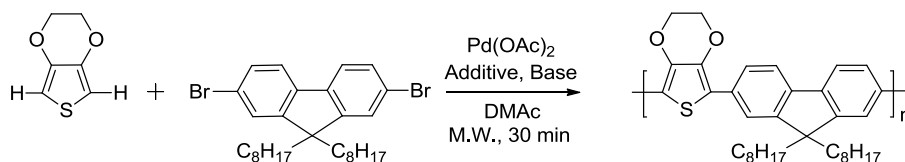
rich and/or electron-deficient groups. A base is also added to assist in C-H bond activation and neutralizes the stoichiometric amount of acid formed. Researchers have widely used this method to prepare conjugated short chain polymers.¹⁴

Y. Fujinami et al.¹⁵ synthesized thiophene and bithiophene based alternating copolymers via Pd catalyzed Direct Arylation reaction. The polycondensation reaction of 3,3',4,4'-tetramethylbithiophene with 2,7-dibromo-9,9-dioctylfluorene gave poly[2,7-(9,9-dioctylfluorene)-alt-5,5'-(3,3',4,4'-tetramethyl-2,2'-bithiophene)] in the presence of Pd(OAc)₂ catalyst (Scheme 4.1).



Scheme 4.1: Synthesis of thiophene- and bithiophene-based conjugated polymers via Direct arylation polymerization

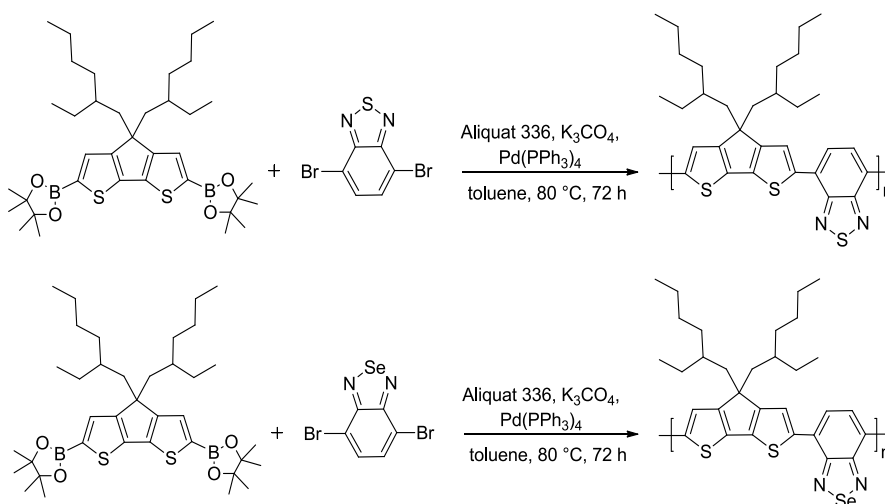
S. J. Choi et al.¹⁶ synthesized poly[(3,4-ethylenedioxythiophene-2,5-diyl)-(9,9-dioctylfluorene-2,7-diyl)] (PEDOTF) by microwave assisted polycondensation via Direct arylation reaction of 3,4-ethylenedioxythiophene with 9,9-dioctyl-2,7-dibromofluorene (Scheme 4.2).



Scheme 4.2: Microwave-assisted polycondensation for synthesis of PEDOTF

Suzuki coupling polymerization involves several advantages like high tolerance to different functional groups and easy work-up after the completion of reaction. Suzuki polymerization is highly effective for the synthesis of highly substituted compounds.¹⁷

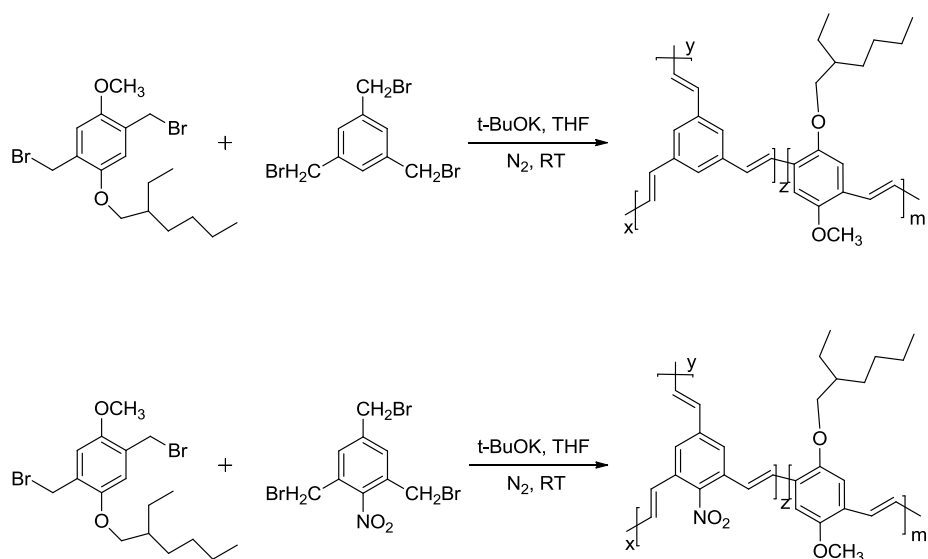
G. L. Gibson et al.¹⁸ synthesized a series of cyclopentadithiophene-benzochalcogenadiazole donor-acceptor copolymers via Suzuki coupling polymerization reactions (Scheme 4.3).



Scheme 4.3: Synthesis of D-A copolymers via Suzuki polymerization

4.1.2 Synthesis of PPV Polymers

Poly(*p*-phenylene vinylene) (PPV) polymers find much application in optoelectronic devices because of their excellent solubility and better thermal stability. The PPV polymers can be used as efficient acceptor materials in polymeric solar cells.^{19,20} R. Li et al.²¹ synthesized hyperbranched PPV polymers by Gilch polymerization route (Scheme 4.4).



Scheme 4.4: Synthesis of hyperbranched PPV polymer via Gilch Reaction

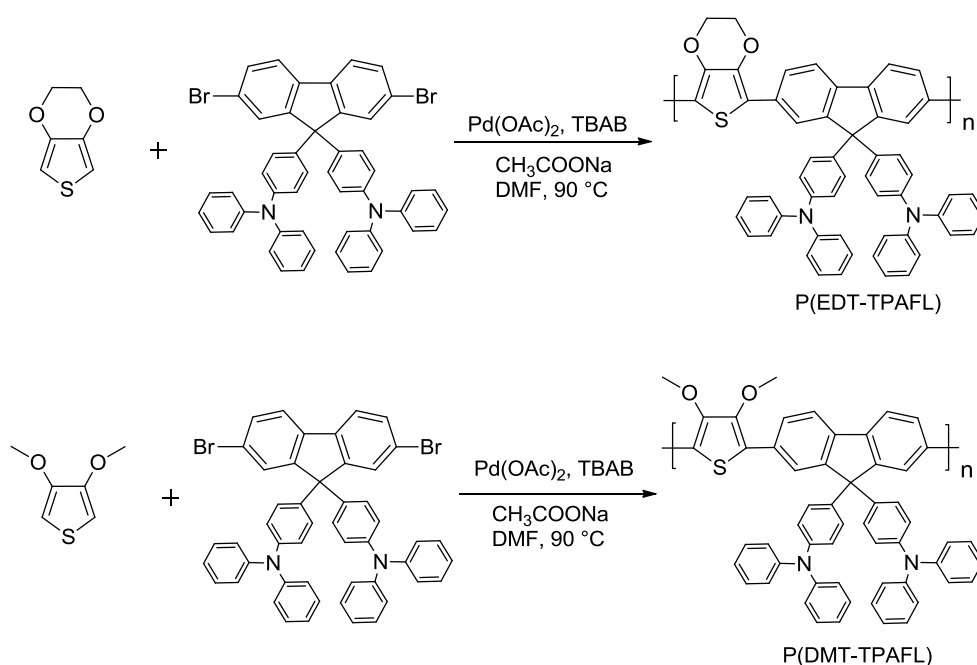
4.2 Results and Discussion

4.2.1 Synthesis of Thiophene Based Polymers

4.2.1.1 P(EDT-TPAFL) and P(DMT-TPAFL)

The two theoretically designed thiophene based polymers, P(EDT-TPAFL) and P(DMT-TPAFL) were synthesized by palladium catalyzed Direct Arylation. Polymerization reaction of 3,4-ethylenedioxythiophene (EDT) and 3,4-dimethoxythiophene (DMT) with 9,9-bis(4-diphenylaminophenyl)

fluorene) (TPAFL) in dry DMF in the presence of palladium catalyst gave the polymers P(EDT-TPAFL) and P(DMT-TPAFL), respectively. The purification process of polymers involved re-precipitation from suitable solvent and soxhlet extraction with different solvents. The synthesized copolymers were soluble in common organic solvents such as tetrahydrofuran (THF), chloroform and chlorobenzene. The synthetic route for the first set of thiophene based polymers is depicted in Scheme 4.5.



Scheme 4.5: Synthesis of P(EDT-TPAFL) and P(DMT-TPAFL)

The two thiophene based polymers synthesized were characterized by ¹H NMR, UV-Visible spectroscopy, GPC, cyclic voltammetry, TGA etc. The molecular weights of the polymers were obtained from gel permeation chromatography in THF referring to polystyrene standards with a flow rate of 1.0 mL/min. The copolymer, P(EDT-TPAFL) exhibited number average

molecular weight (M_n) of 6546 and weight average molecular weight (M_w) of 7839 with polydispersity index (PDI) of 1.20. The copolymer, P(DMT-TPAFL) exhibited number average molecular weight (M_n) of 5922 and weight average molecular weight (M_w) of 9677 with polydispersity index (PDI) of 1.63. Table 4.1 summarizes the molecular weight and polydispersity index (PDI) of the copolymers. M_p is the peak molecular weight. The polymers P(EDT-TPAFL) and P(DMT-TPAFL) showed peak molecular weight of 7218 and 6942, respectively.

Table 4.1: Results of the polymerisation reaction

Polymer	M_n	M_w	M_p	PDI
P(EDT-TPAFL)	6546	7839	7218	1.20
P(DMT-TPAFL)	5922	9677	6942	1.63

The structures of the polymers were confirmed by ^1H NMR spectra. P(EDT-TPAFL) showed resonance peaks corresponding to $-\text{O}-\text{CH}_2-$ protons of ethylenedioxythiophene unit at δ 3.7-4.0 as multiplet. The peaks observed at δ 6.9-7.3 are due to aromatic protons of two triphenylamine rings that are attached to the position 9 of the fluorene molecule. Peaks around δ 7.6-8.0 are due to the aromatic protons of fluorene unit. ^1H NMR spectrum of P(DMT-TPAFL) showed resonance peaks corresponding to $-\text{O}-\text{CH}_3$ protons of dimethoxythiophene unit at δ 4.2-4.5 as multiplet. The peaks observed at δ 7.0-7.4 are due to aromatic protons of two triphenylamine rings that are attached to the position 9 of the fluorene unit. Peaks around δ 7.7-7.9 are due to the aromatic protons of fluorene. The ^1H NMR spectra of the polymers are shown in Figure 4.1.

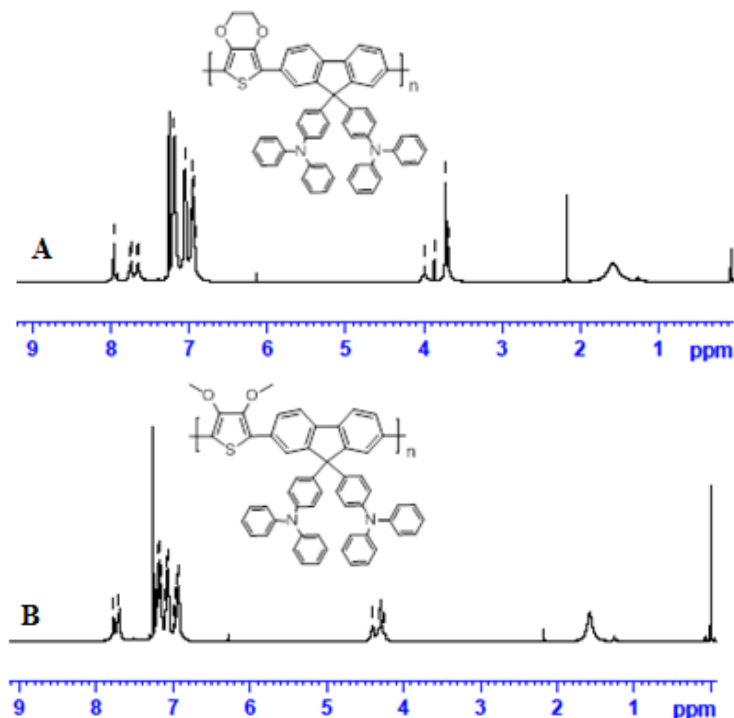


Figure 4.1: ¹H NMR spectra of (A) P(EDT-TPAFL) and (B) P(DMT-TPAFL)

4.2.1.1.1 Optical Properties

Absorption spectra of the polymers were recorded in chloroform. Usually the absorption band below 350 nm arises due to π - π^* transition and peaks at longer wavelengths are due to the intermolecular charge transfer (ICT) band. Here, the synthesized polymers, P(EDT-TPAFL) and P(DMT-TPAFL) showed absorption maximum around 469 nm and 432 nm respectively. The absorption onset of P(EDT-TPAFL) and P(DMT-TPAFL) occurred at 587 nm and 507 nm respectively. The optical band gap calculated was found to be 2.11 eV and 2.44 eV, respectively. From quantum chemical calculations, band gaps obtained were 2.27 eV and 2.36 eV respectively. The band gaps calculated from optical method are in good agreement with the theoretical

values. Figure 4.2 shows the absorption spectra of the two thiophene based copolymers.

Emission spectra of the polymers were recorded in chloroform. Polymers P(EDT-TPAFL) and P(DMT-TPAFL) showed emission peak maxima at 565 nm and 529 nm respectively. Figure 4.3 shows the emission spectra of P(EDT-TPAFL) and P(DMT-TPAFL) in chloroform.

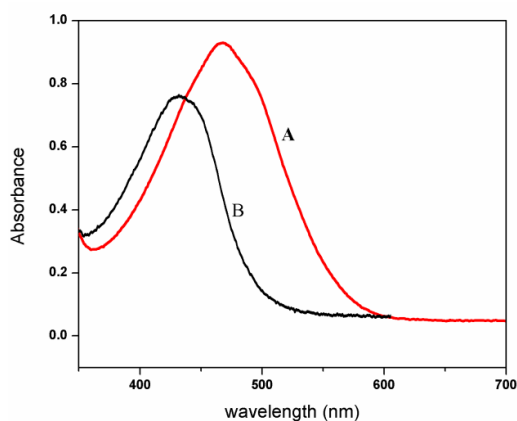


Figure 4.2: UV-Vis spectra: (A) P(EDT-TPAFL) and (B) P(DMT-TPAFL) in chloroform

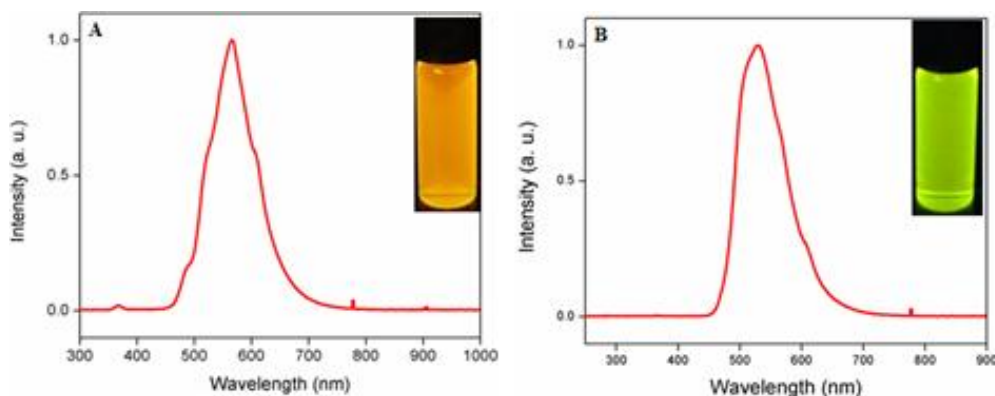


Figure 4.3: Emission spectra of the polymers: (A) P(EDT-TPAFL) and (B) P(DMT-TPAFL) in chloroform (2 mg/10 mL) (Excitation wavelength 365 nm)

4.2.1.1.2 Thermal Properties

The thermal characteristics of the polymers were investigated by TG-DTG analysis. The peak decomposition temperature was defined as the first inflection point in the thermogravimetric curve, corresponding to peak in the first derivative of thermogravimetric data. The onset degradation and degradation temperature are obtained from the TG curve. From the TG traces of the synthesized polymers, it is clear that the polymers, P(EDT-TPAFL) and P(DMT-TPAFL) follow single step degradation pattern. The moisture content present in the polymer was lost below 100 °C. In P(EDT-TPAFL), DTG traces showed onset of degradation around 390 °C and degradation at temperature 420 °C with around 4 % weight loss as the onset loss point. In P(DMT-TPAFL), the onset of degradation was around 386 °C and the degradation temperature was at 410 °C. Here only 3 % weight loss took place at the onset loss point. TG-DTG traces of the polymers are shown in the Figure 4.4.

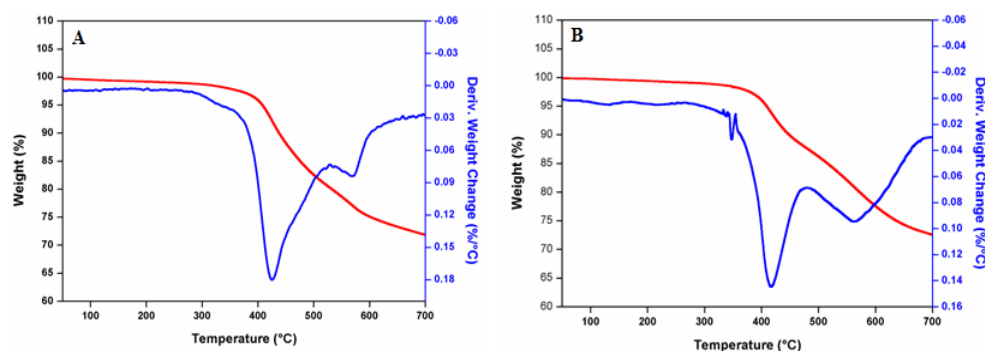


Figure 4.4: TG-DTG traces of the polymers: (A) P(EDT-TPAFL) and (B) P(DMT-TPAFL)

4.2.1.1.3 Electrochemical Studies

Cyclic voltammetric (CV) studies were carried out to determine the HOMO, LUMO levels and band gap of the polymers. CV studies were performed in a solution of Bu_4NPF_6 (0.1 M) in dry acetonitrile at 100 mV/s under nitrogen atmosphere. The set up consists of a Ag/Ag⁺ reference electrode, a platinum button electrode (0.08 cm²) coated with thin copolymer as the working electrode, and a platinum wire as the counter electrode. From the onset of oxidation, the HOMO levels of polymers were calculated by using the equation, $\text{HOMO} = -(4.71 + E_{\text{ox}}^{\text{onset}})$. The LUMO energy levels (from the onset of reduction potentials) were calculated using the equation, $\text{LUMO} = -(4.71 + E_{\text{red}}^{\text{onset}})$. From the onset of oxidation, the HOMO levels of P(EDT-TPAFL) and P(DMT-TPAFL) were calculated to be -5.67 eV and -5.81 eV respectively. The LUMO energy levels (from the onset of reduction potential) of P(EDT-TPAFL) and P(DMT-TPAFL) were calculated to be -3.72 eV and -3.88 eV respectively. The band gaps of the polymers P(EDT-TPAFL) and P(DMT-TPAFL) were calculated to be 1.95 eV and 1.93 eV respectively. The values of HOMO, LUMO and band gap of the first set of thiophene based polymers are shown in Table 4.2. The HOMO and LUMO energies were lowered on copolymerization which indicated the enhanced electron accepting/transporting properties in conjugated polymers. The electrochemical band gaps of these two polymers were found to be lower than that obtained by theoretical and optical methods. This is because, the predicted band gaps are for the isolated gas phase chains and also, the solid state effects such as polarization effects and intermolecular packing forces are neglected.^{22,23} Band gap calculated by means of theoretical, electrochemical and optical methods are depicted in Table 4.3.

Table 4.2: HOMO, LUMO levels and band gap of polymers calculated by means of electrochemical method

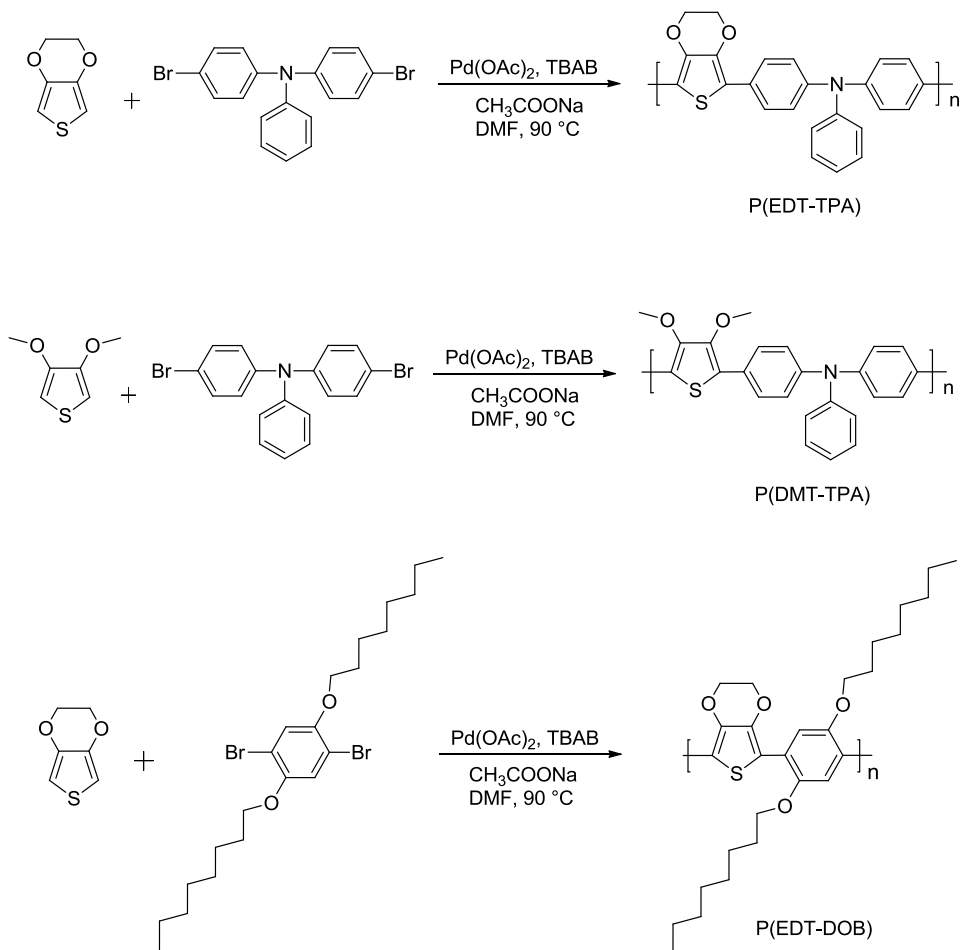
Polymer	HOMO - (4.71 + E _{ox} ^{onset}) (eV)	LUMO - (4.71 + E _{red} ^{onset}) (eV)	E _g (Electrochemical) (eV)
P(EDT-TPAFL)	-5.67	-3.72	1.95
P(DMT-TPAFL)	-5.81	-3.88	1.93

Table 4.3: Band gaps calculated by means of theoretical, electrochemical and optical methods

Polymer	E _g (Theoretical) (eV)	E _g (Electrochemical) (eV)	E _g (Optical) (eV)
P(EDT-TPAFL)	2.27	1.95	2.11
P(DMT-TPAFL)	2.36	1.93	2.44

4.2.1.2 P(EDT-TPA), P(DMT-TPA) and P(EDT-DOB)

The second set of three theoretically designed thiophene based polymers, P(EDT-TPA), P(DMT-TPA) and P(EDT-DOB) were synthesized by palladium catalyzed Direct Arylation polymerization reaction. 3,4-Ethylenedioxythiophene (EDT) and 3,4-dimethoxythiophene (DMT) when treated with 4,4'-dibromotriphenylamine (TPA) in dry DMF in the presence of palladium catalyst gave polymers P(EDT-TPA) and P(DMT-TPA) respectively. The polymer P(EDT-DOB) was synthesized by treating 3,4-ethylenedioxythiophene with 1,4-dibromo-2,5-bis(octyloxy)benzene. The products were washed with methanol and acetone in a soxhlet extractor to remove oligomers and catalyst residues. The synthetic route for the second set of thiophene based polymers is depicted in Scheme 4.6.



Scheme 4.6: Synthesis of P(EDT-TPA), P(DMT-TPA) and P(EDT-DOB)

The copolymer, P(EDT-TPA) exhibited number average molecular weight (M_n) of 4316, weight average molecular weight (M_w) of 5443 and peak molecular weight of 4881 with polydispersity index (PDI) of 1.26. The copolymer, P(DMT-TPA) exhibited number average molecular weight (M_n) of 4663, weight average molecular weight (M_w) of 6704 and peak molecular weight of 5545 with polydispersity index (PDI) of 1.43. The copolymer,

P(EDT-DOB) exhibited number average molecular weight (M_n) of 5465, weight average molecular weight (M_w) of 7689 and peak molecular weight of 7317 with polydispersity index (PDI) of 1.41. Table 4.4 summarizes the molecular weight and polydispersity index (PDI) of the copolymers.

Table 4.4: Results of the polymerisation reaction

Polymer	M_n	M_w	M_p	PDI
P(EDT-TPA)	4316	5443	4881	1.26
P(DMT-TPA)	4663	6704	5545	1.43
P(EDT-DOB)	5465	7689	7317	1.41

^1H NMR spectra of the polymers were recorded and structure of each polymer was assigned. P(EDT-TPA) showed resonance peaks corresponding to $-\text{O}-\text{CH}_2-$ protons of ethylenedioxythiophene unit at δ 3.7-4.4 as multiplet. The peaks observed at δ 7.0-7.7 are due to aromatic protons of the triphenylamine moiety. ^1H NMR spectrum of P(DMT-TPA) showed resonance peaks corresponding to $-\text{O}-\text{CH}_3$ protons of dimethoxythiophene unit at δ 3.9-4.1 as multiplet. Aromatic protons of triphenylamine ring showed peaks at δ 7.1-7.7. ^1H NMR spectrum of the polymer P(EDT-DOB) showed peaks around δ 0.8-2.1 due to aliphatic protons of two octyloxy chains. Resonance peaks corresponding to $-\text{O}-\text{CH}_2-$ protons of ethylenedioxythiophene unit were observed at δ 3.7-4.4 as multiplet. The peaks observed at δ 7.1 and at δ 7.4 are due to the two aromatic protons of benzene ring. The ^1H NMR spectra of the polymers are shown in Figure 4.5.

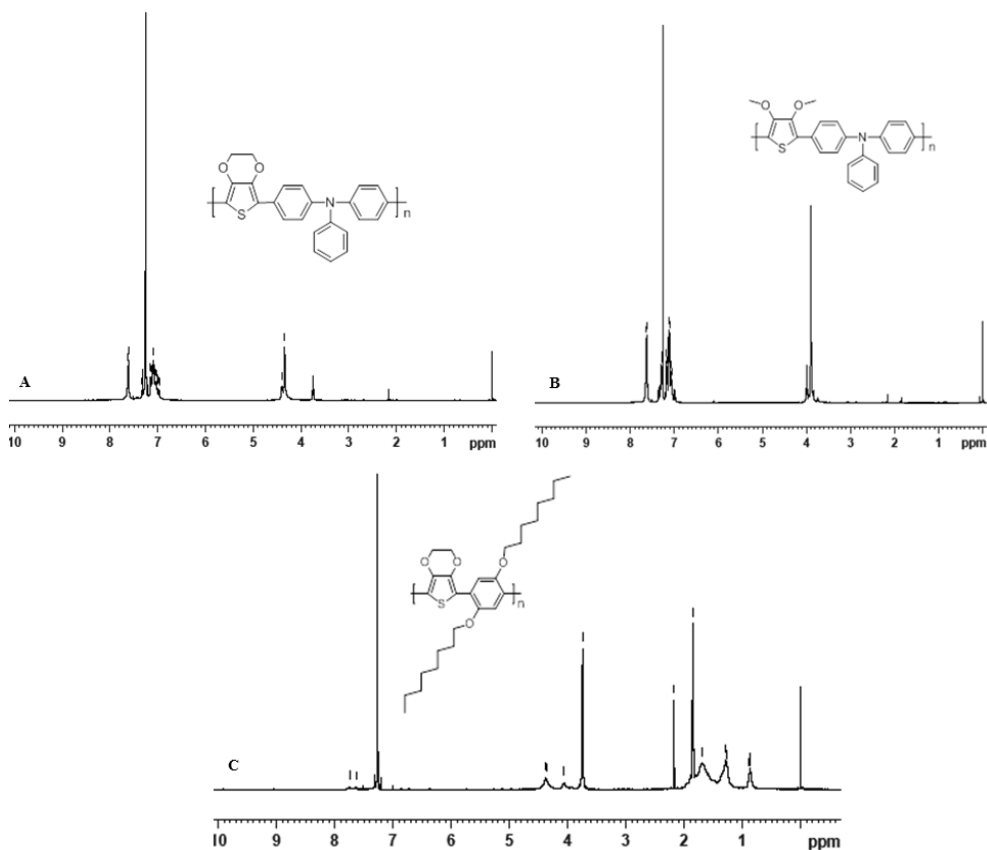


Figure 4.5: ¹H NMR spectra of (A) P(EDT-TPA), (B) P(DMT-TPA) and (C) P(EDT-DOB)

4.2.1.2.1 Optical Properties

Absorption spectra of the second set of three polymers were recorded in chloroform. The synthesized polymers, P(EDT-TPA), P(DMT-TPA) and P(EDT-DOB) showed absorption maximum around 431 nm, 408 nm and 487 nm respectively. The absorption onset of P(EDT-TPA), P(DMT-TPA) and P(EDT-DOB) were observed at 538 nm, 490 nm and 605 nm respectively. The optical band gap values of polymers were calculated to be 2.30 eV, 2.53 eV

and 2.05 eV respectively from the onset of absorption peaks. The theoretical band gaps of the polymers were obtained to be 2.53 eV, 2.77 eV and 2.44 eV respectively from quantum chemical calculations. The band gaps calculated from optical methods are in good agreement with the theoretical values. Figure 4.6 shows the absorption spectra of the second set of thiophene based copolymers.

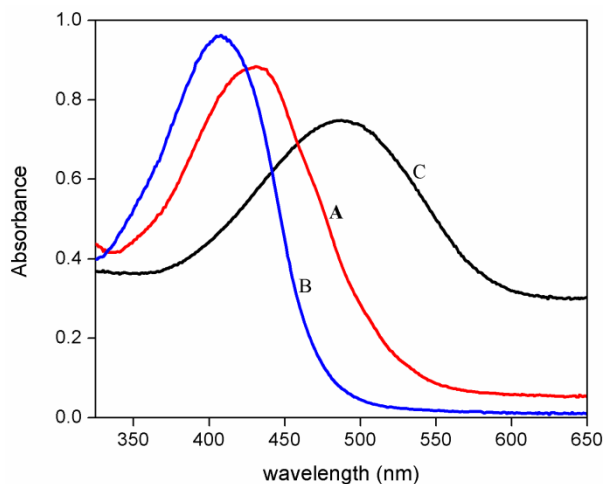


Figure 4.6: UV-Vis spectra: (A) P(EDT-TPA), (B) P(DMT-TPA) and (C) P(EDT-DOB) in chloroform

Emission spectra of the polymers were recorded in chloroform. Polymers P(EDT-TPA), P(DMT-TPA) and P(EDT-DOB) showed emission maxima at 520 nm, 502 nm and 565 nm respectively. Figure 4.7 shows the emission spectra of the three polymers in chloroform.

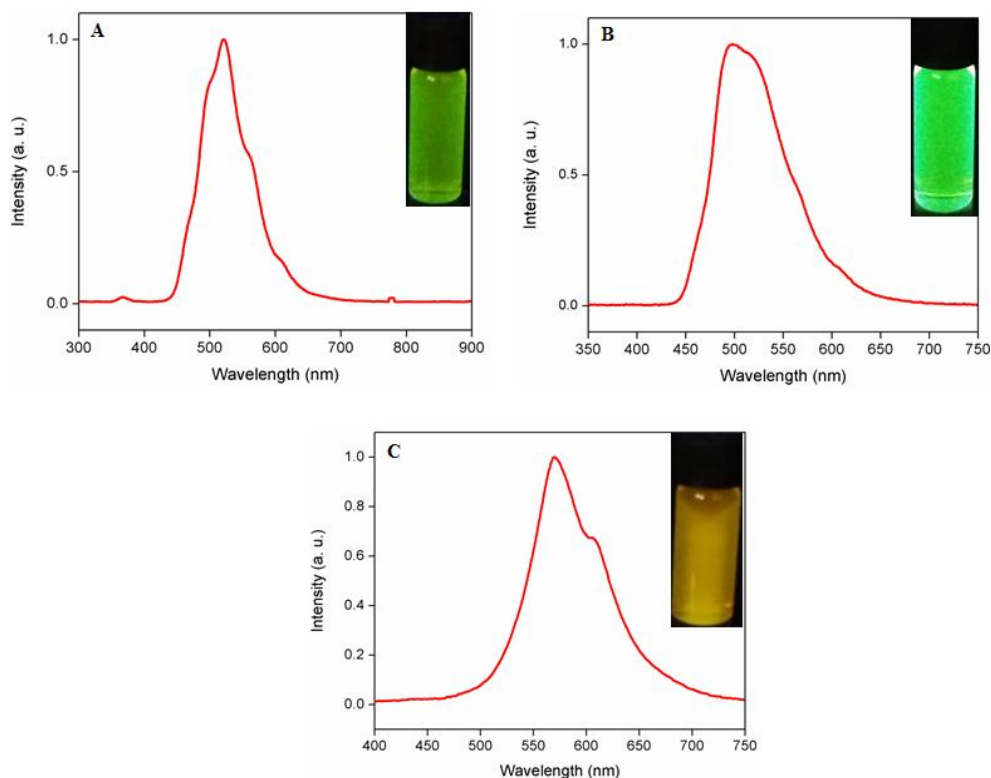


Figure 4.7: Emission Spectra of the polymers: (A) P(EDT-TPA), (B) P(DMT-TPA) and (C) P(EDT-DOB) in chloroform (2 mg/10 mL) (Excitation wavelength 365 nm)

4.2.1.2.2 Thermal Properties

The thermal properties of the polymers were obtained from TG-DTG analysis. The onset degradation and degradation temperature of the polymers were obtained from the corresponding TG curve. The second set of thiophene based polymers P(EDT-TPA), P(DMT-TPA) and P(EDT-DOB) followed single step degradation pattern (Figure 4.8). For P(EDT-TPA), DTG trace showed onset of degradation around 360 °C and degradation temperature at 410 °C with around 4 % weight loss as the onset loss

point. DTG trace of P(DMT-TPA) showed the onset of degradation around 380 °C and the degradation temperature at 405 °C. Here, 5 % weight loss took place at the onset loss point. In the case of P(EDT-DOB), the onset of degradation was observed around 340 °C and the degradation temperature at 400 °C. Here 5 % weight loss took place at the onset loss point.

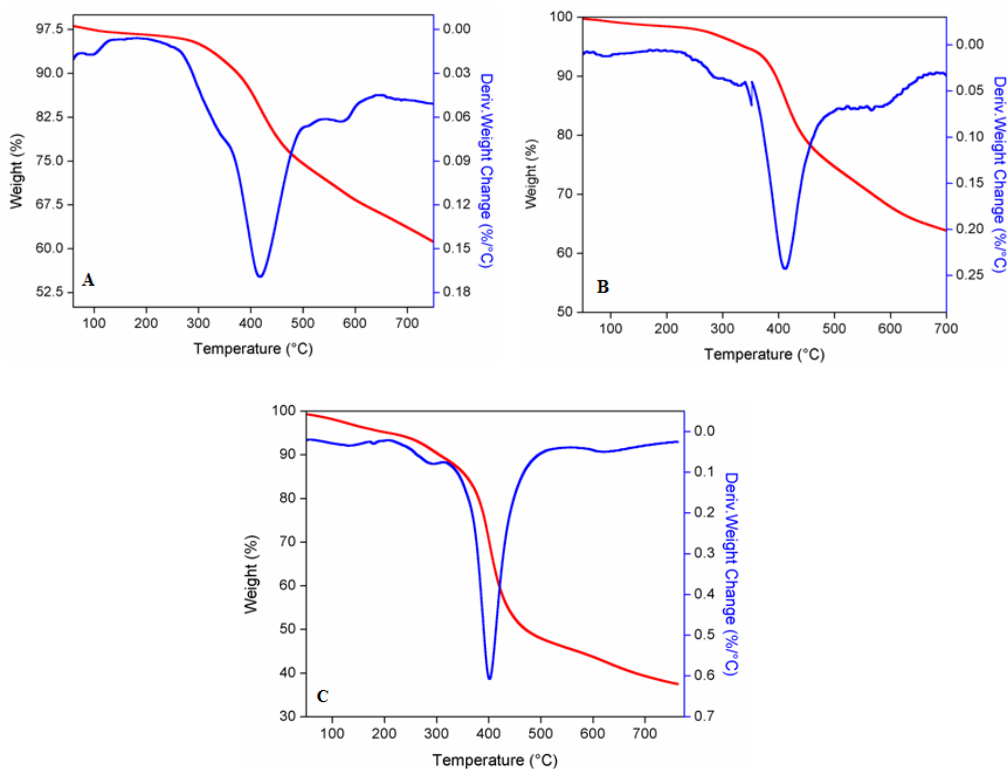


Figure 4.8: TG-DTG traces of the polymers: (A) P(EDT-TPA), (B) P(DMT-TPA) and (C) P(EDT-DOB)

4.2.1.2.3 Electrochemical Studies

To determine the highest occupied molecular orbital (HOMO) and lowest unoccupied molecular orbital (LUMO) levels of the polymers, cyclic voltammetry was carried out. From the onset of oxidation, the HOMO levels of polymers were calculated using the equation, $\text{HOMO} = -(4.71 + E_{\text{ox}}^{\text{onset}})$. The LUMO energy levels (from the onset of reduction potentials) were calculated using the equation, $\text{LUMO} = -(4.71 + E_{\text{red}}^{\text{onset}})$. From the onset of oxidation, the HOMO levels of P(EDT-TPA), P(DMT-TPA) and P(EDT-DOB) were calculated to be -5.46 eV, -5.68 eV and -5.24 eV respectively. The LUMO energy levels (from the onset of reduction potential) of P(EDT-TPA), P(DMT-TPA) and P(EDT-DOB) were calculated to be -3.72 eV, -3.88 eV and -3.58 eV respectively. The band gaps of the polymers P(EDT-TPA), P(DMT-TPA) and P(EDT-DOB) were calculated to be 1.74 eV, 1.80 eV and 1.66 eV respectively. The values of HOMO, LUMO and band gap of the second set of three thiophene based polymers are shown in Table 4.5. The HOMO and LUMO energies were lowered on copolymerization which indicated the enhanced electron accepting / transporting properties in conjugated polymers. The electrochemical band gaps of these three thiophene based polymers were found to be lower than that obtained by theoretical and optical methods which was already mentioned. Another chance for the low values of electrochemical band gaps of synthesized polymers is the uncorresponding behavior of the used supporting electrolyte, Bu_4NPF_6 towards the synthesized polymers. Band gap calculated by means of theoretical, electrochemical and optical methods are depicted in Table 4.6.

Table 4.5: HOMO, LUMO levels and band gap of polymers calculated by means of electrochemical method

Polymer	HOMO - (4.71 + E _{ox} ^{onset}) (eV)	LUMO - (4.71 + E _{red} ^{onset}) (eV)	Eg (Electrochemical) (eV)
P(EDT-TPA)	-5.46	-3.72	1.74
P(DMT-TPA)	-5.68	-3.88	1.80
P(EDT-DOB)	-5.24	-3.58	1.66

Table 4.6: Band gaps calculated by means of theoretical, electrochemical and optical methods

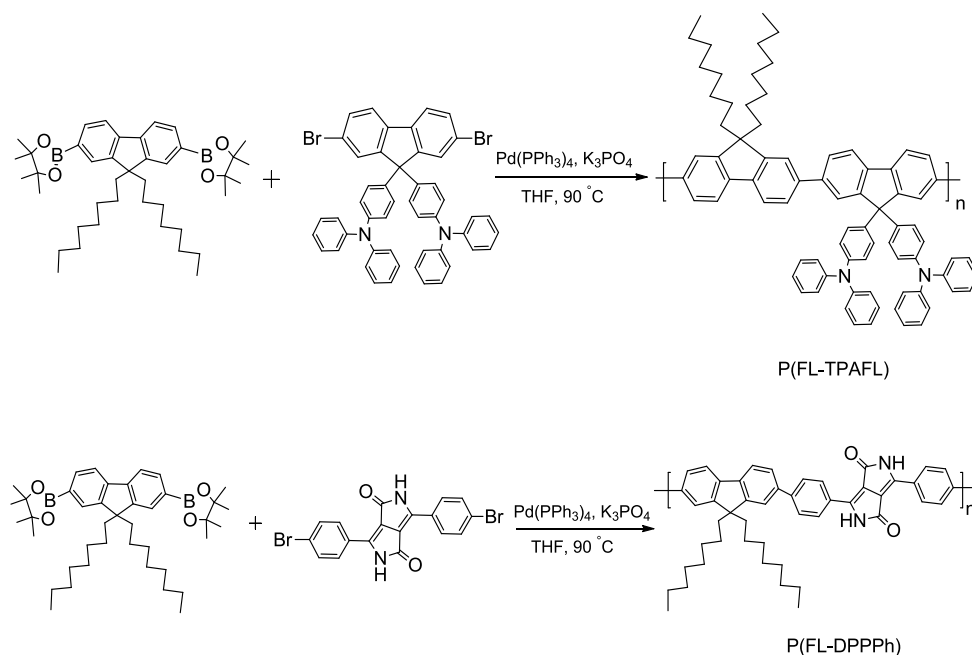
Polymer	Eg (Theoretical) (eV)	Eg (Electrochemical) (eV)	Eg (Optical) (eV)
P(EDT-TPA)	2.53	1.74	2.30
P(DMT-TPA)	2.77	1.80	2.53
P(EDT-DOB)	2.44	1.66	2.05

4.2.2 Synthesis of Fluorene Based Polymers

4.2.2.1 P(FL-TPAFL) and P(FL-DPPPh)

The first set of two theoretically designed fluorene based polymers P(FL-TPAFL) and P(FL-DPPPh) were synthesized by palladium catalyzed Suzuki cross-coupling polymerization reaction using Pd(PPh₃)₄ as catalyst. The fluorene monomer, 2,7-Bis(4,4,5,5-tetramethyl-1,3,2-dioxaborolan-2-yl)-9,9-dioctylfluorene was reacted with 9,9-bis(4-diphenylaminophenyl) fluorene (TPAFL) and 3,6-bis(4-bromophenyl) 2,5-dihydropyrrolo[3,4-c]pyrrole-1,4-dione (DPPPh) in dry THF to give the polymers P(FL-TPAFL) and P(FL-DPPPh), respectively. The synthesized polymers were purified by soxhlet extraction using hexane, methanol and acetone. The

synthetic route for the first set of fluorene based polymers is depicted in Scheme 4.7.



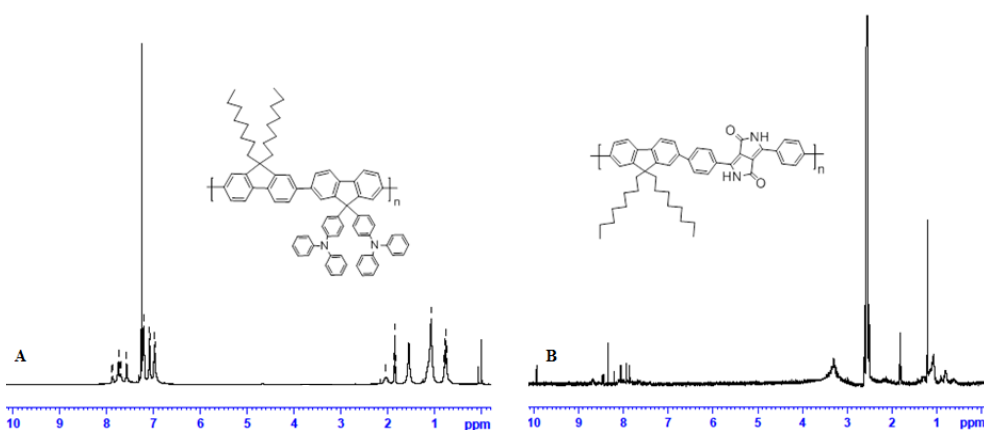
Scheme 4.7: Synthesis of P(FL-TPAFL) and P(FL-DPPPh)

The molecular weights of the polymers were obtained from gel permeation chromatography in THF. The copolymer, P(FL-TPAFL) exhibited number average molecular weight (M_n) of 17000 and weight average molecular weight (M_w) of 24107 with polydispersity index (PDI) of 1.41. The copolymer, P(FL-DPPPh) exhibited number average molecular weight (M_n) of 3994 and weight average molecular weight (M_w) of 6185 with polydispersity index (PDI) of 1.55. Table 4.7 summarizes the molecular weight and polydispersity index (PDI) of the copolymers. The polymers, P(FL-TPAFL) and P(FL-DPPPh) showed peak molecular weight of 21734 and 4475, respectively.

Table 4.7: Results of the polymerization reaction

Polymer	M _n	M _w	M _p	PDI
P(FL-TPAFL)	17000	24107	21734	1.41
P(FL-DPPPh)	3994	6185	4475	1.55

The structures of the polymers were confirmed by ¹H NMR spectra. In the case of P(FL-TPAFL), peaks observed around δ 0.8-2.1 are due to aliphatic protons of alkyl chains. The peaks observed at δ 6.9-7.4 are due to the aromatic protons of triphenylamine rings that are attached to the position 9 of the fluorene moiety. Peaks around δ 7.6-7.9 are due to the aromatic protons of fluorene moieties. ¹H NMR spectrum of P(FL-DPPPh) showed resonance peaks corresponding to aliphatic protons of alkyl chain at δ 1.1-3.3 as multiplet. The peaks observed at δ 7.8-8.7 as multiplet are due to the aromatic protons of phenyl and fluorene units. The ¹H NMR spectra of the polymers are shown in Figure 4.9.

**Figure 4.9: ¹H NMR spectra of (A) P(FL-TPAFL) and (B) P(FL-DPPPh)**

4.2.2.1.1 Optical Properties

Absorption spectra of the polymers were recorded in THF. The polymers, P(FL-TPAFL) and P(FL-DPPPh) showed absorption maximum around 385 nm and 542 nm, respectively. The absorption onset of polymers P(FL-TPAFL) and P(FL-DPPPh) occur at 419 nm and 630 nm respectively. The optical band gap was calculated to be 2.96 eV and 1.97 eV, respectively. From quantum chemical calculations, the theoretical band gaps obtained were 2.80 eV and 1.96 eV respectively. The band gaps calculated from optical methods are in good agreement with the theoretical values. Figure 4.10 shows the absorption spectra of the first set of two fluorene based copolymers.

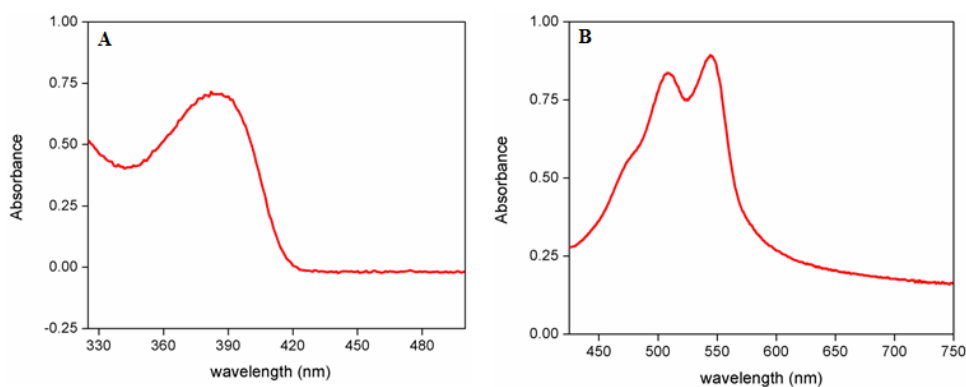


Figure 4.10: UV-Vis spectra: (A) P(FL-TPAFL) and (B) P(FL-DPPPh) in THF

Emission spectra of polymers were recorded in THF. Polymers, P(FL-TPAFL) showed emission peak at 421 nm. Two shoulder peaks were observed around 441 nm and 471 nm. This may be due to the spacial twisting of two triphenylamine rings that are attached to the 9th position of fluorene unit. The polymer, P(FL-DPPPh) showed emission peak at 559 nm with a shoulder peak at 606 nm. This shoulder peak could be due to the spacial twisting of two phenyl rings that are attached covalently to the diketopyrrolopyrrole unit.

Figure 4.11 shows the emission spectra of P(FL-TPAFL) and P(FL-DPPPh) in THF.

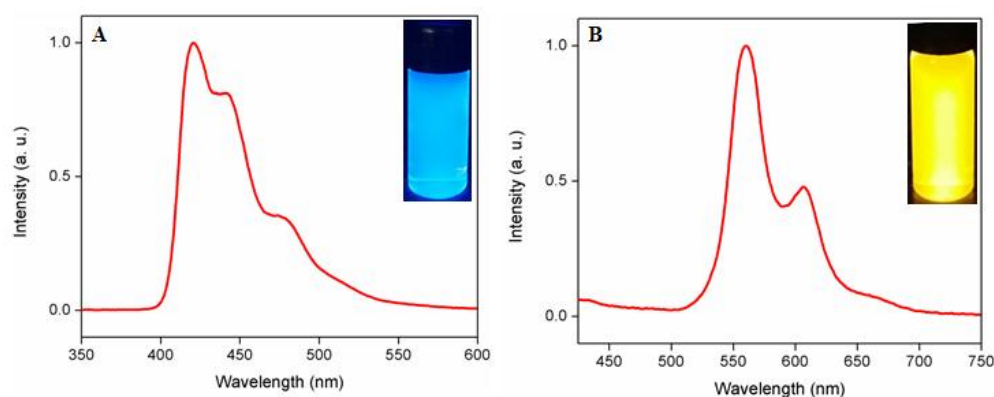


Figure 4.11: Emission spectra of the polymers: (A) P(FL-TPAFL) and (B) P(FL-DPPPh) in THF (2 mg/10 mL) (Excitation wavelength 365 nm)

4.2.2.1.2 Thermal Properties

The thermal degradation patterns of the polymers were obtained from thermogravimetric analysis. The onset of degradation and degradation temperature is obtained from the TG curve. The TG traces of the polymers P(FL-TPAFL) showed a two-step degradation pattern and P(FL-DPPPh) follow single step degradation pattern. In P(FL-TPAFL), DTG traces showed onset of degradation around 450 °C and degradation temperature at 480 °C with about 5 % weight loss as the onset loss point. In P(FL-DPPPh), the onset of degradation was around 330 °C and the degradation temperature was at 405 °C. Here, only 6 % weight loss took place at the onset loss point. As shown by the TG-DTG curves, two polymers showed good thermal stability. TG-DTG traces of the polymers are shown in the Figure 4.12.

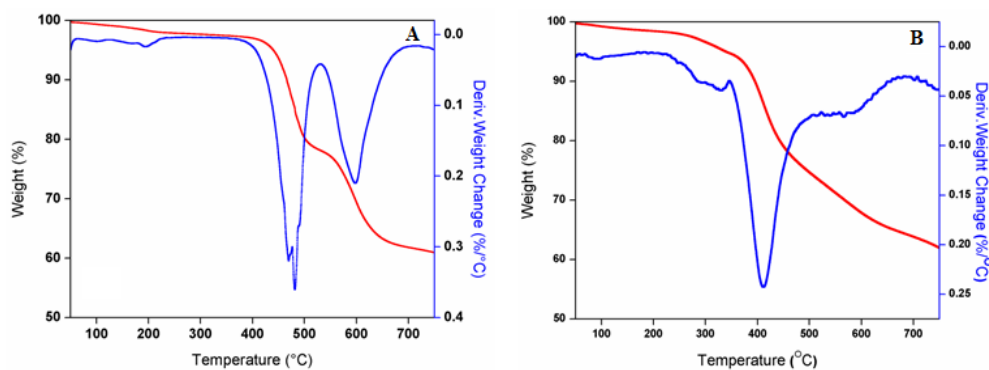


Figure 4.12: TG-DTG traces of the polymers: (A) P(FL-TPAFL) and (B) P(FL-DPPPh)

4.2.2.1.3 Electrochemical Studies

The HOMO, LUMO levels and band gap of the polymers were determined by cyclic voltammetric studies. From the onset of oxidation, the HOMO levels of polymers P(FL-TPAFL) and P(FL-DPPPh) were calculated to be -6.12 eV and -5.77 eV respectively using the equation, $\text{HOMO} = -(4.71 + E_{\text{ox}}^{\text{onset}})$. Similarly the LUMO energy levels were calculated to be -3.71 eV and -3.96 eV using the equation, $\text{LUMO} = -(4.71 + E_{\text{red}}^{\text{onset}})$. The band gaps of the polymers P(FL-TPAFL) and P(FL-DPPPh) were calculated to be 2.41 eV and 1.81 eV, respectively. The values of HOMO, LUMO and band gap of the first set of fluorene based polymers are shown in Table 4.8. Band gap calculated by means of theoretical, electrochemical and optical methods are depicted in Table 4.9.

Table 4.8: HOMO, LUMO levels and band gap of polymers calculated by means of electrochemical method

Polymer	HOMO - (4.71 + E _{ox} ^{onset}) (eV)	LUMO - (4.71 + E _{red} ^{onset}) (eV)	Eg (Electrochemical) (eV)
P(FL-TPAFL)	-6.12	-3.71	2.41
P(FL-DPPPh)	-5.77	-3.96	1.81

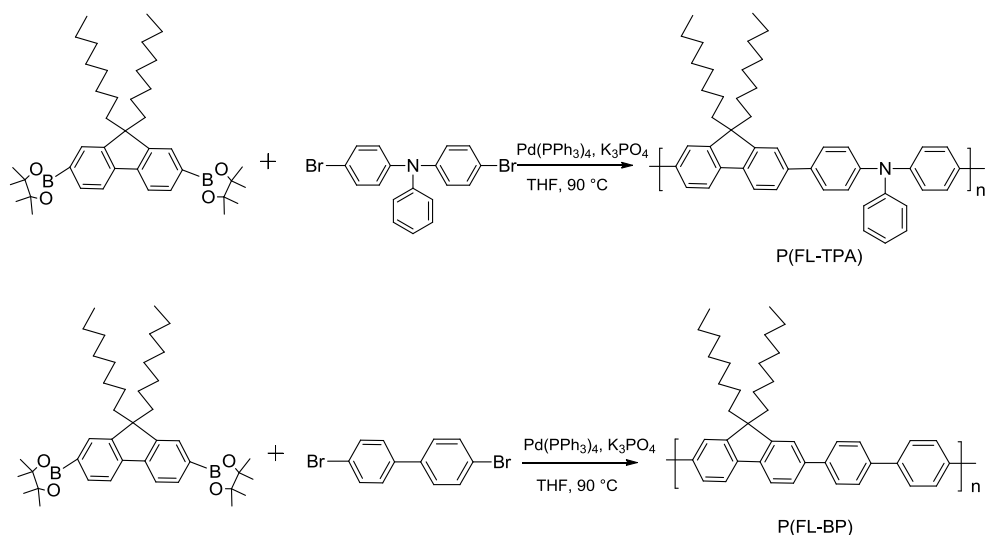
Table 4.9: Band gaps calculated by means of theoretical, electrochemical and optical methods

Polymer	Eg (Theoretical) (eV)	Eg (Electrochemical) (eV)	Eg (Optical) (eV)
P(FL-TPAFL)	2.80	2.41	2.96
P(FL-DPPPh)	1.96	1.81	1.97

4.2.2.2 P(FL-TPA) and P(FL-BP)

The second set of two theoretically designed fluorene based polymers, P(FL-TPA) and P(FL-BP) were synthesized by palladium catalyzed Suzuki cross-coupling polymerization reaction using Pd(PPh₃)₄ as catalyst. The fluorine monomer, 2,7-Bis(4,4,5,5-tetramethyl-1,3,2-dioxaborolan-2-yl)-9,9-dioctylfluorene was reacted with 4,4'-dibromotriphenylamine (TPA) and 4,4'-dibromo-1,1'-biphenyl (BP) in dry THF to give the polymers P(FL-TPA) and P(FL-BP), respectively. The crude products were dissolved in minimum amount of chloroform and re-precipitated from methanol and the product filtered was again purified by soxhlet extraction using hexane, methanol and acetone. The synthesized copolymers were soluble in common organic solvents such as tetrahydrofuran (THF), chloroform and chlorobenzene. The

synthetic route for the second set of fluorene based polymers is depicted in Scheme 4.8.



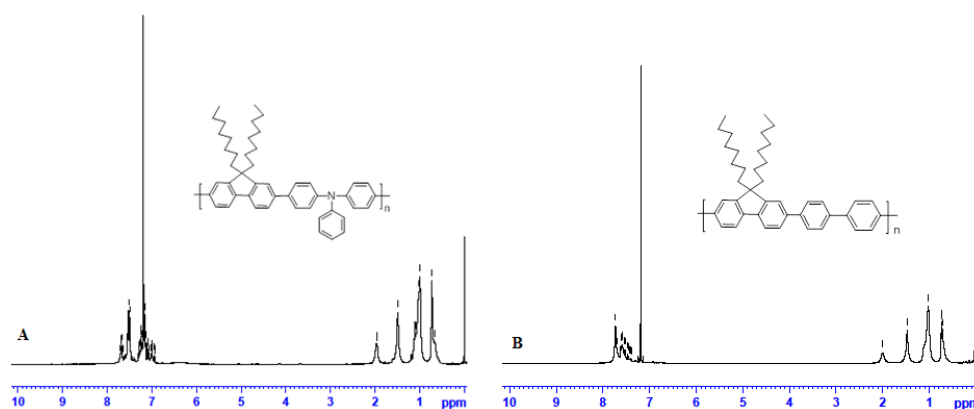
Scheme 4.8: Synthesis of P(FL-TPA) and P(FL-BP)

The two fluorene based polymers were characterized by different spectroscopic and analytical techniques. The molecular weights of the polymers were obtained from gel permeation chromatography in THF. The copolymer, P(FL-TPA) exhibited number average molecular weight (M_n) of 5530 and weight average molecular weight (M_w) of 10085 with polydispersity index (PDI) of 1.82. The copolymer, P(FL-BP) exhibited number average molecular weight (M_n) of 7097 and weight average molecular weight (M_w) of 12960 with polydispersity index (PDI) of 1.83. Table 4.10 summarizes the molecular weights and polydispersity index (PDI) of the copolymers.

Table 4.10: Results of the polymerization reaction

Polymer	M_n	M_w	M_p	PDI
P(FL-TPA)	5530	10085	5571	1.82
P(FL-BP)	7097	12960	7486	1.83

The structure of the polymers were confirmed by ^1H NMR spectra. In the case of P(FL-TPAFL), peaks observed around δ 0.8-2.1 are due to aliphatic protons of alkyl chains. The peaks observed at δ 7.0-7.8 are due to the aromatic protons of triphenylamine and fluorene moiety. ^1H NMR spectrum of P(FL-BP) showed resonance peaks corresponding to aliphatic protons of alkyl chain at δ 0.7-2.0 as multiplet. The peaks observed at δ 7.2-7.8 as multiplet are due to the aromatic protons of biphenyl and fluorene units. The ^1H NMR spectra of the polymers are shown in Figure 4.13.

**Figure 4.13: ^1H NMR spectra of (A) P(FL-TPA) and (B) P(FL-BP)**

4.2.2.2.1 Optical Properties

Absorption spectra of polymers were recorded in THF. The polymers, P(FL-TPA) and P(FL-BP) showed absorption maximum around 379 nm and 353 nm, respectively. The absorption onset of polymers, P(FL-TPA) and P(FL-BP) occurred at 422 nm and 400 nm, respectively. The optical band gap values of polymers were calculated to be 2.94 eV and 3.10 eV, respectively. The theoretical band gap values of polymers were obtained to be 2.94 eV and 3.26 eV, respectively. The band gaps calculated from optical methods are in good agreement with the theoretical values. Figure 4.14 shows the absorption spectra of the second set of two fluorene based copolymers.

Emission spectra of polymers were recorded in THF. Polymer P(FL-TPA) showed emission peak at 430 nm and the polymer, P(FL-BP) showed emission peak at 405 nm. Figure 4.15 shows the emission spectra of P(FL-TPA) and P(FL-BP) in THF.

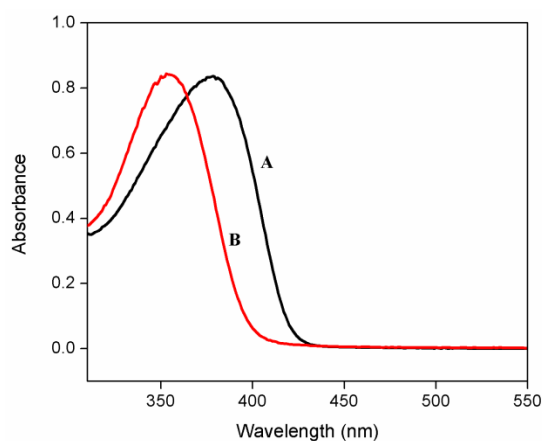


Figure 4.14: UV-Vis spectra: (A) P(FL-TPA) and (B) P(FL-BP) in THF

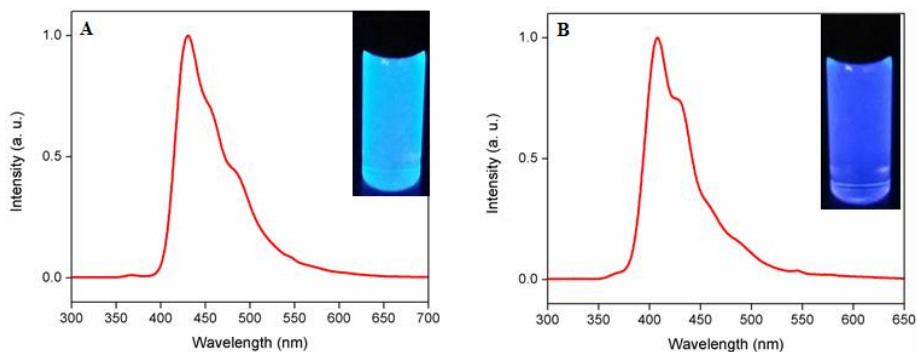


Figure 4.15: Emission spectra of the polymers: (A) P(FL-TPA) and (B) P(FL-BP) in THF (2 mg/10mL) (Excitation wavelength 365 nm)

4.2.2.2 Thermal Properties

The thermal stability of the polymers was investigated by TG-DTG analysis. The onset of degradation and degradation temperature is obtained from the TG traces of the synthesized polymers. It is clear that the polymers, P(FL-TPA) and P(FL-BP) followed single step degradation pattern. In P(FL-TPA), DTG traces showed onset of degradation around 400 °C and degradation temperature at 475 °C with about 12 % weight loss as the onset loss point. In P(FL-BP), the onset of degradation was around 330 °C and the degradation temperature was at 470 °C. Here, only 6 % weight loss took place at the onset loss point. TG-DTG traces of the polymers are shown in the Figure 4.16.

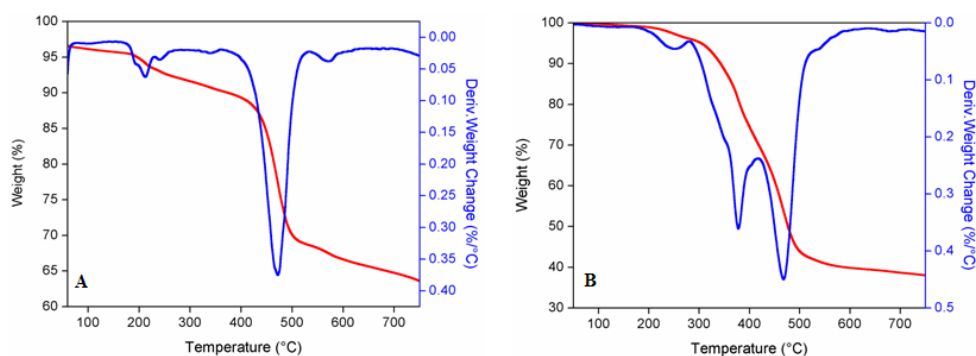


Figure 4.16: TG-DTG traces of the polymers: (A) P(FL-TPA) and (B) P(FL-BP)

4.2.2.2.3 Electrochemical Studies

Cyclic voltammetry was used to assess the HOMO, LUMO levels and band gap of the polymers. From the onset of oxidation, the HOMO levels of polymers, P(FL-TPA) and P(FL-BP) were calculated to be -5.67 eV and -6.12 eV, respectively using the equation, $\text{HOMO} = -(4.71 + E_{\text{ox}}^{\text{onset}})$. The LUMO energy levels (from the onset of reduction potentials) of P(FL-TPA) and P(FL-BP) were calculated to be -3.75 eV and -3.91 eV, respectively using the equation, $\text{LUMO} = -(4.71 + E_{\text{red}}^{\text{onset}})$. The band gaps of the polymers, P(FL-TPA) and P(FL-BP) were calculated to be 1.92 eV and 2.21 eV, respectively. The values of HOMO, LUMO and band gap of the second set of fluorene based polymers are shown in Table 4.11. The electrochemical band gaps of these two polymers were found to be lower than that obtained by theoretical and optical methods. This may be due to the difference in the mechanism of optical excitation and electrochemical oxidation and reduction processes. Optical excitation involved the creation of excitons and the latter process creates ions. The low energy of excitons compared to the ions and solvation of the ions in the electrochemical experiments were reflected in the low value of electrochemical band gap. Band gaps calculated by means of theoretical, electrochemical and optical methods are depicted in Table 4.12.

Table 4.11: HOMO, LUMO levels and band gap of polymers calculated by means of electrochemical method

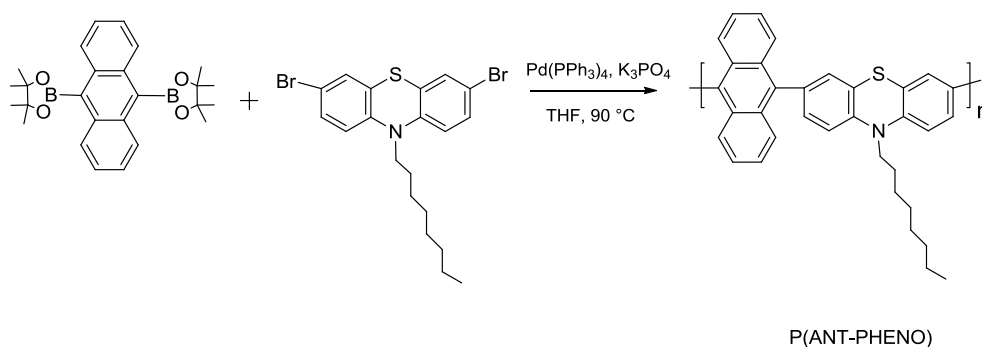
Polymer	HOMO - (4.71 + $E_{\text{ox}}^{\text{onset}}$) (eV)	LUMO - (4.71 + $E_{\text{red}}^{\text{onset}}$) (eV)	Eg (Electrochemical) (eV)
P(FL-TPA)	-5.67	-3.75	1.92
P(FL-BP)	-6.12	-3.91	2.21

Table 4.12: Band gaps calculated by means of theoretical, electrochemical and optical methods

Polymer	E _g (Theoretical) (eV)	E _g (Electrochemical) (eV)	E _g (Optical) (eV)
P(FL-TPA)	2.94	1.92	2.94
P(FL-BP)	3.26	2.21	3.10

4.2.3 Synthesis of Anthracene-phenothiazine copolymer P(ANT-PHENO)

The theoretically designed anthracene-phenothiazine copolymer, P(ANT-PHENO) was synthesized by palladium catalyzed Suzuki cross-coupling polymerization reaction using Pd(PPh₃)₄ as catalyst. 9,10-anthracenediboronic acid bis(pinacol) ester was reacted with 3,7-dibromo-10-octylphenothiazine in dry THF to give the copolymer, P(ANT-PHENO). The product was purified by soxhlet extraction using hexane, methanol and acetone, respectively. The synthetic route for the anthracene based polymer is depicted in Scheme 4.9.

**Scheme 4.9: Synthesis of P(ANT-PHENO)**

The copolymer, P(ANT-PHENO) exhibited number average molecular weight (M_n) of 7022, weight average molecular weight (M_w) of 10627 and peak molecular weight of 5056 with polydispersity index (PDI) of 1.51.

Table 4.13 summarizes the molecular weight and polydispersity index (PDI) of the copolymer.

Table 4.13: Results of the polymerization reaction

Polymer	M_n	M_w	M_p	PDI
P(ANT-PHENO)	7022	10627	8056	1.51

The structure of the polymer, P(ANT-PHENO) was confirmed by ^1H NMR spectrum. The peaks observed around δ 0.8-2.2 are due to aliphatic protons of alkyl chains. The two peaks observed around δ 3.9-4.1 are due to two aliphatic protons of alkyl chains adjacent to the nitrogen hetero atom. The peaks observed at δ 6.9-7.9 are due to the aromatic protons of phenothiazine and anthracene moiety. The ^1H NMR spectrum of the polymer is shown in Figure 4.17.

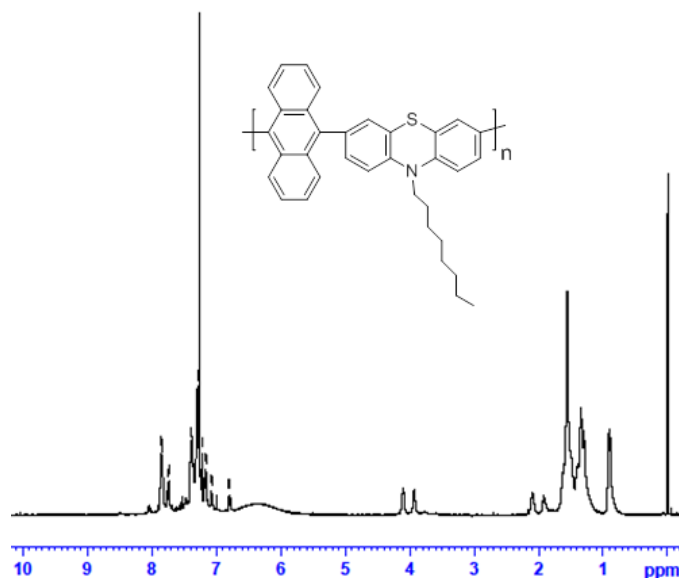


Figure 4.17: ^1H NMR spectrum of P(ANT-PHENO)

4.2.3.1 Optical Properties

Absorption spectrum of the polymer, P(ANT-PHENO) showed absorption maximum and absorption onset around 398 nm and 483 nm, respectively. The shape and structure of UV spectrum is the characteristic of the polynuclear aromatic hydrocarbons. The optical band gap was calculated to be 2.57 eV. From quantum chemical calculations, band gap obtained was 2.86 eV. The band gap calculated from optical method is in good agreement with the theoretical value. Figure 4.18 shows the absorption spectrum of the copolymer.

Emission spectrum of the polymer was recorded in THF. Polymer P(ANT-PHENO) showed emission peak at 532 nm. Figure 4.19 shows the emission spectrum of the copolymer in THF.

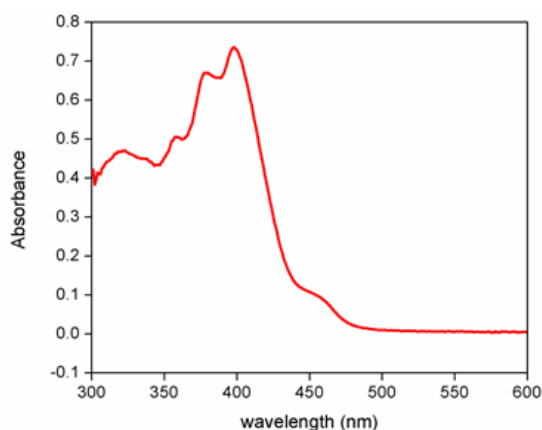


Figure 4.18: UV-Vis spectrum of P(ANT-PHENO) in THF

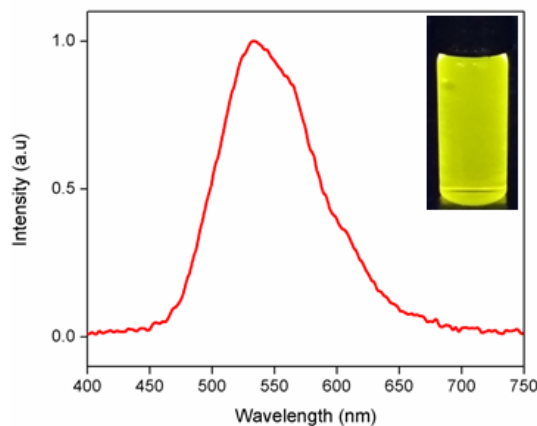


Figure 4.19: Emission spectrum of P(ANT-PHENO) in THF (2 mg/10 mL) (Excitation wavelength 365 nm)

4.2.3.2 Thermal and Electrochemical Properties

The thermal and electrochemical properties of the polymer were investigated. TG-DTG curve of the polymer, P(ANT-PHENO) followed single step degradation pattern (Figure 4.20). It showed onset of degradation around 390 °C and degradation at a temperature of 410 °C with about 6 % weight loss as the onset loss point.

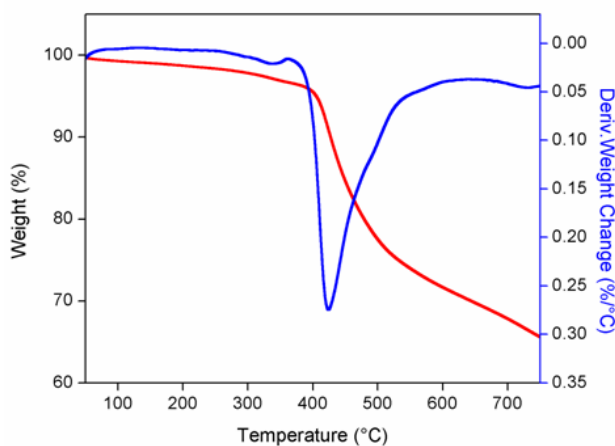


Figure 4.20: TG-DTG trace of P(ANT-PHENO)

The HOMO, LUMO levels and band gap of the polymer were obtained from cyclic voltammetric studies. From the onset of oxidation, the HOMO and LUMO levels of P(ANT-PHENO) were calculated to be -5.69 eV and -3.81 eV, respectively. The band gap of the polymer was calculated to be 1.88 eV. The values of HOMO, LUMO and band gap of the copolymer is presented in Table 4.14. The electrochemical band gap of the polymer was found to be lower than that obtained by theoretical and optical methods. The reason for low value of electrochemical band gap when compared to the theoretical value is that the theoretical calculation included the assumption that the molecules are in the gas phase. But, in the case of electrochemical method the molecule is assumed to be in solid phase. The ordered molecular orientation resulted in the lower band gap value. Band gap calculated by means of theoretical, electrochemical and optical methods are depicted in Table 4.15.

Table 4.14: HOMO, LUMO levels and band gap of polymers calculated by means of electrochemical method

Polymer	HOMO - $(4.71 + E_{\text{ox}}^{\text{onset}})$ (eV)	LUMO - $(4.71 + E_{\text{red}}^{\text{onset}})$ (eV)	Eg (Electrochemical) (eV)
P(ANT-PHENO)	-5.69	-3.81	1.88

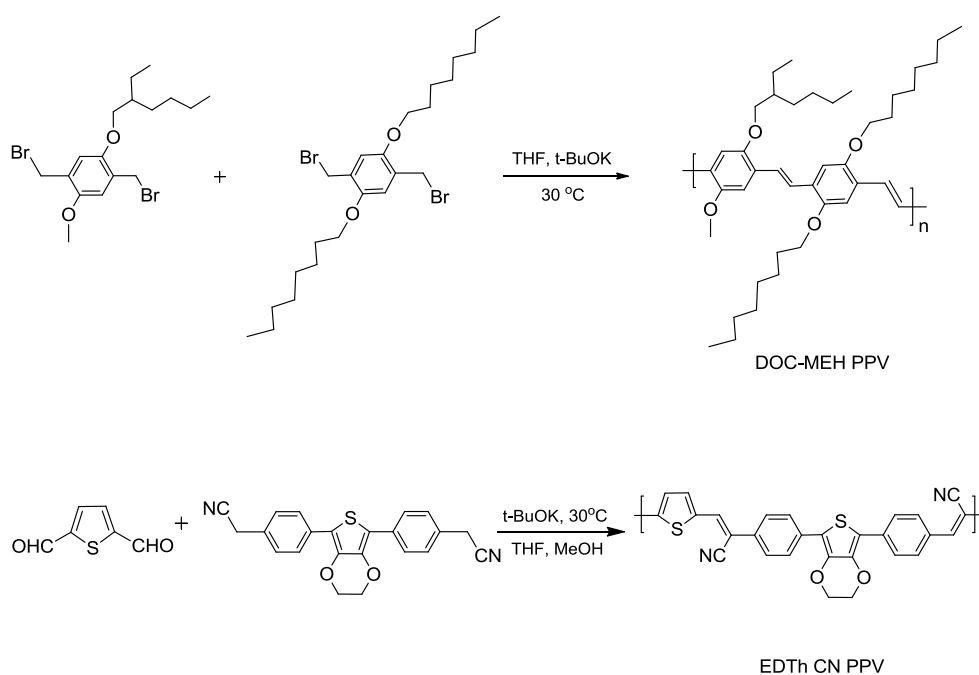
Table 4.15: Band gaps calculated by means of theoretical, electrochemical and optical methods

Polymer	Eg (Theoretical) (eV)	Eg (Electrochemical) (eV)	Eg (Optical) (eV)
P(ANT-PHENO)	2.86	1.88	2.57

4.2.4 Synthesis of Phenylenevinylene Polymers (PPV)

4.2.4.1 DOC-MEH PPV and EDTh CN PPV

The two phenylenevinylene polymers, DOC-MEH PPV and EDTh CN PPV were synthesized by Gilch polymerization reaction and Knoevenagel polycondensation reaction, respectively. These two reactions have taken place in the presence of potassium tertiary butoxide (t-BuOK) at 30 °C. The synthesized copolymers were soluble in tetrahydrofuran (THF). The synthetic route for the phenylenevinylene based polymers is depicted in Scheme 4.10.



Scheme 4.10: Synthesis of DOC-MEH PPV and EDTh CN PPV

The polymer, DOC-MEH PPV exhibited number average molecular weight (M_n) of 15975 and weight average molecular weight (M_w) of 22828 with polydispersity index (PDI) of 1.43. The polymer, EDTh CN PPV exhibited number average molecular weight (M_n) of 3635 and weight average molecular weight (M_w) of 4915 with polydispersity index (PDI) of 1.35. Table 4.16 summarizes the molecular weight and polydispersity index (PDI) of the copolymers. The polymers, DOC-MEH PPV and EDTh CN PPV showed peak molecular weight of 17723 and 4630, respectively.

Table 4.16: Results of the polymerization reaction

Polymer	M_n	M_w	M_p	PDI
DOC-MEH PPV	15975	22828	17723	1.43
EDTh CN PPV	3635	4915	4630	1.35

The ^1H NMR spectra of the polymers are shown in Figure 4.21. ^1H NMR spectrum of DOC-MEH PPV showed resonance peaks corresponding to aliphatic protons of alkyl chain at δ 0.9-1.9 as multiplet. Peaks observed around δ 3.9-4.2 are due to $-\text{O}-\text{CH}_2-$ protons of alkyl chains. The peaks observed at δ 7.1-7.6 are due to the unsaturated aliphatic protons of vinylene linkage and aromatic protons of phenyl rings. ^1H NMR spectrum of EDTh CN PPV showed resonance peaks corresponding to $-\text{OCH}_2-$ protons at δ 5.3. The peaks observed at δ 6.9-7.7 as multiplet are due to the aromatic protons and aliphatic protons of vinylene linkage.

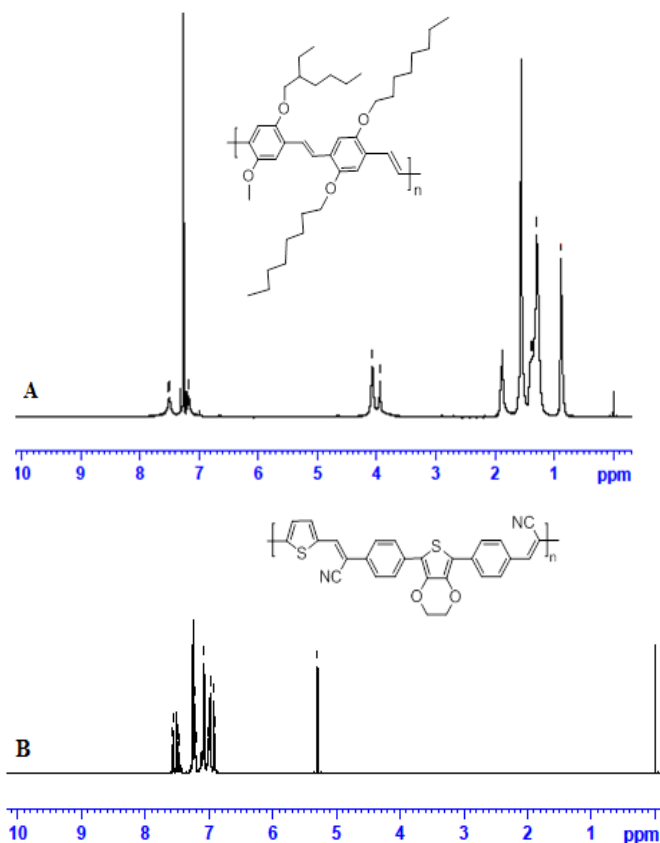


Figure 4.21: ¹H NMR spectra of (A) DOC-MEH PPV and (B) EDTh CN PPV

4.2.4.1.1 Optical Properties

Absorption spectra of polymers were recorded in THF. The polymers DOC-MEH PPV and EDTh CN PPV showed absorption maximum around 492 nm and 457 nm, respectively. The absorption onset of polymers DOC-MEH PPV and EDTh CN PPV occur at 553 nm and 572 nm, respectively. The optical band gap calculated was found to be 2.24 eV and 2.17 eV, respectively. From quantum chemical calculations, band gaps obtained were 1.79 eV and 1.81 eV respectively. Figure 4.22 shows the absorption spectra of the phenylenevinylene polymers.

Figure 4.23 shows the emission spectra of DOC-MEH PPV and EDTh CN PPV in THF. Emission spectrum of polymer DOC-MEH PPV showed emission peak at 554 nm. The polymer, EDTh CN PPV showed emission peak at 580 nm with a shoulder peak at 608 nm. This shoulder peak could be due to the out of the plane twisting of the two phenyl rings that are attached covalently to the 3,4-ethylenedioxythiophene ring.

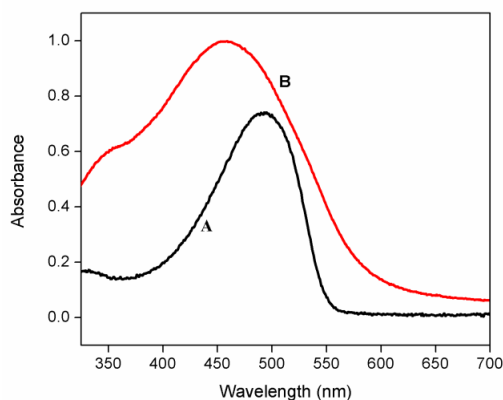


Figure 4.22: UV-Vis spectra: (A) DOC-MEH PPV and (B) EDTh CN PPV in THF

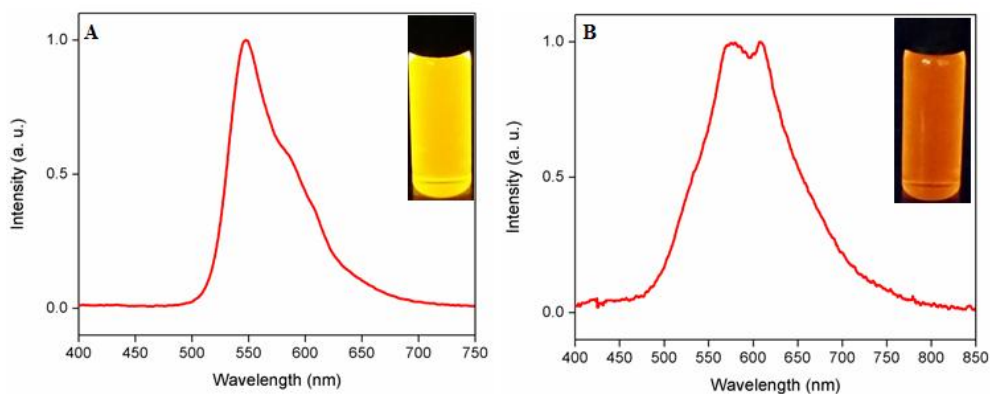


Figure 4.23: Emission spectra of the polymers: (A) DOC-MEH PPV and (B) EDTh CN PPV in THF (2 mg/10mL) (Excitation wavelength 365 nm)

4.2.4.1.2 Thermal Properties

The thermal stability of the polymers were investigated by TG-DTG analysis. From the TG traces of the synthesized polymers, it is clear that the polymers DOC-MEH PPV and EDTh CN PPV followed single step degradation pattern. In DOC-MEH PPV, DTG traces showed onset of degradation around 385 °C and degradation temperature at 435 °C with about 4% weight loss as the onset loss point. In EDTh CN PPV, the onset of degradation is around 380 °C and the degradation temperature is at 415 °C. Here about 6 % weight loss took place at the onset loss point. TG-DTG traces of the polymers are shown in the Figure 4.24.

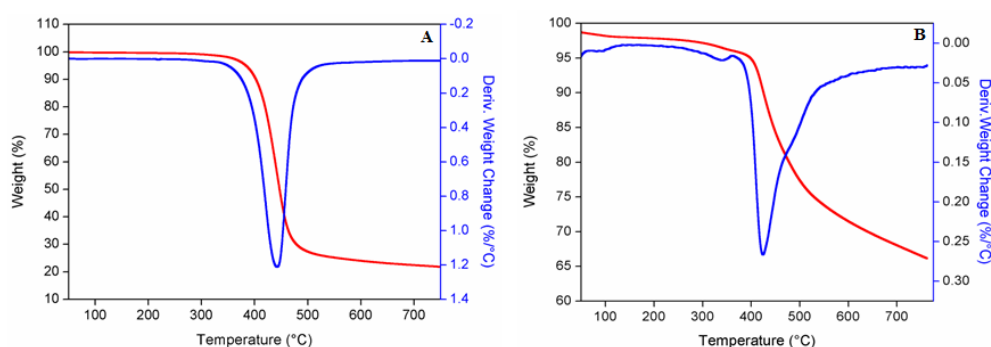


Figure 4.24: TG-DTG traces of the polymers: (A) DOC-MEH PPV and (B) EDTh CN PPV

4.2.4.1.3 Electrochemical Studies

From the cyclic voltammetric traces, the HOMO levels of DOC-MEH PPV and EDTh CN PPV were calculated to be -5.71 eV and -5.71 eV, respectively. The LUMO energy of DOC-MEH PPV and EDTh CN PPV were calculated to be -3.91 eV and -4.05 eV, respectively. The band gaps of the polymers DOC-MEH PPV and EDTh CN PPV were calculated to be 1.80 eV and 1.66 eV, respectively. The values of HOMO, LUMO and band

gap of the phenylenevinylene polymers are shown in Table 4.17. Band gap calculated by means of theoretical, electrochemical and optical methods are depicted in Table 4.18.

Table 4.17: HOMO, LUMO levels and band gap of polymers calculated by means of electrochemical method

Polymer	HOMO - (4.71 + E _{ox} ^{onset}) (eV)	LUMO - (4.71 + E _{red} ^{onset}) (eV)	E _g (Electrochemical) (eV)
DOC-MEH PPV	-5.71	-3.91	1.80
EDTh CN PPV	-5.71	-4.05	1.66

Table 4.18: Band gaps calculated by means of theoretical, electrochemical and optical methods

Polymer	E _g (Theoretical) (eV)	E _g (Electrochemical) (eV)	E _g (Optical) (eV)
DOC-MEH PPV	1.79	1.80	2.24
EDTh CN PPV	1.81	1.66	2.17

4.3 Experimental

4.3.1 Synthesis of Thiophene Based Polymers

4.3.1.1 General Procedure for the Polymerization

To a stirred solution of 3,4-ethylenedioxythiophene/3,4-dimethoxythiophene (0.53 mmol) in 10 mL DMF was added tetrabutylammonium bromide (0.175 g, 0.53 mmol) and sodium acetate (0.29 g, 2.1 mmol). The reaction mixture was stirred at room temperature for 15 min followed by the addition of the dibromo derivative of the monomer (0.53 mmol) and 10 mol % palladium acetate. The reaction mixture was stirred at 90 °C for 48 h. The reaction mixture was cooled to room temperature and poured in to ice cold methanol.

The precipitate was filtered and washed with methanol. The polymers were purified by soxhlet extraction using acetone and methanol for 24 h. The residue was dissolved in minimum amount of chloroform and re-precipitated from methanol. The precipitate was filtered and dried under vacuum.

4.3.1.1.1 Synthesis of P(EDT-TPAFL)

3,4-Ethylenedioxythiophene (0.075 g, 0.53 mmol), tetrabutylammonium bromide (0.175 g, 0.53 mmol), sodium acetate (0.29 g, 2.1 mmol), 9,9-bis(4-diphenylaminophenyl)-2,7-dibromofluorene (0.26 g, 0.53 mmol) and palladium acetate (0.012 g, 0.053 mmol) were used.

Yield : 46 %
UV-Vis (CHCl₃) λ_{\max} : 469 nm
¹H NMR (400 MHz, CDCl₃) : δ 3.7-4.0 (4 H, m), 6.9 (4 H, d), 7.0 (8 H, d),
7.2 (8H, d), 7.3 (8 H, d), 7.6 (2H, d),
8.0 (4 H, d)

4.3.1.1.2 Synthesis of P(DMT-TPAFL)

3,4-Dimethoxythiophene (0.076 g, 0.53 mmol), tetrabutylammonium bromide (0.175 g, 0.53 mmol), sodium acetate (0.29 g, 2.1 mmol), 9,9-bis(4-diphenylaminophenyl)-2,7-dibromofluorene (0.26 g, 0.53 mmol) and palladium acetate (0.012 g, 0.053 mmol) were used.

Yield : 52 %
UV-Vis (CHCl₃) λ_{\max} : 432 nm
¹H NMR (400 MHz, CDCl₃) : δ 4.3 (6 H, m), 6.9 (4 H, d), 7.0 (8 H, d),
7.2 (8H, d), 7.3 (8 H, d), 7.7 (2H, d), 7.8
(4 H, d)

4.3.1.1.3 Synthesis of P(EDT-TPA)

3,4-Ethylenedioxythiophene (0.075 g, 0.53 mmol), tetrabutylammonium bromide (0.175 g, 0.53 mmol), sodium acetate (0.29 g, 2.1 mmol), 4,4'-dibromotriphenylamine (0.21 g, 0.53 mmol) and palladium acetate (0.012 g, 0.053 mmol) were used.

Yield : 40 %
UV-Vis (CHCl₃) λ_{max} : 431 nm
¹H NMR (400 MHz, CDCl₃) : δ 4.3 (4 H, d), 7.1 (6 H, m), 7.4 (3 H, m),
7.7 (4 H, m)

4.3.1.1.4 Synthesis of P(DMT-TPA)

3,4-Dimethoxythiophene (0.076 g, 0.53 mmol), tetrabutylammonium bromide (0.175 g, 0.53 mmol), sodium acetate (0.29 g, 2.1 mmol), 4,4'-dibromotriphenylamine (0.21 g, 0.53 mmol) and palladium acetate (0.012 g, 0.053 mmol) were used.

Yield : 52 %
UV-Vis (CHCl₃) λ_{max} : 408 nm
¹H NMR (400 MHz, CDCl₃) : δ 3.9 (6 H, s), 7.1 (6 H, m), 7.4 (3 H, m),
7.7 (4 H, m)

4.3.1.1.5 Synthesis of P(EDT-DOB)

3,4-Ethylenedioxythiophene (0.075 g, 0.53 mmol), tetrabutylammonium bromide (0.175 g, 0.53 mmol), sodium acetate (0.29 g, 2.1 mmol), 1,4-dibromo-2,5-bis(octyloxy)benzene (0.26 g, 0.53 mmol) and palladium acetate (0.012 g, 0.053 mmol) were used.

Yield : 57 %

UV-Vis (CHCl₃) λ_{max} : 487 nm

¹H NMR (400 MHz, CDCl₃) : δ 0.8 (6 H, m), 1.3, 1.7 (20 H, m),
1.9 (4 H, m), 3.8 (4 H, s), 4.1, 4.4 (4H, s),
7.3 (2 H, s)

4.3.2 Synthesis of Fluorene Based Polymers

4.3.2.1 General Procedure for Polymerization through Suzuki Coupling

Under nitrogen atmosphere, 40 mL of dry THF was added to a flask charged with 10 mol % of Pd(PPh₃)₄. To this round bottomed flask, dibromo derivative of the monomer (0.36 mmol) and 2,7-Bis(4,4,5,5-tetramethyl-1,3,2-dioxaborolan-2-yl)-9,9-dioctylfluorene (0.23 g, 0.36 mmol) were added followed by potassium phosphate (2 equiv, 0.14 g). The mixture was stirred vigorously at 80-90 °C for 72 h. The reaction mixture was cooled to room temperature and added dropwise into stirring ice cold methanol to precipitate the polymer. The precipitate was collected by filtration and washed with methanol and acetone. The polymer was washed continuously with methanol and acetone for 2 days in a soxhlet extractor to remove the oligomers and catalyst residues. The product was dried under reduced pressure.

4.3.2.1.1 Synthesis of P(FL-TPAFL)

9,9-Bis(4-diphenylaminophenyl)-2,7-dibromofluorene (0.29g, 0.36 mmol), 2,7-Bis(4,4,5,5-tetramethyl-1,3,2-dioxaborolan-2-yl)-9,9-dioctylfluorene (0.23 g, 0.36 mmol), potassium phosphate (2 equiv, 0.14 g), Pd(PPh₃)₄ (0.04 g, 0.036 mmol) were used.

Yield : 64 %
UV-Vis (CHCl₃) λ_{max} : 385 nm
¹H NMR (400 MHz, CDCl₃) : δ 0.8 (6 H, s), 1.2 (4 H, s), 1.6 (20 H, s), 1.9 (4 H, s), 6.9 (4 H, d), 7.0 (8 H, d), 7.2 (8H, d), 7.3 (8 H, d), 7.6 (2H, d), 7.9 (10 H, d)

4.3.2.1.2 Synthesis of P(FL-DPPPh)

3,6-Bis(4-bromophenyl) 2,5-dihydropyrrolo[3,4-c]pyrrole-1,4-dione (0.16 g, 0.36 mmol), 2,7-Bis(4,4,5,5-tetramethyl-1,3,2-dioxaborolan-2-yl)-9,9-dioctylfluorene (0.23 g, 0.36 mmol), potassium phosphate (2 equ, 0.14 g), Pd(PPh₃)₄ (0.04 g, 0.036 mmol) were used.

Yield : 44 %
UV-Vis (CHCl₃) λ_{max} : 542 nm
¹H NMR (400 MHz, CDCl₃) : δ 1.2 (6 H, s), 1.8 (4 H, s), 2.7 (20 H, s), 3.4 (4 H, s), 7.8 (2 H, m), 8.1-8.5 (12 H, m), 8.7 (2 H, s)

4.3.2.1.3 Synthesis of P(FL-TPA)

4,4'-Dibromotriphenylamine (0.145 g, 0.36 mmol), 2,7-Bis(4,4,5,5-tetramethyl-1,3,2-dioxaborolan-2-yl)-9,9-dioctylfluorene (0.23 g, 0.36 mmol), potassium phosphate (2 equiv, 0.14 g), Pd(PPh₃)₄ (0.04 g, 0.036 mmol) were used.

Yield : 68 %
UV-Vis (CHCl₃) λ_{max} : 379 nm
¹H NMR (400 MHz, CDCl₃) : δ 0.7 (6 H, s), 1.1 (4 H, s), 1.6 (20 H, s),
2.0 (4 H, s), 7.0 (6 H, m), 7.2 (5 H, m),
7.6 (6H, m), 7.7 (2 H, m)

4.3.2.1.4 Synthesis of P(FL-BP)

4,4'-Dibromobiphenyl (0.11 g, 0.36 mmol), 2,7-Bis(4,4,5,5-tetramethyl-1,3,2-dioxaborolan-2-yl)-9,9-dioctylfluorene (0.23 g, 0.36 mmol), potassium phosphate (2 equiv, 0.14 g), Pd(PPh₃)₄ (0.04 g, 0.036 mmol) were used.

Yield : 51 %
UV-Vis (CHCl₃) λ_{max} : 353 nm
¹H NMR (400 MHz, CDCl₃) : δ 0.7 (6 H, s), 1.1 (4 H, s), 1.6 (20 H, s),
2.0 (4 H, s), 7.1 (6 H, m), 7.5 (4 H, m),
7.8 (4 H, m)

4.3.3 Synthesis of Anthracene-phenothiazine copolymer, P(ANT-PHENO)

3,7-Dibromo-10-octyl-phenothiazine (0.17 g, 0.36 mmol), 9,10-anthracene diboronic acid bis(pinacol) ester (0.155 g, 0.36 mmol), potassium phosphate (2 equiv, 0.14 g), Pd(PPh₃)₄ (0.04 g, 0.036 mmol) were used.

Yield : 48 %
UV-Vis (CHCl₃) λ_{max} : 398 nm
¹H NMR (400 MHz, CDCl₃) : δ 0.8 (3 H, s), 1.4 (10 H, d), 2.0 (2 H, d),
4.0 (2 H, d), 6.9-7.6 (10 H, m), 7.9 (4 H, m)

4.3.4 Synthesis of Phenylenevinylene Polymers

4.3.4.1 Synthesis of DOC-MEH PPV

To a solution of 1,4-bis(bromomethyl)-2-((2-ethylhexyl)oxy)-5-methoxybenzene (0.84 g, 2 mmol) and 1,4-bis(bromomethyl)-2,5-bis(octyloxy)benzene (1.04 g, 2 mmol) in 20 mL of anhydrous THF was added drop wise to a solution of 95 % potassium t-butoxide (2.12 g, 18 mmol) in 80 mL of THF at 30 °C with stirring. The solution was poured into cold methanol. The precipitate was filtered and washed with methanol. The polymer was further purified by soxhlet extraction with acetone and methanol to afford a red solid.

Yield : 35 %
UV-Vis (CHCl₃) λ_{max} : 492 nm
¹H NMR (400 MHz, CDCl₃) : δ 0.9 (12 H, s), 1.4 (28 H, m), 1.7 (4 H, m),
1.9 (1 H, s), 4.0 (5 H, m), 4.2 (4 H, m),
7.3 (4 H, M), 7.6 (4 H, d)

4.3.4.2 Synthesis of EDTh CN PPV

A solution of 2,5-thiophenedicarboxaldehyde (0.14 g, 1 mmol) and 2,2'-((2,3-dihydrothieno[3,4-b][1,4]dioxine-5,7-diyl)bis(4,1 phenylene)) diacetonitrile (0.37 g, 1 mmol) in 20 mL of mixture of anhydrous methanol and THF in 1:1 ratio was placed in a round bottomed flask and stirred under a gentle flow of nitrogen. 3 mmol of potassium t-butoxide in 15 mL of THF was added at 30 °C with stirring. After 15 minutes, 30 mL of methanol was added to the reaction mixture and acidified with conc. HCl. The polymer was filtered and further purified by soxhlet extraction with acetone and methanol.

Yield : 30 %
UV-Vis (CHCl₃) λ_{max} : 457 nm
¹H NMR (400 MHz, CDCl₃) : δ 5.2 (4 H, s), 6.9 (2 H, m), 7.0-7.3 (6 H, m), 7.5 (4 H, m).

4.4 Conclusion

Twelve theoretically designed polymers were synthesized by means of Direct arylation polymerization, Suzuki Coupling polymerization, Gilch polymerization and Knoevenagel polycondensation reactions. All the polymers were characterized by ¹H NMR and UV-visible spectroscopy. Molecular weight of the polymers was determined by GPC analysis. Electrochemical and thermal properties of polymers were obtained from cyclic voltammetry and thermogravimetric analysis. Experimental band gap of the polymers were obtained from optical and electrochemical methods.

References

- [1] C. K. Chiang, M. A. Druy, S. C. Gau, A. J. Heeger, E. J. Louis, A. G. MacDiarmid, Y. W. Park, H. J. Shirakawa, *J. Am. Chem. Soc.*, 1978, **100**, 1013.
- [2] A. J. Heeger, *Angew. Chem.*, 2001, **113**, 2660.
- [3] A. G. McDiarmid, *Angew. Chem.*, 2001, **113**, 2649.
- [4] H. Shirakawa, *Angew. Chem.*, 2001, **113**, 2642.
- [5] W. E. Moerner, S. M. Silence, *Chem. Rev.*, 1994, **94**, 127.
- [6] M. X. Chen, E. Perzon, N. Robisson, S. K. M. Jonsson, M. R. Andersson, M. Fahiman, M. Berggren, *Synth. Met.*, 2004, **146**, 233.
- [7] X. Gong, S. Wang, *Polymer Light-Emitting Diodes: Devices and Materials*, S. S. Sun, L. R. Dalton; CRC Press, Boca Raton, 2008.
- [8] N. Blouin, A. Michaud, D. Gendron, S. Wakim, E. Blair, R. N. Plesu, M. Belletete, G. Durocher, Y. Tao, M. Leclerc, *J. Am. Chem. Soc.*, 2008, **130**, 732.
- [9] E. Bundgaard, F. C. Krebs, *Sol. Energy Mater. Sol. Cells.*, 2007, **91**, 954.
- [10] A. C. Arias, S. E. Ready, R. Lujan, W. S. Wong, K. E. Paul, A. Salleo, M. L. Chabiny, R. Apte, R. A. Street, Y. Wu, P. Liu, B. Ong, *Appl. Phys. Lett.*, 2004, **85**, 3304.
- [11] B. J. de Gans, P. C. Duineveld, U. S. Schubert, *Adv. Mater.*, 2004, **16**, 203.
- [12] J. L. Reddinger, R. J. Reynolds, *Adv. Polym. Sci.*, 1999, **145**, 57.
- [13] C. A. Thomas, *Donor-acceptor methods for band gap reduction in conjugated polymers: The role of electron rich donor heterocycles*, PhD Thesis, University of Florida, 2002.
- [14] L. G. Meercier, M. Leclerc, *Acc. Chem. Res.*, 2013, **46**, 1597.
- [15] Y. Fujinami, J. Kuwabara, W. Lu, H. Hayashi, T. Kanbara, *ACS Macro Lett.*, 2012, **1**, 67.

- [16] S. J. Choi, J. Kuwabara, T. Kanbara, *ACS Sustain. Chem. Eng.*, 2013, **1**, 878.
- [17] M. Baumann, I. R. Baxendale, *Beilstein. J. Org. Chem.*, 2013, **9**, 2265.
- [18] G. L. Gibson, T. M. McCormick, D. S. Seferos, *J. Am. Chem. Soc.*, 2012, **134**, 539.
- [19] K. Colladet, S. Fourier, T. J. Cleij, L. Lutsen, J. Gelan, D. Vanderzande, N. L. Huong, H. Naugebauer, S. Sariciftci, A. Aguirre, G. Janssen, E. Goovaerts, *Macromolecules*, 2007, **40**, 65.
- [20] N. S. Cho, J. H. Park, S. K. Lee, J. Lee, H. K. Shim, M. J. Park, D. H. Hwang, B. J. Jung, *Macromolecules*, 2006, **39**, 177.
- [21] R. Li, Y. Mo, R. Shi, P. Li, C. Li, Z. Wang, X. Wang, S. Li, *Monatsh Chem.*, 2014, **145**, 85.
- [22] P. Puschig, C. A. Draxl, G. Heimel, E. Zojer, R. Resel, G. Leising, M. Kriechbaum, W. Graupner, *Synth. Met.*, 2001, **116**, 327.
- [23] V. J. Eaton, D. Steele, *J. Chem. Soc. Faraday Trans.*, 1973, **2**, 1601.

.....✂.....

Chapter 5

NONLINEAR OPTICAL AND PHOTOVOLTAIC APPLICATIONS OF CONJUGATED POLYMERS

Contents

- 5.1 Introduction
- 5.2 Results and Discussion
- 5.3 Conclusion

In this chapter, third-order nonlinear optical and photovoltaic applications of synthesized polymers are discussed. Third-order nonlinear absorption coefficient (β), imaginary part of nonlinear susceptibility ($\text{Im}\chi^{(3)}$) and optical limiting threshold values of synthesized polymers were evaluated. Inverted and conventional solar cells were fabricated with some of the synthesized polymers blended with PCBM as active layer. Inverted cells were constructed using the device structure ITO/ZnO/Polymer: PCBM/Ag gave better power conversion efficiency.

5.1 Introduction

Conjugated polymers with low band gaps, suitable energy levels and high charge carrier mobility are suitable for functional applications. The band gap can be tuned by introducing suitable donor and acceptor moieties or introducing linker units. The combination of high-lying HOMO levels (residing on the donor units) and low-lying LUMO levels (residing on the acceptor units) results in an overall low band gap for the polymer. The band

gap can be narrowed or widened on the basis of the choice of donor and acceptor units, or more specifically, the difference in electron density between the donor and acceptor units along the polymer backbone.¹ Recently, nonlinear optical (NLO) properties of organic photonic materials have become the subject of current research interest, because of their potential applications in a wide variety of optoelectronic devices.² Nonlinear optical properties, large third-order susceptibility and fast response time and processability of donor-acceptor groups have been studied by several researchers.³ This in turn has attracted the present interest in investigating nonlinear optical properties of copolymers. Donor-acceptor conjugated polymers have strong nonlinear optical (NLO) properties because of their two photon absorption. Two photon absorption (TPA) has considerable interest due to its potential applications in two-photon fluorescence imaging,^{4,5} optical data storage⁶ and optical power limiting.⁷

The development of bulk heterojunction polymer solar cells (PSCs) has become an interesting area of research and has focused on the synthesis of new photovoltaic conjugated polymers and the development of device fabrication technologies. Low band gap materials can harvest photons at longer wavelength which improve the efficiency of organic photovoltaics, due to a better overlap of the absorption spectrum and the solar spectrum.⁸⁻¹⁰ The present chapter is concerned with the third-order nonlinear optical and photovoltaic properties of synthesized conjugated polymers.

5.1.1 Nonlinear Optics

Nonlinear optics (NLO) is the branch of optics that describes the behavior of light in nonlinear media. The field of nonlinear optics developed

gradually with the invention of lasers. In the beginning, research advances were made on inorganic ferroelectric materials followed by semiconductors. In the 1970's, the importance of organic materials was realized because of their nonlinear optical responses, fast optical response, high laser damage thresholds, architectural flexibility, and ease of fabrication. At present, materials can be classified into three categories: inorganic ferroelectrics, semiconductors, and organic materials.¹¹ At low intensity of light, typical of non-laser sources, the properties of materials remain independent of the intensity of illumination. Laser sources can provide sufficiently high light intensities to modify the optical properties of materials. Light waves can then interact with each other, exchanging momentum and energy, and the superposition principle is no longer valid. This interaction of light waves can result in the generation of optical fields at new frequencies, including optical harmonics of incident radiation or sum- or difference-frequency signals.¹²

5.1.1.1 Z-scan Technique

The open aperture Z-scan experiment was performed to determine the third-order nonlinear absorption coefficient, β_{eff} of the synthesized polymers. Nonlinear absorption in a nonlinear optical material are of two types, one is saturable absorption (SA) and the other is reverse saturable absorption (RSA). In SA process, the transmittance increases forming a peak at the focus and in RSA process, valley is formed at the focus.¹³ The nonlinear absorption is occurring due to several mechanisms including two-photon absorption (TPA), RSA, free carrier absorption (FCA) and nonlinear scattering.¹⁴ In semiconductor polymeric materials, along with TPA, FCA is

a higher order nonlinear process that may also contribute to the induced absorption. But, in comparison with TPA, FCA is a weak process and hence its contribution to the nonlinear absorption is relatively less.¹⁵ Using a single, focused laser beam, one measures the transmittance of a sample through a partially obscuring circular aperture (Z-scan). The transmittance is determined as a function of the sample position (Z) measured with respect to the focal plane. The open aperture (OA) Z-scan technique was performed at 532 nm. The open aperture curve exhibits a normalized transmittance valley, indicating the presence of induced absorption in the solution state, indicating the reverse saturation (RSA) type of absorption with a positive NLO absorption coefficient.^{16,17} The normalized transmittance for the standard OA Z-scan is expressed by the Eq. (5.1)

$$T_{(Z)} = \frac{C}{q_0 \sqrt{\pi}} \int_{-\infty}^{\infty} \ln(1 + q_0 e^{-t}) dt \dots\dots\dots (5.1)$$

where, $q_0 = \beta I_0(t) L_{\text{eff}}$ and $L_{\text{eff}} = (1 - e^{-\alpha l})/\alpha$ is the effective thickness with linear absorption coefficient α and I_0 is the irradiance at focus.

The experimental data obtained were fitted with the theoretical curves for RSA and the effective nonlinear absorption coefficient, β for the copolymers was calculated. The imaginary part of the third-order nonlinear susceptibility, $\text{Im}\chi^{(3)}$ of the polymer is calculated by Eq.(5.2)

$$\text{Im}\chi^{(3)} = \frac{n_0^2 c^2 \beta}{240 \pi^2 \omega} \dots\dots\dots (5.2)$$

where, C is the velocity of light in vacuum, ω is the angular frequency of radiation, where $\omega = 2\pi/\lambda$ and $\lambda = 532$ nm.

The copolymers generally show strong optical nonlinearity due to donor-acceptor scheme. Reverse saturable absorption behavior of polymers is mainly due to the nonlinear mechanism such as two photon absorption.¹⁸

5.1.1.2 Optical Power Limiting

The measure of nonlinear transmission as a function of input fluence is used to investigate the optical limiting property of the polymer. A material which transmits light at low input intensities and become opaque at high inputs is called optical limiter. Optical limiting property of a material is mainly due to nonlinear absorption, which corresponds to the imaginary part of third-order susceptibility¹⁹ i.e., it could be due to free carrier absorption, reverse saturation absorption, self-focusing, self-defocusing or induced scattering. Recently, conducting polymers have drawn significant attention as optical limiters for eyes or for sensor protection from high intensity laser. The minimum standard required for a material to behave as an effective optical limiter is to have low limiting threshold, high linear transmittance throughout the bandwidth, stability etc.²⁰ Thus, the optical limiting properties of copolymers were studied by a standard OA z-scan technique at 532 nm. A material with low value of optical limiting threshold is a good optical limiter. The optical limiting curves were plotted by using Eq. (5.3).

$$I_{(z)} = \frac{E}{\pi \left(1 + \left(\frac{z}{z_0}\right)^2\right) \tau \omega_0^2} \dots\dots\dots (5.3)$$

where, $\tau = 7 \times 10^{-9}$ s, $\omega_0 = 42.56 \times 10^{-6}$ m, $E = 135 \mu\text{J}$, the z_0 value is obtained by the relation $z_0 = \pi \omega_0^2 / \lambda$.

5.1.2 Photovoltaics

5.1.2.1 Bulk Heterojunction Devices

A heterojunction is composed of two materials with different electron affinities and ionization potentials. At the interface, potentials created may favor exciton dissociation. The electron will be accepted by the material with the larger electron affinity and the hole will be accepted by the material with the lower ionization potential results in a difference in potential energy which is larger than the exciton binding energy.²¹⁻²⁴ In the case of bulk heterojunction, the two materials which are blended together will act as photoactive layer. The photoactive layer in polymeric bulk heterojunction photovoltaic device is composed of a blend of donor and acceptor with a maximized interfacial area between the materials.²⁵⁻²⁷ The photoactive layer can be processed from solution by spin coating. In a typical polymeric bulk heterojunction photovoltaic device, the photoactive layer is sandwiched between a transparent conductive oxide layer and a metal electrode. The photoactive layer is composed of low band gap conjugated polymer as donor and soluble fullerene derivative as acceptor.²⁷⁻²⁹

5.1.2.1.1 Conventional Photovoltaic Devices

In bulk heterojunction devices, electrons flow from acceptor to the metal electrode and holes flow from donor to the transparent conductive oxide layer (TCO). TCOs are fundamental components in photovoltaic devices. Indium tin oxide (ITO) is the generally used transparent conductive oxide. The work function of ITO is 4.5 eV - 4.7 eV, lying in between the HOMO and LUMO of the conjugated polymers and ITO has the ability to

collect both the holes and electrons.³⁰⁻³² If ITO is coated with hole transporting layer such as MoO₃ or anode buffer layer such as PEDOT:PSS, a conventional solar cell can be processed. Here, ITO can collect holes.

I. Etxebarria et al.³³ fabricated conventional photovoltaic devices in the configuration ITO/PEDOT:PSS/PTB7:PC70BM/Ca/Ag. Here, PEDOT:PSS was spin coated on ITO as hole transport layer.

5.1.2.1.2 Inverted Photovoltaic Devices

An inverted photovoltaic device can be processed by coating electron transporting materials like TiO₂, ZnO or In₂S₃ over ITO.^{34,35} Here, the holes and electrons are generated in the active layer in the reverse manner to that in a conventional photovoltaic device. The electron transporting material, usually an inorganic n-type semiconductor is coated between the ITO and the active layer. The inverted photovoltaic device has the advantage over the conventional devices because of the stability of the device.³⁶ S. Schumann et al.³⁷ fabricated inverted photovoltaic device in which ZnO was coated as electron collective layer between ITO and blended P3HT:PCBM photoactive layer. ZnO layers were controlled either by electro-deposition or spray pyrolysis techniques. The constructed OPV device gave a power conversion efficiency of 4.9 %.

5.1.2.2 I-V Characteristics of a Photovoltaic Device

The current-voltage characteristics of photovoltaic device correspond to a negative shift in amplitude of the dark current in the system as the optical intensity of the light is increased. The current-voltage characteristics

of a photovoltaic device in the dark and under illumination are shown in Figure 5.1. The power delivered by a solar cell is the product of current and voltage ($I \times V$).

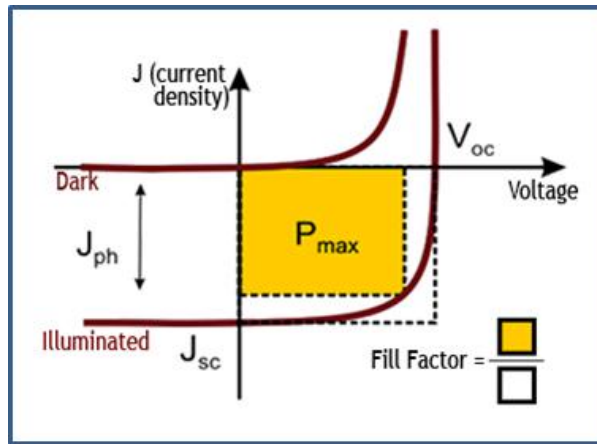


Figure 5.1: Current density-voltage curve of a photovoltaic device

The efficiency of a photovoltaic device is the ratio of the electrical power output P_{out} , compared to the solar power input, P_{in} , into the photovoltaic cell. P_{out} can be taken to be P_{max} since the solar cell can be operated up to its maximum power output to get the maximum efficiency. The power conversion efficiency of a solar cell is determined by the following formula:³⁸

$$\eta = \frac{(V_{oc} \times I_{sc} \times FF)}{P_{in}} \dots\dots\dots (5.4)$$

$$FF = \frac{(V_{mpp} \times I_{mpp})}{(V_{oc} \times I_{sc})} \dots\dots\dots (5.5)$$

where V_{oc} is the open circuit voltage, I_{sc} is the short circuit current, FF is the fill factor and P_{in} is the power density of the incident light. V_{mpp} and I_{mpp} are the voltage and current at the maximum power point.

5.1.2.3 Open Circuit Voltage

Open circuit voltage is the maximum possible voltage across a photovoltaic cell under illumination when disconnected from any circuit. It is the difference of electrical potential between two terminals of a photovoltaic device. In organic photovoltaic devices, the highest occupied molecular orbital level of the donor and lowest unoccupied molecular orbital level of acceptor define the open circuit voltage of the device in a linear way.^{39,40}

5.1.2.4 Short Circuit Current

The short circuit current is the current through the illuminated solar cell when the voltage across the solar cell is zero (i.e., when the solar cell is short circuited). The short circuit current is due to the generation and collection of light-generated carriers. For an ideal solar cell at most moderate resistive loss mechanism, the short circuit current and the light-generated current are identical. Therefore, the short circuit current is the largest current which may be drawn from the solar cell.

5.1.2.5 Fill Factor

Fill factor is the ratio of a photovoltaic cell's actual maximum power output to its theoretical power output if both current and voltage were at their maxima, I_{sc} and V_{oc} , respectively.

In this thesis, photovoltaic property of bulk heterojunctions fabricated in both conventional and inverted manner using some of the polymers as active layer by blending with PCBM has been evaluated.

5.2 Results and Discussion

5.2.1 Open Aperture (OA) Z-scan Measurements of the Polymers

NLO properties of the polymers were measured by the single beam Z-scan technique with nanosecond laser performed with a Q-switched Nd:YAG laser system (Spectra Physics LAB- 1760) with pulse width of 7 ns at 10 Hz repetition rate and 532 nm wavelength. The sample was moved in the direction of light propagation near the focal point of the lens with focal length of 200 mm. The radius of the beam waist was calculated to be 42.56 μm . The Z-scan system was calibrated using CS_2 as standard. The transmitted beam energy, reference beam energy and their ratios were measured simultaneously by an energy ratiometer (REj7620, Laser Probe Corp.) having two identical pyroelectric detector heads (Rjp 735). The effect of fluctuations of laser beam was eliminated by dividing the transmitted power by the power obtained at the reference detector; both being measured using identical photo detectors. The data were analyzed using the procedure described by Bahae et al.⁴¹ and the nonlinear optical coefficients were obtained by fitting the experimental Z-scan plot with the theoretical plots.

5.2.1.1 Thiophene Based Polymers

a) P(EDT-TPAFL) and P(DMT-TPAFL)

The open aperture (OA) Z-scan traces of the polymers, P(EDT-TPAFL) and P(DMT-TPAFL) in CHCl_3 are shown in Figure 5.2.

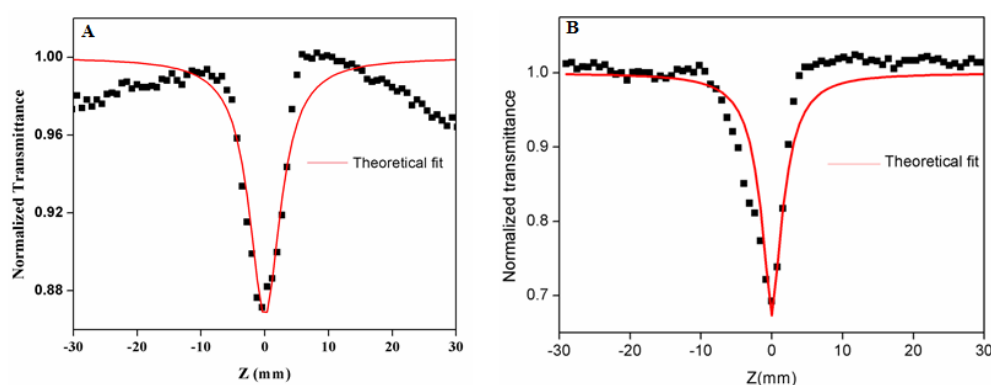


Figure 5.2: Open-aperture Z-scan traces of (A) P(EDT-TPAFL) and (B) P(DMT-TPAFL) in CHCl_3 at $135 \mu\text{J}$

Here, the two copolymers showed a normalized transmittance peak-valley type graph with a positive NLO absorption coefficient. The nonlinear absorption traces of the copolymers were fitted well with the graph derived from two photon absorption (TPA) theory. The two copolymers showed reverse saturable absorption type graph (Figure 5.2). The nonlinear absorption coefficient (β , m^2/W) and imaginary value of third-order nonlinear susceptibility ($\text{Im}\chi^{(3)}$, esu) were calculated.

Optical Power Limiting

The optical limiting properties of copolymers were studied by the standard OA Z-scan technique at 532 nm. Figure 5.3 shows the transmitted energy of the polymers P(EDT-TPAFL) and P(DMT-TPAFL) as a function

of input fluence. At low input fluence, the output varies linearly with input power. The optical limiting threshold is noted as the deviation from linearity. The optical limiting threshold of P(EDT-TPAFL) and P(DMT-TPAFL) was determined to be 0.36 GW cm^{-2} and 0.20 GW cm^{-2} , respectively. The low optical limiting threshold values of these polymers are due to the donor-acceptor scheme. A material with low value of optical limiting threshold is a good optical limiter.

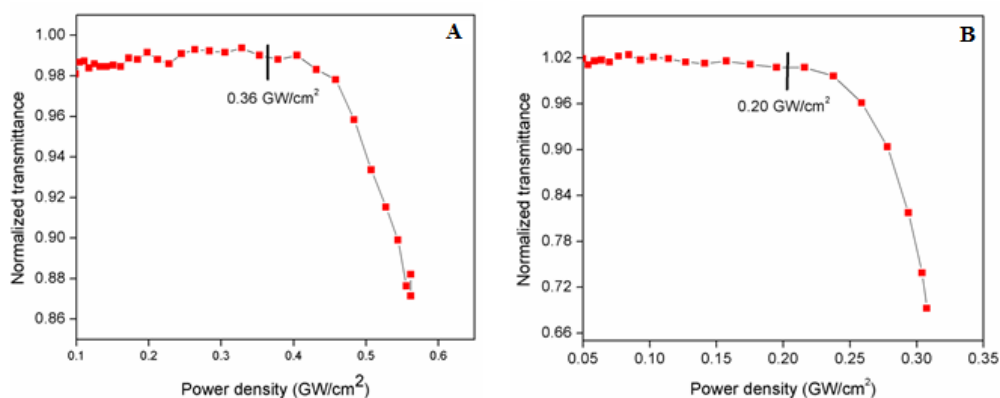


Figure 5.3: Optical limiting curve of (A) P(EDT-TPAFL) and (B) P(DMT-TPAFL)

The calculated values of third-order nonlinear absorption coefficient (β , m/W), imaginary value of third-order nonlinear susceptibility ($\text{Im}\chi^{(3)}$, esu) and optical limiting threshold values are given in the Table 5.1. The polymers showed large optical nonlinearity due to strong delocalization of π electrons. The third-order nonlinear absorption coefficient values of the polymers were found to be in the order of 10^{-10} mW^{-1} which showed that the band gap of each polymer was in the semiconducting range which was already confirmed theoretically and experimentally.

Table 5.1: Third-order nonlinear absorption coefficient (β , m/W), imaginary value of third-order nonlinear susceptibility ($\text{Im } \chi^{(3)}$, esu) and optical limiting threshold (GW/cm^2) of copolymers

Polymer	Nonlinear absorption coefficient (β , mW^{-1})	Imaginary part of nonlinear susceptibility ($\text{Im } \chi^{(3)}$, esu)	Optical limiting threshold (GW/cm^2)
P(EDT-TPAFL)	1.41×10^{-10}	0.29×10^{-11}	0.36
P(DMT-TPAFL)	3.82×10^{-10}	0.85×10^{-11}	0.20

b) P(EDT-TPA), P(DMT-TPA) and P(EDT-DOB)

The open-aperture (OA) Z-scan trace of the three polymers, P(EDT-TPA), P(DMT-TPA) and P(EDT-DOB) in THF are shown in Figure 5.4. The three copolymers P(EDT-TPA), P(DMT-TPA) and P(EDT-DOB) showed a normalized transmittance peak-valley type graph with a positive NLO absorption coefficient. The nonlinear absorption traces of the copolymers were fitted well with the graph derived from two photon absorption (TPA) theory.

The three copolymers showed reverse saturable absorption type graph (Figure 5.4). The third-order nonlinear absorption coefficient (β , m/W) and imaginary value of third-order nonlinear susceptibility ($\text{Im}\chi^{(3)}$, esu) were determined. The values of nonlinear absorption coefficient and imaginary part of nonlinear susceptibility were found to be in the order of 10^{-10} mW^{-1} and 10^{-11} esu respectively. This implied that the band gap values of these three polymers, P(EDT-TPA), P(DMT-TPA) and P(EDT-DOB) were in the semiconducting range. The strong nonlinearity is due to the charge transfer from donor to the acceptor units. The first excited state may be the charge-transfer state.

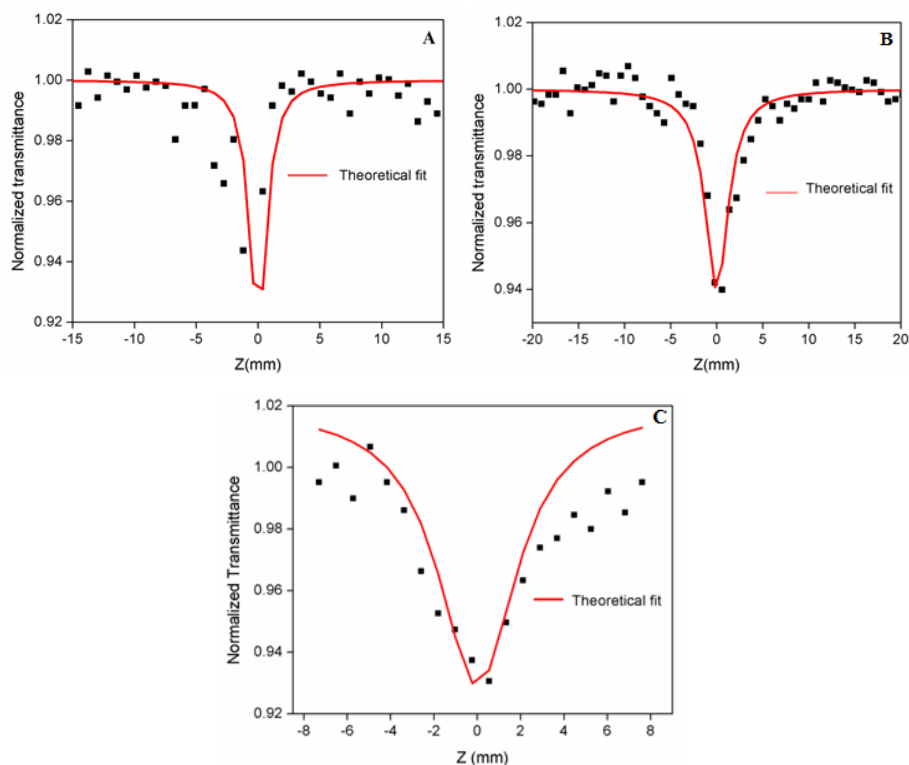


Figure 5.4: Open-aperture Z-scan traces of (A) P(EDT-TPA), (B) P(DMT-TPA) and (C) P(EDT-DOB) in THF at 135 μJ

Optical Power Limiting

Open aperture Z-scan technique was used to determine the optical limiting properties of the three copolymers. Figure 5.5 shows the transmitted energy of the polymers, P(EDT-TPA), P(DMT-TPA) and P(EDT-DOB) as a function of input fluence. The optical limiting threshold of P(EDT-TPA), P(DMT-TPA) and P(EDT-DOB) were determined to be 0.39 GW cm^{-2} , 0.31 GW cm^{-2} and 0.44 GWcm^{-2} , respectively. The low optical limiting threshold values of the polymers implied that the polymers could be chosen as good optical limiters. The calculated values of nonlinear absorption

coefficient (β , m/W), imaginary value of third-order nonlinear susceptibility ($\text{Im}\chi^{(3)}$, esu) and optical limiting threshold values are given in the Table 5.2.

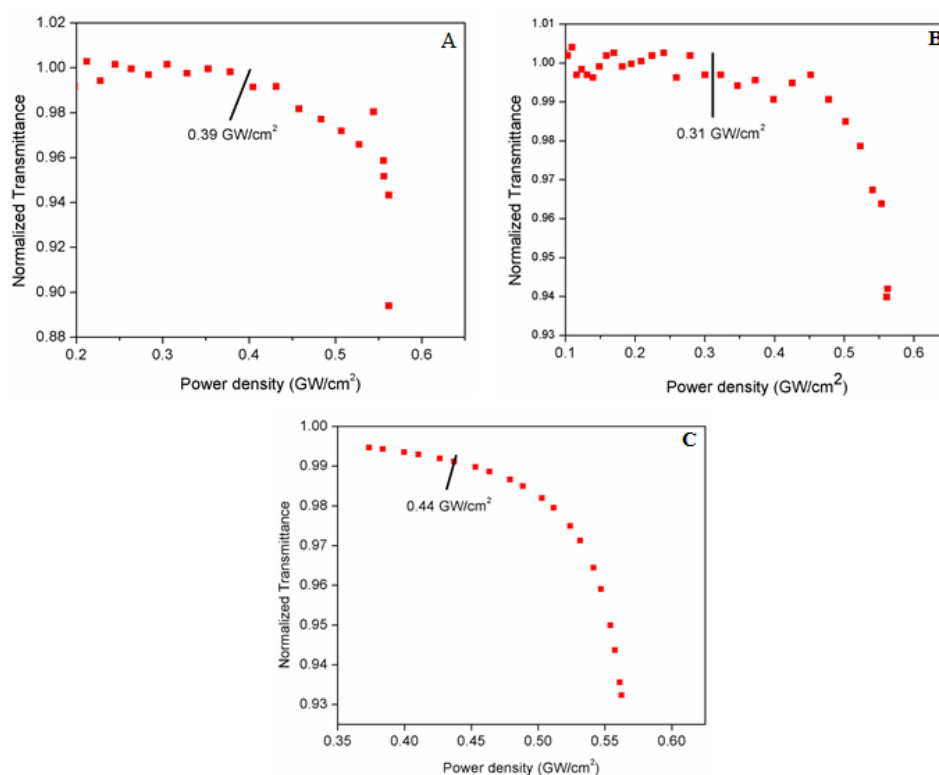


Figure 5.5: Optical limiting curves of (A) P(EDT-TPA), (B) P(DMT-TPA) and (C) P(EDT-DOB)

Table 5.2: Third-order nonlinear absorption coefficient (β , m/W), imaginary value of third order nonlinear susceptibility ($\text{Im}\chi^{(3)}$, esu) and optical limiting threshold (GW/cm^2) of copolymers

Polymer	Nonlinear absorption coefficient (β , mW^{-1})	Imaginary part of nonlinear susceptibility ($\text{Im}\chi^{(3)}$, esu)	Optical limiting threshold (GW/cm^2)
P(EDT-TPA)	0.82×10^{-10}	0.17×10^{-11}	0.39
P(DMT-TPA)	0.57×10^{-10}	0.12×10^{-11}	0.31
P(EDT-DOB)	0.65×10^{-10}	0.14×10^{-11}	0.44

5.2.1.2 Fluorene Based Polymers

a) P(FL-TPAFL) and P(FL-DPPPh)

The open aperture Z-scan trace of the polymers, P(FL-TPAFL) and P(FL-DPPPh) in THF are shown in Figure 5.6. The two copolymers showed a normalized transmittance peak-valley type graph with a positive NLO absorption coefficient. The absorption coefficient values were observed to be in the order of 10^{-10} mW^{-1} . In the case of copolymer P(FL-TPAFL), the comonomer TPAFL acted as donor and FL acted as acceptor which was confirmed theoretically. This donor-acceptor scheme resulted in the strong optical nonlinearity of the copolymer. Where as in the case of copolymer P(FL-DPPPh), the comonomer FL acted as donor unit. The HOMO level of FL was found to be higher than that of comonomer DPPPh. The charge transfer from donor to acceptor unit was responsible for the optical nonlinearity of the polymer. The nonlinear absorption traces of the copolymers were fitted well with the graph derived from two photon absorption (TPA) theory. The two copolymers showed reverse saturable absorption type graph (Figure 5.6). The RSA graph showed that the polymers initially absorb two photos from high intensity laser beam.

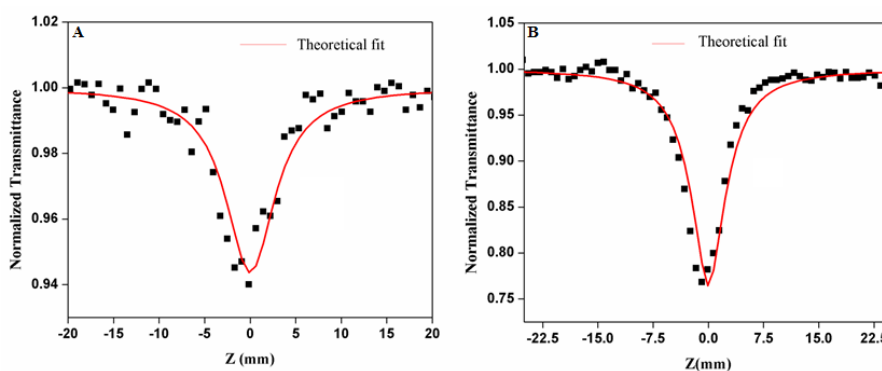


Figure 5.6: Open aperture Z-scan traces of (A) P(FL-TPAFL) and (B) P(FL-DPPPh) in THF at 135 μJ

Optical Power Limiting

To determine the optical limiting behavior of copolymers, open aperture z-scan traces of the polymers were analyzed. Figure 5.7 shows the transmitted energy of synthesized copolymers. The optical limiting threshold of P(FL-TPAFL) and P(FL-DPPPh) were determined to be 0.27 GW cm^{-2} and 0.31 GW cm^{-2} , respectively.

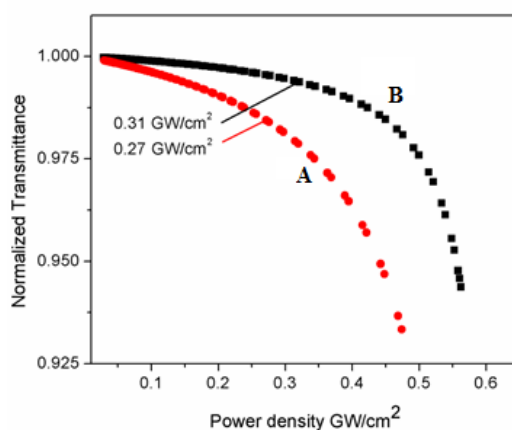


Figure 5.7: Optical limiting curve of (A) P(FL-TPAFL) and (B) P(FL-DPPPh)

The nonlinear absorption coefficient (β , m/W) and imaginary value of third-order nonlinear susceptibility ($\text{Im}\chi^{(3)}$, esu) and optical limiting threshold values were calculated and are given in Table 5.3.

Table 5.3: Third-order nonlinear absorption coefficient (β , m/W), imaginary value of third order nonlinear susceptibility ($\text{Im}\chi^{(3)}$, esu) and optical limiting threshold (GW/cm^2) of copolymers

Polymer	Nonlinear absorption coefficient (β , mW^{-1})	Imaginary part of nonlinear susceptibility ($\text{Im}\chi^{(3)}$, esu)	Optical limiting threshold (GW/cm^2)
P(FL-TPAFL)	0.53×10^{-10}	0.11×10^{-11}	0.27
P(FL-DPPPh)	2.72×10^{-10}	0.58×10^{-11}	0.31

b) P(FL-TPA) and P(FL-BP)

The open aperture (OA) Z-scan traces of the polymers, P(FL-TPA) and P(FL-BP) in THF were taken (Figure 5.8). The solid curves in the figure are the theoretical fit to the experimental data. The two copolymers showed a reverse saturable absorption type graph with a positive NLO absorption coefficient.

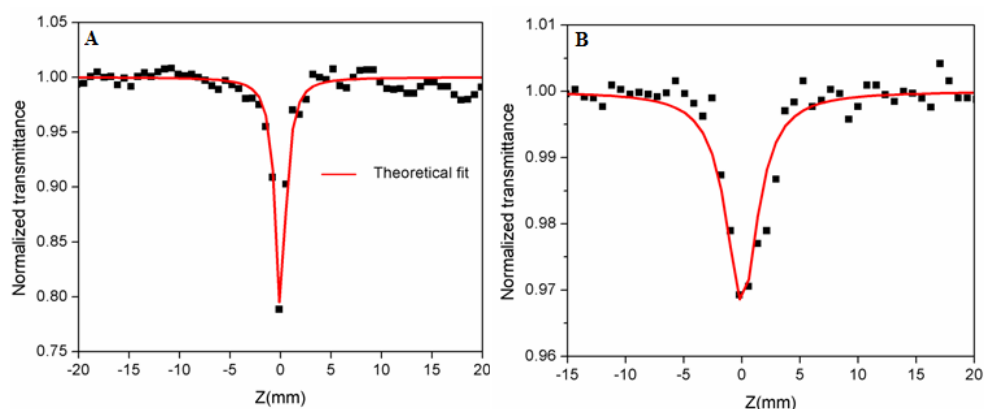


Figure 5.8: Open aperture Z-scan traces of (A) P(FL-TPA) and P(FL-BP) in THF at 135 μJ

The nonlinear absorption traces of the copolymers were fitted well with the graph derived from two photon absorption (TPA) theory. The charge transfer along the donor-acceptor backbone of the polymers resulted in the optical nonlinearity. The third-order nonlinear absorption coefficient (β , m^2/W) and imaginary value of third-order nonlinear susceptibility ($\text{Im } \chi^{(3)}$, esu) are calculated. The values were found to be in good agreement with the semiconducting behavior of the polymers.

Optical Power Limiting

The optical limiting threshold of P(FL-TPA) and P(FL-BP) were determined to be 0.37 GW cm^{-2} and 0.46 GW cm^{-2} , respectively using open aperture Z-scan technique (Figure 5.9). The low limiting threshold values

of the polymers indicate that these polymers can be used for optical power limiting at high laser fluences. The calculated values of nonlinear absorption coefficient (β , m/W), imaginary value of third-order nonlinear susceptibility ($\text{Im}\chi^{(3)}$, esu) and optical limiting threshold values are given in the Table 5.4.

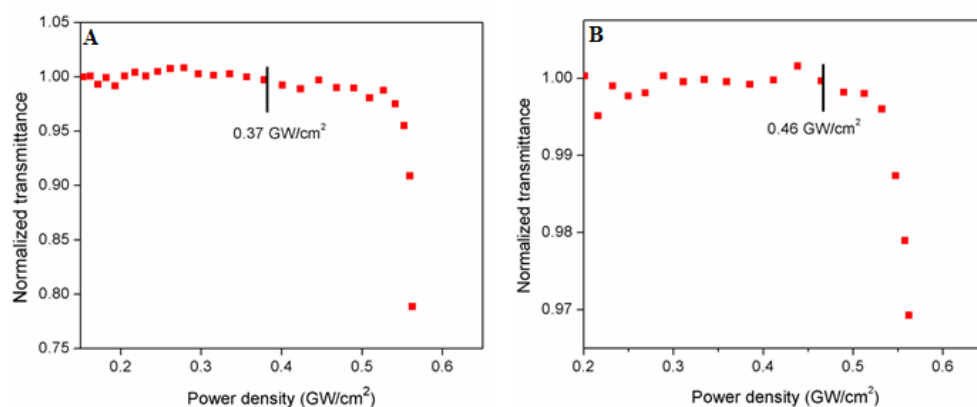


Figure 5.9: Optical limiting curves of (A) P(FL-TPA) and (B) P(FL-BP)

Table 5.4: Nonlinear absorption coefficient (β , m/W), imaginary value of third order nonlinear susceptibility ($\text{Im}\chi^{(3)}$, esu) and optical limiting threshold (GW/cm^2) of copolymers

Polymer	Nonlinear absorption coefficient (β , mW^{-1})	Imaginary part of nonlinear susceptibility ($\text{Im}\chi^{(3)}$, esu)	Optical limiting threshold (GW/cm^2)
P(FL-TPA)	0.47×10^{-10}	0.10×10^{-11}	0.37
P(FL-BP)	0.29×10^{-10}	0.06×10^{-11}	0.46

5.2.1.3 Anthracene-Phenothiazine Copolymer P(ANT-PHENO)

The open aperture Z-scan trace of the polymer P(ANT-PHENO) was recorded in THF (Figure 5.10). Here, the copolymer showed a normalized

transmittance peak-valley type graph with a positive NLO absorption coefficient. The copolymer showed reverse saturable absorption type graph.

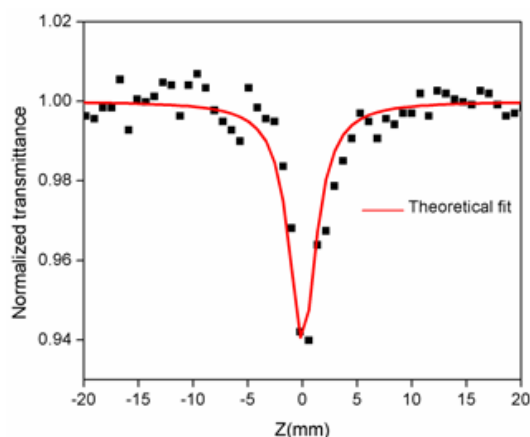


Figure 5.10: Open-aperture z-scan trace of P(ANT-PHENO) in THF at 135 μJ

The nonlinear absorption trace of the copolymer fitted well with the graph derived from two photon absorption (TPA) theory which implied that the process involved in the nonlinear absorption is two photon absorption (TPA). The third-order nonlinear absorption coefficient (β , m^2/W) and imaginary value of third-order nonlinear susceptibility ($\text{Im}\chi^{(3)}$, esu^3) were calculated and were found to be in the semiconducting range.

Optical Power Limiting

The optical limiting threshold of copolymer was investigated by OA z-scan technique at 532 nm. Figure 5.11 shows the transmitted energy of synthesized anthracene-phenothiazine copolymer. The optical limiting threshold of P(ANT-PHENO) was determined to be 0.46 GW cm^{-2} . Because of the low optical limiting threshold value, the polymer could be used in optical limiting devices. Table 5.5 shows the calculated values of nonlinear

absorption coefficient (β , m/W), imaginary value of third-order nonlinear susceptibility ($\text{Im}\chi^{(3)}$, esu) and optical limiting threshold of the copolymer.

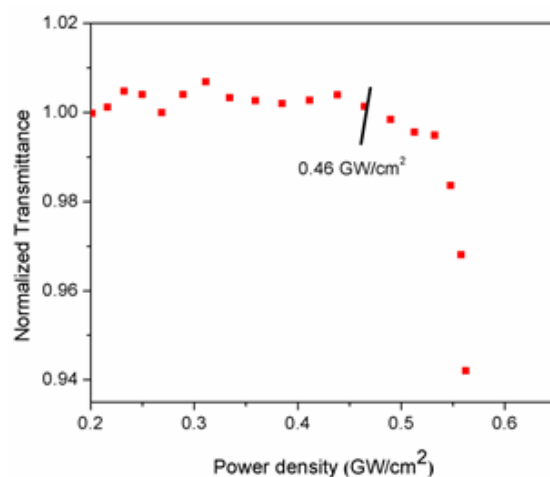


Figure 5.11: Optical limiting curve of P(ANT-PHENO)

Table 5.5: Third-order nonlinear absorption coefficient (β , m/W), imaginary value of third-order nonlinear susceptibility ($\text{Im}\chi^{(3)}$, esu) and optical limiting threshold (GW/cm^2) of the copolymer

Polymer	Nonlinear absorption coefficient (β , mW^{-1})	Imaginary part of nonlinear susceptibility ($\text{Im}\chi^{(3)}$, esu)	Optical limiting threshold (GW/cm^2)
P(ANT-PHENO)	0.57×10^{-10}	0.12×10^{-11}	0.46

5.2.1.4 Phenylenevinylene Polymers (PPVs)

The open aperture (OA) Z-scan traces of two phenylenevinylene polymers, DOC-MEH PPV and EDTh CN PPV showed a normalized transmittance valley-peak type graph with a negative NLO absorption coefficient. The two polymers showed saturable absorption type graph (Figure 5.12).

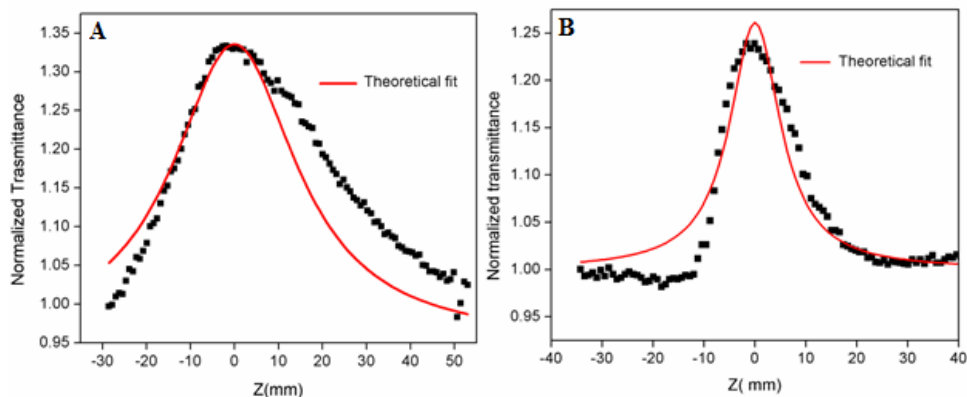


Figure 5.12: Open aperture Z-scan traces of (A) DOC-MEH PPV and (B) EDTh CN PPV in THF at 135 μJ

The switch over from reverse saturable absorption to saturable absorption could be attributed to ground state band bleaching of phenylenevinylene polymers in solution. These polymers could not be used as optical limiter because of these polymers showed enhanced transmittance at focus. The third-order nonlinear absorption coefficient (β , m/W) and imaginary value of third-order nonlinear susceptibility ($\text{Im}\chi^{(3)}$, esu) were calculated. The calculated values of nonlinear absorption coefficient (β , m/W) and imaginary value of third-order nonlinear susceptibility ($\text{Im}\chi^{(3)}$, esu) are given in the Table 5.6.

Table 5.6: Third-order nonlinear absorption coefficient (β , m/W) and imaginary value of third-order nonlinear susceptibility ($\text{Im}\chi^{(3)}$, esu) of phenylenevinylene polymers

Polymer	Nonlinear absorption coefficient (β , mW^{-1})	Imaginary part of nonlinear susceptibility ($\text{Im}\chi^{(3)}$, esu)
DOC-MEH PPV	-1.85×10^{-10}	-0.39×10^{-11}
EDTh CN PPV	-1.56×10^{-10}	-3.29×10^{-11}

5.2.2 Photovoltaic Device Fabrication

Photovoltaic performances of some of the synthesized conjugated polymers were evaluated by constructing both conventional and inverted solar cells.

Conventional solar cell was constructed using polymer:PCBM blend in 2:1 ratio as active layer, with device architecture, ITO/MoO₃/Polymer:PCBM/LiF/Al. MoO₃ act as anode buffer layer and LiF as cathode buffer layer. Both of these layers and Al electrode were deposited by vacuum evaporation technique. Conventional solar cells were also constructed by using Tris(8-hydroxyquinolino)aluminum (Alq₃) as cathode buffer layer and MoO₃ as anode buffer layer in the configuration, ITO/MoO₃/Polymer:PCBM/Alq₃/Al and another one with PEDOT:PSS as anode buffer layer and LiF as cathode buffer layer in the architecture, ITO/PEDOT:PSS/Polymer:PCBM/LiF/Al. In both cases, the open circuit voltage and short circuit current were found to be very low.

For the construction of inverted solar cells, an electron collective ZnO layer was deposited on the ITO substrate using simple, cost effective, non-vacuum, chemical spray pyrolysis (CSP) technique. The device configuration was ITO/ZnO/Polymer:PCBM/Ag. Highly pure silver (99.99 % pure) was vacuum evaporated to form the top contact with an area of 0.03cm². For both cases, active layer was deposited using spin coating (25 mg dissolved in 1 mL chlorobenzene). Current-Voltage characteristics were measured using a source measure unit NI PXI-1033 and illumination was done using Class AAA solar simulator [PET, USA].

5.2.2.1 Photovoltaic Performance of Conventional Solar Cells Constructed using Synthesized Polymers

Schematic diagram of the conventional solar cell constructed using the polymer, P(FL-DPPPh) and PCBM blend in 2:1 ratio as active layer is shown in Figure 5.13. The solar cell configuration is ITO/MoO₃/P(FL-DPPPh):PCBM/LiF/Al. The J-V curve of the conventional solar cell under dark and under illumination is shown in Figure 5.14.

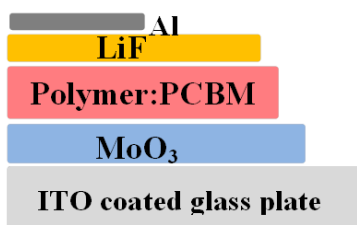


Figure 5.13: Schematic diagram of conventional solar cell

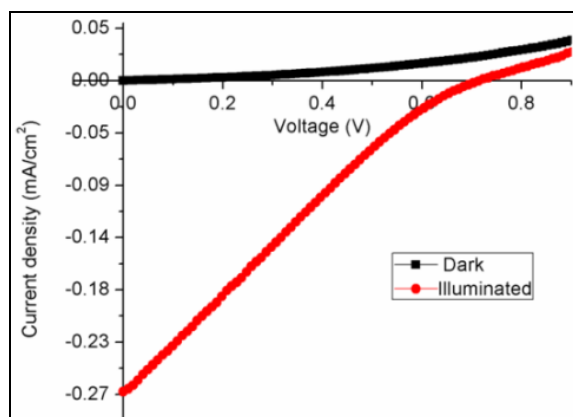


Figure 5.14: J-V curves of conventional solar cell with configuration ITO/MoO₃/P(FL-DPPPh):PCBM/LiF/Al under dark and under illumination

The conventional solar cell under illumination gave open circuit voltage (V_{oc}) of 0.71 V, short circuit current density (J_{sc}) of 0.27 mA/cm²

and fill factor of 23 %. The maximum power conversion efficiency achieved by the solar cell was 0.04 %.

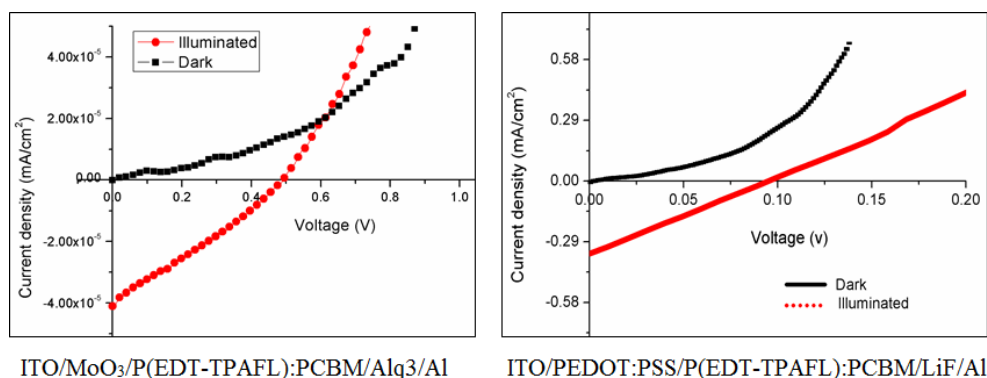


Figure 5.15: J-V curves of conventional solar cells with configuration ITO/MoO₃/P(EDT-TPAFL):PCBM/Alq₃/Al and ITO/PEDOT:PSS/P(EDT-TPAFL):PCBM/LiF/Al

Conventional solar cells were constructed in two different configurations using the polymer P(EDT-TPAFL) and PCBM blend in 2:1 ratio as active layer. The configurations are ITO/MoO₃/P(EDT-TPAFL):PCBM/Alq₃/Al and ITO/PEDOT:PSS/P(EDT-TPAFL):PCBM/LiF/Al. The J-V curves of the conventional solar cells under dark and under illumination are shown in Figure 5.15.

The conventional solar cell constructed in the configuration ITO/MoO₃/P(EDT-TPAFL):PCBM/Alq₃/Al under illumination gave open circuit voltage (V_{oc}) of 0.49 V and short circuit current density (J_{sc}) of the order of 10^{-4} mA/cm². The short circuit current is negligible. The solar cell fabricated in the configuration ITO/PEDOT:PSS/P(EDT-TPAFL):PCBM/LiF/Al under illumination gave open circuit voltage (V_{oc}) of 0.09 V and short circuit current density (J_{sc}) of 0.35 mA/cm².

5.2.2.2 Photovoltaic Performance of Inverted Solar Cells Constructed using Synthesized Polymers

In the inverted structure, as in Figure 5.16 which shows the schematic diagram of the device which has an electron collecting ZnO layer with higher resistivity of $\sim 10^2 \Omega \text{ cm}$ coated over ITO plate.

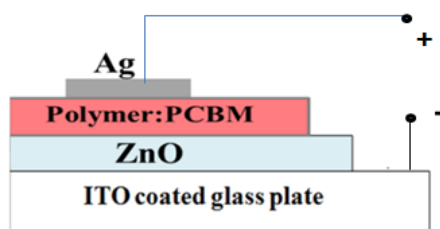


Figure 5.16: Schematic diagram of ZnO/Polymer heterojunction

The photovoltaic performance of inverted solar cell constructed using the polymer P(FL-DPPPh):PCBM blend as active layer in the configuration ITO/ZnO/P(FL-DPPPh):PCBM/Ag was checked and the J-V curves of the inverted solar cell under dark (inset) and under illumination is shown in Figure 5.17.

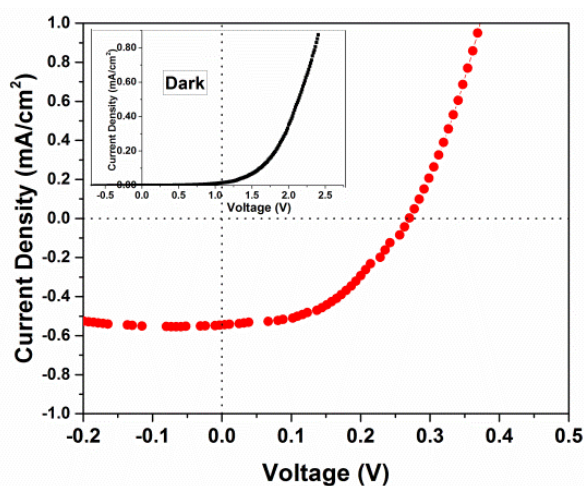


Figure 5.17: J-V curves of inverted solar cell with configuration ITO/ZnO/P(FL-DPPPh):PCBM/Ag

The solar cell under illumination gave open circuit voltage (V_{oc}) of 0.27 V, short circuit current density (J_{sc}) of 0.55 mA/cm^2 and fill factor of 47 %. The maximum power conversion efficiency achieved by the inverted solar cell was 0.07 %.

Inverted solar cells processed from different solvents, were constructed using the polymer P(DMT-TPAFL):PCBM blend as active layer in the configuration ITO/ZnO/P(DMT-TPAFL):PCBM/Ag and the photovoltaic performances of the constructed solar cells were evaluated. The J-V curves of the inverted solar cells processed from different solvents under illumination are shown in Figure 5.18.

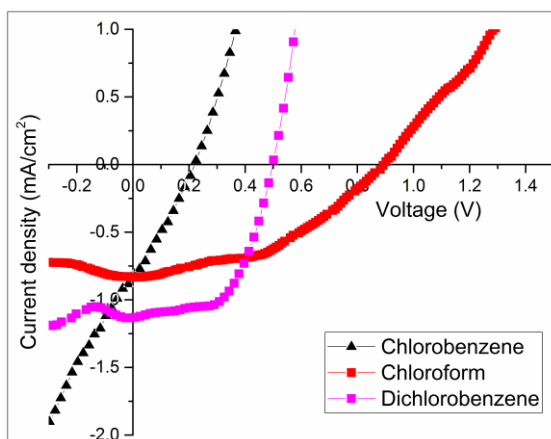


Figure 5.18: J-V curves of inverted solar cell with configuration ITO/ZnO/P(DMT-TPAFL):PCBM/Ag processed from different solvents

The solar cell processed from chlorobenzene, under illumination gave open circuit voltage (V_{oc}) of 0.22 V, short circuit current density (J_{sc}) of 0.82 mA/cm^2 and fill factor of 28 %. The maximum power conversion efficiency achieved by the inverted solar cell was 0.05 %. The solar cell

processed from chloroform under illumination gave open circuit voltage (V_{oc}) of 0.88 V, short circuit current density (J_{sc}) of 0.83 mA/cm^2 and fill factor of 43 %. The maximum power conversion efficiency achieved by the device was 0.32 %. The photovoltaic cell processed from dichlorobenzene, under illumination gave open circuit voltage (V_{oc}) of 0.50 V, short circuit current density (J_{sc}) of 1.15 mA/cm^2 and fill factor of 55 %. The maximum power conversion efficiency achieved by the photovoltaic device was 0.32 %.

The photovoltaic performance of inverted solar cells constructed using the polymer P(EDT-TPAFL):PCBM blend which were processed from different solvents as active layer in the configuration ITO/ZnO/P(EDT-TPAFL):PCBM/Ag were studied. The J-V curves of the inverted solar cells processed from different solvents under illumination are shown in Figure 5.19.

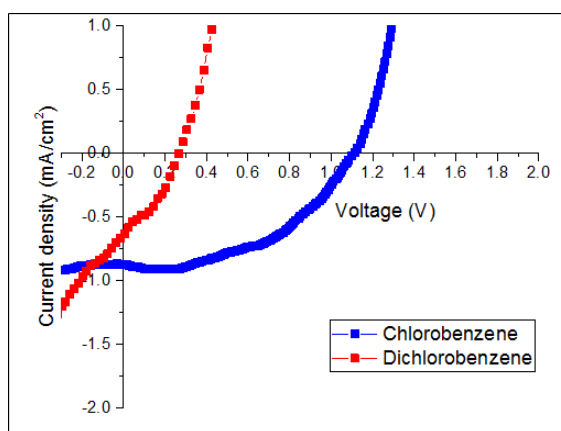


Figure 5.19: J-V curves of inverted solar cell with configuration ITO/ZnO/P(EDT-TPAFL):PCBM/Ag in chlorobenzene and dichlorobenzene

The solar cell processed from dichlorobenzene, under illumination gave open circuit voltage (V_{oc}) of 0.27 V, short circuit current density (J_{sc})

of 0.65 mA/cm² and fill factor of 34 %. The maximum power conversion efficiency achieved by the inverted solar cell is 0.06 %. The solar cell processed from chlorobenzene under illumination gave open circuit voltage (V_{oc}) of 1.12 V, short circuit current density (J_{sc}) of 0.89 mA/cm² and fill factor of 50 %. The maximum power conversion efficiency achieved by the device was 0.50 %.

Inverted solar cell showed better collection of charge carriers which resulted in the better J_{sc} value than the other. Fill factor of a device is a key parameter that determines the quality of the device. The maximum fill factor achieved by the conventional type architecture was below 23 %, whereas the inverted structure gave maximum fill factor value of 55 %, which reveals the better device quality for inverted structure. In the inverted solar cell architecture, electron collective ZnO layer was highly resistive. Replacing this with much more conducting ZnO, by doping with Al or inverted Al doped ZnO, can enhance the charge carrier collection resulting in improvement in short circuit current density and hence efficiency.

5.3 Conclusion

The third-order nonlinear optical absorption characteristics of synthesized copolymers have been studied using open aperture Z-scan technique. It was found that the nonlinear absorption was due to effective two photon absorption process. The Z-scan results indicated that the nonlinear absorption coefficient (β , m W⁻¹) and imaginary part of third-order nonlinear susceptibility ($\text{Im}\chi^{(3)}$, esu) of polymers were in the order of 10⁻¹⁰ and 10⁻¹¹, respectively. The synthesized polymers except two PPV polymers exhibited good optical power limiting behavior at 532 nm. Hence, the polymers could be considered as

potential candidates for optical-power-limiting applications. Inverted and conventional solar cells were fabricated with some of the synthesized polymers blended with PCBM as active layer. Conventional solar cell constructed with polymer P(FL-DPPPh):PCBM blend as active layer, gave a power conversion efficiency of 0.04 %. Inverted solar cell was also constructed with polymer P(FL-DPPPh):PCBM blend as active layer, which gave a power conversion efficiency of 0.07 %. Inverted solar cells constructed using P(EDT-TPAFL):PCBM blend in dichlorobenzene and chlorobenzene and gave power conversion efficiencies of 0.06 % and 0.50 %, respectively. Inverted solar cells were constructed using P(DMT-TPAFL):PCBM blend in dichlorobenzene, chlorobenzene and chloroform gave power conversion efficiencies of 0.32 % , 0.05 % and 0.32 %, respectively. Devices developed with both structures exhibited photovoltaic characteristics with better performance for inverted architecture with cell configuration. ITO/ZnO/P(EDT-TPAFL):PCBM/Ag processed from chlorobenzene gave maximum power conversion efficiency of 0.5 %.

References

- [1] L. G. Gregory, M. M. Theresa, S. S. Dwight, *J. Am. Chem. Soc.*, 2012, **134**, 539.
- [2] M. Bass, J. M. Enoch, E. W. Van Stryland, W. L. Wolfe, Handbook of optics IV, Fiber Optics and Nonlinear Optics, McGraw-Hill, New York, 2nd edn, 2001.
- [3] S. Webster, J. Fu, L. A. Padilha, O. V. Przhonska, D. J. Hagan, E. W. Van Stryland, M. V. Bondar, Y. L. Slominsky, A. D. Kachkovski, *Chem. Phys.*, 2008, **348**, 143.

- [4] W. Denk, J. H. Strickler, W. W. Webb, *Science*, 1990, **248**, 73.
- [5] C. Xu, W. Zipfel, J. B. Shear, R. M. Williams, W. W. Webb, *Proc Natl Acad Sci USA.*, 1996, **93**, 10763.
- [6] D. A. Parthenopoulos, P. M. Rentzepis, *Science*, 1989, **245**, 843.
- [7] J. E. Ehrlich, X. L. Wu, I-Y. S. Lee, Z-Y. Hu, H. Rockel, S. R. Marder, J. W. Perry, *Opt Lett.*, 1997, **22**, 1843.
- [8] W. H. Lee, S. K. Lee, W. S. Shin, S. j. Moon, M. J. Park, S. H. Lee, *Sol. Energ. Mat. Sol. Cells*, 2014, **122**, 190.
- [9] R. R. Sondergaard, M. Hosel, F. C. Krebs, *J. Polym. Sci. Part B Polym. Phys.*, 2013, **51**, 16.
- [10] E. Bundgaard, F. C. Krebs, *Sol. Energ. Mat. Sol. Cells*, 2007, **91**, 954.
- [11] Y. R. Shen, *The Principles of Nonlinear Optics*, Wiley, New York, 1984.
- [12] K. Rottwitt, P. T. Lichtenberg, *Nonlinear Optics Part A: Basic Principles and Materials*, CRC Press, 2014.
- [13] K.K. Nagaraja, S. Pramodini, A. Santhosh Kumar, H.S. Nagaraja, P. Poornesh, Dhananjaya Kekuda, *Opt. Mater.*, 2013, **35**, 431.
- [14] P. G. L. Frobel, S.R. Suresh, S. Mayadevi, S. Sreeja, C. Mukherjee, C.I. Muneera, *Mater. Chem. Phys.*, 2011, **129**, 981.
- [15] V. Kumari, V. Kumar, B. P. Malik, R. M. Mehra, D. Mohan, *Opt. Commun.*, 2012, **285**, 2182.
- [16] S. Narayanan, S. P. Raghunathan, S. Mathew, M.V. Mahesh Kumar, A. Abbas, K. Sreekumar, C. Sudha Kartha, Rani Joseph, *Eur. Polym. J.*, 2015, **64**, 157.
- [17] A. Thankappan, S. Thomas, V. P. N. Nampoore, *Opt. Laser Technol.*, 2014, **58**, 63.
- [18] I. Litty, K. Bindu, V. P. N. Nampoore, P. Radhakrishnan, *Opt. Mater.*, 2008, **31**, 361.

- [19] S. Mathew, A. D. Saran, S. A. Joseph, B. S. Bhardwaj, D. Punj, P. Radhakrishnan, *J. Mater Sci: Mater Electron.*, 2012, **23**, 739.
- [20] N. K. M. Naga Srinivas, S. Venugopal Rao, D.V.G.L.N. Rao, B.K. Kimball, M. Nakashima, B. S. Decristofano, D. Narayana Rao, *J. Porphyr. Phthalocyanines*, 2001, **5**, 549.
- [21] S. E. Shaheen, R. Radspinner, N. Peyghambarian, G. E. Jabbour, *Appl. Phys. Lett.*, 2001, **79**, 2996.
- [22] J. J. M. Halls, C. A. Walsh, N. C. Greenham, E. A. Marseglia, R. H. Friend, S. C. Moratti, A. B. Holmes, *Nature*, 1995, **376**, 498.
- [23] G. Yu, J. Gao, J. C. Hummelen, F. Wudl, A. J. Heeger, *Science*, 1995, **270**, 1789.
- [24] C. J. Brabec, N. S. Sariciftci, J. C. Hummelen, *Adv. Funct. Mater.*, 2001, **11**, 15.
- [25] G. Yu, J. Gao, J. C. Hummelen, F. Wudl, A. J. Heeger, *Science*, 1995, **270**, 1789.
- [26] S. Gunes, H. S. Neugebauer, N. S. Sariciftci, *Chem. Rev.*, 2007, **107**, 1324.
- [27] K. Coakley, M. D. McGehee, *Chem. Mater.*, 2004, **16**, 4533.
- [28] C. J. Brabec, N. S. Sariciftci, J. C. Hummelen, *Adv. Funct. Mater.*, 2001, **11**, 15.
- [29] B. C. Thompson, J. M. J. Frechet, *Angew. Chem., Int. Ed.*, 2008, **47**, 58.
- [30] L. M. Chen, Z. Hong, G. Li, Y. Yang, *Adv. Mater.*, 2009, **21**, 1434.
- [31] Y. Long, *Appl. Phys. Lett.*, 2009, **95**, 193301.
- [32] T. W. Ng, M. F. Lo, Z. T. Liu, F. L. Wong, S. L. Lai, M. K. Fung, C. S. Lee, S. T. Lee, *J. Appl. Phys.*, 2009, **106**, 114501.
- [33] I. Etzebarria, A. Guerrero, J. Albero, G. G. Belmonte, E. Palomares, R. Pacios, *Organic Electronics*, 2014, **15**, 2756.
- [34] M. Niggemann, M. Glatthaar, A. Gombert, A. Hinsch, V. Wittwer, *Thin Solid Films*, 2004, **451**, 619.
- [35] Z. Xu, L. M. Chen, G. Yang, C. H. Huang, J. Hou, Y. Wu, G. Li, C. S. Hsu, Y. Yang, *Adv. Funct. Mater.*, 2009, **19**, 1227.

- [36] F. C. Krebs, S. A. Gevorgyan, J. Alstrup, *J. Mater. Chem.*, 2009, **19**, 5442.
- [37] S. Schumann, R. Da Campo, B. Illy, A. C. Cruickshank, M. A. McLachlan, M. P. Ryan, D. J. Riley, D. W. McComb, T. S. Jones, *J. Mater. Chem.*, 2011, **21**, 2381.
- [38] H. Hoppe, N. S. Sariciftci, *J. Mater. Chem.*, 2004, **19**, 1924.
- [39] C. J. Brabec, A. Cravino, D. Meissner, N. S. Sariciftci, T. Fromhertz, M. Minse, L. Sanchez, J. C. Hummelen, *Adv. Funct. Mater.*, 2001, **11**, 374.
- [40] G. G. Mallairas, J. R. Salem, P. J. Brock, J. C. Scott, *J. Appl. Phys.*, 1998, **84**, 1583.
- [41] M. S. Bahae, A. A. Said, T. H. Wei, D. J. Hagan, E. W. VanStryland, *IEEE J Quantum Electron.*, 1990, **26**, 760.

.....✂.....

SUMMARY AND OUTLOOK

Contents	6.1 <i>Summary of the Work</i>
	6.2 <i>Major Achievements</i>
	6.3 <i>Future Outlook</i>

Conjugated polymers have several advantages over inorganic systems such as stability, processability, low cost, etc. The main focus of the present study was to synthesize low band gap conjugated polymers for nonlinear optical and photovoltaic applications. This chapter summarizes the major findings in the overall research work done. Theoretically designed conjugated polymers were synthesized via different synthetic strategies like Direct Arylation Polymerization, Suzuki Coupling Polymerization, Gilch Polymerization and Knoevenagel Polycondensation. The nonlinear optical properties and photovoltaic performances of the synthesized polymers have been investigated. Scope of the future work is also outlined here.

6.1 Summary of the work

The major intention of the present work was to synthesize conjugated polymers which are suitable for applications in photovoltaics and nonlinear optics. One well-established approach to obtain conjugated polymers with the above two desired properties are based on the strategy of incorporating an electron donating and/or withdrawing unit into the polymer backbone. Computational design combined with chemical intuition was used to predict electronic properties of the donor-acceptor polymers.

Table 6.1: Theoretical and Experimental band gap of copolymers

Polymer	E_g (Theoretical) (eV)	E_g (Electrochemical) (eV)	E_g (Optical) (eV)
P(EDT-TPAFL)	2.27	1.95	2.11
P(DMT-TPAFL)	2.36	1.93	2.50
P(EDT-TPA)	2.53	1.74	2.30
P(DMT-TPA)	2.77	1.80	2.53
P(EDT-DOB)	2.44	1.66	2.05
P(FL-TPAFL)	2.80	2.41	2.96
P(FL-DPPPh)	1.96	1.81	1.97
P(FL-TPA)	2.94	1.92	2.94
P(FL-BP)	3.26	2.20	3.10
P(ANT-PHENO)	2.86	1.88	2.57
DOC-MEH PPV	1.79	1.80	2.27
EDTh CN PPV	1.81	1.66	2.10

In this work, twelve low band gap conjugated polymers were designed. Monomers and D-A units were optimized using density functional theory (DFT) and total optimization process included DFT/B3LYP/6-31G formalism. Band gap, oscillator strength and excitation energies were calculated using time dependent density functional theory (TD-DFT) calculations. Conjugated polymers were optimized by applying periodic boundary condition (PBC). All the designed conjugated polymers were synthesized by different synthetic strategies like Direct arylation polymerization, Suzuki coupling polymerization, Gilch polymerization and Knoevenagel polycondensation. All the polymers were characterized by different spectroscopic and analytical techniques. The

redox behavior of the copolymers were investigated using cyclic voltammetry. HOMO and LUMO energy values and electrochemical band gap of copolymers were calculated. Band gaps obtained from optical and electrochemical methods were in good agreement with the band gaps obtained from theoretical calculations.

Third-order nonlinear optical properties of all the polymers were investigated using Z-scan technique. The open aperture Z-scan traces of ten copolymers gave reverse saturable absorption type graphs and all the traces were fitted with the theoretical plot derived from the two photon absorption (TPA) theory. This implied that the mechanism involved in the optical nonlinearity could be TPA. Nonlinear absorption coefficients of all the ten polymers were in the order of 10^{-10} mW^{-1} and imaginary part of nonlinear susceptibility values were of the order of 10^{-11} esu, which implied that all the polymers exhibited strong optical nonlinearity at 532 nm. The remaining two PPV polymers gave saturable absorption type graphs. Thus all the synthesized conjugated polymers showed very good third-order nonlinear optical properties because of the strong intermolecular charge transfer between the donor and the acceptor units and can be used as ideal candidates in nonlinear optical applications. All the synthesized polymers, except PPV polymers, showed good optical limiting property at 532 nm due to two-photon absorption (TPA) process. The polymer P(DMT-TPAFL) showed superior optical power limiting property.

Table 6.2: Nonlinear absorption coefficient (β , m/W), imaginary value of third-order nonlinear susceptibility ($\text{Im}\chi^{(3)}$, esu) and optical limiting threshold (GW/cm^2) of copolymers

Polymer	β 10^{-10} (m/W)	$\text{Im}\chi^{(3)}$ 10^{-11} (esu)	Optical limiting threshold (GW/cm^2)
P(EDT-TPAFL)	1.41	0.29	0.36
P(DMT-TPAFL)	3.82	0.85	0.20
P(EDT-TPA)	0.82	0.17	0.39
P(DMT-TPA)	0.57	0.12	0.31
P(EDT-DOB)	0.65	0.14	0.44
P(FL-TPAFL)	0.53	0.11	0.27
P(FL-DPPPh)	2.72	0.58	0.31
P(FL-TPA)	0.47	0.10	0.37
P(FL-BP)	0.29	0.06	0.46
P(ANT-PHENO)	0.57	0.12	0.46
DOC-MEH PPV	-1.85	-0.39	-
EDTh CN PPV	-1.56	-3.29	-

Photovoltaic performances of some of the copolymers were checked by constructing both classical and inverted bulk heterojunction solar cells using polymer:PCBM blend in 2:1 ratio as active layer. In inverted solar cells, ZnO was used as electron transport layer and cell configuration adopted was ITO/ZnO/Polymer:PCBM/Ag. Inverted solar cell constructed with polymer P(FL-DPPPh):PCBM blend as active layer, gave a power conversion efficiency of 0.07 %. Conventional solar cell was constructed with polymer P(FL-DPPPh):PCBM blend as active layer in a configuration ITO/MoO₃/PL:PCBM/LiF/Al, which gave a power conversion efficiency of 0.04 %.

Inverted solar cells were constructed using P(EDT-TPAFL):PCBM blend in dichlorobenzene and chlorobenzene and gave power conversion efficiencies of 0.06 % and 0.50 %, respectively. Inverted solar cells were constructed using P(DMT-TPAFL):PCBM blend in dichlorobenzene, chlorobenzene and chloroform and gave power conversion efficiencies of 0.32 % , 0.05 % and 0.32 %, respectively.

Table 6.3: Photovoltaic performances of synthesized polymers

Polymer:PCBM	Area (cm ²)	Voc (mV)	Jsc (mA/cm ²)	FF (%)	Efficiency (%)
P(FL-DPPPh) in chlorobenzene ITO/MoO ₃ /PL:PCBM/LiF/Al	0.22	715	0.27	23	0.04
P(FL-DPPPh) in chlorobenzene ITO/ZnO/PL:PCBM/Ag	0.03	270	0.55	47	0.07
P(EDT-TPAFL) in dichlorobenzene	0.03	270	0.65	34	0.06
P(EDT-TPAFL) in chlorobenzene	0.03	1120	0.89	50	0.50
P(DMT-TPAFL) in dichlorobenzene	0.03	500	1.15	55	0.32
P(DMT-TPAFL) in chlorobenzene	0.03	224	0.82	28	0.05
P(DMT-TPAFL) in chloroform	0.03	879	0.83	43	0.32

6.2 Major Achievements

- Theoretically designed and synthesized twelve conjugated polymers for nonlinear optical and photovoltaic applications.
- All the synthesized polymers showed third-order nonlinear optical properties.

- The conjugated polymers showed good optical power limiting behavior at 532 nm.
- Both conventional and inverted photovoltaic devices were constructed using three synthesized conjugated polymers in different cell configurations.
- Inverted solar cell constructed using P(EDT-TPAFL) with a device structure ITO/ZnO/P(EDT-TPAFL):PCBM/Ag processed from chlorobenzene gave maximum power conversion efficiency of 0.5 %.

6.3 Future Outlook

Three of the synthesized polymers showed photovoltaic activity when blended with PCBM as active layer both in conventional and inverted device architecture. The variation in power conversion efficiencies of these polymers could be checked by changing both the anode and cathode buffer layers. The role of thickness of active layer in a photovoltaic device is also to be investigated. The rest of the polymers could be subjected to more studies to explore the suitability of these polymers in photovoltaic devices and light emitting diodes.

.....❧.....

||| List of Publications |||

Publications

- [1] **C. P. Anjali** and K. Sreekumar, *Synthesis, Characterization and Third Order Nonlinear Optical Properties of 3,4-ethylenedioxythiophene-9,9-bis(4-diphenylaminophenyl fluorene) Copolymer*, ISBN No: :978-93-80095-738, 2016.
- [2] **C. P. Anjali** and K. Sreekumar, *Synthesis, Theoretical Investigation and Nonlinear Optical Properties of poly(3,4-dimethoxythiophene-9,9-bis(4-diphenylaminophenyl fluorene) and poly(EDOT-9,9-bis(4-diphenylaminophenyl fluorene)) Copolymers via Direct Arylation Polymerization Route*, ISBN:978-81-930558-2-3, 2017.
- [3] **C. P. Anjali**, M. V. Mahesh Kumar, R. Geethu, Rosemary Davis, Sona Narayanan, S. Mathew, K. P. Vijayakumar, P. Predeep and K. Sreekumar, *Theoretical Investigation, Nonlinear Optical Properties and Photovoltaic Performances of two Fluorene based Donor-Acceptor Copolymers* (communicated)

Papers presented in Conferences

- [4] **C. P. Anjali**, Sowmya Xavier and K. Sreekumar, paper presented entitled “*Synthesis and Third-order Nonlinear Optical Properties of 3,4-dimethoxythiophene-9,9-bis(4-diphenylaminophenyl fluorene) Copolymer*” in the National Conference on Recent Trends in Bio-Inorganic & Organometallic Chemistry (NCBOC-2015) held at SSIET, Coimbatore, October 2015.

- [5] **C. P. Anjali** and K. Sreekumar, poster presentation entitled “*Synthesis of a new conjugated polymer, poly(edot-9,9-bis(4-diphenylaminophenyl fluorene)*” in the International Conference on Advances in Applied Mathematics, Materials Science and Nanotechnology for Engineering and Industrial Applications, (ICMMN 2K16) held at FISAT, Angamaly, Kerala, January 2016.
- [6] **C. P. Anjali** and K. Sreekumar, oral presentation entitled “*Synthesis and Optical Limiting Properties of 3,4-dimethoxythiophene-9,9-bis(4-diphenylaminophenyl fluorene) Copolymer*” in the International Conference on Advances in Polymer Technology, (APT 2016) held at Dept. of PS & RT, CUSAT, February, 2016.
- [7] **C. P. Anjali**, Sowmya Xavier and K. Sreekumar, poster presentation entitled “*Theoretical Design, Synthesis and Nonlinear Optical Properties of two Novel Thiophene-based Polymers via Direct Arylation Polymerization route*” in the 29th Kerala Science Congress held at Mar.Thoma college, Tiruvalla, Pathanamthitta, Kerala, January 2017.

.....❧.....

List of Abbreviations

A	Acceptor
ANT	Anthracene
ANT-PHENO	(Anthracene)- (10-octylphenothiazine)
B3LYP	Becke, three parameter, Lee-Yang-Parr
BHJ	Bulk heterojunction
BLA	Bond length alteration
BP	Biphenyl
Bu ₄ NPF ₆	Tetrabutylammonium hexafluorophosphate
C ₆₀	Fullerene
CT	Charge-transfer
CV	Cyclic Voltammetry
D-A	Donor-Acceptor
DCM	Dichloromethane
DFT	Density functional theory
DMF	Dimethyl formamide
DMT	3,4-dimethoxythiophene
DMT-TPA	(3,4-dimethoxythiophene)-(triphenylamine)
DMT-TPAFL	(3,4-dimethoxythiophene)-(9,9-bis(4-diphenylaminophenyl)-fluorene)
DOB	2,5-bis (octyloxy) benzene
DOC	1,4-dimethyl-2,5-bis(octyloxy)benzene
DPP	Diketopyrrolopyrrole
DPPPh	3,6-diphenyl- 2,5-dihydropyrrolo [3,4-c] pyrrole-1,4-dione
DTG	Differential Thermogravimetry
EDT	3,4-ethylenedioxythiophene
EDT-DOB	(3,4-ethylenedioxythiophene)-(2,5-bis(octyloxy)benzene)
EDTPhCN	2,2'-((2,3-dihydrothieno[3,4-b][1,4]dioxine-5,7-diyl)bis(1,4-phenylene)) diacetonitrile
EDT-TPA	(3,4-ethylenedioxythiophene)-(triphenylamine)

List of Abbreviations

EDT-TPAFL	(3,4-ethylenedioxythiophene)-(9,9-bis(4-diphenylaminophenyl)-fluorene)
FL	9,9-dioctylfluorene
FL-BP	(9,9-dioctylfluorene)-(biphenyl)
FL-DPPPh	(9,9-dioctylfluorene)- (3,6-diphenyl-2,5-dihydropyrrolo [3,4-c] pyrrole-1,4-dione)
FL-TPA	(9,9-dioctylfluorene)-(triphenylamine)
FL-TPAFL	(9,9-dioctylfluorene)-(9,9-bis(4-diphenylaminophenyl)fluorene)
f_{osc}	Oscillator strength
GPC	Gel Permeation Chromatography
$^1\text{H NMR}$	^1H Nuclear magnetic resonance
HOMO	Highest occupied molecular orbital
HPLC	High Performance Liquid Chromatography
HSE06	Heyd-Scuseria-Ernzerhof
ICT	Intramolecular charge transfer
$\text{Im } \chi^{(3)}$	Imaginary part of the third-order susceptibility
ITO	Indium tin oxide
LEDs	Light emitting diodes
LUMO	Lowest unoccupied molecular orbital
M. P.	Melting point
MEH	1,4-dimethyl-2-((2-ethylhexyl)oxy)-5-methoxybenzene
Mn	Number average molecular weight
Mw	Weight average molecular weight
Nd:YAG	Neodymium-doped yttrium aluminium garnet
NLO	Nonlinear optical
NLR	Nonlinear refraction
OA	Open-aperture
OFETs	Organic field-effect transistors
OPV	Organic photovoltaic
P(ANT-PHENO)	Poly(anthracene)-alt-10-octylphenothiazine)

P(DMT-TPA)	Poly(3,4-dimethoxythiophene-alt-triphenylamine)
P(DMT-TPAFL)	Poly(3,4-dimethoxythiophene-alt-9,9-bis(4-diphenylaminophenyl)-fluorene)
P(EDT-DOB)	Poly(3,4-ethylenedioxythiophene-alt-2,5-bis(octyloxy)benzene)
P(EDT-TPA)	Poly(3,4-ethylenedioxythiophene-alt-triphenylamine)
P(EDT-TPAFL)	Poly(3,4-ethylenedioxythiophene-alt-9,9-bis(4-diphenylaminophenyl)-fluorene)
P(FL-BP)	Poly(9,9-dioctylfluorene)-alt-biphenyl)
P(FL-DPPPh)	Poly(9,9-dioctylfluorene)- alt-3,6-bis(phenyl) 2,5-dihydropyrrolo [3,4-c] pyrrole-1,4-dione)
P(FL-TPA)	Poly(9,9-dioctylfluorene)-alt-triphenylamine)
P(FL-TPAFL)	Poly(9,9-dioctylfluorene)-alt-9,9-bis(4-diphenylaminophenyl)-fluorene)
PBC	Periodic boundary condition
PC ₆₁ BM	[6,6]-Phenyl C ₆₁ butyric acid methyl ester
PC ₇₁ BM	[6,6]-Phenyl C ₇₁ -butyric acid methyl ester
PDI	Poly dispersity index
PL	Photoluminescence spectrum
PSC	Polymer solar cell
RSA	Reverse saturation absorber
SA	Saturation absorber
TBAB	Tetrabutylammoniumbromide
TG	Thermogravimetry
ThCHO	2,5-thiophene dicarboxaldehyde
THF	Tetrahydrofuran
TPA	Two photon absorption
TPA	Triphenylamine
TPAFL	9,9-bis(4-diphenylaminophenyl)-fluorene
UV-Visible	Ultraviolet-Visible

